2-7-2024

Stromal Reprogramming by FAK Inhibition Overcomes Radiation Resistance to Allow for Immune Priming and Response to Checkpoint Blockade

Varintra Lander
Washington University in St. Louis

WASHINGTON UNIVERSITY IN ST. LOUIS

Division of Biology and Biomedical Sciences

Immunology

Dissertation Examination Committee:

David G. DeNardo, Chair

Gregory D. Longmore

Robert D. Schreiber

Julie K. Schwarz

Sheila A. Stewart

Stromal Reprogramming by FAK Inhibition Overcomes Radiation Resistance to Allow for Immune Priming and Response to Checkpoint Blockade

by

Varintra Edlyn Lander

A dissertation presented to
Washington University in St. Louis
in partial fulfillment of the
requirements for the degree
of Doctor of Philosophy

May 2024
St. Louis, Missouri

Table of Contents

List of Figures

List of Tables

Acknowledgments

My time at Washington University has been a tremendous blessing and I can think of no words to fairly describe it. I have learned so much and gained many irreplaceable mentors, colleagues, and friends along the way – I thank God every day for all these blessings. First and foremost, I would like to thank my mentor and thesis advisor, **Dr. David DeNardo**. David has been an instrumental scientific advisor and I cannot thank him enough for his patience, time, and energy to shape me into an independent scientist that I have become today. His passion for science and enthusiasm for new discoveries, especially in translational research, have been contagious ever since I joined his lab; I could not have asked for a better lab than his for my thesis project. David: thank you for being my advocate, for all your support and understanding of my shortcomings as a growing scientist, and for always being there for the highs and lows of my graduate school training. Thank you for teaching me resilience through failure and for showing me perseverance can be fruitful. Thank you for teaching me to always try my best and to not be afraid to fail – I am forever grateful for your many scientific and life advice. I hope I will continue to love science and research as you have showed and taught me.

David played a pivotal role in the accomplishment of my thesis work, but the rest of my committee members were as essential in my journey to become an independent scientist. **Dr. Julie Schwarz**, **Dr. Gregory Longmore**, **Dr. Robert Schreiber**, and **Dr. Sheila Stewart**: I would like to extend my deepest gratitude for all your generous time and expertise. Throughout my training, my committee members have challenged me and have given rigorous scientific ideas and priceless advice. As a physician scientist herself,

Dr. Julie Schwarz has been a great mentor and I have been very blessed to be able to learn under her supervision. Without Dr. Schwarz's expertise in radiation oncology, Dr. Longmore's expertise in cancer extracellular matrix, Dr. Schreiber's expertise in cancer immunology, and Dr. Stewart's expertise in cancer-associated fibroblasts, I would not have been able to complete my thesis project successfully. I am very fortunate to be able to get training in this very collaborative environment.

The rest of the DeNardo lab members have made it easy for me to come to lab every morning feeling excited. **Brett Knolhoff**, **Xiuting Liu**, **Liang-I Kang**, **Jad Belle**, **Natalie Kingston**, **John Baer**, **Chong Zuo**, **Graham Hogg**, **Brett Herzog**, **Savannah Bogner**, **Samarth Hegde**, and **John Herndon**: you all have been one of my greatest support systems going through graduate school. Over the past 5 years, you have been the best colleagues anyone could have asked for. I consider you more than just colleagues, but also friends. Thank you for your patience in listening to my failed experiments and for your generous encouragement. I also have David to thank for giving me this richly educational and engaging environment for me to thrive as a budding scientist. I will forever treasure my time in the DeNardo lab, and I will deeply miss everyone.

My passion for science started when I was an undergraduate researcher at the University of Washington in **Dr. Phil Greenberg**'s lab. In his lab, I first learned about cancer immunology from **Dr. Andrea Schietinger** and fell in love with the field that I continued to do my thesis project in the same field. Andrea is the one who has supported me from the very beginning to pursue a career as a physician scientist, and for that I am forever grateful. Thank you for taking me under your wings when you started your own lab at MSKCC. I am very grateful for all the career advice you have given me and for

being such a wonderful mentor you always have been. I cannot thank you enough for nurturing me and for advocating and supporting me. I hope one day I can be a successful scientist like you and David.

I know I could not have gone through my training at Washington University alone. I have met numerous wonderful friends along the way, and I would like to thank each and every one of them for being so impactful in my life. **Tsehay**, **Samuel**, **Mary Morgan**, and **Tim**: thank you for life group, for all the time you have listened about my life crisis, and for being more than supportive every single time. Life in St. Louis would have been miserable without you all and I hope our friendships will continue way beyond our time at WashU.

I don't even know how to start thanking my **(Krisnawan) family**. **Daddy** and **Mommy**: thank you for moving all the way from Indonesia to the US for our education. Thank you for your countless sacrifices, your continuous prayers and support, your advice, your encouragement, your patience, and your unconditional love. I know I can never repay for all the things you have given me, but I hope one day I can make you proud. **Andrew** and **Clarissa (Goodie)**: thank you for being the best siblings and for allowing me to be the annoying older sister. Thank you for the joy, laughter, and the time we've spent together. Going back home to Seattle to visit you guys have always been a reprieve in the middle of my training and I thank you for being my safe haven I know I can always go to.

One of the greatest blessings I received during my time at WashU is **Daniel Lander**. Daniel: thank you for being my greatest confidant and my best friend. Thank you for being a good listener and for shouldering the burden with me whenever things get rough. Thank you for teaching me how to work hard and how to be tough. Despite your busy schedule

and lack of sleep, thank you for making time for me whenever I need it. Thank you for your patience and your unending support in my seemingly endless training to become a physician scientist. I pray that we both will continue to support each other yet to never lose track of what is most important in life.

Varintra Lander

Washington University in St. Louis

May 2024

ABSTRACT OF THE DISSERTATION

Stromal Reprogramming by FAK Inhibition Overcomes Radiation Resistance to Allow for Immune Priming and Response to Checkpoint Blockade

by

Varintra Edlyn Lander

Doctor of Philosophy in Biology and Biomedical Sciences

Immunology

Washington University in St. Louis, 2024

Professor David G. DeNardo, Chair

Pancreatic Ductal Adenocarcinoma (PDAC) is one of the most lethal malignancies. While immune checkpoint blockade (ICB) is effective in many solid cancers, it has not been effective in PDAC. Furthermore, clinical trials combining ICB with standard of care chemo- or radio-therapy (RT), which should be able to prime anti-tumor immunity and unlock ICB, have not been overwhelmingly successful. Thus, understanding the effect of RT on PDAC tumor immunity is critical to plan better combination treatment strategies for this highly recalcitrant cancer.

To elucidate if RT can prime antigen specific T cell responses, we first looked at human PDAC resections. In our RT-treated human PDAC cohort, we found no increase in the number of tumor infiltrating T cells in the tumor stroma compared to a control group. Additionally, using genetically engineered PDAC model, the p48-Cre/LSL-$Kras^{G12D}$/$p53^{Flox/Flox}$/$OVA\text{-}GFP^{+}$ (KPC-OG) mice, RT alone, despite inducing temporary

tumor control, similarly did not prime new antigen specific T cell responses. These data suggest that RT gives us no evidence of T cell priming. We postulated that the unique PDAC tumor microenvironment (TME), which is characterized by a fibrotic desmoplastic stroma, might play a role in limiting RT-induced immune priming.

To study the role of PDAC TME, we developed a 3D organoid co-culture system. We found fibroblasts and collagen work synergistically to mitigate RT efficacy, which is mediated in part through Focal Adhesion Kinase (FAK). In mice, FAK inhibitor (FAKi) rescued RT resistance leading to significant tumor regression and enhanced survival. Associated with this regression, we found increased dendritic cells and tumor specific $CD8^+$ T cells numbers. Single cell RNA seq and CyTOF revealed that the dual treatment primed immune cells and cancer associated fibroblasts to participate in better anti-tumor immunity in the form of enhanced antigen processing and presentation and T cell activation. This positive data prompted us to initiate a phase Ib study in which FAKi will be given in combination with RT to patients with locally advanced PDAC (NCT04331041). This clinical trial is currently underway with interesting early biomarker results, which mirrored our pre-clinical findings showing stromal reprogramming toward more anti-tumor phenotypes.

Based on the anti-tumor changes brought by the dual treatment, we next hypothesized the combination of RT and FAKi would render ICB effective. Pre-clinical studies in mouse PDAC models showed that while RT and ICB was ineffective at tumor control, the triple combination of RT, FAKi, and ICB led to extended long-term survival. Overall, these data suggest that stromal modulation can be used to allow RT to prime anti-tumor immunity in PDAC and unlock ICB efficacy.

Chapter 1: Introduction

Cancer is a very devastating disease and is among the leading causes of death worldwide. In 2021, it was estimated that more than 1,898,160 individuals were diagnosed with cancer with more than 608,570 estimated deaths (seer.cancer.gov, as of March 16, 2022). Furthermore, cancer continues to be a growing issue. Data from 2015-2017 showed that approximately 39.5% of men and women will be diagnosed with cancer at some point during their lifetimes. According to the International Agency for Research on Cancer (part of World Health Organization), by 2040, the number of new cancer cases per year is expected to rise to 29.5 million and the number of cancer-related deaths to 16.4 million. It is evident that cancers affect many people.

Cancers arise when cells in the body divide uncontrollably and spread into surrounding tissues. This change in normal homeostasis is usually caused by genetic mutations in the cellular DNA, which allow the mutated cells to bypass signals that normally tell cells to stop dividing or to die. Through this, cancer cells require many abilities to survive and continue to grow undetected.

There are multiple treatment options for cancer, which include, but not limited to: surgery, chemotherapy, radiation therapy (RT), immunotherapy, hormone therapy, and targeted therapy. Numerous patients can benefit from these treatments, but many patients eventually face the same problem known as treatment resistance. Even though we have a lot more treatment options now compared to decades ago, patients can still succumb to cancer due to treatment resistance that can develop quickly, within a matter of weeks after the start of treatment, or even years later. Given how tricky it is to treat cancer cells, researchers believe that to combat many cancer types, nowadays, one way

to overcome or delay treatment resistance is to treat cancer patients with a combination of treatment modalities.

The general goal of my thesis dissertation was to elucidate the factors that cause pancreatic cancer to be resistant to treatment, focusing on radiation therapy (RT), and how to overcome this recalcitrant nature of pancreatic cancer in clinic using multiple-pronged treatment approach. First, I will illustrate that, unlike in other cancer such as sarcoma, RT is insufficient to prime robust T cell responses in pancreatic cancer. Second, I will show that the pancreatic cancer's stromal elements are responsible to repress RT efficacy and the induction of interferons. Third, I will demonstrate that by reprogramming the stroma, through inhibition of Focal Adhesion Kinase (FAK), we can reverse stromal-induced RT resistance and thus promote the remodeling of PDAC stroma to promote immunogenicity which include T cell priming. And lastly, I will portray that the combination of RT and FAK inhibition renders immune checkpoint blockade therapy effective and significantly improves survival. This introductory chapter will review pancreatic cancer and its tumor microenvironment (TME), RT and components of the TME that can trigger RT resistance, and FAK signaling and advances to target FAK in cancer.

1.1. Pancreatic Cancer

Pancreatic cancer is currently the 3rd leading cause of cancer-related deaths and predicted to be the 2nd leading by 2030[1] (**Table 1.1**). Pancreatic ductal adenocarcinoma (PDAC) accounts for more than 90% of pancreatic cancer cases and remains to be a highly lethal malignancy with a 5-year survival rate of less than 10%[2]. The only potential for curative treatment for PDAC is complete surgical resection, but 80-90% of patients

are diagnosed at unresectable stages[2,3]. For patients with non-resectable or borderline-resectable PDAC, systemic chemotherapy is considered standard-of-care first-line treatment modality, which includes Gemcitabine, Capecitabine, 5-Fluorouracil (5-FU), Abraxane, or Oxaliplatin, in monotherapy settings or in combination with other treatment modality such as RT. Combinatorial chemotherapies, such as FOLFIRINOX (a mixture of Folinic acid, 5-FU, Irinotecan, and Oxaliplatin) and Gem/Abraxane (a combination of Gemcitabine and albumin-bound Paclitaxel, Abraxane) have been shown to significantly improve patient survival, albeit at the cost of significantly higher toxicity[2]. RT has been utilized in many PDAC patients to improve resectability in locally advanced or primarily inoperable or borderline-operable patients with conflicting results from multiple trials[2,3]. Immunotherapies, including immune checkpoint blockade (ICB), adoptive cell transfer, cancer vaccines, and agents that manipulate the immune microenvironment in the TME, have made tremendous impacts in many cancers; however, no immunotherapeutic approaches have shown promising results so far in PDAC patients[4], except maybe in a minority of PDAC patients with high tumor mutational burden[5]. Clearly, there is a lack of durable and effective treatment option for PDAC patients, and more research needs to be done to overcome this recalcitrant nature of PDAC.

PDAC develops overtime in a multi-step carcinogenesis process due to accumulating mutations in the pancreatic acinar cells[2,3,6]. There are three precursor lesions of invasive pancreatic ductal adenocarcinomas: 1) PanIN (pancreatic intraepithelial neoplasm), which is the most common out of the three, 2) MCN (mucinous cystic neoplasm), and 3) IPMN (intraductal papillary mucinous neoplasm). Acinar cells need to first acquire activating mutation of the proto-oncogene *KRAS* to initiate the acinar-to-ductal metaplasia

needed to generate PanINs[3,6]. Somatic driver mutations are very common in PDAC with activating *KRAS* mutation being found in >90% of patients, followed by mutations of *P53* found in 60-70% of patients, *CDKN2A* in >50% of patients, and *SMAD4* inactivation in 50% of patients[3,6]. However, even with these common genetic perturbations, when compared to other cancers like melanoma, non-small cell lung cancer, head and neck cancer, and cervical cancer, PDAC has a fairly low mutational burden and response to immunotherapy[7]. Furthermore, PDAC is unique compared to other solid cancers due to its characteristic abundance of stromal cells, which can constitute up to 90% of the tumor volume, and a paucity of epithelial malignant cells[2]. The recalcitrant nature of PDAC has been linked in part to its unique TME[8]. Thus, to strategically and effectively target PDAC, we need to understand its unique TME.

1.2. The Tumor Microenvironment in Pancreatic Cancer

One hallmark of PDAC is that it is one of the most stroma-rich cancers[3,8]. PDAC's TME is very heterogeneous and is characterized by both cellular and acellular components, which include abundant cancer associated fibroblasts (CAFs), immune cells, pancreatic stellate cells (PSCs), endothelial cells, dense collagen-rich extracellular matrix (ECM), and soluble proteins like cytokines, chemokines, and growth factors[8-11]. PDAC's fibrotic stroma has been associated with PDAC's proliferation, survival, metastasis, escape from immune control, and resistance to therapies[3,8]. Thus, understanding the components of the PDAC TME and how they interact with the PDAC tumor cells should help us better design future treatment plans.

The PDAC CAFs constitute of a very heterogenous and diverse metabolically active stromal cells with numerous roles in the TME[12]. CAFs are thought to be derived from mesenchymal cells of various origins that can either be resident or recruited to the pancreas. A major source of PDAC CAFs is PSCs[13]. Activated CAFs can comprise between 15-85% of the stromal cells in the PDAC TME[12]. However, it is not easy to identify CAFs in the PDAC TME due to the lack of specific cell surface markers that are expressed only on the CAFs and not on other cells. Hence, CAFs are identified by cell morphology and lack of lineage markers for other cell types such as epithelial cells, immune cells, and endothelial cells. Many would agree that the expression of Podoplanin (PDPN), Vimentin, and platelet-derived growth factor receptor-α and -β (PDGFRα and PDGFRβ) are commonly used to identify CAFs. PDAC CAFs are thought to be one of the major players responsible for the desmoplasia and fibrotic response, which occur throughout PDAC tumorigenesis[12]. Interestingly, many studies have reported both tumor-supportive and tumor-suppressive roles of the PDAC CAFs[12,14-20]. However, it is not yet clear how plastic these CAF populations are. Currently, there are four proposed models for the diverse functions and phenotypes of CAFs[18]: 1) One class of CAFs with multiple functions; 2) Two classes of CAFs with either tumor-promoting or tumor-restraining functions; 3) Several CAF classes with only one main function, falling into either tumor-promoting or tumor-restraining; or 4) Several classes of CAFs, each with one main function that is either tumor-promoting or tumor-restraining depending on the context. Further complicating the matter, it has been shown that the characteristics and interactions of CAFs with other cells types in the TME could change dynamically as the

cancers evolve[18]. Given how complex CAFs' functions and phenotypes are, it has not been a trivial endeavor to study CAFs.

Recent studies using single cell RNA sequencing, mass cytometry, and genetically engieneered mouse models have made it possible to begin to understand the heterogeneity and the functional roles of PDAC CAFs. Broadly in PDAC, CAFs can be divided into three main subtypes[13,18,21,22]: 1) Myofibroblastic CAFs (myCAFs, defined by markers αSMA, THY1, TAGLN, CTGF, IGFBP3, COL12A1, THBS2, and LRRC15); 2) Inflammatory CAFs (iCAFs, defined by markers CLEC3B, COL14A1, and LY6C); and 3) Antigen-presenting CAFs (apCAFs, defined by markers CD74, SLP1, SAA3, MHC-II, and FSP1). Works published by the Tuveson Lab have nicely eluciated the differences among these three CAF subtypes[13,21,22]. myCAFs are characterized by αSMA expression, TGFβ signaling, ECM production, and are found proximal to the tumor ducts and interact with the PDAC cells through juxtacrine mechanisms. iCAFs are characterized by LY6C expression, JAK/STAT signaling, having a secretory phenotype, and are found farther from the tumor ducts within the stroma and interact with the PDAC cells and other cells through inflammatory cytokines. apCAFs are characterized by CD74 and MHC-II expressions, STAT1 signaling, antigen presentation signaling pathways, and have immunomodulatory abilities, such as interacting with $CD4^+$ T cells to activate them, albeit at a lower level than professional immune antigen presenting cells (APCs). Although much have been discovered in the last decade regarding the PDAC CAFs, there are still many outstanding questions which need to be answered. We still do not have a clear understanding on how cancer therapies will shift these PDAC CAF subsets and the relative influences of these CAF subsets on therapeutic response and/or resistance.

CAFs are not the only population in the PDAC TME which are diverse. The immune landscape of the PDAC TME is also composed of various different immune cell types, which have been shown to have both tumor-promoting and tumor-restraining roles[23]. Because of this, the immune microenvironment of PDAC has been more recently used as a prognostic feature of the disease[23]. The PDAC immune microenvironment is considered highly immunosuppressive due to the abundance of tumor associated macrophages (TAMs), $CD4^+$ $T_{regulatory}$ cells, myeloid-derived suppressor cells (MDSCs), and hardly any $CD8^+$ $T_{cytotoxic}$ cells and conventional dendritic cells (cDCs) infiltrating the tumors[8,24,25]. This imbalance of pro-tumorigenic to anti-tumorigenic immune cells could explain the resistance of PDAC to immunotherapies and the poor prognosis of the disease.

TAMs in PDAC play a huge role in the immunusppressive TME of PDAC. For example, TAMs in PDAC: 1) secrete immunosuppressive cytokines and enzymes, such as TGFβ, IL-10, and VEGF; 2) interfere with the metabolism and suppress the activity of $CD4^+$ $T_{effector}$ cells and $CD8^+$ $T_{cytotoxic}$ cells; 3) recruit $CD4^+$ $T_{regulatory}$ cells; and 4) activate PSCs into CAFs, further contributing to the immunosuppressive TME[8]. The presence of TAMs has generally been correlated with poor prognosis in PDAC and other cancers. TAMs have also been shown to cause chemo-, radio-, and immuno-therapy resistance[26]. Because of their immunosuppressive nature, many therapies have been aimed to either deplete or repolarize TAMs to have more anti-tumor phenotypes and functions.

There is an inverse correlation between the infiltration of myeloid cells and $CD8^+$ T cells in PDAC[27]. This is not surprising given that TAMs are considered to be the most abundant pro-tumorigenic immune cells in PDAC. $CD8^+$ T cells are important anti-tumor

immune players and their presence in PDAC has been correlated with good prognosis[28]. However, the $CD8^+$ T cells found in many PDAC patients express higher levels of inhibitory and exhaustion markers which imply their immune dysfunction and diminished cytotoxic ability[27]. Furthermore, the $CD8^+$ T cells found in the PDAC TME are mostly found at greater distances from the tumor cells due the desmoplastic TME[24,25], which may hinder their ability to kill the tumor cells[29-31]. Moreover, the harsh PDAC TME has been shown to be metabolically incompatible for effective T cell function, making it even harder for them to perform their cytolytic functions[8]. Therefore, many immunotherapies are aimed to unleash the inhibitory checkpoints on T cells, to increase their infiltration into the tumors, and to render the TME to be more supportive of T cell functions.

Just like $CD8^+$ T cells in the PDAC TME, conventional dendritic cells are essential in tumor immunology. cDCs are professional antigen presenting cells (APCs), which process and present antigens to T cells, and are necessary for their initial priming; hence they are considered as a bridge between the innate and adaptive immune system[32,33]. cDCs are broadly categorized into: 1) cDC1 (marked by CD141 and XCR1 in human, and CD103, CD24, Xcr1, and CD8 and the transcription factor *Batf3* and *Irf8* in mouse), which predominantly stimulate $CD8^+$ T cells; and 2) cDC2 (marked by Sirpα and CD1c in human, and CD11b and CD4 and the transcription factor *Irf4* in mouse), which predominantly activate $CD4^+$ T cells[34]. While cDC2s are important for regulating immune responses to extracellular pathogens, parasites, and allergens, and hence the induction of Th17 and Th2 cell immune responses, cDC1s are important for regulating immune responses to intracellular pathogens and hence the induction of type 1 immunity (Th1) through the production of IL-12[34,35]. There is another type of dendritic cells, known as plasmacytoid

DCs, which play a role through cytokine secretion, mainly type-I interferon, but are thought to not participate directly in the presentation of antigens to T cells[34,35]. Although plasmacytoid DCs are also important in cancer immunology, I will mainly focus on conventional DCs.

Exogenous antigens, including cancer antigens, can be presented on MHC-I molecules of cDCs through a process known as “cross-presentation.” This process is essential for the initiation of $CD8^+$ T cell responses in many conditions including cancers[36,37]. More importantly, cDC1’s role to fully prime $CD8^+$ T cells also requires the presence and function of $CD4^+$ T cells for the process of “licensing,” which occurs when CD40 on cDCs is activated through interacting with CD40L on $CD4^+$ T cells[38-40]. Moreover, recent data suggest that cDC1s can also prime $CD4^+$ T cells and that these $CD4^+$ T cells participate in the licensing of cDC1s for enhanced $CD8^+$ T cell responses to tumors, questioning the original dogma that cDC1s only prime $CD8^+$ T cells[41]. In this newer model, cDC1 is the central cell type that primes both $CD8^+$ and $CD4^+$ T cells. The interaction between CD40L and CD40 on the $CD4^+$ T cell and cDC1 respectively, is essential for strong licensing of cDC1s and lack of this ligation can lead to failure of tumor rejection by $CD8^+$ T cells, highlighting the importance of this 3-cell interaction for anti-tumor immunity[41].

In addition to their direct interaction with T cells, upon type-I interferon stimulation, cDC1s can also secrete important cytokines and chemokines that can recruit and activate T cells, including CXCL9, CXCL10, and CXCL11[42-44]. Furthermore, immune checkpoint blockade (ICB) therapies used in cancers, such as αPD-1 and αCTLA-4, require the presence and action of cDC1s to be effective[45]. Therefore, cDC1s remain the focus in

cancer immunology due their role for anti-tumor T cell trafficking and T cell functions[35,42] and it is to be expected that their presence is necessary for T cell-mediated anti-tumor control[46,47].

Lastly, besides the diverse cellular PDAC stromal elements, PDAC also has a fibrotic and desmoplastic acellular ECM[8]. The PDAC ECM components include collagen, fibronectin, hyaluronic acid, proteoglycans, as well as other enzymes and proteinases. The accumulation of this dense ECM components deforms normal organ architecture of the pancreas, which includes abnormal configuration of blood and lymphatic vessels, which make PDAC to be considered to have a hypoxic and harsh environment[8]. This PDAC TME contributes to poor drug delivery and deprived infiltration of anti-tumor immune cells among many others, which can explain the chemo- and immuno-therapy resistance.

In summary, the PDAC TME has a very diverse CAFs and immune populations and dense ECM components. Many of these aspects have been linked to PDAC resistance to chemo-, radio-, and immuno-therapies[48-52]. Although not at all comprehensive, I have mentioned some cell types that have tumor-promoting and other cell types with tumor-repressing roles. Even within the same cell type, there is known to be a spectrum of different phenotypes. These cells' phenotype, composition, distribution, and spatial proximity to each other are undoubtedly important to understanding cancer progression and response or resistance to treatment. My project aims to elucidate a part of this central question.

1.3. Radiation Therapy (RT) and Stromal-Mediated RT Resistance

Tumor Microenvironment as a Regulator of Radiation Therapy: New Insights into Stromal-Mediated Radioresistance

Krisnawan, V. E., Stanley, J. A., Schwarz, J. K. & DeNardo, D. G. Tumor Microenvironment as a Regulator of Radiation Therapy: New Insights into Stromal-Mediated Radioresistance. Cancers 12, 2916 (2020).

Simple Summary: Cancer is multifaceted and consists of more than just a collection of mutated cells. These cancerous cells reside along with other non-mutated cells in an extracellular matrix which together make up the tumor microenvironment or tumor stroma. The composition of the tumor microenvironment plays an integral role in cancer initiation, progression, and response to treatments. In this review, we discuss how the tumor microenvironment regulates the response and resistance to radiation therapy and what targeted agents have been used to combat stromal-mediated radiation resistance.

Abstract: A tumor is a complex “organ” composed of malignant cancer cells harboring genetic aberrations surrounded by a stroma comprised of non-malignant cells and an extracellular matrix. Considerable evidence has demonstrated that components of the genetically “normal” tumor stroma contribute to tumor progression and resistance to a wide array of treatment modalities, including radiotherapy. Cancer-associated fibroblasts can promote radioresistance through their secreted factors, contact-mediated signaling, downstream pro-survival signaling pathways, immunomodulatory effects, and cancer stem cell-generating role. The extracellular matrix can govern radiation responsiveness by influencing oxygen availability and controlling the stability and bioavailability of growth factors and cytokines. Immune status regarding the presence of pro- and anti-tumor immune cells can regulate how tumors respond to radiation therapy. Furthermore, stromal

cells including endothelial cells and adipocytes can modulate radiosensitivity through their roles in angiogenesis and vasculogenesis, and their secreted adipokines, respectively. Thus, to successfully eradicate cancers, it is important to consider how tumor stroma components interact with and regulate the response to radiation. Detailed knowledge of these interactions will help build a preclinical rationale to support the use of stromal-targeting agents in combination with radiotherapy to increase radiosensitivity.

1.3.1. Focused Introduction

The field of oncology has evolved from a malignant mutated cancer cell-centered view to the understanding of cancer as a complex "organ" composed of both malignant cells and diverse nonmalignant cellular and non-cellular components termed the tumor stroma or tumor microenvironment (TME)[53-57]. The concept of cancer as a disease focusing only on malignant tumor cells has been deemed inaccurate; in some cancers, stromal cells represent the majority of cell types, as is frequently seen in pancreatic and breast cancers[58]. These cellular stromal components often include activated cancer-associated fibroblasts (CAFs), leukocytes, and vascular cells, but they also sometimes include other adjacent normal tissue/cells such as non-transformed epithelia, adipose tissue, or neurons[53-57]. The non-cellular compartment of the tumor stroma comprises extracellular matrix (ECM) components like collagens, laminins, fibrinogen, elastin, and proteoglycan, and secreted factors such as cytokines, chemokines, and sequestered growth factors[53-63]. Accumulating evidence highly suggests that malignant cancer cells and the tumor stroma reciprocally communicate with and influence one another, but this relationship is complex and remains poorly understood. To treat cancer as a disease, we cannot single-mindedly focus on cancer cells with their autonomous genetic mutations; we need to

simultaneously consider the TME because its interactions with tumor cells often contribute to disease initiation, progression, and treatment response[54-56,58,64].

Radiation therapy (RT) is a powerful anti-cancer therapeutic used to treat up to 50−60% of cancer patients[64,65]. The goal of RT is to target highly proliferative cancer cells while sparing normal tissue. The concept of dose fractionation—delivering small daily RT doses over several days—is designed to exploit cancer cells' vulnerabilities in repairing DNA damage, leading to their demise, while giving normal healthy cells a chance to activate their DNA repair and cell cycle mechanisms[65-68]. Historically, radiobiology has utilized linear quadratic modeling to estimate the therapeutic treatment ratio, with increasing radiation toxicity to cancer cells while avoiding surrounding normal tissue. This "therapeutic ratio" is based on differences between the DNA damage and repair kinetics of cancer and normal cells. The linear-quadratic model utilizes the α and β parameters to describe the linear and quadratic portions of the cell survival curve, respectively, and experimental evidence suggests that these parameters and the α:β ratio differ widely across and even within some tumor types[69,70]. Classical modeling predicts that delivering small doses of radiation over the course of multiple treatments (i.e., conventional dose fractionation) can increase the therapeutic ratio compared to single-dose delivery, and early studies using small and large animal models confirmed these effects[69-71]. However, recent evidence has called into question whether small doses of radiation delivered over a protracted treatment course (conventional fractionation) are required to achieve these effects.

Standard of care for the majority of solid tumors requires 50 to 70 Gy total radiation dose delivered with conventionally fractionated schedules, most commonly utilizing 1.8

to 2 Gy per fraction. Over the past decade significant technologic advances in image-guided radiation, tumor tracking, beam intensity modulation, and beam shaping have facilitated the capacity to precisely deliver higher dose per fraction to the tumor while sparing larger volumes of surrounding normal structures. This concept of hypofractionation, or higher fractional doses of radiation over fewer total fractions and commonly delivered with stereotactic guidance via stereotactic body radiotherapy (SBRT) or stereotactic radiosurgery (SRS), has demonstrated safety and efficacy in many tumor types[72-75]. However, data also suggest that the clinical effects of hypofractionation are not solely due to differences in tumor and normal tissue DNA repair kinetics but also to the effects of radiotherapy on the TME. Although largely anecdotal, TME alterations can be demonstrated through the observation of "out-of-field" or abscopal responses to focused radiation as first described in the early 1950s[76]. Since then, additional work has demonstrated that the abscopal response is dependent on alterations in the immune system and the surrounding stromal tissue. Radiation can result in immune cell priming, neoantigen and cytokine release, modification of tumor vasculature, and alteration of the ECM, all of which have the potential to be optimized to enhance RT efficacy[77-81].

Despite RT designed to target malignant tumor cells, and the knowledge that RT can be used to prime the immune system, the complex interaction between malignant tumor cells and other cells within the TME is important because the stroma can impact malignant cells' response and contribute to treatment resistance[64]. Additionally, there are reports that RT can cause numerous changes in stromal cells within the TME that further promote undesirable tumor growth, invasion, and treatment resistance[64]. To successfully eradicate cancers, these reciprocal interactions between the tumor cells and tumor stroma must be

characterized in detail. Moreover, the use of stromal-targeting agents in combination with RT is a largely unaddressed therapeutic option. These topics deserve more attention to broaden our knowledge to design better treatment strategies to combat cancers, particularly those characterized by a high density of stromal cells and other stromal components within the TME. In this review, we summarize the roles of stromal components and the TME that contribute to cancer cell radioresistance (**Figure 1.1**) and discuss how they may be targeted for possible therapeutic benefit (**Figure 1.2**).

1.3.2. The Impact of RT on the Tumor Stroma

RT seeks to exploit DNA repair deficiencies in malignant tumor cells, but even in perfect scenarios, it invariably affects stromal cells within the tumor mass or at its boundaries[82]. Although many RT-mediated stromal changes are beneficial, such as the revival of or polarization toward tumor-suppressing immunity, RT can act as a double-edged sword in tumors[65]. Specifically, deleterious side effects could facilitate cancer progression and treatment resistance. These are the byproducts of RT we hope to avoid by carefully designing and planning RT dose regimens and combinatorial treatments.

One impact of RT on the tumor stroma is chronic inflammation that drives RT-induced fibrosis marked by an increased number of stromal cells and ECM components, through several mechanisms that have been reviewed elsewhere[83]. RT-induced fibrosis is a well-known side effect that can arise in some patients[53,83,84]. RT can completely transform the TME by inducing rapid and chronic loss of hyaluronic acid[85] and collagen remodeling[86] by altering how CAFs regulate their collagen production[62,87]. Furthermore, RT-treated CAF populations can undergo modifications and alterations in terms of their diversity, secretome, and phenotype[88]. Additionally, RT enhances activation of proliferating

machinery involving the RAS and mitogen-activated protein kinase (MAPK) cascades; the invasion pathways, which involve matrix metalloproteins (MMPs), laminin 5, and filamin A; transforming growth factor beta (TGFβ) signaling, which is involved in tumor progression, resistance, and metastasis[54,59,89]. Likewise, RT to the stroma can increase tumor invasiveness due to increased hepatocyte growth factor (HGF)/c-Met (HGF receptor) signaling and MAPK activity, which enhances tumor mobility and can be deleterious[90]. Taken together, these reports suggest that RT can activate stromal features indicative of potential stromal-mediated treatment resistance.

It is still unclear how different fractionated RT regimens alter the stromal components of the TME and how these changes affect subsequent responses of cancer cells to RT. Similarly, the attempts to combine stromal-disrupting agents with RT to overcome stromal-mediated radioresistance remain unclear and merit further study.

1.3.3. The Impact of CAFs on RT Efficacy

CAFs are heterogeneous and the major contributors to the tumor stroma[55,56]. CAFs have been shown to control tumor phenotype at all stages of tumor progression. Their roles have been reviewed elsewhere and include the ability to shape the ECM; modulate innate and adaptive immune microenvironments; recruit and regulate leukocyte migration and inflammation via cytokines, chemokines, and growth factors; provide metabolic support (amino acids, lipids, and tricarboxylic acid cycle intermediates); and contribute to paracrine activation of mitogenic and pro-survival cellular signaling via cell surface receptor-ligand interaction and secreted proteins or exosomes[55,56,91]. The mechanisms by which CAFs contribute to radioresistance are likely mediated through their secreted factors, contact-mediated signaling, immunomodulatory effects, and ECM alterations[92].

CAFs secrete a number of different active factors that have diverse effects on tumor phenotype[55,56]. For example, through their active secretory function, tumor stromal fibroblasts can transfer RNA within exosomes to cancer cells. This exosome transfer mechanism has been implicated in paracrine anti-viral RIG-I and juxtacrine NOTCH (NOTCH3-JAG1) signaling pathways, which both contributed to the expansion of therapy-resistant tumor-initiating cells. Stromal cells, which include CAFs and some bone marrow cells, protected breast cancer cells by inducing an interferon (IFN)-related DNA damage resistance signature in a STAT1-dependent manner and caused the tumors to be chemo- and radioresistant[93]. In another model, conditioned media (CM) from pancreatic stellate cells (PSCs), which are the central mediator of desmoplasia and major contributors of pancreatic CAFs, dose-dependently enhanced pancreatic tumor cell proliferation, migration, invasion, and colony formation and caused resistance to gemcitabine and RT. The CM was found to activate the MAPK AKT pathways in tumor cells, and the authors postulated that factors such as interleukin-1β (IL-1β) and TGFβ were responsible[94]. The TME of glioblastoma is known to produce abundant TGFβ, a pleiotropic cytokine that promotes an effective DNA damage response. Glioma-initiating cells were protected from RT-induced cell death by this increase in TGFβ production, which promoted an effective DNA damage response and self-renewal via C-X-C chemokine receptor type 4 (CXCR4) and NOTCH1. TGFβ inhibition prevented tumor cell DNA repair and enhanced RT efficacy in this glioblastoma model[95]. Furthermore, CAFs can promote irradiated cancer cell recovery and tumor relapse after RT by producing insulin-like growth factor-1/2 (IGF-1/2), C-X-C motif chemokine ligand 12 (CXCL12), and β-hydroxybutyrate. These secreted factors increase reactive oxygen species (ROS) levels post-RT, which enhanced protein

phosphatase 2A activity and repressed the mammalian target of rapamycin activation, therefore inducing autophagy in cancer cells to promote cancer cell recovery. It was argued that blocking IGF-2 and autophagy can reduce CAF-promoted tumor relapse in mice after RT and could be a promising RT sensitization therapeutic strategy (**Figure 1.2**)[96].

CAF-secreted factors trigger many downstream autocrine and/or paracrine signaling pathways that regulate treatment response. A network of paracrine signaling among cancer cells, myeloid cells, and stromal cells such as endothelial cells can drive the processes of treatment resistance and metastasis[97]. CXCL1 signaling is an example of paracrine signaling that contributes to radioresistance. Along with cancer cells, CAFs highly express and secrete CXCL1, which inhibits expression of the ROS-scavenging enzyme superoxide dismutase 1, leading to ROS accumulation following RT[98]. In this scenario, tumor cells take advantage of ROS accumulation to enhance DNA damage repair mechanisms and ultimately cause radioresistance. This radioresistance is also mediated by activation of the mitogen-activated protein kinase ERK kinase/extracellular-signal-regulated kinase (MEK/ERK) signaling pathway important for malignant transformation[99,100]. Crosstalk between CAFs and tumor cells through CXCL1 expression in an autocrine/paracrine signaling loop is responsible for the radioresistance phenotype[98]. Together, these studies showed that through their secreted active factors, CAFs can confer radioresistance to tumor cells.

CAFs are embedded in the tumor stroma, allowing them to actively communicate with other cells present in their surrounding environment through various mechanisms[55,56]. Besides acting through their secreted factors, CAFs also induce radioresistance through

direct contact-mediated signaling between cancer cells and CAFs[55]. In pancreatic cancer, PSCs promote radioprotection and stimulate the proliferation of pancreatic cancer cells through β1 integrin signaling. β1 integrin is known to modulate the cellular response to genotoxic stress including RT[101]. It was found that this effect is independent of phosphoinositide 3-kinase (PI3K) but depends on focal adhesion kinase (FAK). β1 integrin inhibition or FAK knockout can abolish PSC-mediated radioprotection in pancreatic cancer cells to single-dose and fractionated RT[102]. These findings indicate that downstream cellular signaling pathways activated due to direct interactions between CAFs and tumor cells can mediate radioresistance.

Additionally, CAFs can work through paracrine networking to enrich cancer stem cells (CSCs), which have been implicated in chemo- and radioresistance. In pancreatic cancer, the presence of PSCs can induce CSC characteristics by increasing the epithelial-mesenchymal transition (EMT) phenotype. A proteomic screen revealed that TGFβ is involved in the radioresistance phenotype, and TGFβ neutralizing antibody can inhibit the EMT and CSC phenotype, thus sensitizing tumor cells to RT and reducing tumorigenicity in vivo[103]. In another setting, IGF-1 receptor (IGF-1R) signaling activation in cancer cells in the presence of CAFs expressing IGF-2 induced Oct3/4, Nanog, and Sox2 expression and promoted stemness pathways related to IGF-1R, EMT, PI3K, TGFβ, WNT, and Hedgehog signaling. This group showed that CAF-derived HGF, IGF-2, basic fibroblast growth factor (bFGF), WNT, and oncostatin M regulated CSC-like characteristics in a paracrine manner through counterpart receptor signaling components and stemness factors. They found that blocking IGF-2/IGF-1R/AKT/Nanog signaling reduced CSC stemness and concluded that there were potential clinical applications of targeted therapy

to improve chemo- and radioresistance (**Figure 1.2**)[104]. Furthermore, CSCs play an important role in disease recurrence after RT as a result of their high DNA repair and antioxidative capabilities. Fractionated RT can enhance IGF-1 secretion and subsequent upregulation of IGF-1R in CSCs. IGF-1R upregulation exerts a dual radioprotective effect by inducing upregulation of AKT/ERK survival signaling and FoxO3 activation, which results in radiation protection. Additionally, they showed that inhibition of IGF-1R signaling reverses CSC radioresistance[105]. Collectively, these findings showed that CAFs can trigger radioresistance through their CSC-promoting roles.

In addition to CAFs' de novo roles in mediating radioresistance, changes in CAFs due to RT can mediate further treatment resistance. This is important because most anti-cancer treatment regimens, including RT, are given in multiple treatment cycles with gaps to allow for normal cell recovery[84]. These gaps between treatment cycles can be exploited by both the tumor and stromal cells to take advantage of survival mechanisms. Thus, changes in the TME in between treatment cycles are important to consider with regard to the subsequent treatment response and resistance[84]. CAFs are not usually killed by RT; they are highly radioresistant due to the defective p53/p21 response pathway and high expression of the cancer marker Survivin[106]. Irradiated fibroblasts can promote the invasive growth of squamous cell carcinoma through the induction of c-Met, RAS, MAPK cascade (Raf-1, MEK1, ERK-1/2), MMP-1, MMP-9, laminin 5, and filamin A. Irradiated fibroblasts also express high levels of TGFβ1[89]. The effects these irradiated fibroblasts can have on non-irradiated neighboring cells are referred to as radiation-induced bystander effects[107], and there is evidence that many of these factors can promote radioresistance.

There are several examples by which RT-induced changes in CAFs contribute to radioresistance. After genotoxic stress, CAFs can secrete WNT16B to the TME and promote prostate cancer therapy resistance. WNT16B, a secreted protein that is activated in fibroblasts through the nuclear factor (NF)κB pathway after DNA damage, subsequently activates the canonical WNT program and promotes EMT in neoplastic cells through paracrine signaling. This process attenuates the effects of both chemo- and radiotherapies and promotes tumor cell survival and disease progression[108]. Moreover, exposure to low-dose RT (<20 cGy) can induce premature senescence in stromal fibroblasts. In one setting, these senescent CAFs are responsible for stimulating enhanced proliferation of breast carcinoma cells and are correlated with radioresistance, which is partly mediated by the AKT pathway[109]. In addition, senescent CAFs can induce a senescence-associated secretory phenotype that includes the production of IL-6, IL-8, and osteopontin that are considered to be pro-tumorigenic factors and have been associated with immunosuppression and stromal-mediated therapeutic resistance[55,58,110]. RT can also promote EMT transition and invasion of pancreatic cancer cells by activating CAFs. CAF-derived CXCL12 directly promoted tumor cell EMT and invasion by acting through CXCR4 on tumor cells and downstream activation of the P38 pathway. Blocking CXCL12/CXCR4 signaling between pancreatic cancer cells and CAFs could attenuate RT-induced tumor cell invasion[111]. Indeed, HGF secretion by irradiated CAFs can increase phosphorylation of c-Met and MAPK activity in pancreatic tumor cells, which translates into enhanced invasion. This unwanted byproduct of RT can be overcome by blocking HGF signaling with an HGF antagonist[90]. Finally, exposure of CAFs to 18 Gy RT resulted in potent induction of multiple DNA damage response (DDR) foci; induced

premature cellular senescence; and inhibited proliferative, migrative, and invasive capacity of CAFs. This RT dose increased the expression of integrins α2, β1, and α5 and dramatically augmented and redistributed focal contacts[112]. The increase in β1 integrin has been correlated with radioresistance[102]. All of these examples point to RT-induced changes in CAFs that can promote further radioresistance. This should encourage us to find therapeutic regimens that target both the tumor and stroma to successfully deliver anti-cancer treatment.

CAF-secreted factors, contact-mediated signaling, downstream pro-survival signaling pathways, CSC-generating role, and changes due to RT all comprise intricate crosstalk between CAFs and cancer cells to render tumor cells radioresistant. While we understand that CAFs play a critical role in shaping responses to RT, there are several areas where we do not fully understand their impact. First, CAFs in tumors are a diverse heterogeneous population that can have opposing roles[55,56,91]. While an abundance of literature supports the tumor-supporting roles of CAFs, some studies also suggest that certain CAF subsets may have tumor-restraining abilities[14,113]. These diverse CAF subsets may have differential effects on radioresistance and, in turn, be shaped differently by RT. Second, the plasticity, diverse origins, and spatial location of CAFs[13,21,22,92] may complicate things further in terms of their contributions to radioresistance. RT may alter CAF phenotypes temporally and spatially, and this will also affect cancer cells' responses to RT. Lastly, RT dose fractionation may differentially impact CAF diversification. Our understanding of CAF diversity and plasticity is still limited, but it is logical to assume that CAF-mediated radioresistance is a problem in RT success and needs further study.

1.3.4. The Impact of ECM on RT Efficacy

The ECM plays an essential role in regulating cancer progression and radiosensitivity. Tumor ECMs are dynamic structures that are remodeled during tumor progression and/or treatment[60]. Among the approximately 300 proteins present in the ECM that are known to regulate tissue homeostasis, inflammation, and disease, collagen is the most abundant, constituting up to 90% of the tumor ECM. In addition to collagens, other prominent fibrous proteins are elastins, fibronectins, and laminins, which are also involved in controlling tumor phenotype[60]. Tumor ECM is typically denser and mechanically stiffer than normal ECM, due to the quantity of ECM as well as structural changes in molecular architecture such as the extent of crosslinking[114]. These changes in ECM density, composition, and stiffness significantly impact malignant cell invasion, survival, and proliferation[115,116]. Variations in ECM stiffness and density have been correlated with disease aggressiveness, progression-free survival, and in some cases, resistance to different treatment modalities[60].

The ability of tumor-promoting ECM to drive treatment resistance is particularly applicable to RT. Tumor cells can interact with the ECM through direct interaction (cell-protein contact), and one major way is through the engagement with integrins[101]. ECM stiffness can facilitate integrin clustering, which can lead to activation of downstream FAK activation and MAP/ERK kinase signaling pathways leading to cell survival, proliferation, migration, and invasion. Integrin-mediated adhesions can also activate transcription factors NFκB, inositol lipid metabolism, and MMP activity[101], in addition to the activation of PI3K/AKT and RAS/MAPK pathways. Integrin activation is important in regulating tumor phenotypes and has been associated with processes such as angiogenesis, survival, invasion, metastasis, and treatment resistance[54,56]. Further complicating this is

the fact that RT can increase the expression of integrins α2, α5, β1, and β6; therefore, we need to consider how RT fractionation controls subsequent treatment resistance[112,117,118]. For example, it was found that β1 integrin controls radioresistance by resisting cellular apoptosis from RT through the activation of AKT signaling. Inhibition of β1 integrin can resensitize tumor cells to RT by decreasing proliferation and increasing apoptosis (**Figure 1.2**)[119,120]. Another group also found that β1 integrin-mediated adhesion confers RT resistance through downstream FAK-interacting proteins (p130Cas and paxillin) and PI3K/AKT-mediated pro-survival signaling pathways[121]. Together, these examples showed that contact-mediated signaling between tumor cells and ECM proteins in cancers can contribute to radioresistance.

The ECM also contains secreted soluble signaling molecules from tumor and stromal cells. The ECM acts as a reservoir for these cytokines, chemokines, and growth factors. Two prominent examples of these secreted factors that control tumor phenotype are TGFβ and various members of the MMP family. Besides interacting directly with the stromal cells and surface proteins in the ECM, tumor cells are constantly and sophisticatedly communicating with these secreted regulatory molecules[62]. Many of these proteins are already known to be capable of inducing radioresistance, such as TGFβ[94,95,103]. Moreover, RT can further increase TGFβ levels, which can accelerate tumor progression. Inhibition with TGFβ neutralizing antibodies has been shown to prevent radiation-induced metastatic progression[122]. Another class of secreted proteins that are highly abundant in the ECM and mediate tumor progression are the different MMPs[54,60,123]. MMP2 is known to degrade collagen IV and plays a role in RT-induced lung injury. MMP2 inhibition prior to RT abrogated the induction of FoxM1 expression, reduced

p53 and p21 expression, decreased expression of DNA repair genes XRCC1 and Chk2/1, and abrogated G2 cell cycle arrest, leading to apoptosis and enhanced radiosensitivity[124]. These examples showed that the ECM serves as a tumor growth factor and cytokine sink, which contributes to tumor radioresistance and worthy of consideration in future therapeutic planning.

Besides controlling the stability and bioavailability of numerous growth factors and cytokines, ECM structure and integrity also influence oxygen availability, acidity, and interstitial fluid pressure in tumors, through its regulation of the tumor vascular system, so it has important effects in terms of controlling treatment response (**Figure 1.1**)[60,114]. Oxygen availability is critical for RT response as hypoxic cells are generally 2.5−3 times less radiosensitive than normoxic cells[125-128]. The indirect effects of RT produce ROS through the hydrolysis of water, which then propagate and modify lipids, membranes, and proteins[62]. Using nitric oxide-dependent arteriole vasorelaxation as a way to increase the partial pressure of oxygen in tumors, multiple groups found that low-dose nitrite can sensitize tumors to RT, leading to a significant tumor growth delay and longer survival[129,130]. Antiangiogenic therapy such as vascular endothelial growth factor (VEGF) receptor 2 blockade, which can create a “normalization window” that increases tumor oxygenation, has also been shown to enhance the RT response (**Figure 1.2**). This effect is dependent on the increased pericyte coverage of tumor vessels via the upregulation of angiopoietin 1 and degradation of the pathologically thick basement membrane via MMP activation[131]. Thalidomide, an angiogenesis inhibitor, can also increase tumor reoxygenation correlated with reduced interstitial fluid pressure and increased perfusion, sufficient to radiosensitize tumors[132]. Non-steroidal anti-inflammatory drugs (NSAIDs) are

another radiosensitizing drug class that works through increasing tumor oxygenation via either a decrease in macrophage recruitment or inhibiting mitochondrial respiration. Using four different NSAIDs (diclofenac, indomethacin, piroxicam, and NS-398), radiation sensitivity in tumor cells can be increased by enhancing radioinduced apoptosis and inhibiting repair of sublethal RT damage[133]. These studies showed that tumor ECM governs oxygen bioavailability in cancers, controls radiosensitivity, and that RT requires sufficient tumor oxygenation to avoid radioresistance (**Figure 1.1**).

In most cancers, tumor cells are embedded in stromal cells with abundant ECM components, that, as described above, govern radioresistance through direct interaction with tumor cells and the ECM's roles as protein reservoirs and a major controller of tumor oxygen bioavailability. Even though many of these factors negatively impact RT efficacy, there are known inhibitors that can successfully reverse ECM-mediated radioresistance. As with CAFs, our current knowledge is still lacking on how RT dose fractionation may differentially impact ECM alterations and how they contribute to radioresistance.

1.3.5. The Impact of Immune Cells on RT Efficacy

RT is a powerful therapeutic approach used in many patients due to its numerous beneficial effects leading to tumor cell eradication. Besides the direct killing of highly proliferating tumor cells by mitotic catastrophe or apoptosis or necrosis, RT is increasingly appreciated to have immunomodulatory effects, which can take advantage of the fact that our immune cells can target and kill abnormal cancerous cells[63,65,82,84,134]. RT modulates the immunogenicity and adjuvanticity of tumors by increasing the expression and release of tumor-associated antigens, increasing the expression of major histocompatibility complex I (MHC-I), inducing immunogenic cell death (ICD) and its downstream anti-tumor

pathways, and releasing danger signals and chemokines that recruit inflammatory anti-tumor immune cells to the TME, including antigen-presenting cells that can activate cytolytic T cells[123,135,136]. RT can also enhance tumor killing by increasing the number of tumor-infiltrating immunostimulatory cells and neoantigen expression[137-139]. However, there are reports that RT can induce immunosuppression on top of anti-tumor immune promoting effects[64,84]. The balance between the two variables predicts the treatment response. Due to its double-edged sword effects on immune modulation, precise dosing regimens and combinatorial treatments of RT must be carefully considered to avoid unwanted immunosuppressive effects[59,61-63,65,82,84,134,135].

As we have discussed with CAFs and ECM, radiosensitivity depends on the complex interaction of malignant cancer cells with their immune TME[134]. Notably, the host immune status also determines the efficacy of treatments, including RT (**Figure 1.1**). The presence and activation status of dendritic cells (DCs) and $CD8^+$ T cells and anti-tumor cytokines such as IFNγ determine the responsiveness to RT[140-143]. IFN-related DNA damage resistance signature (IRDS) genes including STAT1, IFN-stimulated genes 15 (ISG15), and IFN-induced protein with tetratricopeptide repeats 1 (IFIT1) are associated with resistance to chemotherapy and/or RT across different tumor cell lines[117]. Additionally, the intratumoral immune response after RT also determines the therapeutic response. RT success is dependent on the antigen-specific nature of immune activation, which can be enhanced by combining RT with immune checkpoint blockade therapies like αPD-1 and αCTLA-4[78,135,144,145]. Increases in intratumoral anti-tumor immune cells and IFNγ were found to imbue $CD8^+$ T cells with lytic activity against tumor cells, and the addition of IL-12 as immunotherapy can augment this RT-induced anti-tumor

immunity[142,146]. Radiation can upregulate the expression of programmed death ligand 1 (PD-L1) on tumor cells in numerous in vivo models, which binds with immune checkpoint receptor PD-1 expressed by CTLs and thereby promotes their dysfunction. The combination of radiation and inhibition of this immune checkpoint has been shown to improve the radiation-induced anti-tumor response through activation of cytotoxic T cells and diminished the influx of myeloid-derived suppressive cells (MDSCs) into the TME[147-149]. Interestingly, several studies in mice and humans have demonstrated abscopal effects, with response of both the primary tumor and distant disease to combination therapy of RT and immune checkpoint blockade[150]. Although most of these studies were conducted utilizing hypofractionated or single-dose ablative radiation schemes, the optimal dose, fractionation, and timing to achieve this effect are unknown[151]. In vivo studies have demonstrated that PD-L1 expression peaks at 3 days post-irradiation, and that concurrent but not sequential treatment with checkpoint inhibitors is necessary for a T cell-mediated tumor response[141,149]. Interestingly, in the KEYNOTE-001 trial, patients who received radiation at any time prior to immune checkpoint therapy had significantly increased progression-free survival, with median time ranging from 9.5 to 11.5 months[152,153]. Despite these appealing data, larger studies demonstrating sufficient survival benefits to lead to approval of regimens containing RT in combination with immune checkpoints have not been published. However, these findings showed the importance of the host's immune status as one major contributor that can predict radiosensitivity.

Like CAFs, immune cells in the TME are very diverse and have different roles. Tumor-associated macrophages (TAMs), MDSCs, and $CD4^+$ regulatory T cells (T_{regs}) are known

to be immune suppressive and pro-tumorigenic; on the other hand, immune cells such as DCs, $CD8^+$ T cells, and NK cells are anti-tumorigenic[64]. Likewise, these immune cells also differentially regulate radiosensitivity in cancers (**Figure 1.1**). The presence of TAMs correlates with increased radioresistance in many different tumors[154]. Radiation plays a role in the recruitment and phenotype modulation of TAMs in the TME. Recruitment of TAMs occurs irrespective of dose and fractionation[155]. Conventional fractionation leads to transcription of colony-stimulating factor 1 (CSF1), which when blocked in prostate cancer models reduces TAM recruitment. Conversely, hypofractionated regimens promote TAM recruitment in hypoxic conditions, where in glioma models radiation-induced hypoxia-inducible factor 1 (HIF-1) expression leads to the increased density of TAMs[156,157]. Co-implantation of tumor cells with bone marrow-derived macrophages increased tumor radioresistance, so depletion of TAMs using a systemic or local injection of macrophage-depleting liposomal clodronate before RT can increase anti-tumor effects in different RT dosing regimens. Radioresistance coming from TAMs is mediated by the tumor necrosis factor (TNF) signaling-dependent upregulation of VEGF, and anti-VEGF or anti-TNF therapy can reverse this radioresistance (**Figure 1.2**)[158]. The effect of the radiation-induced influx of TAMs in the TME depends on the exact phenotype they acquire once infiltrated. The decision tree for macrophage polarization, unlike recruitment, does appear to be dependent on the radiation dose and fraction. Anti-tumor phenotypes may be favored in conventionally fractionated dosing, which can in turn enhance T cell-mediated tumor control[159,160]. Importantly, this effect may be lost in hypofractionated and single-dose ablative regimens. One reason may be that hypoxia which results from vascular impairment by RT promotes macrophage immunosuppressive and pro-

tumorigenic tissue remodeling functions[161-163]. However, this is likely an oversimplification, and the true impact of TAMs may depend on the organ- and cancer-specific context in which radiation is employed. RT itself can cause an influx of MDSCs into tumors that eventually polarize the TME into an immune-suppressive environment. This polarization is dependent on transcriptional regulation by the NFκB p50 subunit, as mice lacking NFκB p50 are much more sensitive to RT[164]. Additionally, MDSCs can be recruited further into the TME from RT in a fractionated RT regimen due to the recruitment of DNA damage-induced kinase ABL1 into cell nuclei where it binds the CSF1 gene promoter and enhances its transcription. Hence, blocking macrophage migration with a CSF1 inhibitor radiosensitizes tumors[98]. Another group also found that a neutralizing antibody to CSF1 or a small molecular inhibitor to the CSF1 receptor kinase efficiently depletes macrophages and delays tumor regrowth following RT (**Figure 1.2**). This delay is a reflection of the increased presence of $CD8^+$ T cells and reduced presence of $CD4^+$ T cells, the main source of T helper 2 (Th2) cytokines IL-4 and IL-13. The authors proposed that the response to RT could be enhanced by reducing TAMs in tumors or blocking their induction of Th2 polarization[165]. Moreover, treatment with the small tyrosine kinase inhibitor sunitinib resulted in a significant reduction of MDSCs and phospho-STAT3 and increased T cell proliferative activity in cancer patients. Sunitinib's ability to increase RT efficacy in tumors is mediated through the reduction in the number and function of immunosuppressive MDSCs and is significantly correlated with lower $CD4^+$ T_{reg} and B cell numbers and augmentation of Tbet expression in primary $CD4^+$ and $CD8^+$ T cells[166,167]. Finally, due to the intrinsic radioresistant nature of $CD4^+$ T_{regs} and its immunosuppressive roles, $CD4^+$ T_{reg} presence in tumors has also been correlated with

radioresistance[168,169]. T_{regs} are essential to generating immune tolerance, are radioresistant compared to other T cell subtypes, and demonstrate a relative increase in the TME after irradiation. T_{regs} are known to increase in mice receiving whole-body radiation[170], and studies of human cervical cancers treated with 10-30 Gy demonstrate decreased $CD8^+$ and $CD4^+$ T cells, without any effect on T_{reg} numbers[171]. In vivo tumor models with systemically depleted T_{regs} demonstrate significant determent of primary and metastatic tumor progression. When these tumors are irradiated, these models demonstrate significantly reduced tumor burden post-RT and improved overall survival[172-177]. Dose and fractionation have also been demonstrated to play a role in the balance of immune priming and immunosuppression post-RT. A B16 murine model receiving a single 5 Gy dose of irradiation showed a relative increase in the T_{reg} population compared to cytotoxic T cells. However, a single 10 Gy dose resulted in a relative decrease of T_{regs}, while a single 15 Gy dose increased both T_{reg} and effector T cells[178]. Systemic elimination of $CD4^+$ T_{regs} using anti-CD25 monoclonal antibody enhances radiotherapeutic benefits via immune modulation (**Figure 1.2**)[170]. Collectively, these studies showed that pro-tumorigenic immune cells can modulate radioresistance in many cancers.

While initially thought to create an immunosuppressive TME, radiation has recently gained momentum clinically as a means to prime the immune system to recognize and remove tumor cells. To achieve this end, cross-presentation of tumor antigen by DCs to cytotoxic T cells must be upregulated. Radiation has been shown to increase IFN-I signaling, leading to expansion and activation of DCs, through induction of the stimulator of IFN genes (STING) pathway[78,141,179,180]. Additionally, tumor cell removal requires the induction of cell death pathways, which can be variable, and include apoptosis, necrosis,

autophagy, and mitotic catastrophe. Immunogenic cell death upregulation is frequently observed following irradiation. This involves three key molecular signals: calreticulin, which undergoes translocation from the endoplasmic reticulum to the plasma membrane to signal uptake of dying tumor cells by DCs; high-mobility group protein B1 (HMGB1), which is released from the dying cells to bind Toll-like receptor 4 on DCs promoting antigen cross-presentation; and adenosine triphosphate (ATP), which activates cytotoxic T cells through inflammasome activation via the P2XR7 pathway[134,180-183]. In vitro experiments have demonstrated that the generation of these three key signaling molecules is dependent on irradiation dose[136]. However, the optimal dose and fractionation of irradiation required to induce ICD in vivo is influenced by the TME[123,134,181]. Utilizing a B16 melanoma mouse model expressing ovalbumin antigen, several groups have demonstrated that single-dose, 15-20 Gy irradiation was more effective in generating activated cytotoxic T cells than more conventional fractionated schedules of 15 Gy in 5 daily fractions and 20 Gy in 4 bi-weekly fractions. This indicated that the prescribed dose per fraction and also the specific timing of individual dose delivery are important to elicit RT-induced immune responses[78,179]. Clinical investigations of this mechanism in patients with colorectal and prostate cancer demonstrated a detectable increase in circulating cytotoxic T cells (Survivin- and/or prostate-specific antigen-specific) in post-irradiation blood samples[184,185]. Additionally, early-stage non-small cell lung cancer patients treated with SBRT, 48 Gy in 6-8 fractions, showed increased circulating cytotoxic T cells[186]. Many studies have indicated that ablative radiation doses are required for activation of T cell immunity, and this is corroborated by clinical evidence suggesting that conventional fractionation can have a detrimental effect on the TME as a

result of the death of infiltrating anti-tumor lymphocytes[84,187-189]. In preclinical studies, mice bearing bilateral flank implants of CT26 colon carcinoma treated with conventional fractionation (10 Gy in 5 fractions) initially demonstrated T cell reductions after each dose of radiation; however, this regimen at 7 days post-therapy led to an expansion of local polyclonal T cells responses and infiltrating T cells, revealing a treatment duration effect in this model system[190]. Several groups have moved away from flank models, due to the prevailing theory that to initiate tumor growth you create a wound stimulating a subsequent acute immune response. Instead, several groups have adopted genetically-engineered mouse models (GEMMs) that spontaneously form tumors. Recent publications utilizing GEMMs of pancreatic cancer and sarcoma have demonstrated that reprogramming the TME can induce T cell immunity and sensitize tumors to radiation[24,25,191] from both single high-dose and hypofractionated RT schemes.

Radiation also plays an important role in overcoming T cell exclusion from the TME. One barrier is the dampened homing of effector T cells, which is modulated by cytokines released from tumor cells and the surrounding stroma. Irradiation can significantly enhance the secretion of CXCL16 by mouse and human breast cancer cells; this chemokine binds to CXCR6 on activated cytotoxic T cells and plays an important role in their recruitment to inflammation sites. CXCL16 can be induced in vitro by a single fraction dose of 5 Gy; while in vivo induction was found to be dose-dependent, reaching a plateau at 12 Gy[192,193]. In another study, mice deficient in IFNγ, a cytokine that is critical for innate and adaptive immunity, received tumor-localized irradiation and demonstrated decreased expression of MHC-I and CXCL9/CXCL10, which are important chemoattractants for cytotoxic T cells[193,194]. TNFα can also be induced by single-fraction irradiation in tumor

cell lines[195]. Radiation also leads to upregulation of anti-inflammatory cytokines, like TGFβ, which will suppress the function of DCs and cytotoxic T cells and promote maturation of T_{regs}. Single fraction radiation from 5-10 Gy in mouse mammary tumors upregulated TGFβ in both tumor cells and the surrounding adipose stroma[86,196]. In irradiated tissues, there is a relative increase in ROS, leading to activation of TGFβ. Mouse models of mammary carcinoma demonstrate that activation of DCs and priming of cytotoxic T cells during RT can be improved by administering TGFβ-neutralizing antibodies[147,196].

Tumors counteract this influx of activated cytotoxic T cells through the downregulation of antigen-presenting MHC-I proteins. Historical studies revealed that radiation increases MHC-I protein expression on tumor cells, leading to restored antigen recognition by cytotoxic T cells. In primary glioblastoma lines, increasing doses of radiation up to 12 Gy led to increased MHC-I expression, and a similar effect was demonstrated in ovarian and cervical cancer cell lines with doses of 25 to 100 Gy[197-200]. Conventionally fractionated radiation also can induce MHC-I expression, where conditioned media from breast cancer lines treated with 6-10 Gy delivered in 3-5 fractions was able to stimulate expression of total cellular and surface MHC-I in recipient cells[201].

The interactions between tumor cells and their immune microenvironment is very complex due to their abundance, diversity, and varying roles. Evidence showing the presence of anti-tumor immune cells and IRDS genes being important to determine RT efficacy and the roles of pro-tumor immune cells to promote radioresistance should inspire us to design therapeutic regimens with different immune-modulating drugs to synergize with RT. However, it is still unclear how different RT fractions affect immune

TME. Additionally, it was recently discovered that distinct immune cell origins (bone marrow or embryonic) have different roles in controlling tumor phenotype[202]. How the immune cell origin contributes to immune-mediated radioresistance is still a largely unaddressed question in the field and needs to be studied[26,203].

1.3.6. Immunomodulatory Roles of CAFs and the ECM and How Their Interactions Regulate RT Efficacy

With recent discoveries, it is increasingly appreciated that malignant tumor cells interact with their TME in a complex and reciprocal manner to regulate tumor progression and treatment response[53-57]. In addition to the ability of the individual stromal components to directly control tumor cell phenotype, interactions among the components of the TME themselves can also exert the same effects[58,114]. Immune cells in the TME are regulated by their microenvironment, including the CAFs and ECM in addition to the tumor cells. These communal interactions in the TME are important to consider because they can inadvertently affect treatment response[63,84,134].

CAFs have various pro-tumorigenic roles by regulating tumor immunity, ECM, and hypoxia, among many other factors[114]. One group reported that fibroblast activation protein $(FAP)^+$ CAFs, one subtype of CAFs, are responsible for suppressing anti-tumor immunity and thus contribute to uncontrollable tumor growth. Depleting FAP-expressing cells provides some tumor growth control through a process involving IFNγ and TNFα[204]. In a cervical cancer model, mesenchymal stromal cells were responsible for immunosuppression through their ability to dampen $CD8^+$ T cell proliferation, activation, and effector functions. This was found to be mediated by the expression of CD39 and CD73 ectonucleotidases and the generation of adenosine by the stromal cells[205]. Lastly,

CAFs can support tumorigenesis and mediate tumor-enhancing inflammation by enhancing tumor angiogenesis, proliferation, and invasion. These tumor-promoting characteristics are mediated by NFκB pathways[206]. These tumor-promoting roles of CAFs, through their modulation of tumor immunity, may apply to the mechanisms of stromal-mediated radioresistance.

CAFs can control tumor immunity through multiple mechanisms[114,207]. CAFs regulate both adaptive and innate immune cell functions, including T cell and immunosuppressive myeloid cells. CAFs can negatively impair the function of $CD8^+$ T cells including cytolytic activity and cytokine production through the production of soluble factors, such as TGFβ and VEGF, metabolic reprogramming via indoleamine 2,3-dioxygenase and arginase, and expression of checkpoint inhibitors like PD-L1[114,208]. Many of these factors were discussed previously in the other sections as they are implicated in radioresistance[94,95,103,158]. CAFs can also affect myeloid cell and DC maturation status and function[209-212]. These immune cells are essential mediators of radiosensitivity[140-143,154]. More importantly, many recent discoveries have shown how targeting the stroma can reawaken anti-tumor immunity and synergize with immunotherapy[213-215], as reviewed elsewhere[114]. The concept of how stromal interactions with the immune microenvironment affect immunotherapy response may also hold true for RT responses.

One way by which CAFs regulate the immune TME is through their secreted factors. CAFs secrete many active factors to the TME which are eventually stored in the ECM reservoir, including the various MMPs[54,60,62,123]. MMP14 mediates tumor progression through vascular and immune-modulatory effects. The anti-MMP14 inhibitory antibody can inhibit tumor growth, reduce tissue hypoxia, increase macrophage number, and shift

cell phenotype towards the more anti-tumor M1-like phenotype due to reduced active TGFβ and SMAD2/3 signaling, hence synergistically enhancing RT effects (**Figure 1.2**)[216]. This example demonstrates that CAF interactions with the ECM and the immune microenvironment can regulate tumor cell radiosensitivity.

CAFs and the ECM have many immunomodulatory functions, which can control tumor cells' treatment response, including RT efficacy. Even on their own, CAFs, ECM, and immune cells can directly confer a radioresistance phenotype to tumor cells, and their interactions among themselves also affect how tumor cells respond to RT. It is presently unclear how these relationships among the tumor stroma components are affected by host immune status and vice versa. Similarly, it is not known how different RT doses and fractionations change these complex interactions and their ensuing tumor-regulating phenotype. It will be fascinating to see how new technologies such as single-cell RNA sequencing will help us discover novel stromal and immune cells and shape our understanding of the immunomodulatory functions of stromal cells in cancers.

1.3.7. The Impact of Other Stromal Cells on RT Efficacy

The TME contains other stromal cells present besides CAFs: blood endothelial cells, lymphatic endothelial cells, adipocytes, mesenchymal stem cells, fibrocytes, pericytes, neurons, etc. Although their contribution is small in terms of their numbers in the TME, they still play important roles in tumor progression, treatment response, treatment resistance, and cancer metastasis[53,59].

Endothelial cells are important players in many different types of cancer. They supply nutrients for tumor growth, provide routes for metastatic dissemination, and contribute to chemo- and radioresistance[128,217,218]. Hence, it is important to understand the tumor

vasculature to comprehend endothelial cell-mediated radioresistance. Tumors have two main ways to develop vasculature: angiogenesis and vasculogenesis. Angiogenesis is the process in which vessels are developed from nearby endothelial cells, while vasculogenesis is the formation of blood vessels from circulating cells postulated to come from the bone marrow[128]. It is clear that angiogenesis is an important process fundamental to treatment refractoriness, but vasculogenesis is especially imperative in RT resistance due to the fact that local RT abrogates local angiogenesis, forcing tumors to rely heavily on the vasculogenesis pathway for blood vessel regrowth post-RT. This mechanism poses another barrier to T cell infiltration. Dysfunctional tumor-associated vasculature has endothelial cells lining the vessels that suppress T cell activity, target them for destruction, and block entry into the TME[219]. Studies of ablative doses of radiation as high as 25 Gy led to the infiltration of TAMs expressing immunosuppressive enzymes[220]. Notably, single-fraction ablative doses also induce significant endothelial cell death, causing reduced vascular flow, hampering T cell recruitment, and inducing a hypoxic and immunosuppressive TME[221,222]. These ablative doses have been evaluated by bioinformatic studies, demonstrating that alteration of tumor vasculature post-irradiation accounts for 20−30% of the radiographic response of brain metastases in stereotactic radiosurgery cases[223]. In contrast, radiation doses <10 Gy have been shown to promote vascular relaxation and increase tumor oxygenation, with fractionated schedules providing the maximal benefit on tumor growth delay due to tumor reoxygenation[224,225]. Low-dose radiation also plays a role in the reprogramming of macrophages, which are important during the angiogenesis process, allowing increased T cell extravasation in vivo through inducible nitric oxide synthetase[160]. There is an influx

of $CD11b^+$ myeloid cells following tumor irradiation, and increased tumor hypoxia increases HIF-1 levels and subsequently upregulates stromal cell-derived factor 1 (SDF1, also known as CXCL12) to initiate vasculogenesis[128]. Many angiogenic inhibitors have been used in the clinic and have proven efficacy as radiosensitizing agents because of multiple different mechanisms related to the "normalization" of tumor vessels and their subsequent oxygen content and acidity (**Figure 1.2**)[54,58,84]. One group claims that the use of the VEGF receptor inhibitor axitinib radiosensitized tumor endothelium and enabled tumor control[226]. Another group found that angiogenesis-promoting factors that protect against endothelial damage can diminish the RT response. Reversing this effect with a VEGF inhibitor promotes RT-induced endothelial injury through the generation of the second messenger ceramide through acid sphingomyelinase trafficking to the plasma membrane. This tumor endothelial cell RT resensitization was shown to mediate tumor control[226]. These studies demonstrated that endothelial cells are important mediators of tumor radioresistance due to their ability to form vessels and control tumor oxygen content.

Adipocytes are also active players in the TME that control cancer development, progression, metastasis, and treatment response, especially in cancers that interact closely with adipose tissue-like breast cancers[227]. Cancer-associated adipocytes (CAAs) are energetic cells capable of secreting a heterogeneous group of molecules known as adipokines that include hormones, growth factors, and cytokines. Some examples of adipokines are leptin, adiponectin, autotaxin, IL-6, TNFα, IGF-1, and HGF. In addition, CAAs actively participate in metabolic remodeling that supports cancer cell growth by regulating the fatty acid reservoir to increase mitochondrial β-oxidation. They also interact

closely with CAFs and ECM molecules through ECM remodeling. More importantly, they act as obstacles to various anti-cancer therapies as they are involved in diverse resistance mechanisms[53,59].

One mechanism of adipocyte-mediated radioresistance is through their secreted adipokines. Some of these adipokines such as TNFα, IGF-1, and HGF were discussed earlier with regard to their contributions to stromal-mediated radioresistance (**Figure 1.1**)[90,104,158,204]. Another group reported that these adipokines can increase the gene expression of NFκB and cyclin D to induce anti-apoptotic transcription and stabilize pro-oncogenic factors such as β-catenin and cyclin-dependent kinases[227]. It was also found that breast cancer cells co-cultured with adipocytes are radioresistant, and the mechanism is through adipocyte secretion of IL-6 resulting in the phosphorylation of Chk1 associated with decreased cancer cell death[227,228]. Another mechanism of adipocyte-mediated radioresistance is the initiation of autotaxin (ATX)–lysophosphatidic acid (LPA) signaling. This group found that CAAs, which closely interact with adjacent tumor cells, can become inflamed from tumor-derived cytokines, which results in the stimulation of adipocytes' ATX secretion and subsequent LPA production. This further promotes inflammatory cytokine production in a vicious feed-forward cycle. RT-induced adipocyte injury triggers increased levels of ATX, cyclooxygenase-2 (COX-2), IL-1β, IL-6, IL-10, TNFα, and LPA1 and LPA2 receptors. This inflammatory response depends on the DNA damage response pathways ATM, ATR, and PARP-1 and inflammatory mediators COX-2 and NFκB, which can potentially be inhibited to reverse radioresistance. Induction of LPA signaling enhances lymphocyte invasion and cytokine and VEGF production to stimulate angiogenesis required for tumor growth[229]. As detailed earlier, angiogenesis is

one factor that contributes to tumor cell radioresistance[60]. These studies showed that adipocytes are not dormant “fat” cells; they are active contributors to tumor phenotype through their active metabolism and secreted factors.

Even though endothelial cells and adipocytes do not make up a significant portion of the tumor stroma, they contribute to tumor radioresistance. Multiple groups have shown that we should not negate their roles in controlling RT response to prevent the formation of radioresistant cancer cells. However, the complexity of different RT doses and fractionation regimens has left the field with an unanswered question regarding their effect on stromal cells present in cancers.

1.3.8. Focused Conclusions

Malignant tumor cells that harbor genetic aberrations are in close proximity with the tumor stroma composed of diverse cellular and non-cellular entities including CAFs, ECM components, immune cells, endothelial cells, adipocytes, and secreted bioactive molecules. At every step of the tumor lifecycle, there is reciprocal communication between these malignant cancer cells and their neighbors. Their highly dynamic interactions control tumor initiation, progression, invasion, metastasis, and treatment resistance, which complicates cancer therapeutic planning[53-58,60,62-65,230]. Here, we reviewed how the tumor stroma can contribute to cancer radioresistance; many of which are mediated through secreted factors, cell surface receptors, and downstream pro-survival and/or anti-apoptotic signaling pathways. The tumor stroma is very diverse, and our current knowledge of distinct cell types is still lacking. It will be interesting to see how new technologies to discover novel CAFs and immune cell types will broaden our knowledge of tumor-stromal interactions.

Further complicating the concept of stromal-mediated radioresistance is the fact that with successive treatments tumor and stromal cells can become more resistant, which could be a problem for many anti-cancer treatment regimens given in cycles, such as chemo- and radiotherapies. Based on the potential of these tumor stroma to induce radioresistance, it seems plausible to include stromal-targeted agents in combination with RT for therapeutic benefit. Multi-directed treatments toward both the tumor cells and the tumor stroma could help eradicate cancers and prevent therapeutic resistance and tumor relapse.

Lastly, RT is a rapidly evolving field. Ultra-high dose rate of RT (FLASH-RT) is a new technology that enables the ultra-fast delivery of doses while sparing normal tissues[231,232]. It will be important to see how FLASH-RT influences tumor-stroma communications and stromal-mediated radioresistance. Despite many recent discoveries, there are still many remaining questions in the field to be addressed, such as how CAF diversity affects radioresistance and how the tumor stroma changes with different RT dosing and fractionation regimens. Future discoveries about these mechanisms can be used for the design of novel RT and drug combinations to target stromal-mediated RT resistance.

1.4. Focal Adhesion Kinase (FAK) in Cancer

Focal Adhesion Kinase (FAK – also known as protein tyrosine kinase 2, PTK2) is a nonreceptor tyrosine kinase that is part of a crucial signaling element to control cell adhesion, spreading, and migration[233]. FAK is activated by a variety of things, including integrins, cytokine receptors, GPCRs, receptor tyrosine kinases, and intracellular pH changes, and FAK helps transmit extracellular signals into intracellular signaling

pathways[233]. FAK expression and activation are elevated in many malignancies[214,233-235], including in PDAC as our lab has previously shown[214]. Increased cell-ECM tension and increased matrix stiffness associated with collagen fiber crosslinking trigger increases in FAK phosphorylation and tumor progression[214,236]. This is particularly very important in PDAC due to its dense fibrotic stroma and increased cell-ECM tension and matrix stiffness[3,8,214].

In the tumor cells, FAK activity can promote invasive cell type, promote survival and growth, enhance cell cycle progression, inhibit apoptosis, and more importantly, promote treatment resistance[235]. Notably, FAK can also regulate pro-inflammatory pathway activation and cytokine production through both its kinase-dependent and kinase-independent mechanisms[233,237]. FAK also has many roles in the stroma. For example, in PDAC, high FAK activation level has been associated with low number of cytotoxic T cells and high number of immunosuppressive myeloid cells[214]. In the endothelial cells, FAK activity can promote vascular permeability, angiogenesis, and tumor intravasation and extravasation leading to metastasis[238,239]. FAK activity in cancer can stimulate macrophage and fibroblast recruitment[240-242]. Moreover, FAK can also promote the tumor-promoting factors of CAFs[243-245]: Barker et al. found that tumor-secreted LOXL2 activate stromal fibroblasts to enhance cancer progression through integrin-mediated FAK activation[243] and Greenberg et al. found that FAK activation could contribute to myofibroblast differentiation, thereby subsequent fibrosis, through FGF/h signaling pathway[244]. Overall, in the stromal cells, FAK activity has been shown to be able to promote spreading, adhesion, survival, and enhanced production of ECM synthesis or remodeling to promote tumor spreading and/or progression[235]. Furthermore, FAK activity

has been correlated with increased malignancy and poor survival in cancer patients[214,215,235]. Together, these data demonstrate that FAK hyperactivation is highly unfavorable and needs to be targeted.

Due to FAK's tumor-promoting properties, many FAK inhibitors have been developed. However, because there is a closely related FAK ortholog, which can compensate for some FAK functions after FAK loss, called Proline-rich tyrosine kinase 2 (Pyk2 – also known as protein tyrosine kinase 2b, PTK2b), many FAK-targeted therapies are developed to target both FAK and Pyk2[235,246]. One important rationale for using a FAK inhibitor is that it not only affects tumor cells directly, but also impacts the surrounding tumor-promoting stroma. In line with prior research detailing FAK's tumor-promoting capabilities, inhibition of FAK has been shown to be highly effective at preventing tumor growth, metastasis, and angiogenesis in multiple mouse models and cancer types[214,235,247]. Early Phase I in-human clinical trials of dual FAK/Pyk2 inhibitors (NCT00666926, NCT00996671, NCT00787033, and NCT01951690) found the compounds to be tolerated with low adverse events. They even showed that some patients demonstrated stable disease while being treated, which was promising[248]. However, FAK inhibitor alone in patients did not cause tumor regression and thus needs to be combined with other agents.

Multiple research groups have shown the efficacy of inhibiting FAK signaling when combined with other therapeutic agents to reverse the failure of treatments and to enhance their efficacy[214,215,249-254]. FAK inhibitor has been successfully combined with both chemotherapies and immunotherapies in pre-clinical mouse models[214,255-257]. Data from our own group and others prompted the initiation of clinical trials testing these

combinations (NCT01778803 NCT03287271, NCT02546531, NCT02758587, NCT03727880, and NCT04201145).

More importantly, FAK signaling has been implicated in radiotherapy resistance[251-253], and thus it is promising to combine FAKi with radiotherapy. These data, including preliminary data from my thesis work, have successfully shown the benefits of using FAKi as a radiosensitizer and thus we initiated the first in-human clinical trial of combining radiotherapy and FAK inhibitor in PDAC patients (NCT04331041). It is still too early to conclude the results of these clinical trials combining FAK inhibitor with other therapeutic agents; however, preliminary human data so far has indicated promising results. This is something to look forward to with enthusiasm.

Given the powerful actions of FAK inhibitor in PDAC, my thesis dissertation work is aimed at understanding how the fibrotic stroma of PDAC impacts the effectiveness of RT and how to utilize this stromal reprogramming agent to increase RT efficacy.

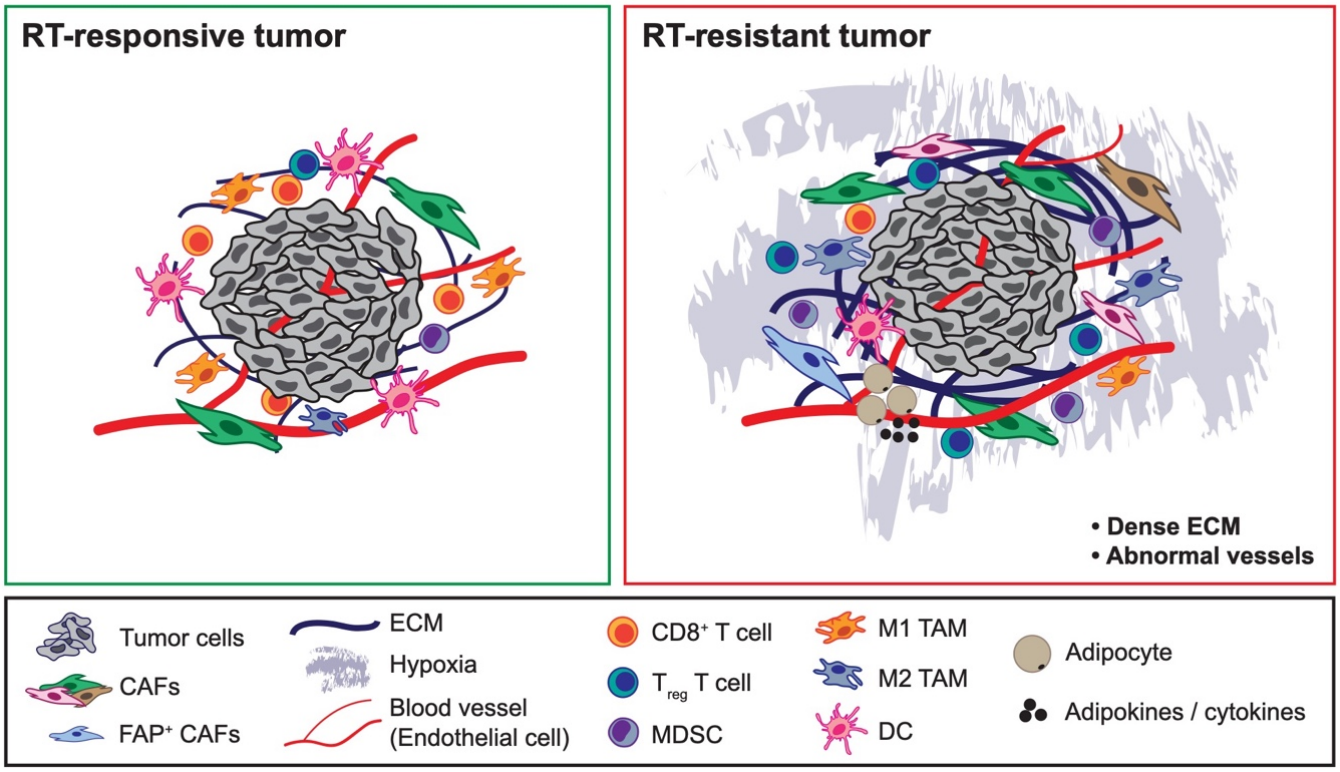

Figure 1.1: Components of the tumor microenvironment governing radiotherapy responsiveness. Components of the tumor stroma differentially dictate whether tumor cells are radiotherapy (RT)-responsive (Left) vs. RT-resistant (Right). Some tumor-promoting cancer-associated fibroblast (CAF) populations can cause tumors to be resistant to RT, such as fibroblast activated protein $(FAP)^+$ CAFs. While immune cells such as $CD8^+$ T cells, dendritic cells, and M1-like tumor-associated macrophages (TAMs) have been linked with RT-responsive tumors, pro-tumorigenic immune cells such as $CD4^+$ T regulatory (T_{reg}) cells, myeloid-derived suppressor cells, and M2-like TAMs have been associated with RT-resistant tumors. Dense extracellular matrix and abnormal endothelial cells and vessel formation, which contribute to tumor hypoxia, have been associated with RT-resistant tumors. Likewise, adipokines secreted by cancer-associated adipocytes can similarly cause tumors to be resistant to RT.

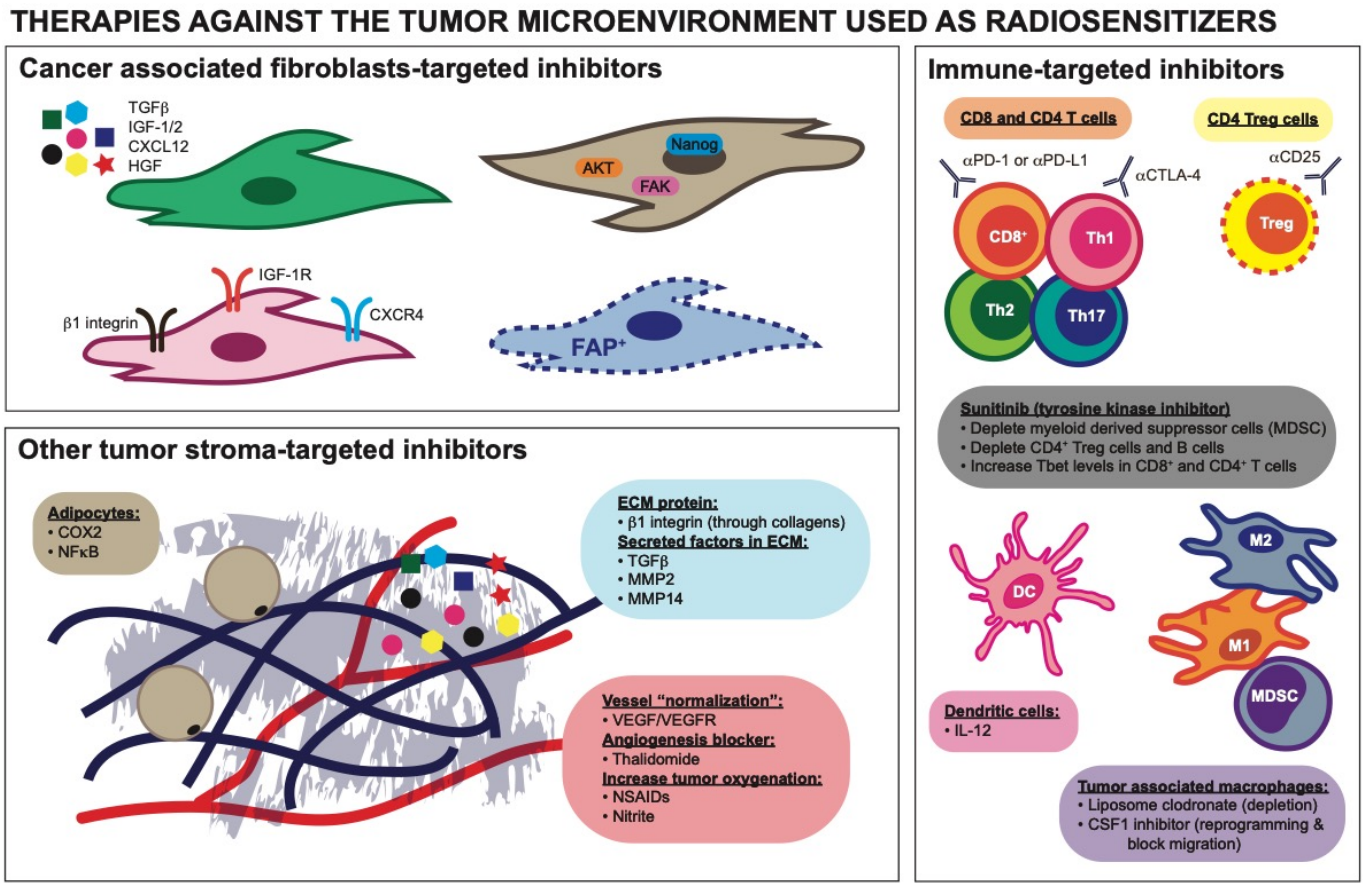

Figure 1.2: Therapies directed against distinct tumor stromal components used as radiosensitizers. Targeted inhibitors against CAFs' secretory molecules, CAFs' downstream cytosolic and nuclear signaling pathways, and CAFs' receptors can increase RT efficacy. Targeting a unique population of CAFs, FAP^+ CAFs, specifically for depletion can also radiosensitize tumors. Components of the ECM can activate β1 integrin receptor on CAFs and targeting β1 integrin can reverse tumor radioresistance. Targeted inhibitors against secreted factors reserved in the ECM have been shown to be radiosensitizing agents. "Normalizing" tumor vessels using VEGF/VEGFR inhibitors and Thalidomide can reverse tumor radioresistance. NSAIDs and nitrite have also been used as radiosensitizers due to their ability to increase tumor oxygenation. Inhibitors of COX-2

and NFκB targeted against cancer-associated adipocytes can reverse the radioresistance in tumors. Immune checkpoint inhibitors (αPD-1 or αPD-L1 and αCTLA-4 antibodies) can rescue “dysfunctional” $CD8^+$ and/or $CD4^+$ T cells and are beneficial when combined with RT. Depletion antibody αCD25 targeted against $CD4^+$ T regulatory cells (T_{regs}) can render tumor cells more radiosensitive. Interleukin-12 capable of enhancing the function of dendritic cells can increase the efficacy of RT. TAMs depletion agent, liposome clodronate, and CSF1 inhibitor can increase RT sensitivity. CSF1 inhibitor can also reprogram/polarize TAMs into having a more anti-tumorigenic phenotype. The tyrosine kinase inhibitor, sunitinib, has been used as a radiosensitizer due to its immunomodulatory ability.

Cancer type	# of deaths/year (2020)	5-year survival		
		All	Local	Distant
Lung	136,084	22%	60%	6%
Colon	51,869	65%	91%	15%
Pancreas	46,774	11%	42%	3%
Breast	42,275	90%	99%	29%
Prostate	32,707	98%	>99%	31%

Table 1.1: Cancer occurrence and 5-year survival rate. Data from: SEER.Cancer.Gov Report (2011-2017); American Cancer Society (2022); CDC.gov (as of March 16, 2022).

Chapter 2: Stromal reprogramming by FAK inhibition overcomes radiation resistance to allow for immune priming and response to checkpoint blockade

Varintra E. Lander, Jad I. Belle, Natalie L. Kingston, John M. Herndon, Graham D. Hogg, Xiuting Liu, Liang-I Kang, Brett L. Knolhoff, Savannah Bogner, John M. Baer, Chong Zuo, Cedric Mpoy, Jalen Scott, Michael Zahner, Buck E. Rogers, Julie K. Schwarz, Hyun Kim, and David G. DeNardo

Cancer Discovery, in revision (2022)

2.1. Focused Introduction

Pancreatic ductal adenocarcinoma (PDAC) is a highly lethal malignancy with a poor 5-year survival rate[258]. To date, the only potentially curative treatment is complete surgical resection, but 85-90% of patients are diagnosed at unresectable stages[259]. While many recent advances in diagnosis, chemotherapy, and even radiation therapies (RT) have made a positive impact on patient survival, these treatments have not been proven to be curative[260,261]. The majority of locally advanced PDAC patients still cannot attain sufficient tumor regression to achieve resectability and metastatic PDAC is incurable[259,262-266]. Additionally, there are no approved immunotherapies for the treatment of PDAC.

Oncogenic mutations in Kras, with help from frequent loss in tumor suppressors like p53 or INK4a, can drive PDAC initiation, progression, treatment resistance, and metastatic spread[267]. Kras accomplishes this through tumor-intrinsic changes in cellular signaling and metabolism, as well as promoting tumor-permissive interactions with surrounding stroma[267]. Additionally, the nature of the fibrotic desmoplastic stroma, composed of dense collagen-rich extracellular matrix and cancer associated fibroblasts (CAFs), likely also contributes to PDAC's resistance to therapy[8-11,13,18,52,53,259]. While checkpoint immunotherapies have been groundbreaking in many solid malignancies[268-270], these same regimens have not been effective in PDAC[259,271,272]. Furthermore, combination treatments of immunotherapies with standard of care chemotherapy or RT, which are aimed to prime anti-tumor immunity and unlock immunotherapies, have not been tremendously efficacious in gastrointestinal tumors[273-275]. Thus, understanding why RT fails to prime anti-tumor immunity in PDAC may be important.

The recalcitrant nature of PDAC has been linked in part to its unique tumor microenvironment (TME). In this TME, the complex communication between the malignant tumor cells and the non-malignant tumor stroma can play a significant role in dictating PDAC's resistance to therapy[18,52,53,259]. Further complicating things, PDAC has a very heterogeneous CAF population, which plays diverse roles and can dictate divergent treatment outcomes[21,22,276,277]. Additionally, PDAC's fibrotic stroma contributes to poor drug delivery and deprived infiltration of anti-tumor immune cells. These two aspects of PDAC's TME have been hypothesized as drivers of PDAC resistance to both chemo- and immuno-therapies[48-51]. However, it is not clear how the PDAC-associated fibrosis might impact efficacy to RT and if this affects RT-induced immune priming.

Historically, studies have focused on RT as a direct mechanism to damage proliferating tumor cells leading to the accumulation of double-strand DNA breaks and cellular death[278]. However, recent studies have shown that numerous factors, including matrix stiffness, can dampen sensitivity to DNA damaging agents and its subsequent DNA repair mechanisms[279,280]. In addition to RT's direct effect on tumor cells, RT can also prime anti-tumor immunity by releasing tumor-derived antigens and danger signals, and this likely plays a critical role in long term RT efficacy in multiple cancer types[281]. Nevertheless, it is unclear if these immune priming functions of RT are intact in highly fibrotic cancers such as PDAC.

Focal adhesion kinases include Focal Adhesion Kinase 1 (FAK, also known as FAK1 or PTK2) and the closely related Protein Tyrosine Kinase 2 beta (PTK2b, also known as FAK2). Both are non-receptor tyrosine kinases that have been heavily studied and attributed to contribute to cancer cell migration, proliferation, and survival, but notably can

also regulate pro-inflammatory pathway activation and cytokine production[215,235,257]. As such, FAK signaling has been shown to be important in wound healing and pathologic fibrosis in many different tissues[241,282]. FAK signaling is hyperactivated in many cancers, including PDAC, and has been correlated with poor survival[114,233,283]. Our group and others have shown that FAK signaling is an integral driver of the fibrotic and immunosuppressive microenvironment that protects PDAC from immune surveillance and drives resistance to immunotherapy[114,284]. In this study, we address the role of stromal-induced RT resistance in immune priming, and we show FAK inhibition can sensitize PDAC to RT and restore RT-induced immune priming and response to immunotherapy.

2.2. Abstract and Significance

ABSTRACT

The effect of radiation therapy (RT) on tumor immunity in PDAC is not well understood. To better understand if RT can prime antigen-specific T cell responses, we analyzed human PDAC tissues and PDAC GEMMs. In both settings, we found little to support evidence of RT-induced T cell priming. Using *in-vitro* systems, we found tumor stromal components, including fibroblasts and collagen, synergize to both blunt RT efficacy and impair RT-induced interferon signaling. Focal Adhesion Kinase (FAK) inhibition rescued RT efficacy *in-vitro* and *in-vivo*, leading to tumor regression, T cell priming, and enhanced long-term survival in PDAC mouse models. Based on these data, we initiated a clinical trial of VS-6063 in combination with SBRT in PDAC patients (NCT04331041). Analysis of PDAC tissues from these patients showed stromal reprogramming mirroring our findings in GEMMs. Finally, the addition of checkpoint immunotherapy to RT and FAKi in animal models led to complete tumor regression and long-term survival.

SIGNIFICANCE

Checkpoint immunotherapeutics have not been effective in PDAC, even when combined with radiation therapy. One possible explanation is that radiation therapy fails to prime T cell responses in PDAC. Here, we show data that FAK inhibition allows radiation therapy to prime tumor immunity and unlock responsiveness to checkpoint immunotherapy.

2.3. Results

Radiation therapy (RT) is insufficient to prime robust T cell responses in PDAC

To study the effect of RT on T cell infiltration, we first performed immunohistochemistry (IHC) on human surgical resection samples from patients who received neoadjuvant RT or no neoadjuvant therapy. We found no difference in the number of tumor-infiltrating $CD8^+$ T cells (**Fig. 2.1A**). In contrast to T cells, we observed increased stromal area and collagen deposition in patients who received prior neoadjuvant RT (**Fig. 2.1B**). These data raise the possibility that while RT can lead to temporary disease control in PDAC patients[285,286], it may fail to prime tumor T cell immunity, thus limiting the long-term benefit. However, due to the heterogeneity of human PDAC tumors and patients, these human studies in un-matched patient populations cannot fully answer this question.

To better understand whether RT can directly affect anti-tumor immunity in PDAC, we utilized the p48-Cre/LSL-$Kras^{G12D}$/$p53^{Flox/Flox}$ (KPC) genetically engineered mouse model (GEMM). The KPC mice mimic the treatment-resistant nature of human disease and have abundant tumor stroma[287]. Previously, studies on the impact of RT on PDAC TME in pre-clinical models have been difficult to perform due to the lack of precision to deliver RT doses into the pancreata of mice. To overcome this, we employed a Small Animal Radiation Research Platform (SARRP)[288], which incorporates CT guidance for image-guided delivery of high doses of radiation (**Fig. 2.2A**). With this instrument, we can safely deliver relevant doses of radiation to the mouse pancreas while limiting the dose to surrounding normal tissues. KPC GEMMs with ultrasound-diagnosed tumors were treated with hypofractionated RT (6Gy x 5) and monitored for tumor progression (**Fig. 2.1C**). We found RT could only modestly control tumor growth as measured by

longitudinal ultrasound imaging or tumor weights at days 7 and 14 after RT start (**Fig. 2.1D-E, 2.2B-D**). After modest disease control, all KPC mice treated with RT eventually rapidly progressed, which was translated into no benefit in overall mouse long-term survival (**Fig. 2.1F**). These data agree with other studies showing, unlike transplantable tumors, this highly fibrotic KPC GEMMs exhibit limited RT response[163,289]. To understand if induction of DNA damage was impaired, we analyzed γH2Ax$^+$ foci formation. As expected, at 6- and 24-hours post completion of hypofractionated RT, significant γH2Ax$^+$ foci were observed in most PDAC cells and stroma, but 48 hours post the last RT dose, most γH2Ax$^+$ foci resolved, suggesting DNA repair was intact in this model (**Fig. 2.1G**). Analysis of Cleaved Caspase 3$^+$ (CC3$^+$) cells found no induction of apoptosis at 7 or 14 days after RT start. Surprisingly, we also observed no change in the number of Ki67$^+$ proliferating cells on day 7, but by day 14, tumor proliferation in RT treated tumors was elevated compared to controls (**Fig. 2.1H, 2.2E**). Together these data show RT has limited efficacy in killing PDAC cells in stroma-rich KPC GEMMs.

Next, we sought to determine if RT could prime T cell immunity in KPC GEMMs. We found that RT did not lead to increased PDAC infiltrating CD8$^+$ or CD4$^+$ T cell numbers (**Fig. 2.1I, 2.2F**). We also did not observe any increase in the number of Ki67$^+$ CD8$^+$ T cells, but found CD44$^+$ CD62L$^-$ activated T cell fraction was slightly decreased. These data were consistent across 7 and 14 days post RT timepoints (**Fig. 2.1I, 2.2F**). While there were no major changes in myeloid cell populations, we noted a trend toward increased monocytes, TAMs, granulocytes, and eosinophils at both days 7 and 14 post RT start (**Fig. 2.2G**). To eliminate the possibility that RT did not prime new T cell responses because of the low neoantigen burden characteristic of KPC GEMMs, we

studied RT's ability to induce tumor specific T cell responses in p48-Cre/LSL-Kras^{G12D}/p53$^{Flox/Flox}$/LSL-OVA-GFP^{+} (KPC-OG) PDAC GEMMs[24]. KPC-OG mice harbor inducible neoantigen, ovalbumin (OVA) and green fluorescent protein (GFP) expression, which allows for the tracking of tumor-antigen specific T cells. Despite neoantigen expression in KPC-OG mice, we found that RT (6Gy x 5) did not lead to an increase in either total or OVA-specific (Dextramer^{+}) CD8^{+} T cells in PDAC tissues 14 days after treatment start. In keeping with the lack of immune priming effects of RT in this model, we also observed no increase in OVA-specific Dextramer^{+} T cells in pancreas draining lymph nodes (**Fig. 2.1J**).

To contrast with these KPC-OG GEMMs, we used littermate mice to evaluate RT-induced T cell immunity in sarcoma tumors. These LSL-Kras^{G12D}/p53$^{Flox/Flox}$/LSL-OVA-GFP^{+} mice (called KPS-OG here-in) were injected with Adenovirus-Cre into the hindleg muscle to generate sarcoma tumors[290]. In contrast to KPC-OG littermates, KPS-OG mice treated with RT (6Gy x 5) had a sustained reduction of tumor progression, decreased Ki67^{+} proliferating tumor cells, and increased tumor-infiltrating CD8^{+} T cells as well as increased OVA-specific T cells in both the tumor tissues and draining lymph nodes (**Fig. 2.1K, 2.2H-I**). Taken together, these data suggest that in genetically equivalent mice, RT increases antigen-specific T cells in sarcoma GEMMs but fails to prime tumor immunity in pancreas GEMMs. While both models were driven by Kras mutation and p53 loss, one key difference we noted was that the KPC-OG PDAC tissues had higher stromal desmoplasia compared to their KPS-OG sarcoma counterparts (**Fig. 2.1J-K, 2.2J**). These data suggest that the effects of RT on tumor control and T cell priming may be related to stromal differences.

Stromal elements repress RT efficacy and induction of interferons

PDAC tumors are often characterized by dramatic desmoplastic stroma comprised of dense extracellular collagen deposition and diverse CAF populations[291,292]. To test the role of PDAC stroma in RT-induced cell death, we used heterotypic organoid cell culture models. These models allow for the co-culture of PDAC organoids with fibroblasts and ECM components. PDAC organoids (KPOG) were derived from KPC-OG mice and growth was tracked by GFP fluorescence (**Fig. 2.3A**). We found that while PDAC organoids alone were sensitive to RT, the addition of pancreas-derived fibroblasts rendered tumor cells less sensitive to RT and the heterotypic organoid co-cultures rapidly grew after RT exposure (**Fig. 2.3A**). Similarly, increasing collagen-I density in this culture system also conferred resistance to RT (**Fig. 2.4A**). The presence of both pancreatic fibroblasts and collagen-I synergistically protected PDAC organoids from RT-induced growth inhibition (**Fig. 2.3B, 2.4B**). To further understand how the PDAC stroma affects RT efficacy, we looked at markers of proliferation, apoptosis, and DNA damage using IHC. First, we found the induction of γH2Ax measured 6-hours post RT was identical in the presence or absence of fibroblasts, suggesting that DNA-damage induction by RT was not impacted, at least in the short term (**Fig. 2.3C**). Similarly, pancreatic fibroblasts did not impact the induction of apoptosis, measured by CC3 at 3 days following RT (**Fig. 2.3D**). However, fibroblasts did significantly increase the number of PDAC cells that re-entered cell cycle 3 days post RT as measured by BrdU incorporation (**Fig. 2.3E**). These data suggest that even though RT can induce apoptosis in some cells, RT was not able to fully blunt the proliferation in the presence of PDAC stroma.

To understand if there are potential changes in RT-regulated immune signaling due to the collagen-rich stroma, we measured the expression of interferon (IFN)-related genes. We found that when organoids were cultured in basement membrane extract alone, robust increases in IFN-related genes expression were observed 24 to 48 hours after RT (**Fig. 2.3F, 2.4C**). This included increases in IFNα, IFNβ, IFNγ, IRF3, IRF7, IRF9, STAT1, CXCL9, CXCL10, and CXCL11 genes. However, when collagen was added to these cultures, the induction of IFN-related genes was severely dampened (**Fig. 2.3F, 2.4C**). Other inflammatory genes such as IL1α were not altered, suggesting some specificity for IFN signaling (**Fig. 2.3F**). These data suggest that stromal elements may limit not only RT-induced growth suppression, as shown by others[119-121], but also RT-induced IFN signaling, which may relate to RT-induced tumor immunity *in-vivo*.

To determine if RT alone changes how PDAC cells interact with the TME, we performed RNA sequencing (RNA-seq) and Reverse Phase Protein Array (RPPA) to look at both the gene and protein levels, respectively, after RT. As expected, compared to vehicle-treated cells, RT-treated cells have higher expression of DNA damage and repair proteins, such as γH2Ax, ATM, Rad17, and Rad51 (**Fig. 2.4D**) and increase in gene sets related to DNA damage, reactive oxygen species (ROS) and DNA repair post RT (**Fig. 2.4E**). However, RT also induced collagen, integrin signaling, and focal adhesion assembly gene signatures (**Fig. 2.4E**). Together, these data suggest that RT may also "prime" PDAC cells to engage with the surrounding stroma through integrin and focal adhesion signaling.

Inhibition of Focal Adhesion Kinase (FAK) overcomes stromal-induced RT resistance

While seldomly mutated, FAK is hyperactivated in >80% of PDAC tumors and plays an integral role in disease progression[214,233]. Furthermore, FAK signaling is amplified by stromal density and can be critical to ECM/integrin-induced survival signaling[214,233]. To understand whether we can overcome stromal-mediated RT resistance through FAK inhibition, we tested RT in combination with a FAK inhibitor, VS-4718 (FAKi). As above, the presence of fibroblasts and collagen enhanced the growth of PDAC organoids and made them much less responsive to RT (**Fig. 2.5A-C**). However, the combination of FAKi and RT led to complete inhibition of PDAC organoid growth, in a FAKi dose-dependent manner (**Fig. 2.5B-C**). This was true whether PDAC cells were grown in the presence of CAFs, collagen, or both (**Fig. 2.5C, 2.6A-B**). These findings show that FAKi could be a potential radiosensitizer for PDAC and that FAKi may increase RT efficacy.

To elucidate the effects of adding FAKi to RT, we again looked at markers of proliferation, apoptosis, and DNA damage using IHC. We did not see a difference in the short-term induction of DNA damage as measured by γH2Ax between RT and RT+FAKi in the presence or absence of fibroblasts, suggesting that neither FAK inhibition, nor the presence of stroma, regulates the amount of initial (first 6 hours) DNA-damage induced by RT in PDAC cells (**Fig. 2.5D**). Next, we found that the combination of RT+FAKi dramatically increased the number of $CC3^+$ apoptotic cells and decreased the number of $Ki67^+$ proliferating cells by 3 days post treatment and these effects were irrespective of the presence of stroma (**Fig. 2.5D**). These data suggest that FAK inhibition can improve RT-induced cell death.

To further understand if the cell death induced by the combination of FAKi and RT would have an immunomodulatory effect, we performed parallel RNA-seq and RPPA on KPOG organoids and the KP2 and KRAS-INK (KI) PDAC cell lines. We found PDAC cells treated with either RT or RT+FAKi had significant upregulation of DNA damage response gene sets and proteins, including DNA damage and ROS-related genes and AMPK, p-ERK, DNA Ligase-IV, TIGAR and Rad17 proteins (**Fig. 2.5E, 2.6C**). However, unlike RT-treated cells, RT+FAKi-treated cells had downregulation of gene set related to DNA damage repair and ROS response, as well as down-regulation of key DNA damage repair signaling proteins (NQO1, JAB1, KEAP1, Rad23, DDB-1, **Fig. 2.5E, 2.6C**). As expected, RT+FAKi-treated cells also had changes in cell cycle gene sets and cell cycle proteins CDK1, p27, Cdc2, CyclinD3, CDK9 corresponding to the observed changes in growth arrest (**Fig. 2.5E-F, 2.6C**). Finally, we observed that RT+FAKi treatment may change key metabolic pathways, including downregulation in genes related to oxidative phosphorylation, glycolysis, cholesterol homeostasis, and DNA replication (**Fig. 2.5E-G, 2.6C**). However, whether these metabolic changes were associated with unique biology or just cell cycle arrest and death is unclear. Taken together, these suggest that while both RT and RT+FAKi can induce DNA damage response, only RT+FAKi inhibits the ability of PDAC cells to repair damage, leading to growth arrest.

Next, we examined the expression of key proliferative signaling mediators for PDAC cells and we observed RT+FAKi led to downregulation of numerous MAPK proteins and pro-survival/apoptosis related proteins, including MEK2, ERK5, p38, PLCγ, Notch1, AKT, XIAP and PARP and upregulation of mTOR/autophagy related proteins ATG7, p70-S6K1, mTOR pS2448, Rictor, S6 and ULK1 (**Fig. 2.5E, 2.6C**). Notably, some of these changes

were also seen with FAKi alone treatment, suggesting that inhibition of FAK drives these changes in our system.

To understand the potential immunologic impact of RT+FAKi treatment, we analyzed changes in the inflammatory pathways in PDAC cells and organoids. By RNA-seq, we observed upregulation of gene sets involved in TNFa-, IFNβ- and IFNg-signaling (**Fig. 2.5F-H, 2.6C**). Additionally, RT+FAKi-treated PDAC cells had increased expression level of genes related to antigen processing and presentation (**Fig. 2.5G-H**), possibly downstream of increased IFN signaling. Correspondingly, increases in NFκB, JNK, and c-Jun pathways were observed at the protein level with RT+FAKi treatment, while Stat3 and Jak2 protein expression was decreased (**Fig. 2.5E, 2.6C**). Using orthogonal approaches, we found that STING and phospho-IRF3 were increased by western blot analysis and IFNα, IFNβ, and IFNγ genes were upregulated by RT-PCR in KI cells treated with RT+FAKi (**Fig. 2.6D-E**). To confirm the observed changes in STAT/IFN signaling *in-vivo*, we performed multiplex IHC (mIHC) on PDAC tissues from KPC mice and found that RT+FAKi treatment elevated phospho-STAT1 (pSTAT1) expression in $CK19^{+}$ PDAC cells (**Fig. 2.5I**). Taken together, these data suggest that FAK inhibition overcomes stromal-induced RT resistance by mitigating pro-survival and DNA damage repair signaling, which ultimately leads to sustained activation of IFN pathways in PDAC cells.

Combining FAKi with RT leads to immune priming *in-vivo*

We next sought to determine if FAK inhibition could improve RT efficacy and immune priming *in-vivo*. To accomplish this, we treated KPC GEMMs with the combination of RT and FAKi (**Fig. 2.7A**). Longitudinal ultrasound imaging showed that RT+FAKi led to

dramatic PDAC tumor regression in nearly 100% of mice (**Fig. 2.7B-C**). These imaging data were verified by absolute pancreas weights from mice sacrificed 7 and 14 days after RT start (**Fig. 2.7D, 2.8A**). Additionally, RT+FAKi was superior to the combination of RT and the chemotherapeutic drug gemcitabine, which has been used to treat PDAC patients (**Fig. 2.7B-C**). Similarly, RT+FAKi lead to tumor regression and long-term survival in KPC-OG GEMMs and syngeneic KP2 PDAC tumor models (**Fig. 2.7G-H, 2.8B**). Corresponding with the observed efficacy, at both 7- and 14-days post RT, RT+FAKi markedly reduced cell proliferation ($Ki67^+$ cells) and $CK19^+$ tumor cells and increased the number of $CC3^+$ apoptotic cells and necrotic tumor areas, compared to tissues from RT alone mice (**Fig. 2.7E-F, 2.8C-D**). Together these data suggest RT+FAKi led to improved tumor cell killing *in-vivo*.

To determine if the observed efficacy of RT+FAKi also corresponded with treatment-induced T cell priming, we assessed change in tumor-antigen specific T cells in KPC-OG GEMMs. Analysis of these mice at 14 days after treatment showed that, while RT+FAKi did not have a large increase in total T cells number, we found more activated $CD44^+$ $CD8^+$ and more tumor-specific OVA-$Dextramer^+$ T cells in PDAC tissue (**Fig. 2.7I, 2.8E**). We next analyzed draining lymph nodes from these mice and found that RT+FAKi treatment dramatically increased the total number activated $CD44^+$ $CD8^+$ T cells and OVA-$Dextramer^+$ $CD8^+$ T cells (**Fig. 2.7I**, **2.8E**), suggesting evidence for treatment-induced immune priming not seen with RT alone. Analysis of other immune cell populations showed that RT+FAKi decreased the total number of $CD4^+$ $Foxp3^+$ T regulatory cells, TAMs, granulocytes, and eosinophils and increased conventional type 1 dendritic cells (cDC1s) but not type 2 dendritic cells (cDC2s) (**Fig. 2.7J-K**). In particular,

the increase in cDC1, which was >13-fold, and the increase in ratio of cDC1 to TAMs, which was >24-fold, may be directly contributing to the treatment-induced increase in tumor-specific $CD8^+$ T cells in KPC-OG GEMMs. We next sought to determine whether T cells were critical to initial tumor regression and/or improved long-term disease control. To accomplish this, we depleted $CD4^+$ and $CD8^+$ T cells in mice bearing syngeneic KP2 PDAC tumors and found that loss of T cells did not affect short-term tumor regression (**Fig. 2.7L, 2.8F**), but was critical for long-term disease control (**Fig. 2.7M, 2.8F**). These data suggest that RT+FAKi remodeled the immune TME to favor T cell priming and that this is critical for long term disease control.

Tumor-infiltrating immune cells from RT+FAKi treated mice have better anti-tumor signatures

To further understand treatment-induced changes in the immune TME, we performed parallel single cell RNA sequencing (scRNA-seq) and Mass Cytometry (CyTOF). For scRNA-seq, we analyzed $CD45^+$ cells from the PDAC tissues of KPC GEMMs treated with vehicle, RT, FAKi or RT+FAKi. Using Uniform Manifold Approximation and Projection (UMAP) representation, we could distinguish all major immune cell populations (**Fig. 2.9A, 2.10A**). To elucidate differences in TAM phenotype, we re-clustered these cells and observed five TAM clusters (termed “Cd74-TAMs, Arg1-TAMs, Ifitm6-TAMs, Ccl7-TAMs, and Proliferating-TAMs”) and one monocyte cluster (**Fig. 2.9B, 2.10B**). Among these, we observed shifts in TAM subsets in RT+FAKi-treated tumors compared to all other treatments. This included decreased frequencies of Arg1-TAMs and an increased Ifitm6-TAMs and Ccl7-TAMs (**Fig. 2.9C**), suggesting possible changes toward T cell supportive

and IFN-responsive phenotypes. To further investigate this, we performed Gene Set Enrichment Analysis (GSEA) across all TAMs subsets from vehicle and RT+FAKi-treated mice and found upregulation of pathways associated with type-I and type-II interferons, T cell activation, phagocytosis, antigen processing and presentation, and ROS production (**Fig. 2.9D-E, 2.10C-D**). In agreement with scRNA-seq, CyTOF analysis of TAMs showed increased CD80, CD86, CD11c, and PDL2 expressions and decreased VISTA in RT+FAKi-treated mice compared to RT-treated mice (**Fig. 2.9F-G, 2.10E-F**). These data suggest that RT+FAKi shift TAMs away from immunosuppressive phenotypes, and perhaps toward immune supportive roles.

As cDCs are critical to the induction of T cell priming, we next sought to determine how RT+FAKi altered their phenotype. We first isolated and reclassified DC populations by UMAP analysis to define four distinct clusters: cDC1, cDC2, Migratory cDC, and plasmacytoid DC (pDC) (**Fig. 2.9H, 2.10G**). Mirroring our flow cytometry data (**Fig. 2.7K**), we found that PDAC tissue from RT+FAKi-treated mice had increased frequency of cDC1's (**Fig. 2.10H**). GSEA and Over Representation analyses found that RT+FAKi increased expression of genes in the type-I and type-II interferon, TNFα, and IL-12 pathways, as well as an increase in signatures for phagocytosis, antigen processing and presentation, and T cell activation across multiple cDC populations (**Fig. 2.9I-L**). By contrast, we observed decreases in pathways associated with integrins and MYC targets (**Fig. 2.9I-J**). Corroborating the changes in antigen presentation, we observed that RT+FAKi upregulated CD80 and CD86 in cDC1s and cDC2s, and decreased Tim3 in the cDC1s by CyTOF analysis (**Fig. 2.9G**). Together, these data suggest that cDCs are both

numerically increased and phenotypically shifted toward improved anti-tumor phenotypes.

Finally, we utilized parallel scRNA-seq and CyTOF to assess the net impact these changes had on T cell phenotypes. To accomplish this, we identified CD4 and CD8 a/b T cells by UMAP analysis of the adaptive immune cells in our scRNA-seq data sets (**Fig. 2.9M, 2.10I**). Agreeing with the increase in activated $CD8^+$ T cells found following RT+FAKi by flow cytometry (**Fig. 2.8E**), GSEA analyses by scRNA-seq found increases in pathways involved in secretory/zymogen granules, downstream T cell receptor (TCR) signaling, AP1, NFAT, and IL12 signaling (**Fig. 2.9N-O, 2.10J-L**). Heatmap of the activation/effector marker genes also showed that many are upregulated in the dual RT+FAKi treatment compared to vehicle or monotherapies (**Fig. 2.10M**). CyTOF analysis of T cells defined several clusters (**Fig. 2.9P-Q, 2.10N-O**). OVA-Dextramer$^+$ $CD8^+$ T cells were prominent in exhausted effector (high for PD1, LAG3 and Tim3, but not Ki67) and proliferative effector (high for Tbet, Eomes, and Ki67) compartments (**Fig. 2.9Q, 2.10O**). We also noted that RT+FAKi-treated mice had increased activation/effector markers Tbet, CD44, and OX40 expressions in OVA-Dextramer$^+$ $CD8^+$ T cells and increased the frequency of $Ki67^+$ Dextramer$^+$ $CD8^+$ T cells compared other treatments (**Fig. 2.9R-S, 2.10P**). However, many OVA-Dextramer$^+$ T cells were in the exhausted cluster with high PD1, LAG3 and Tim3 expression and RT+FAKi increased the fraction of Dextramer-negative $CD8^+$ T cells that clustered in the exhausted fraction (**Fig. 2.9Q,T, 2.10O**). These data suggest that T cell checkpoint may be engaged during treatment. Analysis of $CD4^+$ effector T cells showed increased OX40 and CD69 expression in PDAC tissue form mice treated with RT+FAKi, suggesting that though not as dominant, $CD4^+$ T cells may also

play a role (**Fig. 2.10Q**). Taken together our data suggest that both innate and adaptive tumor-infiltrating immune cells from RT+FAKi-treated mice acquired a more anti-tumor phenotype; however, it is unclear if this will be confounded or aided by changes in desmoplastic stromal responses.

FAKi alters CAFs to participate in tumor immunity

Like tumor-infiltrating immune cells, CAFs, which are abundant in PDAC, can play a large role in determining treatment response[8,18,22,52,213,276]. To further understand how our treatments changed the PDAC CAFs, we performed scRNA-seq from CAF-enriched $CD45^-$, $CD31^-$, $EPCAM^-$, $PDPN^+$ cells isolated by fluorescence-activated cell sorting (FACS) from KPC mice 14 days after treatment start. UMAP analysis of these CAFs generated seven unique subclusters (**Fig. 2.11A, 2.12A**). Using known CAF markers[21,22], we were able to identify the classic myofibroblastic CAFs (myCAFs) marked by *Acta2* and *Col12a1*, inflammatory CAFs (iCAFs) marked by *Cxcl12* and *Ly6c*, and antigen-presenting CAFs (apCAFs) marked by *Cd74* and *H2-Ab1* (**Fig. 2.12A-B**). Interestingly, treatments containing FAK inhibitors generated distinct CAF clusters that did not fall into the 3 classical CAF clusters identified in vehicle or RT samples (**Fig. 2.11A-C, 2.12B**). We named these FAKi-treatment induced CAFs “FAK-CAF1, FAK-CAF2, FAK-CAF3, and RTFAK-CAF” based on the treatments which induced them (**Fig. 2.11B-C**). These FAKi-induced phenotypic clusters were also seen with multiple data normalization and integration strategies, suggesting these population shifts were treatment-induced and not due to batch or computational effects but a true treatment-induced shift in transcriptional phenotype (**Fig. 2.12C-E**). We observed FAKi-induced CAFs subsets became enriched

in FAKi-treated samples at the expense of myCAFs subsets (**Fig. 2.11B-C, 2.12C-E**). In conjunction with these data, we observed decreased number of αSMA$^+$ CAFs by IHC and collagen density by Sirius Red staining in both FAKi- and RT+FAKi-treated mice compared to controls (**Fig. 2.11D-E**). These data suggest that FAKi treatment significantly altered the CAF composition/phenotype.

To elucidate the phenotypic differences in these CAF subsets, we first performed GSEA and Over Representation analyses comparing myCAFs in Vehicle-treated mice to FAKi-induced CAFs subsets (FAK-CAFs #1-3) in FAKi-treated mice. In comparison to myCAFs, all the FAK-CAFs had upregulation of pathways associated with TNFα, NFκB, IFNα, IFNγ, and AP1 signaling, and downregulation of pathways associated with angiogenesis, TGFβ, MYC targets, oxidative phosphorylation, and glycolysis (**Fig. 2.11F-G, 2.12F-G**). As expected, we also saw downregulation of FAK and integrin signatures in CAFs in FAKi-treated mice (**Fig. 2.12G**).

To confirm that we retain the same anti-tumor phenotypes generated by FAKi treatment, we performed GSEA and Over Representation analyses comparing myCAFs in Vehicle treated mice to RT+FAKi-induced CAFs subsets (RTFAK-CAF) in RT+FAKi-treated mice. In comparison to myCAFs, RTFAK-CAFs also had upregulation of pathways associated with TNFα, IFNα, IFNγ, and inflammatory response (**Fig. 2.11H-I**), similar to FAK-CAFs. We also observed a downregulation of MYC, integrins, MAPK, TGFβ, IL-6, and FAK signaling pathways, and upregulation of leukocyte migration and chemotaxis in RTFAK-CAFs compared to vehicle myCAFs (**Fig. 2.11H-J, 2.12H**). To cross-validate the upregulation of IFN signaling in CAFs, we performed mIHC for CK19, PDPN, and pSTAT1 and found RT+FAKi-treated mice had an upregulation of pSTAT1$^+$ in CK19$^-$ PDPN$^+$ CAFs

(**Fig. 2.11K**). Taken together, these data suggest that inhibition of FAK signaling remodeled the PDAC CAFs to augment IFN signaling in the stroma.

FAK inhibition in combination with RT in PDAC patients activates interferon signaling

Based on the data above, we initiated a clinical trial of a FAK inhibitor (VS-6063) in combination with stereotactic body radiation therapy (SBRT) in locally advanced PDAC patients (NCT04331041). In the patients we have accrued to date, we performed scRNA-seq on tissues from pre- and post-treatment biopsies (**Fig. 2.13A**). In data from the first four patients, UMAP analysis identified PDAC cells, CAFs, and major immune populations (**Fig. 2.13B, 2.14A**). Mirroring what we found in our pre-clinical studies (**Fig. 2.5**), gene set enrichment analysis of the PDAC cells showed that the combination treatment led to upregulation of multiple interferon pathways and TNFα signaling and downregulation of MYC and DNA repair pathways (**Fig. 2.13C, 2.14B**), which suggest that these PDAC cells might also be deprived of their proliferative and repair mechanisms. To further understand how SBRT + VS-6063 treatment changed the TME in our patients, we re-clustered the CAFs and TAMs populations separately and compared differentially expressed genes and pathways in these pre- and post-treatment biopsies. In CAFs, we observed that SBRT + VS-6063 increased the IFNα, IFNβ, and TNFα signaling pathways, and decreased the TGFβ and integrin signaling pathways (**Fig. 2.13D, 2.14C-F**). Similarly, in TAMs, we observed increases in IFNα, IFNβ, and TNFα, and decreases in glycolysis and hypoxia pathways in SBRT + VS-6063 post-treatment samples (**Fig. 2.13E-F, 2.14G-H**). These results from both CAFs and TAMs in humans parallel our results obtained in mice,

which demonstrate activation of IFN signaling in both the target tumor compartment and the tumor-associated stroma. Together, our mouse models and human data suggest that combining FAK inhibition with RT can reprogram the TME to support IFN signaling and tumor immunity.

FAK inhibition in combination with RT renders checkpoint blockade effective

Our data suggest that adding FAK inhibition to RT leads to tumor regression and priming of tumor antigen-specific T cells (**Fig. 2.7B-D,I, 2.8A-B**); but, these effects in turn drive upregulation of T cell exhaustion (**Fig. 2.9Q,T, 2.10O**). This suggests that these newly primed $CD8^+$ T cells might become limited by checkpoints. To test this, we treated mice bearing established syngeneic KP2-OVA PDAC tumors and treated with RT+FAKi in combination with αPD1 and αCTLA4 IgGs (immune checkpoint blockade, ICB, **Fig. 2.13G**). Mirroring our T cell depletion studies, short-term tumor regression by RT+FAKi was not impacted by the addition of ICB (**Fig. 2.13H**); however, the triple combination of RT+FAKi+ICB led to progressive tumor regression over time and long-term survival in 8 of 9 mice in the treatment group, which was superior to all other treatment groups (**Fig. 2.13I**). We repeated this in the KRAS-INK PDAC model and observed the addition of ICB to RT+FAKi also sustained more durable tumor regression (**Fig. 2.14I-J**). Together, these data suggest that the changes brought by RT+FAKi into the immune cells can be further enhanced with the addition of checkpoint immunotherapy, which could translate short-term tumor regression into long-term tumor control and/or eradication.

2.4. Figures

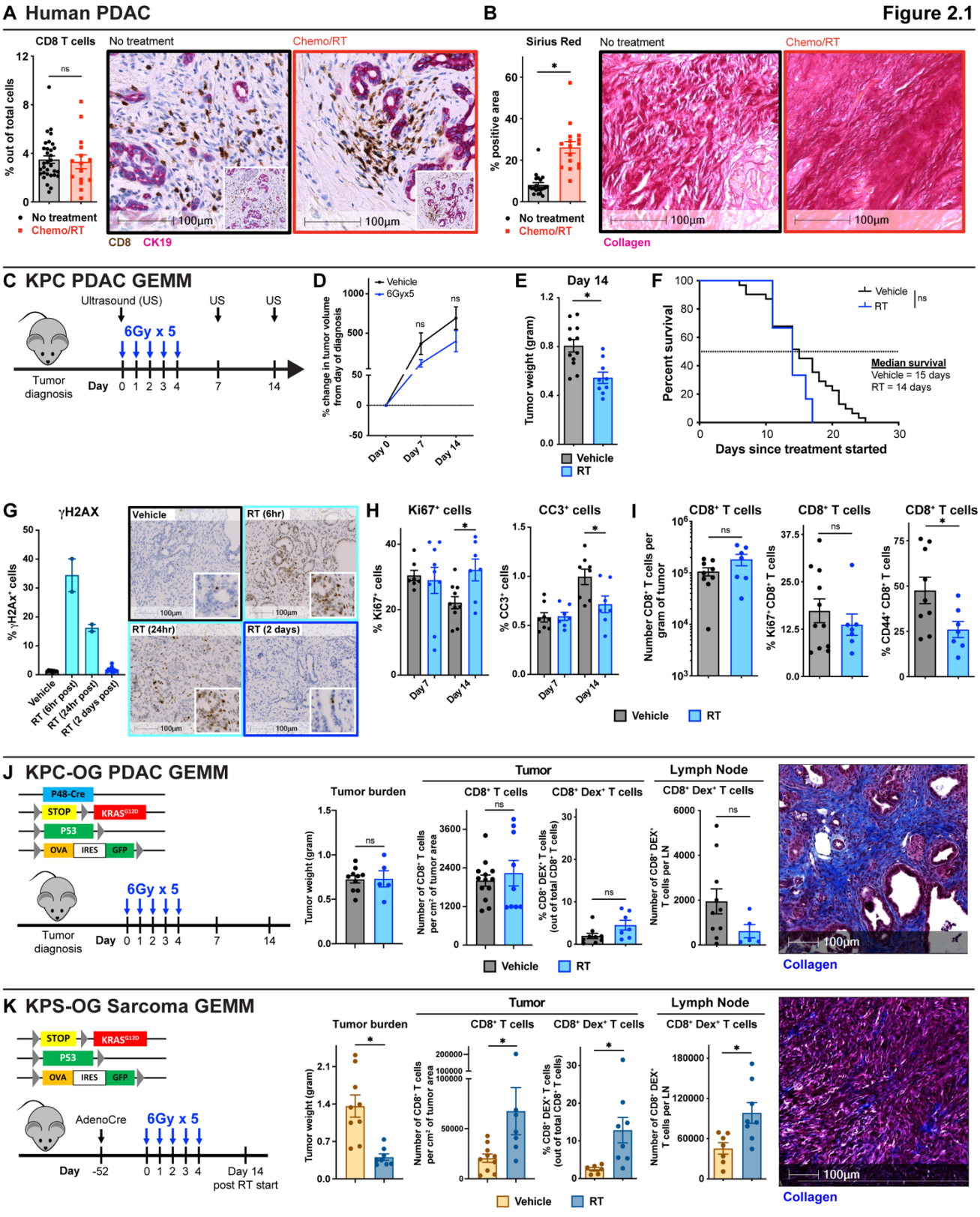
A Human PDAC
B
Figure 2.1
CD8 T cells
No treatment
Chemo/RT
% out of total cells
ns
No treatment
Chemo/RT
100μm
CD8 CK19
Sirius Red
% positive area
*
Collagen
C KPC PDAC GEMM
Ultrasound (US)
6Gy x 5
Tumor diagnosis
Day 0 1 2 3 4 7 14
D
Vehicle
6Gyx5
% change in tumor volume from day of diagnosis
Day 0
Day 7
Day 14
E
Day 14
Tumor weight (gram)
Vehicle
RT
F
Percent survival
Days since treatment started
Median survival
Vehicle = 15 days
RT = 14 days
G
γH2AX
% γH2Ax+ cells
Vehicle
RT (6hr)
RT (24hr)
RT (2 days)
H
Ki67+ cells
CC3+ cells
% Ki67+ cells
% CC3+ cells
I
CD8+ T cells
Number CD8+ T cells per gram of tumor
% Ki67+CD8+ T cells
% CD44+ CD8+ T cells
J KPC-OG PDAC GEMM
P48-Cre
STOP
KRASG12D
P53
OVA
IRES
GFP
Tumor
Lymph Node
Tumor burden
CD8+ T cells
CD8+ Dex+ T cells
Number of CD8+ T cells per cm2 of tumor area
% CD8+ DEX+ T cells (out of total CD8+ T cells)
Number of CD8+ DEX+ T cells per LN
K KPS-OG Sarcoma GEMM
AdenoCre
Day -52
Day 14 post RT start

<u>Figure 2.1</u>: Radiation therapy is insufficient to prime robust T cell responses in PDAC

(A-B) Analysis of CD8α T cell number and collagen density in surgical resection samples from patients who received neoadjuvant RT or no neoadjuvant therapy. Representative CD8α/CK19 IHC and Sirius Red images and quantification are depicted. n = 15-32 patients/group. **(C)** Schematic of RT administration and tumor burden monitoring in KPC GEMMs. KPC mice diagnosed with ultrasound (US) were treated with hypofractionated RT (6Gy x 5) and longitudinally assessed for tumor burden. **(D)** Tumor growth kinetics of Vehicle and RT-treated KPC mice from (C) quantified by US measurements. n = 8-12 mice/group. **(E)** Day 14 pancreas weight from KPC mice from (C). n = 9-13 mice/group. **(F)** Kaplan-Meier survival curve of KPC mice from (C). n = 6-31 mice/group. **(G)** Analysis of DNA damage (γH2Ax) on tissues from KPC Vehicle or RT-treated mice at various time points (n = 2-10 mice/group). Representative γH2Ax IHC images are depicted. **(H)** Analysis of proliferation (Ki67) and apoptosis (CC3) by IHC on tissues from KPC mice at Days 7 and 14 post RT. n = at least 7 mice/group. **(I)** Quantification of total $CD8^+$ T cells number and percentage of $Ki67^+$ or $CD44^+$ $CD8^+$ T cells out of total $CD8^+$ T cells number by flow cytometry in KPC Vehicle or RT-treated mice at Day 14. n = at least 7 mice/group. **(J)** Genetic loci for KPC-OG PDAC GEMMs and schematic of RT administration. Pancreas weight of KPC-OG Vehicle or RT-treated mice. Analysis of CD8α T cell number from KPC-OG Vehicle or RT-treated mice by IHC. Quantification of total $CD8^+$ OVA-$Dextramer^+$ tumor specific T cells number from tumor and pancreas draining lymph nodes in KPC-OG Vehicle or RT-treated mice by flow cytometry. Representative Trichrome image from KPC-OG Vehicle-treated mice is depicted. All analyses were done at Day 14

post RT start. n = at least 6 mice/group. **(K)** Genetic loci for KPS-OG sarcoma GEMMs and schematic of AdenoCre injection and RT administration. Tumor weight of KPS-OG Vehicle or RT-treated mice. Analysis of CD8α T cell number from KPS-OG Vehicle or RT-treated mice by IHC. Quantification of total $CD8^+$ OVA-$Dextramer^+$ tumor specific T cells number from tumor and draining lymph nodes in KPS-OG Vehicle or RT-treated mice by flow cytometry. Representative Trichrome image from KPS-OG Vehicle-treated mice is depicted. All analyses were done at Day 14 post RT start. n = at least 7 mice/group.
All graphs depict mean +/- SEM. For comparisons between two groups * denotes $p < 0.05$ by two-tailed t-test, one-way ANOVA, or Kaplan-Meyer as appropriate. ns denotes not significant.

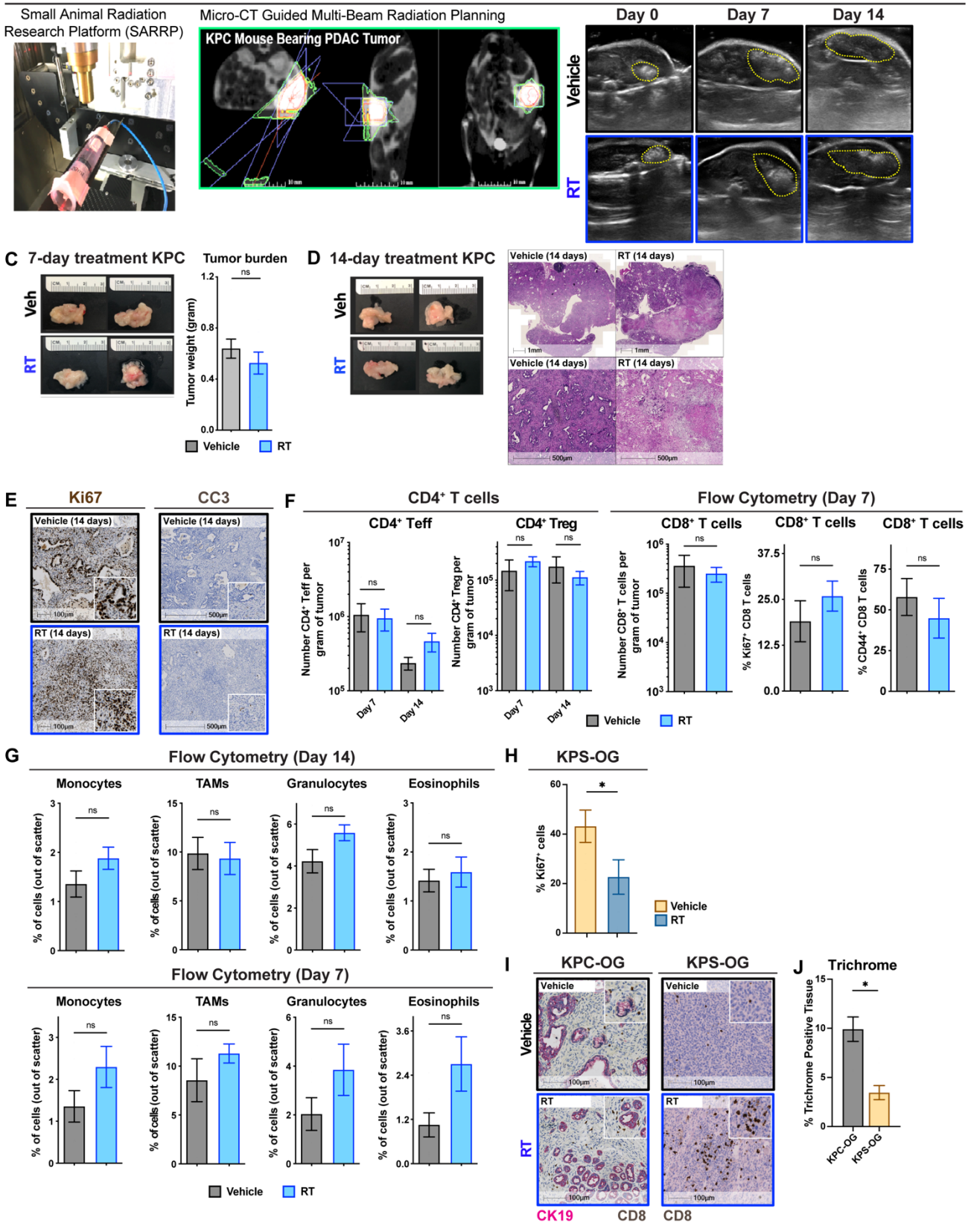
A
Small Animal Radiation Research Platform (SARRP)
Micro-CT Guided Multi-Beam Radiation Planning
KPC Mouse Bearing PDAC Tumor
B
Day 0
Day 7
Day 14
Vehicle
RT
C 7-day treatment KPC
Tumor burden
Veh
RT
Tumor weight (gram)
ns
Vehicle
RT
D 14-day treatment KPC
Vehicle (14 days)
RT (14 days)
E
Ki67
CC3
F
CD4⁺ T cells
CD4⁺ Teff
CD4⁺ Treg
Number CD4⁺ Teff per gram of tumor
Number CD4⁺ Treg per gram of tumor
Day 7
Day 14
Flow Cytometry (Day 7)
CD8⁺ T cells
Number CD8⁺ T cells per gram of tumor
% Ki67⁺ CD8 T cells
% CD44⁺ CD8 T cells
G
Flow Cytometry (Day 14)
Monocytes
TAMs
Granulocytes
Eosinophils
% of cells (out of scatter)
H
KPS-OG
% Ki67⁺ cells
I
KPC-OG
KPS-OG
CK19
CD8
J
Trichrome
% Trichrome Positive Tissue

Figure 2.2: Radiation therapy is insufficient to prime robust T cell responses in PDAC

(A) Schematic of Small Animal Radiation Research Platform (SARRP) machine with CT-guided multi-beam radiation planning utilized for precise RT targeting. **(B)** Representative US images from KPC Vehicle or RT-treated mice at Days 0, 7, and 14 for tumor growth kinetics in **Fig. 2.1D**. **(C)** Representative gross tissue images and Day 7 pancreas weight from KPC Vehicle or RT-treated mice from **Fig. 2.1C**. n = at least 7 mice/group. **(D)** Representative gross tissue and H&E images from KPC Vehicle or RT-treated mice at Day 14. n = at least 7 mice/group. **(E)** Representative Ki67 and CC3 IHC images from **Fig. 2.1H**. n = at least 7 mice/group. **(F)** Quantification of total $CD4^+$ T effector and $CD4^+$ $Foxp3^+$ T regulatory cells by flow cytometry in KPC mice at Days 7 and 14. Quantification of total $CD8^+$ T cells number and percentage of $Ki67^+$ or $CD44^+$ $CD8^+$ T cells out of total $CD8^+$ T cells number by flow cytometry in KPC mice at Day 7. n = at least 7 mice/group. **(G)** Quantification of various myeloid infiltrates: (i) Monocytes ($CD45^+$ $CD3^-$ $CD19^-$ $Ly6C^+$), (ii) TAMs ($CD45^+$ $CD3^-$ $CD19^-$ $Ly6C^-$ $Ly6G^-$ $CD11b^+$ $F4/80^+$ $MHC\text{-}II^+$), (iii) Granulocytes ($CD45^+$ $CD3^-$ $CD19^-$ $Ly6C^-$ $Ly6G^+$), and (iv) Eosinophils ($CD45^+$ $CD3^-$ $CD19^-$ $Ly6C^-$ $Ly6G^-$ $CD11b^+$ $F4/80^-$ $MHC\text{-}II^-$) by flow cytometry in KPC Vehicle or RT-treated mice at Days 7 and 14. n = at least 7 mice/group. **(H)** Analysis of Ki67 by IHC on tissues from KPS-OG mice at Day 14 post RT. n = at least 7 mice/group. **(I)** Representative $CD8\alpha$/CK19 IHC in KPC-OG mice and $CD8\alpha$ IHC in KPS-OG mice from **Fig. 2.1J-K**. n = at least 7 mice/group. **(J)** Analysis of collagen content in KPC-OG and KPS-OG Vehicle mice in **Fig. 2.1J-K**. n = at least 7 mice/group.

All graphs depict mean +/- SEM. For comparisons between two groups * denotes $p < 0.05$ by two-tailed t-test. ns denotes not significant.

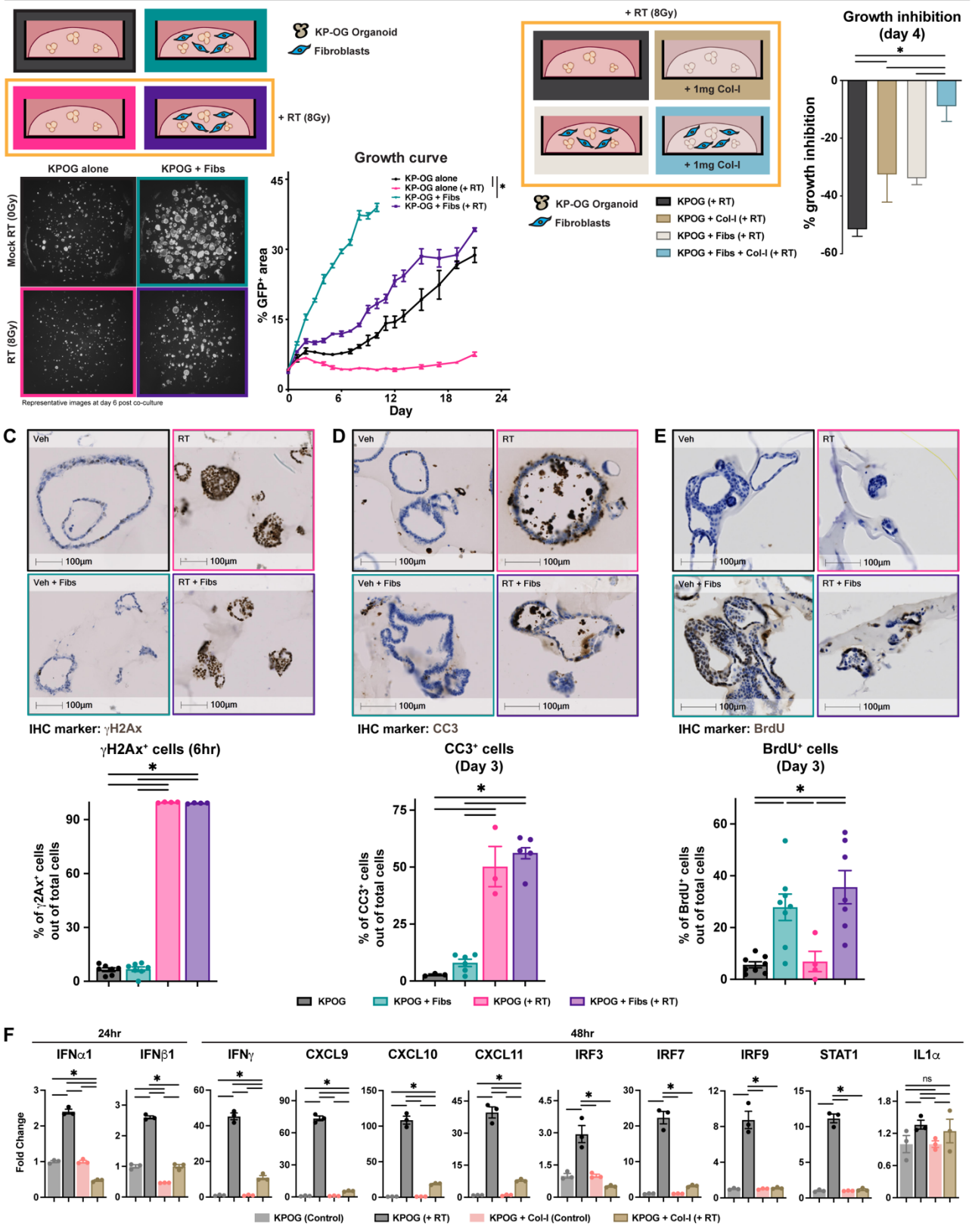
A KPOG organoid in vitro culture system
KP-OG Organoid
Fibroblasts
+ RT (8Gy)
KPOG alone
KPOG + Fibs
Mock RT (0Gy)
RT (8Gy)
Representative images at day 6 post co-culture
Growth curve
KP-OG alone
KP-OG alone (+ RT)
KP-OG + Fibs
KP-OG + Fibs (+ RT)
% GFP+ area
Day
B
+ RT (8Gy)
+ 1mg Col-I
+ 1mg Col-I
KP-OG Organoid
Fibroblasts
KPOG (+ RT)
KPOG + Col-I (+ RT)
KPOG + Fibs (+ RT)
KPOG + Fibs + Col-I (+ RT)
Growth inhibition (day 4)
% growth inhibition
C
Veh
RT
Veh + Fibs
RT + Fibs
100µm
IHC marker: γH2Ax
γH2Ax+ cells (6hr)
% of γ2Ax+ cells out of total cells
D
IHC marker: CC3
CC3+ cells (Day 3)
% of CC3+ cells out of total cells
E
IHC marker: BrdU
BrdU+ cells (Day 3)
% of BrdU+ cells out of total cells
KPOG
KPOG + Fibs
KPOG (+ RT)
KPOG + Fibs (+ RT)
F
24hr
48hr
IFNα1
IFNβ1
IFNγ
CXCL9
CXCL10
CXCL11
IRF3
IRF7
IRF9
STAT1
IL1α
Fold Change
ns
KPOG (Control)
KPOG (+ RT)
KPOG + Col-I (Control)
KPOG + Col-I (+ RT)

Figure 2.3: Stromal elements repress RT efficacy and induction of interferons

(A) Experimental schematic of KPOG organoids co-culture conditions with fibroblasts (10^5 cells). Cells were cultured and left to equilibrate for one day before treated with RT (8Gy). Representative GFP images taken with a fluorescent microscope at day 6 post co-culture. Tumor growth analysis of KPOG organoids tracked overtime. n = at least 3/group. **(B)** Experimental schematic of KPOG organoids co-culture conditions with fibroblasts (10^5 cells) and Collagen-I (1mg). Cells were cultured and left to equilibrate for one day before treated with RT. Quantification of tumor growth inhibition taken at day 4. n = at least 3/group. **(C)** Analysis and representative IHC images of γH2Ax by IHC on KPOG organoid cultures taken 6hr post RT. n = at least 3 sets/group. **(D-E)** Analysis and representative IHC images of CC3 (D) and 5hr-pulsed BrdU (E) by IHC on KPOG organoid cultures taken 3 days post RT. n = at least 3/group. **(F)** Bar graph displaying fold change of IFN-related genes measured by RT-PCR on KPOG organoid cultures treated with different conditions. n = at least 3/group.

All graphs depict mean +/- SEM. * denotes $p < 0.05$ by two-tailed t-test or one-way ANOVA as appropriate. ns denotes not significant.

Figure 2.4

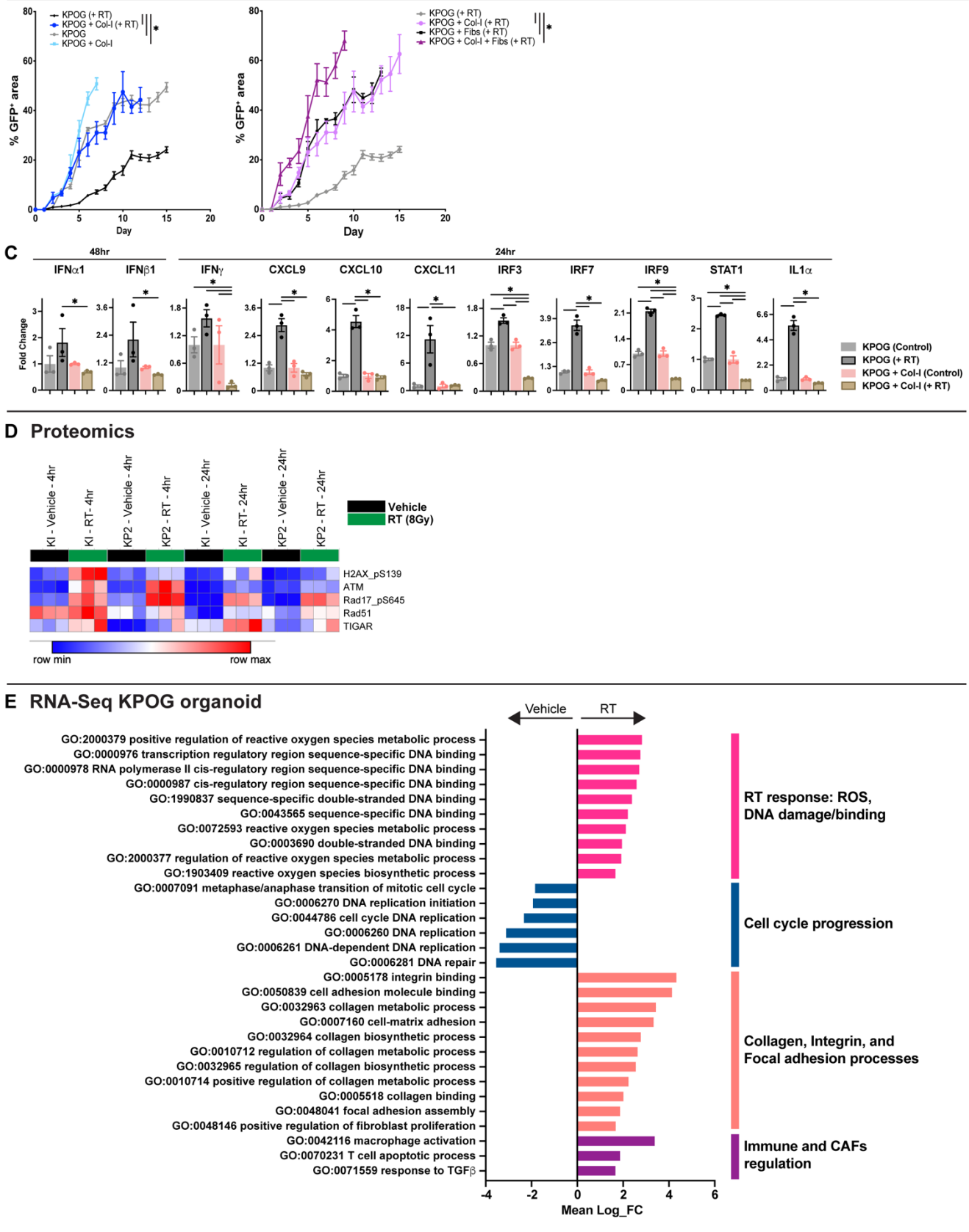
A
B
KPOG (+ RT)
KPOG + Col-I (+ RT)
KPOG
KPOG + Col-I
KPOG + Fibs (+ RT)
KPOG + Col-I + Fibs (+ RT)
% GFP+ area
Day
C
48hr
24hr
IFNα1
IFNβ1
IFNγ
CXCL9
CXCL10
CXCL11
IRF3
IRF7
IRF9
STAT1
IL1α
Fold Change
KPOG (Control)
KPOG (+ RT)
KPOG + Col-I (Control)
KPOG + Col-I (+ RT)
D Proteomics
KI - Vehicle - 4hr
KI - RT- 4hr
KP2 - Vehicle - 4hr
KP2 - RT - 4hr
KI - Vehicle - 24hr
KI - RT- 24hr
KP2 - Vehicle - 24hr
KP2 - RT - 24hr
Vehicle
RT (8Gy)
H2AX_pS139
ATM
Rad17_pS645
Rad51
TIGAR
row min
row max
E RNA-Seq KPOG organoid
Vehicle
RT
GO:2000379 positive regulation of reactive oxygen species metabolic process
GO:0000976 transcription regulatory region sequence-specific DNA binding
GO:0000978 RNA polymerase II cis-regulatory region sequence-specific DNA binding
GO:0000987 cis-regulatory region sequence-specific DNA binding
GO:1990837 sequence-specific double-stranded DNA binding
GO:0043565 sequence-specific DNA binding
GO:0072593 reactive oxygen species metabolic process
GO:0003690 double-stranded DNA binding
GO:2000377 regulation of reactive oxygen species metabolic process
GO:1903409 reactive oxygen species biosynthetic process
GO:0007091 metaphase/anaphase transition of mitotic cell cycle
GO:0006270 DNA replication initiation
GO:0044786 cell cycle DNA replication
GO:0006260 DNA replication
GO:0006261 DNA-dependent DNA replication
GO:0006281 DNA repair
GO:0005178 integrin binding
GO:0050839 cell adhesion molecule binding
GO:0032963 collagen metabolic process
GO:0007160 cell-matrix adhesion
GO:0032964 collagen biosynthetic process
GO:0010712 regulation of collagen metabolic process
GO:0032965 regulation of collagen biosynthetic process
GO:0010714 positive regulation of collagen metabolic process
GO:0005518 collagen binding
GO:0048041 focal adhesion assembly
GO:0048146 positive regulation of fibroblast proliferation
GO:0042116 macrophage activation
GO:0070231 T cell apoptotic process
GO:0071559 response to TGFβ
Mean Log_FC
RT response: ROS, DNA damage/binding
Cell cycle progression
Collagen, Integrin, and Focal adhesion processes
Immune and CAFs regulation

Figure 2.4: Stromal elements repress RT efficacy and induction of interferons

(A-B) Tumor growth analysis of KPOG organoids +/- 1 mg/mL Collagen-I (A) and KPOG organoids +/- 10^5 fibroblasts +/- 1 mg/mL Collagen-I (B) treated with RT tracked overtime. n = at least 3/group. **(C)** Bar graph displaying fold change of IFN-related genes measured by RT-PCR on KPOG organoid cultures treated with different conditions. n = at least 3/group. **(D)** Heatmap displaying expression level of DNA damage response/repair proteins from Reverse Protein Phase Array (RPPA) analysis. Proteins were taken from KRAS-INK (KI) and KP2 cells at 4hr and 24hr post RT. n = at least 3/group. **(E)** Bar graph displaying mean log fold change analysis of DEGs of KPOG organoids to known biological functions in Gene Ontology (GO) database. All graphs displayed comparisons of Vehicle to RT-treated cells. All pathways were filtered with p value < 0.05.

All graphs depict mean +/- SEM. * denotes $p < 0.05$ by two-tailed t-test or one-way ANOVA as appropriate. ns denotes not significant.

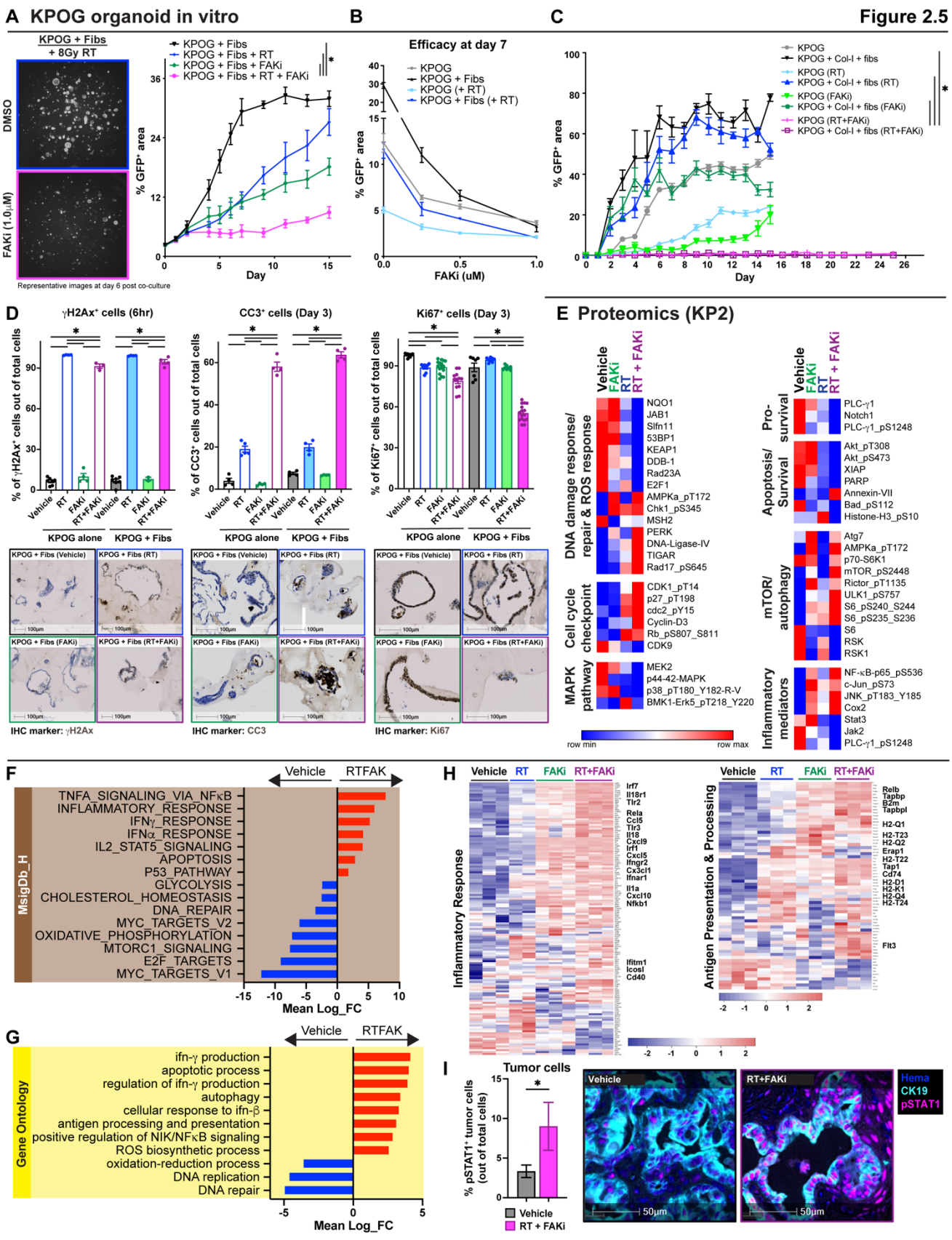
A KPOG organoid in vitro
B
C
Figure 2.5
KPOG + Fibs
+ 8Gy RT
DMSO
FAKi (1.0μM)
Representative images at day 6 post co-culture
KPOG + Fibs
KPOG + Fibs + RT
KPOG + Fibs + FAKi
KPOG + Fibs + RT + FAKi
% GFP+ area
Day
Efficacy at day 7
KPOG
KPOG + Fibs
KPOG (+ RT)
KPOG + Fibs (+ RT)
FAKi (uM)
KPOG + Col-I + fibs
KPOG (RT)
KPOG + Col-I + fibs (RT)
KPOG (FAKi)
KPOG + Col-I + fibs (FAKi)
KPOG (RT+FAKi)
KPOG + Col-I + fibs (RT+FAKi)
D
γH2Ax+ cells (6hr)
CC3+ cells (Day 3)
Ki67+ cells (Day 3)
% of γH2Ax+ cells out of total cells
% of CC3+ cells out of total cells
% of Ki67+ cells out of total cells
Vehicle
RT
FAKi
RT+FAKi
KPOG alone
KPOG + Fibs
KPOG + Fibs (Vehicle)
KPOG + Fibs (RT)
KPOG + Fibs (FAKi)
KPOG + Fibs (RT+FAKi)
IHC marker: γH2Ax
IHC marker: CC3
IHC marker: Ki67
E Proteomics (KP2)
Vehicle
FAKi
RT
RT + FAKi
DNA damage response/ repair & ROS response
NQO1
JAB1
Slfn11
53BP1
KEAP1
DDB-1
Rad23A
E2F1
AMPKa_pT172
Chk1_pS345
MSH2
PERK
DNA-Ligase-IV
TIGAR
Rad17_pS645
Cell cycle checkpoint
CDK1_pT14
p27_pT198
cdc2_pY15
Cyclin-D3
Rb_pS807_S811
CDK9
MAPK pathway
MEK2
p44-42-MAPK
p38_pT180_Y182-R-V
BMK1-Erk5_pT218_Y220
row min
row max
Pro-survival
PLC-γ1
Notch1
PLC-γ1_pS1248
Apoptosis/ Survival
Akt_pT308
Akt_pS473
XIAP
PARP
Annexin-VII
Bad_pS112
Histone-H3_pS10
mTOR/ autophagy
Atg7
AMPKa_pT172
p70-S6K1
mTOR_pS2448
Rictor_pT1135
ULK1_pS757
S6_pS240_S244
S6_pS235_S236
S6
RSK
RSK1
Inflammatory mediators
NF-κB-p65_pS536
c-Jun_pS73
JNK_pT183_Y185
Cox2
Stat3
Jak2
PLC-γ1_pS1248
F
Vehicle
RTFAK
MsigDb_H
TNFA_SIGNALING_VIA_NFκB
INFLAMMATORY_RESPONSE
IFNγ_RESPONSE
IFNα_RESPONSE
IL2_STAT5_SIGNALING
APOPTOSIS
P53_PATHWAY
GLYCOLYSIS
CHOLESTEROL_HOMEOSTASIS
DNA_REPAIR
MYC_TARGETS_V2
OXIDATIVE_PHOSPHORYLATION
MTORC1_SIGNALING
E2F_TARGETS
MYC_TARGETS_V1
Mean Log_FC
G
Gene Ontology
ifn-γ production
apoptotic process
regulation of ifn-γ production
autophagy
cellular response to ifn-β
antigen processing and presentation
positive regulation of NIK/NFκB signaling
ROS biosynthetic process
oxidation-reduction process
DNA replication
DNA repair
H
Inflammatory Response
Irf7
Il18r1
Tlr2
Rela
Ccl5
Tlr3
Il18
Cxcl9
Irf1
Cxcl5
Ifngr2
Cx3cl1
Ifnar1
Il1a
Cxcl10
Nfkb1
Ifitm1
Icosl
Cd40
Antigen Presentation & Processing
Relb
Tapbp
B2m
Tapbpl
H2-Q1
H2-T23
H2-Q2
Erap1
H2-T22
Tap1
Cd74
H2-D1
H2-K1
H2-Q4
H2-T24
Flt3
I
Tumor cells
% pSTAT1+ tumor cells (out of total cells)
Vehicle
RT + FAKi
Hema
CK19
pSTAT1
50μm

Figure 2.5: Inhibition of Focal Adhesion Kinase (FAK) overcomes stromal-induced RT resistance

(A) Tumor growth analysis of KPOG organoids co-cultured with fibroblasts treated with RT +/- FAKi (1.0μM) tracked overtime. Cells were cultured as in **Fig. 2.3A**. Representative GFP images at day 6 post co-culture. n = at least 3/group. **(B)** Growth analysis of KPOG organoids co-cultured with fibroblasts treated with RT +/- FAKi at varying concentrations (0, 0.25, 0.5, 1.0 μM) at day 7 post co-culture. Cells were cultured as in **Fig. 2.3A**. n = at least 3/group. **(C)** Tumor growth analysis of KPOG organoids co-cultured with fibroblasts and Col-I treated with RT +/- FAKi tracked overtime. Cells were cultured as in **Fig. 2.3A**. n = at least 3/group. **(D)** Analysis of γH2Ax by IHC on KPOG organoid cultures taken 6hr post RT. Analysis of CC3 and Ki67 by IHC on KPOG organoid cultures taken 3 days post RT. Representative γH2Ax, CC3, and Ki67 IHC images are depicted. n = at least 3/group. **(E)** Heatmap displaying expression level of proteins related to: (i) DNA damage response/repair and ROS response, (ii) Cell cycle checkpoint, (iii) MAPK pathway, (iv) Pro-survival, (v) Apoptosis/survival, (vi) mTOR/autophagy, and (vii) Inflammatory mediators from RPPA analysis. Proteins were taken from KP2 cells at 24hr post RT. n = at least 3/group. **(F-G)** Bar graph displaying overrepresentation analysis of DEGs on KPOG organoids to known biological functions in MsigDb_Hallmark (F) and GO (G) database. All graphs displayed comparisons of Vehicle to RT+FAKi-treated cells. All pathways were filtered with p value < 0.05. **(H)** Heatmap displaying expression level of genes related to inflammatory cytokines and chemokines in MsigDb_Hallmark database for inflammatory response and antigen processing and presentation in GO database. **(I)**

mIHC analysis of $CK19^+$ $pSTAT1^+$ cells from KPC mice from **Fig. 2.7A**. Representative CK19 and pSTAT1 fused mIHC images are depicted. n = at least 6 mice/group.

All graphs depict mean +/- SEM. * denotes $p < 0.05$ by two-tailed t-test or one-way ANOVA as appropriate.

Figure 2.6

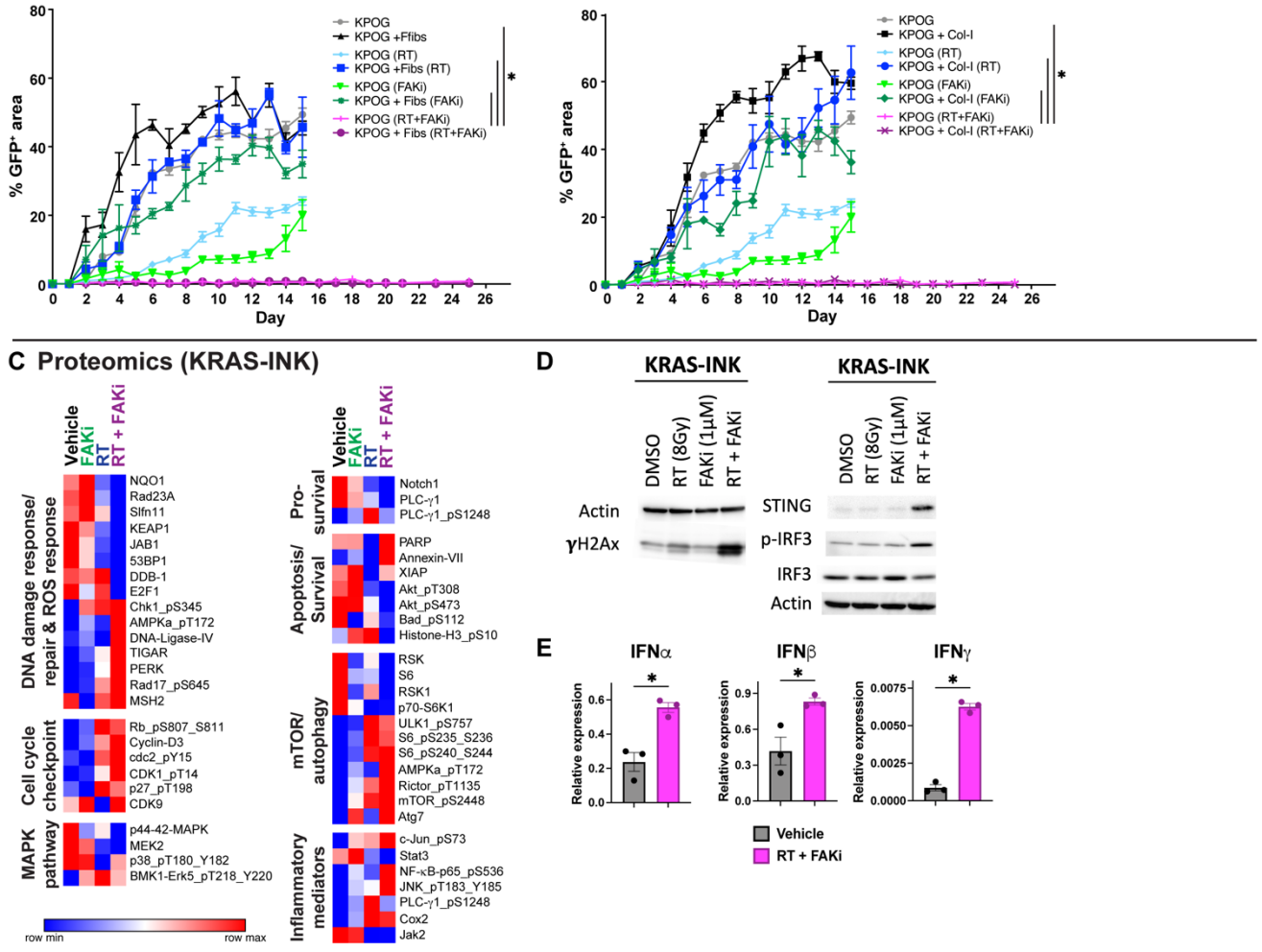
A
B
% GFP+ area
Day
KPOG
KPOG +Ffibs
KPOG (RT)
KPOG +Fibs (RT)
KPOG (FAKi)
KPOG + Fibs (FAKi)
KPOG (RT+FAKi)
KPOG + Fibs (RT+FAKi)
KPOG + Col-I
KPOG + Col-I (RT)
KPOG + Col-I (FAKi)
KPOG + Col-I (RT+FAKi)
*
C Proteomics (KRAS-INK)
Vehicle
FAKi
RT
RT + FAKi
DNA damage response/ repair & ROS response
NQO1
Rad23A
Slfn11
KEAP1
JAB1
53BP1
DDB-1
E2F1
Chk1_pS345
AMPKa_pT172
DNA-Ligase-IV
TIGAR
PERK
Rad17_pS645
MSH2
Cell cycle checkpoint
Rb_pS807_S811
Cyclin-D3
cdc2_pY15
CDK1_pT14
p27_pT198
CDK9
MAPK pathway
p44-42-MAPK
MEK2
p38_pT180_Y182
BMK1-Erk5_pT218_Y220
row min
row max
Pro-survival
Notch1
PLC-γ1
PLC-γ1_pS1248
Apoptosis/ Survival
PARP
Annexin-VII
XIAP
Akt_pT308
Akt_pS473
Bad_pS112
Histone-H3_pS10
mTOR/ autophagy
RSK
S6
RSK1
p70-S6K1
ULK1_pS757
S6_pS235_S236
S6_pS240_S244
AMPKa_pT172
Rictor_pT1135
mTOR_pS2448
Atg7
Inflammatory mediators
c-Jun_pS73
Stat3
NF-κB-p65_pS536
JNK_pT183_Y185
PLC-γ1_pS1248
Cox2
Jak2
D
KRAS-INK
KRAS-INK
DMSO
RT (8Gy)
FAKi (1μM)
RT + FAKi
Actin
γH2Ax
STING
p-IRF3
IRF3
Actin
E
IFNα
IFNβ
IFNγ
Relative expression
Vehicle
RT + FAKi

<u>Figure 2.6</u>: Inhibition of Focal Adhesion Kinase (FAK) overcomes stromal-induced RT resistance

(A-B) Tumor growth analysis of KPOG organoids co-cultured with 10^5 fibroblasts (A) and KPOG organoids co-cultured with addition of 1 mg/mL Collagen-I (B) treated with RT +/- FAKi tracked overtime. Cells were cultured as in **Fig. 2.3A**. n = at least 3/group. **(C)** Heatmap displaying expression level of proteins related to: (i) DNA damage response/repair and ROS response, (ii) Cell cycle checkpoint, (iii) MAPK pathway, (iv) Pro-survival, (v) Apoptosis/survival, (vi) mTOR/autophagy, and (vii) Inflammatory mediators from RPPA analysis. Proteins were taken from KRAS-INK cells at 24hr post treatment. n = at least 3/group. **(D)** Western Blot analysis of γH2Ax, STING, p-IRF3, and total IRF3 proteins from KRAS-INK cells 24hr post RT. n = at least 3/group. **(E)** RT-PCR analysis of IFNα, IFNβ, and IFNγ genes from KRAS-INK cells 24hr post RT. n = at least 3/group.

All graphs depict mean +/- SEM. * denotes $p < 0.05$ by two-tailed t-test or one-way ANOVA as appropriate.

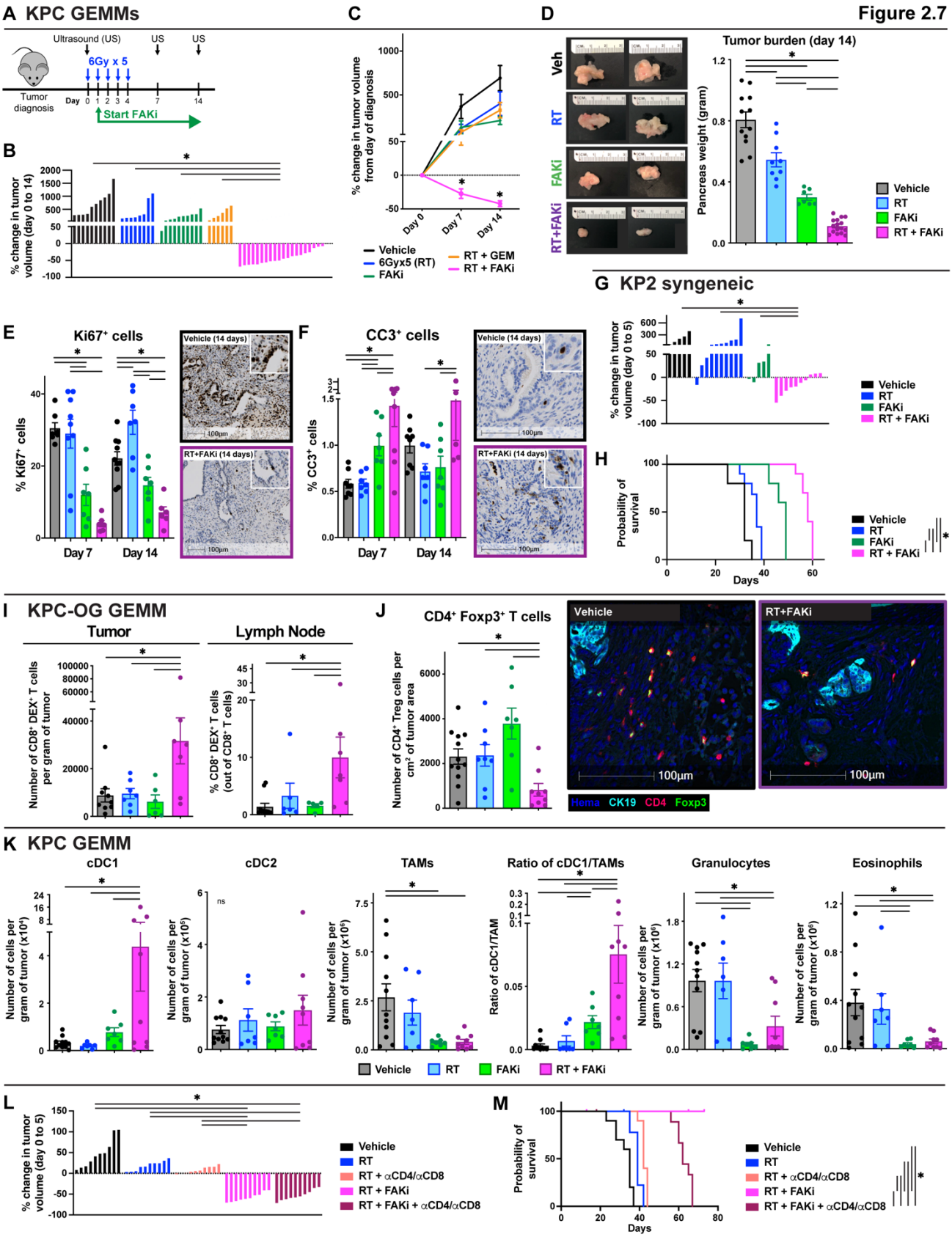
A KPC GEMMs
Ultrasound (US)
US
US
6Gy x 5
Tumor diagnosis
Day 0 1 2 3 4 7 14
Start FAKi
B
% change in tumor volume (day 0 to 14)
C
% change in tumor volume from day of diagnosis
Day 0
Day 7
Day 14
Vehicle
6Gyx5 (RT)
FAKi
RT + GEM
RT + FAKi
D
Figure 2.7
Veh
RT
FAKi
RT+FAKi
Tumor burden (day 14)
Pancreas weight (gram)
Vehicle
RT
FAKi
RT + FAKi
G KP2 syngeneic
% change in tumor volume (day 0 to 5)
H
Probability of survival
Days
E
Ki67⁺ cells
% Ki67⁺ cells
Day 7
Day 14
Vehicle (14 days)
RT+FAKi (14 days)
100µm
F
CC3⁺ cells
% CC3⁺ cells
I KPC-OG GEMM
Tumor
Lymph Node
Number of CD8⁺ DEX⁺ T cells per gram of tumor
% CD8⁺ DEX⁺ T cells (out of CD8⁺ T cells)
J
CD4⁺ Foxp3⁺ T cells
Number of CD4⁺ Treg cells per cm² of tumor area
Vehicle
RT+FAKi
100µm
Hema CK19 CD4 Foxp3
K KPC GEMM
cDC1
cDC2
TAMs
Ratio of cDC1/TAMs
Granulocytes
Eosinophils
Number of cells per gram of tumor (x10⁶)
Ratio of cDC1/TAM
ns
Vehicle
RT
FAKi
RT + FAKi
L
% change in tumor volume (day 0 to 5)
Vehicle
RT
RT + αCD4/αCD8
RT + FAKi
RT + FAKi + αCD4/αCD8
M
Probability of survival
Days

Figure 2.7: Combining FAKi with RT leads to immune priming *in-vivo*

(A) Schematic of RT (6Gy x 5) and FAKi (75mg/kg bid) administration and tumor burden monitoring in KPC GEMMs. KPC mice diagnosed with US were treated and longitudinally assessed for tumor burden. **(B)** Waterfall plot of KPC GEMMs from (A) evaluating tumor growth difference from Day 0 to Day 14 by US measurement. Gemcitabine (GEM) was given at a dose of 75mg/kg every 5 days starting at Day 0. n = 6-20 mice/group. **(C)** Tumor growth kinetics of KPC mice from (B) quantified by US measurements. n = 6-20 mice/group. **(D)** Day 14 pancreas weight of KPC mice from (A). Representative gross tissue images are depicted. n = 6-20 mice/group. **(E-F)** Analysis of Ki67 (E) and CC3 (F) by IHC on tissues from KPC mice at Days 7 and 14 post treatment start. Representative Ki67 and CC3 IHC images are depicted. n = at least 7 mice/group. **(G)** Waterfall plot of KP2 syngeneic tumor-bearing mice treated as depicted in (A) evaluating tumor growth difference from Day 0 to Day 5. n = 5-10 mice/group. **(H)** Kaplan-Meier survival curve for KP2 syngeneic tumor-bearing mice from (G). n = 5-10 mice/group. **(I)** Quantification of total $CD8^+$ OVA-$Dextramer^+$ T cells number in tumor and pancreas draining lymph node from KPC-OG mice treated as in (A) by flow cytometry. n = at least 7 mice/group. **(J)** Multiple IHC (mIHC) analysis of $CD4^+$ $Foxp3^+$ T regulatory cells from KPC mice from (A). Representative CK19, CD4, and Foxp3 fused mIHC images are depicted. n = at least 7 mice/group. **(K)** Quantification of various innate immune infiltrates: (i) cDC1 ($CD45^+$ $CD3^-$ $CD19^-$ $Ly6C^-$ $Ly6G^-$ $F4/80^{lo}$ $MHC\text{-}II^{hi}$ $CD24^{hi}$ $CD103^+$), (ii) cDC2 ($CD45^+$ $CD3^-$ $CD19^-$ $Ly6C^-$ $Ly6G^-$ $F4/80^{lo}$ $MHC\text{-}II^{hi}$ $CD24^{hi}$ $CD11b^+$), (iii) TAMs ($CD45^+$ $CD3^-$ $CD19^-$ $Ly6C^-$ $Ly6G^-$ $CD11b^+$ $F4/80^+$ $MHC\text{-}II^+$), (iv) Granulocytes ($CD45^+$ $CD3^-$ $CD19^-$ $Ly6C^-$ $Ly6G^+$), and (v) Eosinophils ($CD45^+$ $CD3^-$ $CD19^-$ $Ly6C^-$ $Ly6G^-$ $CD11b^+$ $F4/80^-$ $MHC\text{-}II^-$) by flow cytometry

in KPC mice from (A). n = at least 7 mice/group. **(L)** Waterfall plot of KP2 syngeneic tumor-bearing mice treated as in (A) evaluating tumor growth difference from Day 0 to Day 5. Depleting αCD4 and αCD8 IgGs were given starting at Day -2 every 4 days for a total of 30 days. n = 10 mice/group. **(M)** Kaplan-Meier survival curve for KP2 syngeneic tumor-bearing mice from (L). n = 10 mice/group.

All graphs depict mean +/- SEM. * denotes $p < 0.05$ by two-tailed t-test or one-way ANOVA or Kaplan-Meyer as appropriate. ns denotes not significant.

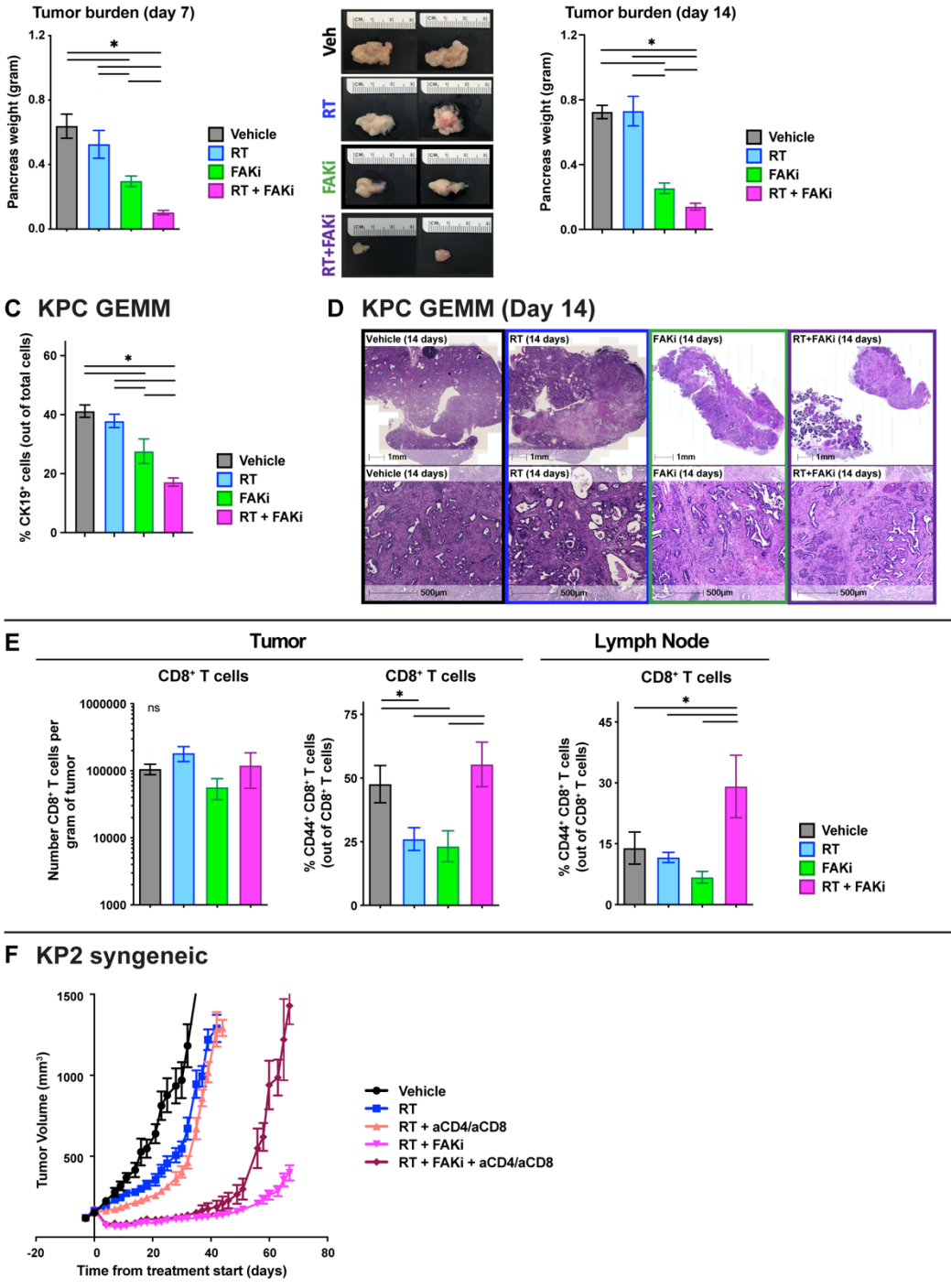
A KPC GEMM
Tumor burden (day 7)
Pancreas weight (gram)
Vehicle
RT
FAKi
RT + FAKi
Veh
RT
FAKi
RT+FAKi
B KPC-OG GEMM
Tumor burden (day 14)
C KPC GEMM
% CK19+ cells (out of total cells)
D KPC GEMM (Day 14)
Vehicle (14 days)
RT (14 days)
FAKi (14 days)
RT+FAKi (14 days)
E
Tumor
Lymph Node
CD8+ T cells
Number CD8+ T cells per gram of tumor
% CD44+ CD8+ T cells (out of CD8+ T cells)
ns
F KP2 syngeneic
Tumor Volume (mm3)
Time from treatment start (days)
RT + aCD4/aCD8
RT + FAKi + aCD4/aCD8

Figure 2.8: Combining FAKi with RT leads to immune priming *in-vivo*

(A) Day 7 pancreas weight of KPC mice from **Fig. 2.7A**. Representative gross tissue images are depicted. n = at least 7 mice/group. **(B)** Day 14 pancreas weight of KPC-OG mice from **Fig. 2.7I** treated as depicted in **Fig. 2.7A**. n = at least 7 mice/group. **(C)** Analysis of $CK19^+$ tumor cell number of KPC mice from **Fig. 2.7A** at Day 14. n = at least 7 mice/group. **(D)** Representative H&E images of KPC mice from **Fig. 2.7A** at Day 14. n = at least 7 mice/group. **(E)** Quantification of total $CD8^+$ T cells number and percentage of $CD44^+$ $CD8^+$ T cells out of total $CD8^+$ T cells number by flow cytometry in KPC mice from **Fig. 2.7A** at Day 14. n = at least 7 mice/group. **(F)** Tumor growth kinetics of KP2 syngeneic tumor-bearing mice from **Fig. 2.7L**. n = 10 mice/group.

All graphs depict mean +/- SEM. * denotes $p < 0.05$ by two-tailed t-test or one-way ANOVA as appropriate. ns denotes not significant.

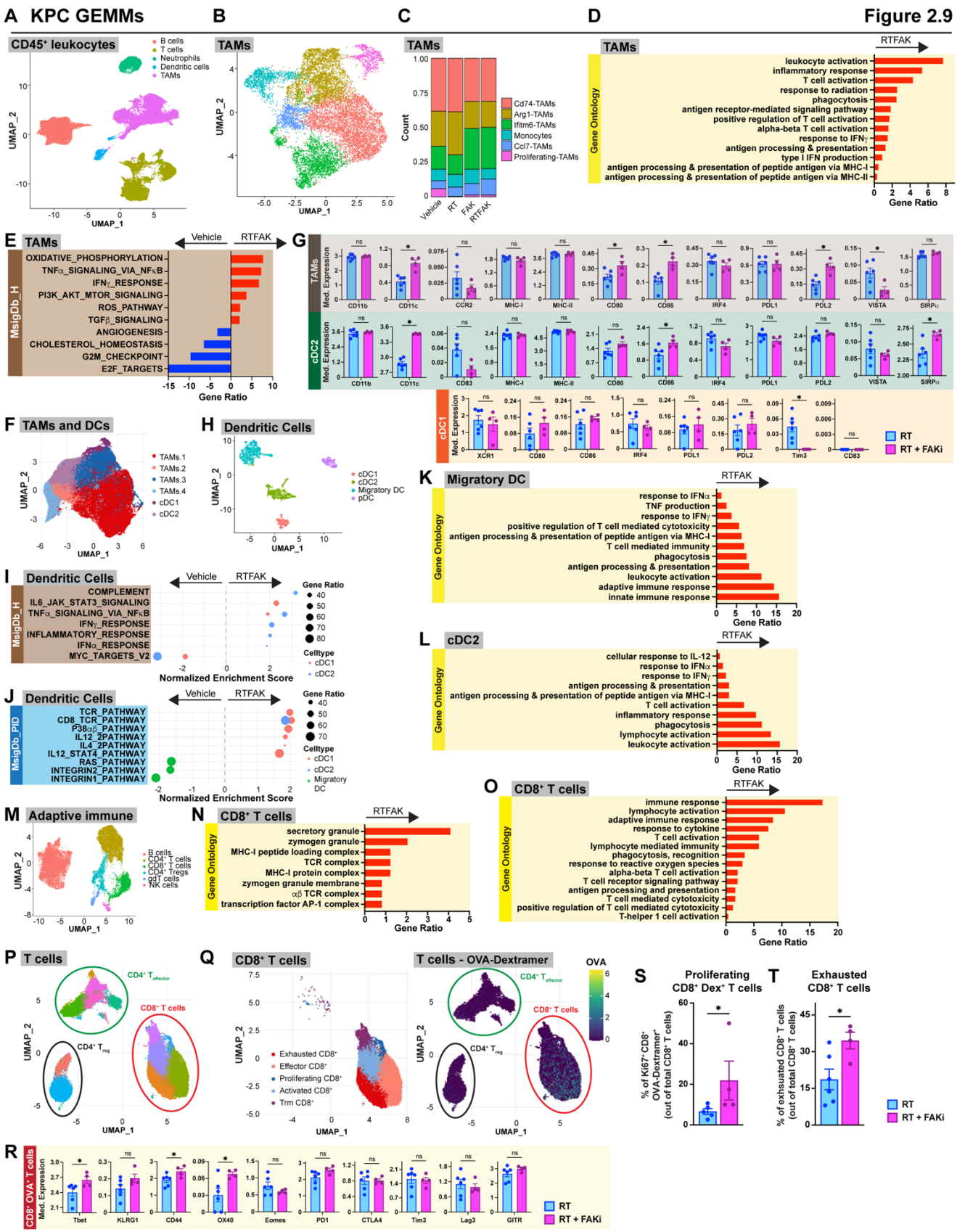
A KPC GEMMs
B
C
D
Figure 2.9
CD45⁺ leukocytes
B cells
T cells
Neutrophils
Dendritic cells
TAMs
UMAP_1
UMAP_2
TAMs
Cd74-TAMs
Arg1-TAMs
Ifitm6-TAMs
Monocytes
Ccl7-TAMs
Proliferating-TAMs
Count
Vehicle
RT
FAK
RTFAK
Gene Ontology
leukocyte activation
inflammatory response
T cell activation
response to radiation
phagocytosis
antigen receptor-mediated signaling pathway
positive regulation of T cell activation
alpha-beta T cell activation
response to IFNγ
antigen processing & presentation
type I IFN production
antigen processing & presentation of peptide antigen via MHC-I
antigen processing & presentation of peptide antigen via MHC-II
Gene Ratio
E TAMs
Vehicle
RTFAK
MsigDb_H
OXIDATIVE_PHOSPHORYLATION
TNFα_SIGNALING_VIA_NFκB
IFNγ_RESPONSE
PI3K_AKT_MTOR_SIGNALING
ROS_PATHWAY
TGFβ_SIGNALING
ANGIOGENESIS
CHOLESTEROL_HOMEOSTASIS
G2M_CHECKPOINT
E2F_TARGETS
Gene Ratio
G
TAMs
cDC2
cDC1
Med. Expression
CD11b
CD11c
CCR2
MHC-I
MHC-II
CD80
CD86
IRF4
PDL1
PDL2
VISTA
SIRPα
CD83
XCR1
Tim3
RT
RT + FAKi
F TAMs and DCs
TAMs.1
TAMs.2
TAMs.3
TAMs.4
cDC1
cDC2
H Dendritic Cells
cDC1
cDC2
Migratory DC
pDC
K Migratory DC
response to IFNα
TNF production
response to IFNγ
positive regulation of T cell mediated cytotoxicity
antigen processing & presentation of peptide antigen via MHC-I
T cell mediated immunity
phagocytosis
antigen processing & presentation
leukocyte activation
adaptive immune response
innate immune response
I Dendritic Cells
MsigDb_H
COMPLEMENT
IL6_JAK_STAT3_SIGNALING
TNFα_SIGNALING_VIA_NFκB
IFNγ_RESPONSE
INFLAMMATORY_RESPONSE
IFNα_RESPONSE
MYC_TARGETS_V2
Normalized Enrichment Score
Celltype
L cDC2
cellular response to IL-12
response to IFNα
response to IFNγ
antigen processing & presentation
antigen processing & presentation of peptide antigen via MHC-I
T cell activation
inflammatory response
phagocytosis
lymphocyte activation
leukocyte activation
J Dendritic Cells
MsigDb_PID
TCR_PATHWAY
CD8_TCR_PATHWAY
P38αβ_PATHWAY
IL12_2PATHWAY
IL4_2PATHWAY
IL12_STAT4_PATHWAY
RAS_PATHWAY
INTEGRIN2_PATHWAY
INTEGRIN1_PATHWAY
Migratory DC
O CD8⁺ T cells
immune response
lymphocyte activation
adaptive immune response
response to cytokine
T cell activation
lymphocyte mediated immunity
phagocytosis, recognition
response to reactive oxygen species
alpha-beta T cell activation
T cell receptor signaling pathway
antigen processing and presentation
T cell mediated cytotoxicity
positive regulation of T cell mediated cytotoxicity
T-helper 1 cell activation
M Adaptive immune
B cells
CD4⁺ T cells
CD8⁺ T cells
CD4⁺ Tregs
γδT cells
NK cells
N CD8⁺ T cells
secretory granule
zymogen granule
MHC-I peptide loading complex
TCR complex
MHC-I protein complex
zymogen granule membrane
αβ TCR complex
transcription factor AP-1 complex
P T cells
CD4⁺ T effector
CD8⁺ T cells
CD4⁺ T reg
Q CD8⁺ T cells
Exhausted CD8⁺
Effector CD8⁺
Proliferating CD8⁺
Activated CD8⁺
Trm CD8⁺
T cells - OVA-Dextramer
OVA
S Proliferating CD8⁺ Dex⁺ T cells
% of Ki67⁺ CD8⁺ OVA-Dextramer⁺ (out of total CD8⁺ T cells)
T Exhausted CD8⁺ T cells
% of exhausted CD8⁺ T cells (out of total CD8⁺ T cells)
R CD8⁺ OVA⁺ T cells
Tbet
KLRG1
CD44
OX40
Eomes
PD1
CTLA4
Tim3
Lag3
GITR
RT
RT + FAKi

Figure 2.9: Tumor-infiltrating immune cells from RT+FAKi treated mice have better anti-tumor signatures

(A) UMAP dimensionality reduction plot of scRNAseq data on $CD45^+$ leukocytes from KPC mice treated with vehicle or RT +/- VS-4718 (FAKi) as depicted in **Fig. 2.7A**. Annotation shows different cell types. **(B)** UMAP analysis of TAMs subsets isolated from (A). 6 different TAM clusters are depicted. **(C)** Count ratio of the TAM clusters from (B). **(D-E)** Bar graph displaying overrepresentation analysis of DEGs on all the TAMs in (B) to known biological functions in Gene Ontology (GO) database (D) and Molecular Signatures database (MsigDb) (E). All graphs displayed comparisons of Vehicle to RT+FAKi-treated mice. All pathways were filtered with p value < 0.05. **(F)** UMAP dimensionality reduction plot of CyTOF data on TAMs and cDCs from KP2-OVA tumor-bearing RT- and RT+FAKi-treated mice treated as depicted in **Fig. 2.7A**. Annotation shows different cell types. **(G)** Analysis of median expression levels of various markers on all the TAMs, cDC1, and cDC2 in (F). n = at least 4 groups of pooled mice/group. **(H)** UMAP analysis of cDCs subsets isolated from (A). 4 different cDC clusters are depicted. **(I-J)** Dot plot displaying Gene Set Enrichment Analysis (GSEA) results from MsigDb_Hallmark (I) and MsigDb_PID (J) databases comparing different cDCs clusters from (H). All graphs displayed comparisons of Vehicle to RT+FAKi-treated mice. All pathways were filtered with p value < 0.05. **(K-L)** Bar graph displaying overrepresentation analysis of DEGs on Migratory DC (K) and cDC2 (L) from (H) to known biological functions in GO database. All graphs displayed comparisons of Vehicle to RT+FAKi-treated mice. All pathways were filtered with p value < 0.05. **(M)** UMAP dimensionality reduction plot of scRNAseq data on the adaptive immune cells from KPC mice treated with vehicle or RT

+/- VS-4718 (FAKi) as depicted in **Fig. 2.7A**. Annotation shows different cell types. **(N-O)** Bar graph displaying overrepresentation analysis of DEGs on $CD8^+$ T cells in (M) to known biological functions in GO database. All graphs displayed comparisons of Vehicle to RT+FAKi-treated mice. All pathways were filtered with p value < 0.05. **(P)** UMAP dimensionality reduction plot of CyTOF data on $CD8^+$ and $CD4^+$ T cell populations from KP2-OVA tumor-bearing RT- and RT+FAKi-treated mice. Annotation shows different cell types. **(Q)** UMAP dimensionality reduction plot of CyTOF data on $CD8^+$ T cell populations from (P). Annotation shows five different $CD8^+$ T cell subclusters. OVA-Dextramer expression levels projected onto UMAP plots in (P). **(R)** Analysis of median expression levels of various markers on $CD8^+$ OVA-$Dextramer^+$ T cells in (P). n = at least 4 groups of pooled mice/group. **(S)** Quantification of proliferating $CD8^+$ OVA-$Dextramer^+$ T cells out of total $CD8^+$ T cells in (P) from mice treated with vehicle or RT +/- FAKi. n = at least 4 groups of pooled mice/group. **(T)** CyTOF quantification analysis of proliferating and exhausted $CD8^+$ T cell numbers in **Fig. 2.9P**. n = at least 4 groups of pooled mice/group. All graphs depict mean +/- SEM. * denotes p < 0.05 by two-tailed t-test or one-way ANOVA as appropriate. ns denotes not significant.

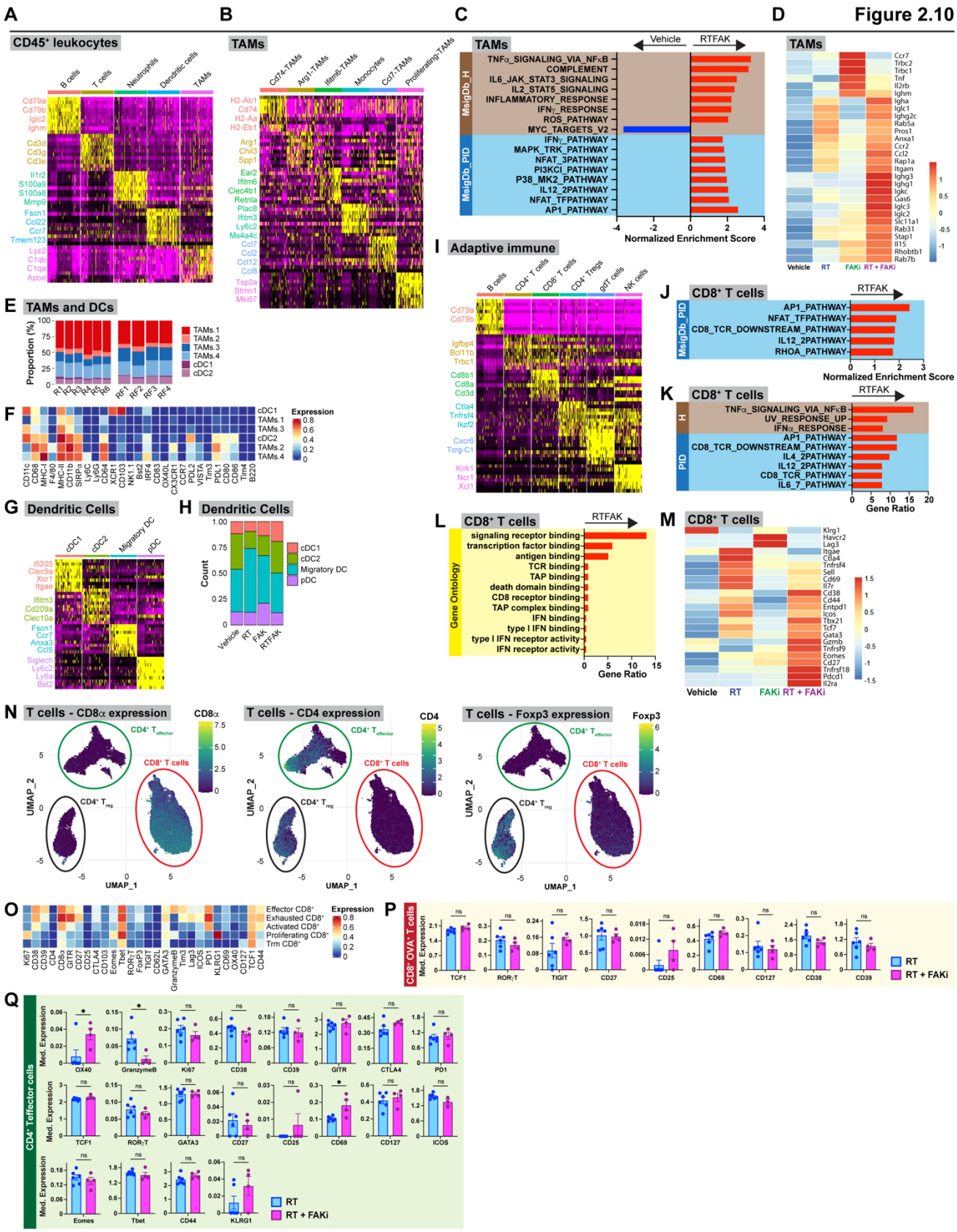
A
B
C
D
Figure 2.10
CD45⁺ leukocytes
B cells
T cells
Neutrophils
Dendritic cells
TAMs
TAMs
Cd74-TAMs
Arg1-TAMs
Ifitm-TAMs
Monocytes
Cd7-TAMs
Proliferating-TAMs
TAMs
Vehicle
RTFAK
MsigDb_H
MsigDb_PID
TNFα_SIGNALING_VIA_NFκB
COMPLEMENT
IL6_JAK_STAT5_SIGNALING
IL2_STAT5_SIGNALING
INFLAMMATORY_RESPONSE
IFNγ_RESPONSE
ROS_PATHWAY
MYC_TARGETS_V2
IFNγ_PATHWAY
MAPK_TRK_PATHWAY
NFAT_3PATHWAY
PI3KCI_PATHWAY
P38_MK2_PATHWAY
IL12_2PATHWAY
NFAT_TFPATHWAY
AP1_PATHWAY
Normalized Enrichment Score
TAMs
Vehicle
RT
FAKi
RT + FAKi
E
TAMs and DCs
Proportion (%)
TAMs.1
TAMs.2
TAMs.3
TAMs.4
cDC1
cDC2
F
Expression
I
Adaptive immune
B cells
CD4⁺ T cells
CD8⁺ T cells
CD4⁺ Tregs
gdT cells
NK cells
J
CD8⁺ T cells
RTFAK
MsigDb_PID
AP1_PATHWAY
NFAT_TFPATHWAY
CD8_TCR_DOWNSTREAM_PATHWAY
IL12_2PATHWAY
RHOA_PATHWAY
Normalized Enrichment Score
K
CD8⁺ T cells
RTFAK
H
PID
TNFα_SIGNALING_VIA_NFκB
UV_RESPONSE_UP
IFNα_RESPONSE
AP1_PATHWAY
CD8_TCR_DOWNSTREAM_PATHWAY
IL4_2PATHWAY
IL12_2PATHWAY
CD8_TCR_PATHWAY
IL6_7_PATHWAY
Gene Ratio
G
Dendritic Cells
cDC1
cDC2
Migratory DC
pDC
H
Dendritic Cells
Count
Vehicle
RT
FAK
RTFAK
L
CD8⁺ T cells
RTFAK
Gene Ontology
signaling receptor binding
transcription factor binding
antigen binding
TCR binding
TAP binding
death domain binding
CD8 receptor binding
TAP complex binding
IFN binding
type I IFN binding
type I IFN receptor activity
IFN receptor activity
Gene Ratio
M
CD8⁺ T cells
Vehicle
RT
FAKi
RT + FAKi
N
T cells - CD8α expression
T cells - CD4 expression
T cells - Foxp3 expression
CD4⁺ T effector
CD8⁺ T cells
CD4⁺ T reg
UMAP_1
UMAP_2
O
Effector CD8⁺
Exhausted CD8⁺
Activated CD8⁺
Proliferating CD8⁺
Trm CD8⁺
Expression
P
CD8⁺ OVA⁺ T cells
Med. Expression
RT
RT + FAKi
Q
CD4⁺ Teffector cells
Med. Expression
RT
RT + FAKi

Figure 2.10: Tumor-infiltrating immune cells from RT+FAKi treated mice have better anti-tumor signatures

(A) Heatmap displaying top 10 genes of different immune cells in **Fig. 2.9A**. **(B)** Heatmap displaying top 10 genes of different TAMs in **Fig. 2.9B**. **(C)** Bar graphs displaying GSEA results from MsigDb_Hallmark and MsigDb_PID databases comparing TAMs in **Fig. 2.9B**. All graphs displayed comparisons of Vehicle to RT+FAKi-treated mice. All pathways were filtered with p value < 0.05. **(D)** Heatmap displaying relative expression level of genes related to antigen processing and presentation taken from MsigDb_Hallmark database in TAMs from **Fig. 2.9B**. **(E)** Count ratio from CyTOF analysis of the 4 TAM clusters and 2 cDC clusters from **Fig. 2.9F**. R1-R6 denotes RT-treated samples. RF1-RF4 denotes RT+FAKi-treated samples. **(F)** Heatmap displaying expression levels of markers used in CyTOF analysis for cell clustering in **Fig. 2.9F**. **(G)** Heatmap displaying top 10 genes of different cDCs in **Fig. 2.9H**. **(H)** Count ratio from scRNAseq analysis of the 4 cDC clusters from **Fig. 2.9H**. **(I)** Heatmap displaying top 10 genes of different adaptive immune cells in **Fig. 2.9M**. **(J-L)** Bar graph displaying GSEA analysis from MsigDb_PID (J), overrepresentation analysis to known biological functions in MsigDb_Hallmark and MsigDb_PID (K) and GO database (L) taken from DEGs of $CD8^+$ T cells in **Fig. 2.9M**. All graphs displayed comparisons of Vehicle to RT+FAKi-treated mice. All pathways were filtered with p value < 0.05. **(M)** Heatmap displaying effector/activation markers from $CD8^+$ T cells in **Fig. 2.9M**. **(N)** CD8, CD4, and Foxp3 expression levels projected onto UMAP plots in **Fig. 2.9P**. **(O)** Heatmap displaying expression levels of markers used in CyTOF analysis for cell clustering in **Fig. 2.9Q**. **(P-Q)** Analysis of median expression levels of various markers on $CD8^+$ OVA-Dextramer$^+$ T

cells (P) and $CD4^+$ T effector cells (Q) in **Fig. 2.9P**. n = at least 4 groups of pooled mice/group.

All graphs depict mean +/- SEM. * denotes $p < 0.05$ by two-tailed t-test or one-way ANOVA as appropriate. ns denotes not significant.

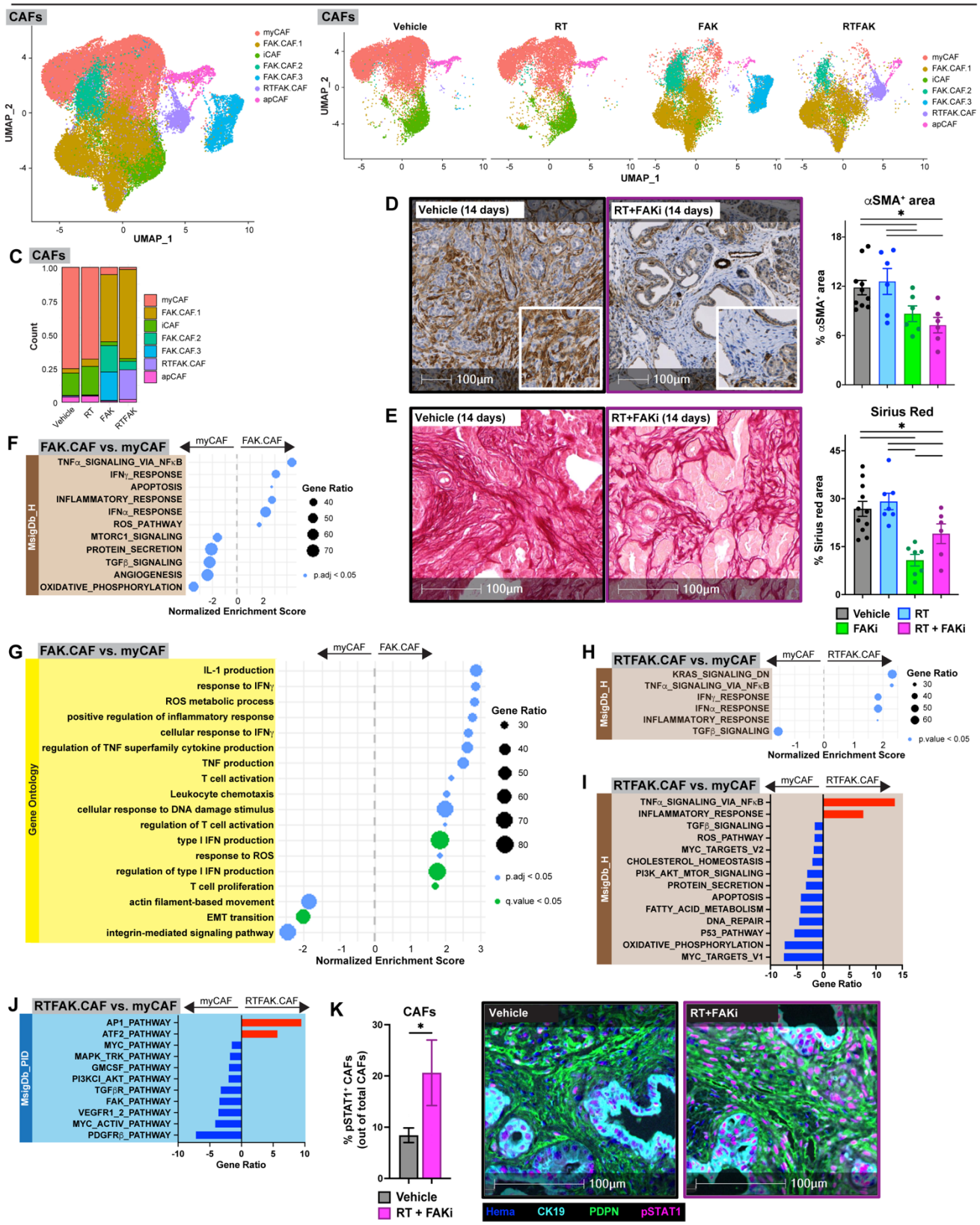
A KPC GEMMs
B
CAFs
myCAF
FAK.CAF.1
iCAF
FAK.CAF.2
FAK.CAF.3
RTFAK.CAF
apCAF
UMAP_1
UMAP_2
Vehicle
RT
FAK
RTFAK
C
Count
D
Vehicle (14 days)
RT+FAKi (14 days)
100µm
αSMA⁺ area
% αSMA⁺ area
E
Sirius Red
% Sirius red area
Vehicle
RT
FAKi
RT + FAKi
F
FAK.CAF vs. myCAF
myCAF
FAK.CAF
MsigDb_H
TNFα_SIGNALING_VIA_NFκB
IFNγ_RESPONSE
APOPTOSIS
INFLAMMATORY_RESPONSE
IFNα_RESPONSE
ROS_PATHWAY
MTORC1_SIGNALING
PROTEIN_SECRETION
TGFβ_SIGNALING
ANGIOGENESIS
OXIDATIVE_PHOSPHORYLATION
Gene Ratio
p.adj < 0.05
Normalized Enrichment Score
G
FAK.CAF vs. myCAF
Gene Ontology
IL-1 production
response to IFNγ
ROS metabolic process
positive regulation of inflammatory response
cellular response to IFNγ
regulation of TNF superfamily cytokine production
TNF production
T cell activation
Leukocyte chemotaxis
cellular response to DNA damage stimulus
regulation of T cell activation
type I IFN production
response to ROS
regulation of type I IFN production
T cell proliferation
actin filament-based movement
EMT transition
integrin-mediated signaling pathway
p.adj < 0.05
q.value < 0.05
Normalized Enrichment Score
H
RTFAK.CAF vs. myCAF
KRAS_SIGNALING_DN
p.value < 0.05
I
RTFAK.CAF vs. myCAF
MsigDb_H
CHOLESTEROL_HOMEOSTASIS
PI3K_AKT_MTOR_SIGNALING
FATTY_ACID_METABOLISM
DNA_REPAIR
P53_PATHWAY
MYC_TARGETS_V1
MYC_TARGETS_V2
Gene Ratio
J
RTFAK.CAF vs. myCAF
MsigDb_PID
AP1_PATHWAY
ATF2_PATHWAY
MYC_PATHWAY
MAPK_TRK_PATHWAY
GMCSF_PATHWAY
PI3KCI_AKT_PATHWAY
TGFβR_PATHWAY
FAK_PATHWAY
VEGFR1_2_PATHWAY
MYC_ACTIV_PATHWAY
PDGFRβ_PATHWAY
Gene Ratio
K
CAFs
% pSTAT1⁺ CAFs (out of total CAFs)
Vehicle
RT + FAKi
Hema
CK19
PDPN
pSTAT1

Figure 2.11: FAKi alters CAFs to participate in tumor immunity

(A) UMAP dimensionality reduction plot of scRNAseq data on $CD45^-$ $CD31^-$ $Epcam^-$ $PDPN^+$ FACS-sorted CAFs-enriched from KPC mice treated with vehicle or RT +/- VS-4718 (FAKi) as depicted in **Fig. 2.7A**. Annotation shows different cell types. **(B-C)** UMAP distribution from (A) split by treatment conditions (B) and count ratio of the CAF clusters (C). **(D-E)** Analysis of αSMA (a marker of myCAFs) (D) and collagen content (E) on tissues from KPC mice (n = at least 7 mice/group). Representative αSMA IHC and Sirius Red images are depicted. **(F-G)** Dot plot displaying Gene Set Enrichment Analysis (GSEA) results from MsigDb_Hallmark (F) and GO (G-H) databases CAFs in (A). All graphs displayed comparisons of myCAFs from Vehicle mice to all FAK-CAFs # 1-3 from FAKi-treated mice. All pathways were filtered with p value < 0.05. **(H-J)** Dot plot displaying Gene Set Enrichment Analysis (GSEA) results from MsigDb_Hallmark (H) and bar graphs displaying overrepresentation analysis of DEGs on CAFs in (A) to known biological functions in MsigDb_Hallmark (I) and MsigDb_PID (J) databases. All graphs displayed comparisons of myCAFs from Vehicle mice to all RTFAK-CAFs from RT+FAKi-treated mice. All pathways were filtered with p value < 0.05. **(K)** mIHC analysis of $CK19^+$ $PDPN^+$ $pSTAT1^+$ cells from KPC mice from **Fig. 2.7A**. Representative CK19, PDPN, and pSTAT1 fused mIHC images are depicted. n = at least 6 mice/group.

All graphs depict mean +/- SEM. * denotes p < 0.05 by two-tailed t-test or one-way ANOVA as appropriate.

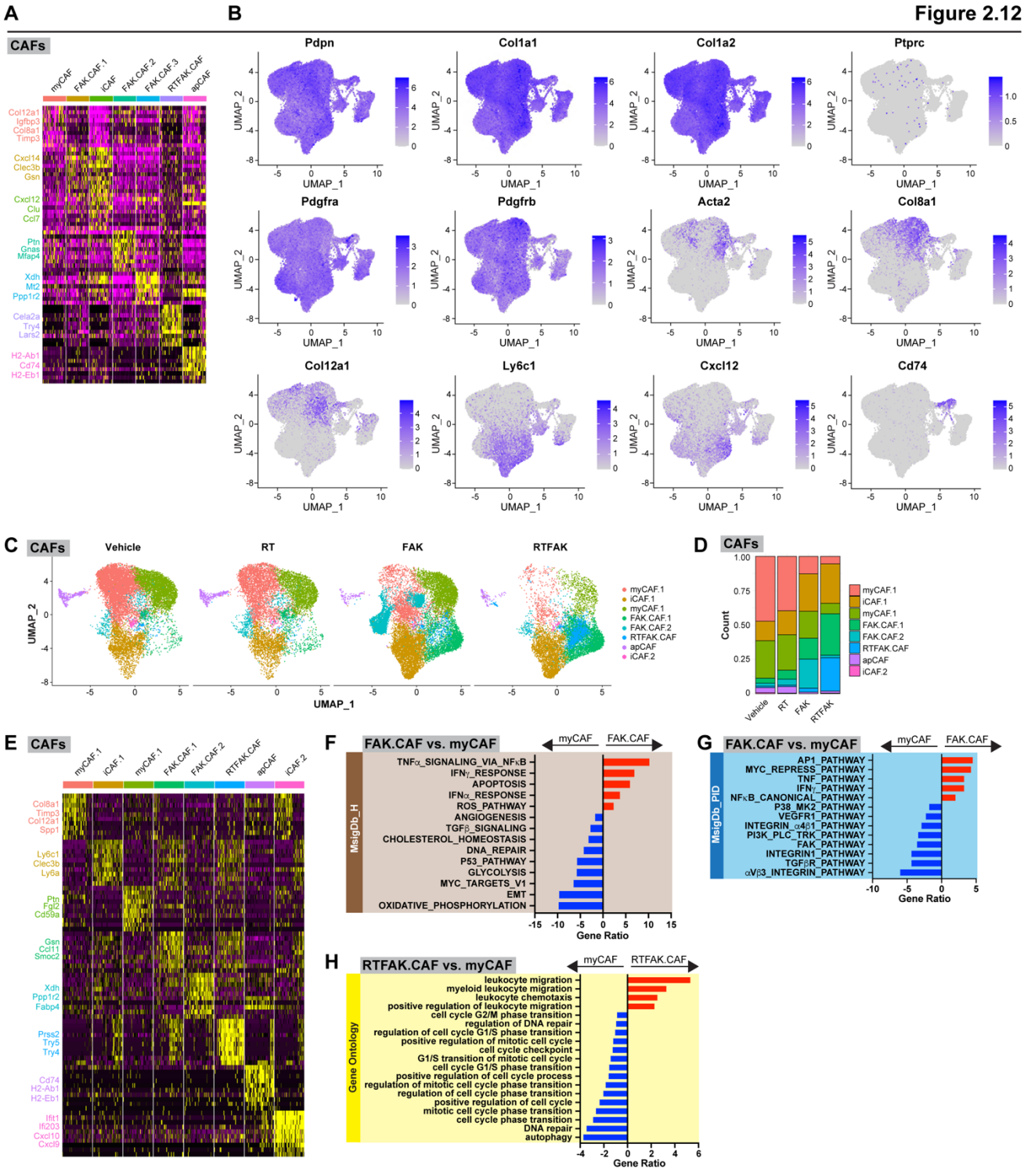
A
CAFs
myCAF
FAK.CAF.1
iCAF
FAK.CAF.2
FAK.CAF.3
RTFAK.CAF
apCAF
Col12a1
Igfbp3
Col8a1
Timp3
Cxcl14
Clec3b
Gsn
Cxcl12
Clu
Ccl7
Ptn
Gnas
Mfap4
Xdh
Mt2
Ppp1r2
Cela2a
Try4
Lars2
H2-Ab1
Cd74
H2-Eb1
B
Pdpn
Col1a1
Col1a2
Ptprc
Pdgfra
Pdgfrb
Acta2
Col8a1
Col12a1
Ly6c1
Cxcl12
Cd74
UMAP_1
UMAP_2
C
CAFs
Vehicle
RT
FAK
RTFAK
myCAF.1
iCAF.1
myCAF.1
FAK.CAF.1
FAK.CAF.2
RTFAK.CAF
apCAF
iCAF.2
D
CAFs
Count
Vehicle
RT
FAK
RTFAK
E
CAFs
Col8a1
Timp3
Col12a1
Spp1
Ly6c1
Clec3b
Ly6a
Ptn
Fgl2
Cd59a
Gsn
Col1
Smoc2
Xdh
Ppp1r2
Fabp4
Prss2
Try5
Try4
Cd74
H2-Ab1
H2-Eb1
Ifit1
Ifi203
Cxcl10
Cxcl9
F
FAK.CAF vs. myCAF
myCAF
FAK.CAF
MsigDb_H
TNFα_SIGNALING_VIA_NFκB
IFNγ_RESPONSE
APOPTOSIS
IFNα_RESPONSE
ROS_PATHWAY
ANGIOGENESIS
TGFβ_SIGNALING
CHOLESTEROL_HOMEOSTASIS
DNA_REPAIR
P53_PATHWAY
GLYCOLYSIS
MYC_TARGETS_V1
EMT
OXIDATIVE_PHOSPHORYLATION
Gene Ratio
G
FAK.CAF vs. myCAF
myCAF
FAK.CAF
MsigDb_PID
AP1_PATHWAY
MYC_REPRESS_PATHWAY
TNF_PATHWAY
IFNγ_PATHWAY
NFκB_CANONICAL_PATHWAY
P38_MK2_PATHWAY
VEGFR1_PATHWAY
INTEGRIN_α4β1_PATHWAY
PI3K_PLC_TRK_PATHWAY
FAK_PATHWAY
INTEGRIN1_PATHWAY
TGFβR_PATHWAY
αVβ3_INTEGRIN_PATHWAY
Gene Ratio
H
RTFAK.CAF vs. myCAF
myCAF
RTFAK.CAF
Gene Ontology
leukocyte migration
myeloid leukocyte migration
leukocyte chemotaxis
positive regulation of leukocyte migration
cell cycle G2/M phase transition
regulation of DNA repair
regulation of cell cycle G1/S phase transition
positive regulation of mitotic cell cycle
cell cycle checkpoint
G1/S transition of mitotic cell cycle
cell cycle G1/S phase transition
positive regulation of cell cycle process
regulation of mitotic cell cycle phase transition
regulation of cell cycle phase transition
positive regulation of cell cycle
mitotic cell cycle phase transition
cell cycle phase transition
DNA repair
autophagy
Gene Ratio

Figure 2.12: FAKi alters CAFs to participate in tumor immunity

(A) Heatmap displaying top 10 genes of different CAFs in **Fig. 2.11A**. **(B)** Feature plots of known CAF marker genes superimposed onto UMAP in **Fig. 2.11A**. **(C)** UMAP dimensionality reduction plot of scRNAseq data on the same cells in **Fig. 2.11A** when Harmony integration was included in analysis. Annotation shows different cell types. **(D)** Count ratio of the CAF clusters in (B). **(E)** Heatmap displaying top 10 genes of the different CAFs in (B). **(F-G)** Bar graphs displaying overrepresentation analysis of DEGs on CAFs in **Fig. 2.11A** to known biological functions in MsigDb_Hallmark (F) and MsigDb_PID (G) databases. All graphs displayed comparisons of myCAFs from Vehicle mice to all FAK-CAFs # 1-3 from FAKi-treated mice. All pathways were filtered with p value < 0.05. **(H)** Bar graph displaying overrepresentation analysis from GO database. All graphs displayed comparisons of myCAFs from Vehicle mice to all RTFAK-CAFs from RT+FAKi-treated mice. All pathways were filtered with p value < 0.05.

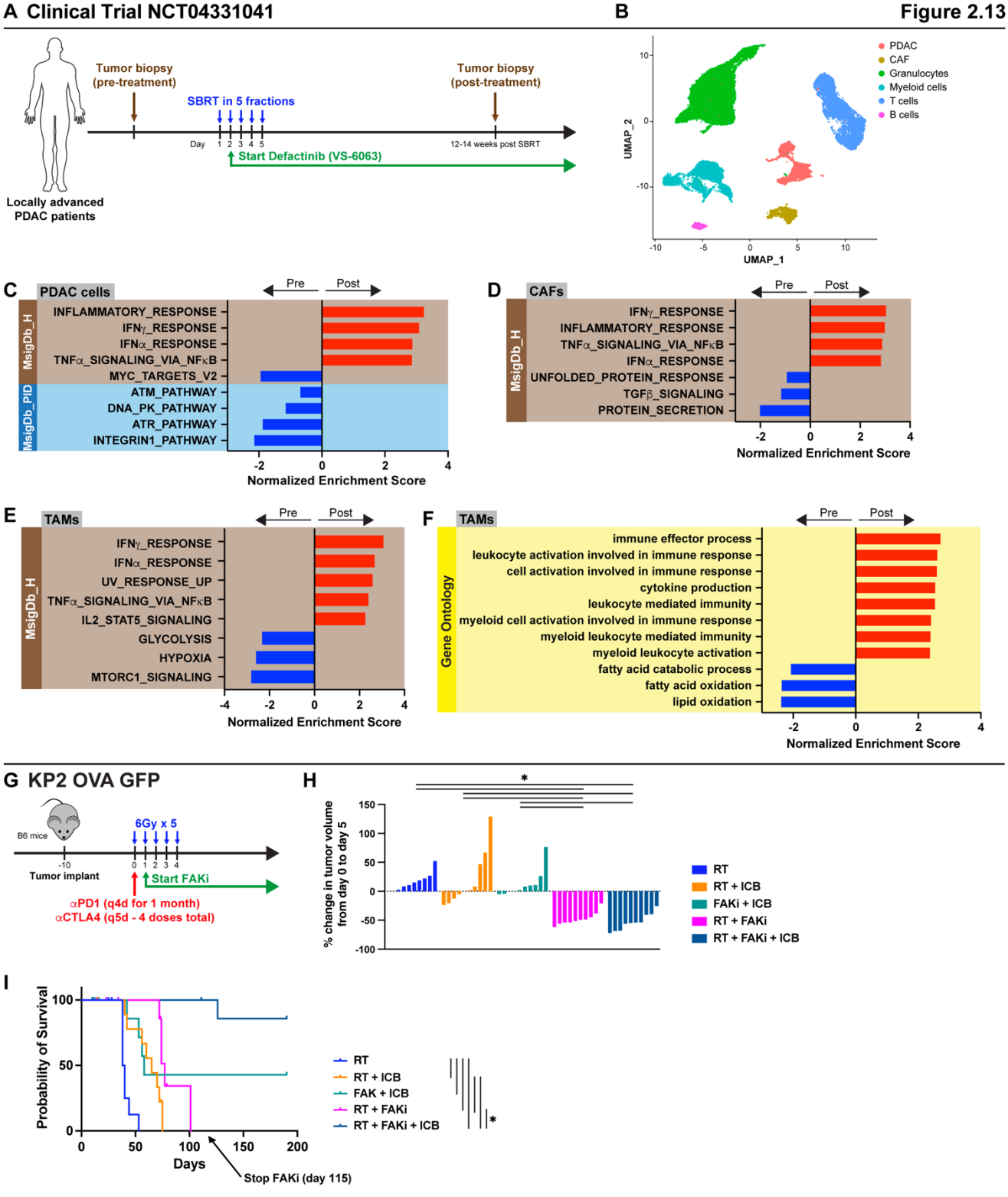
A Clinical Trial NCT04331041
B
Figure 2.13
Tumor biopsy (pre-treatment)
SBRT in 5 fractions
Day 1 2 3 4 5
Tumor biopsy (post-treatment)
12-14 weeks post SBRT
Start Defactinib (VS-6063)
Locally advanced PDAC patients
PDAC
CAF
Granulocytes
Myeloid cells
T cells
B cells
UMAP_1
UMAP_2
C
PDAC cells
Pre
Post
MsigDb_H
INFLAMMATORY_RESPONSE
IFNγ_RESPONSE
IFNα_RESPONSE
TNFα_SIGNALING_VIA_NFκB
MYC_TARGETS_V2
MsigDb_PID
ATM_PATHWAY
DNA_PK_PATHWAY
ATR_PATHWAY
INTEGRIN1_PATHWAY
Normalized Enrichment Score
D
CAFs
MsigDb_H
IFNγ_RESPONSE
INFLAMMATORY_RESPONSE
TNFα_SIGNALING_VIA_NFκB
IFNα_RESPONSE
UNFOLDED_PROTEIN_RESPONSE
TGFβ_SIGNALING
PROTEIN_SECRETION
Normalized Enrichment Score
E
TAMs
MsigDb_H
IFNγ_RESPONSE
IFNα_RESPONSE
UV_RESPONSE_UP
TNFα_SIGNALING_VIA_NFκB
IL2_STAT5_SIGNALING
GLYCOLYSIS
HYPOXIA
MTORC1_SIGNALING
Normalized Enrichment Score
F
TAMs
Gene Ontology
immune effector process
leukocyte activation involved in immune response
cell activation involved in immune response
cytokine production
leukocyte mediated immunity
myeloid cell activation involved in immune response
myeloid leukocyte mediated immunity
myeloid leukocyte activation
fatty acid catabolic process
fatty acid oxidation
lipid oxidation
Normalized Enrichment Score
G KP2 OVA GFP
B6 mice
6Gy x 5
Tumor implant
Start FAKi
αPD1 (q4d for 1 month)
αCTLA4 (q5d - 4 doses total)
H
% change in tumor volume from day 0 to day 5
RT
RT + ICB
FAKi + ICB
RT + FAKi
RT + FAKi + ICB
I
Probability of Survival
Days
RT
RT + ICB
FAK + ICB
RT + FAKi
RT + FAKi + ICB
Stop FAKi (day 115)

Figure 2.13: FAK inhibition in combination with RT in PDAC patients activates interferon signaling

(A) Schematic of clinical trial (NCT04331041). Patients received SBRT with a total of 50Gy given in 5 fractions. VS-6063 was given at a dose of 400mg BID starting the end of day 2 post-SBRT and continued up to one year. Tissues were obtained pre-treatment and after 12-14 weeks post-SBRT. **(B)** UMAP analysis of six pre- and post-treatment biopsies from (A). **(C)** Bar graph displaying GSEA analysis of DEGs on all the PDAC cells in (B) to known biological functions in MsigDb_Hallmark and MsigDb_PID databases. All graphs displayed comparisons of pre-treatment to post-treatment biopsies. All pathways were filtered with p value < 0.05. **(D)** Bar graph displaying GSEA analysis of DEGs on all the CAFs in (B) to known biological functions in MsigDb_Hallmark database. All graphs displayed comparisons of pre-treatment to post-treatment biopsies. All pathways were filtered with p value < 0.05. **(E-F)** Bar graphs displaying GSEA analysis of DEGs on all the TAMs in (B) to known biological functions in MsigDb_Hallmark (E) and GO (F) databases. All graphs displayed comparisons of pre-treatment to post-treatment biopsies. All pathways were filtered with p value < 0.05. **(G)** Schematic of RT (6Gy x 5), FAKi (75mg/kg bid), and ICB (αPD1, 200μg and αCTLA4, 200μg) administration in B6 KP2-OVA-GFP tumor-bearing mice. Mice were treated and longitudinally assessed for tumor burden. **(H)** Waterfall plot of KP2-OVA tumor-bearing mice from (E) evaluating tumor growth difference from Day 0 to Day 5. n = 10 mice/group. **(I)** Kaplan-Meier survival curve for KP2-OVA mice from (A). n = 10 mice/group.

For comparison between multiple groups, * denotes p < 0.05 by two-tailed t-test, one-way ANOVA, or Kaplan-Meyer as appropriate.

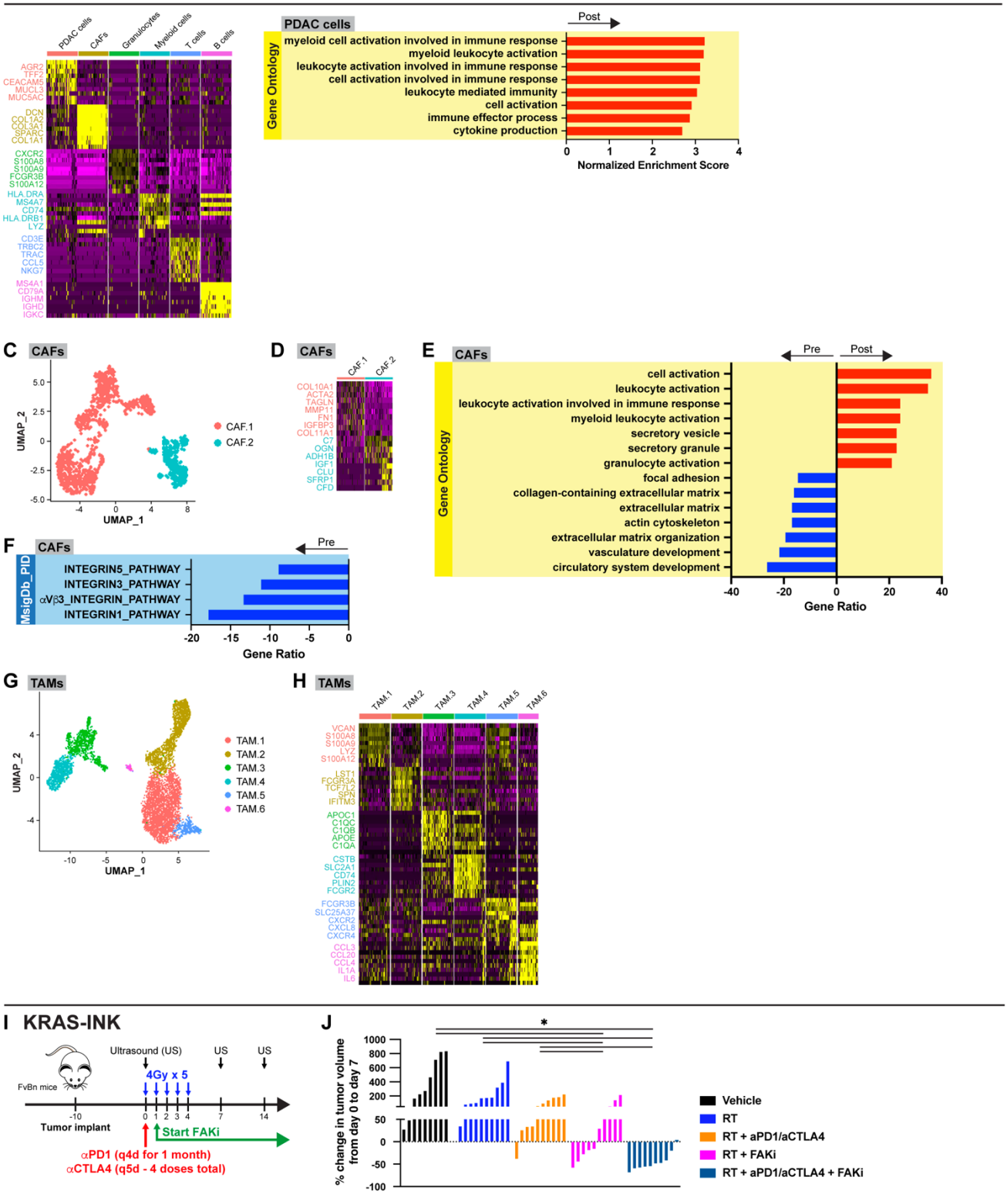
A Clinical Trial
B
PDAC cells
CAFs
Granulocytes
Myeloid cells
T cells
B cells
Post
Gene Ontology
myeloid cell activation involved in immune response
myeloid leukocyte activation
leukocyte activation involved in immune response
cell activation involved in immune response
leukocyte mediated immunity
cell activation
immune effector process
cytokine production
Normalized Enrichment Score
C CAFs
UMAP_1
UMAP_2
CAF.1
CAF.2
D CAFs
E CAFs
Pre
Post
cell activation
leukocyte activation
leukocyte activation involved in immune response
myeloid leukocyte activation
secretory vesicle
secretory granule
granulocyte activation
focal adhesion
collagen-containing extracellular matrix
extracellular matrix
actin cytoskeleton
extracellular matrix organization
vasculature development
circulatory system development
Gene Ratio
F CAFs
MsigDb_PID
INTEGRIN5_PATHWAY
INTEGRIN3_PATHWAY
αVβ3_INTEGRIN_PATHWAY
INTEGRIN1_PATHWAY
Gene Ratio
G TAMs
TAM.1
TAM.2
TAM.3
TAM.4
TAM.5
TAM.6
H TAMs
I KRAS-INK
FvBn mice
Ultrasound (US)
4Gy x 5
Tumor implant
Start FAKi
αPD1 (q4d for 1 month)
αCTLA4 (q5d - 4 doses total)
J
% change in tumor volume from day 0 to day 7
Vehicle
RT
RT + aPD1/aCTLA4
RT + FAKi
RT + aPD1/aCTLA4 + FAKi

Figure 2.14: Human PDAC patients and checkpoint blockade

(A) Heatmap displaying top 10 genes of different cell clusters in **Fig. 2.13B**. **(B)** Bar graph displaying GSEA analysis of DEGs on all the PDAC cells in **Fig. 2.13B** to known biological functions in GO database. All graphs displayed comparisons of pre-treatment to post-treatment biopsies. All pathways were filtered with p value < 0.05. **(C)** UMAP analysis of CAFs isolated from **Fig. 2.13B**. **(D)** Heatmap displaying top 10 genes of different cell clusters in (C). **(E-F)** Bar graph displaying Over Representation analysis of DEGs on all the CAFs in **Fig. 2.13B** to known biological functions in GO (E) and MsigDb_PID (F) databases. All graphs displayed comparisons of pre-treatment to post-treatment biopsies. All pathways were filtered with p value < 0.05. **(G)** UMAP analysis of TAMs isolated from **Fig. 2.13B**. **(H)** Heatmap displaying top 10 genes of different cell clusters in (G). **(I)** Schematic of RT (4Gy x 5), FAKi (75mg/kg bid), and ICB (αPD1, 200μg and αCTLA4, 200μg) administration and tumor burden monitoring in KRAS-INK orthotopic tumor-bearing mice. Mice were treated and longitudinally assessed for tumor burden by US. **(J)** Waterfall plot of KRAS-INK tumor-bearing mice from (D) evaluating tumor growth difference from Day 0 to Day 7 by US measurement. n = 10 mice/group.

For comparisons between multiple groups * denotes p < 0.05 by one-way ANOVA or two-tailed t-test as appropriate.

2.5. Methods

Genetic mice and other models

p48-Cre/LSL-Kras^{G12D}/p53$^{Flox/Flox}$ (KPC) and p48-Cre/LSL-Kras^{G12D}/p53$^{Flox/Flox}$/OVA-GFP^{+} (KPC-OG) mice used in these studies were bred to C57Bl/6J background and verified by congenic markers. The generation and studies entailing the details of the KPC-OG mouse were published by our lab[24]. KPC and KPC-OG mice were enrolled for treatment studies when the first >0.5 cm tumor was detected by biweekly palpation corroborated by ultrasound measurement. Thereafter, tumor size was assessed weekly by ultrasound (SonoSite m-Turbo). Survival events were scored when mice lost >15% body weight, tumor burden reached >1.8 cm in diameter, moribund appearance, severe cachexia, or per absolute survival. For all studies, care was taken to include negative littermates as well as sex- and age-match in the same experimental setup.

LSL-Kras^{G12D}/p53$^{Flox/Flox}$/OVA-GFP^{+} mice, littermates of KPC-OG mice, were injected with Adenoviral-Cre at 8-10 weeks old of age which generated sarcoma GEMMs (KPS-OG) 7-8 weeks post inoculation. Tumor size was assessed by caliper measurement for randomization.

Human subjects

All human PDAC tissues were obtained under informed consent from patients. Washington University Ethics committee approved the study under institutional review board protocol #201108117 and #201704078 and clinical trial NTC04331041.

Cell lines

3D organoid cell lines (KPOG) were derived from tumor-bearing female KPC-OG mice. *Kras-Ink* or KI cells used in certain orthotopic transplant experiments were derived from Pdx1-Cre/LSL-Kras^{G12D}/Ink/Arf$^{Flox/Flox}$ mice in Dr. Hanahan's laboratory (EPFL, Lausanne). KP2 cells were derived from PDAC tumor tissue obtained from 6-month-old p48-Cre/LSL-KrasG12D/p53$^{Flox/+}$ mice, which were screened for C57BL/6 identity. Cells were grown out on collagen-coated plastic for <12 passages and were tested for CK19, αSMA, Vimentin and CD45 to verify their identity and purity. KP2-OVA-GFP cells were derived from tumor-bearing female KPC-OG, which were used in certain syngeneic subcutaneous experiments.

Three independent WT pancreatic fibroblast primary cell lines were derived from WT C57Bl/6J background mice. Pancreas was harvested (detailed below) and plated on tissue culture flasks under standard antibiotics and the addition of Gentamycin and Amphotericin B. No additional growth factors were supplemented in culture media. After ~3 passages, the culture was composed of pure fibroblasts only. For organoid growth studies, only fibroblasts with passage <10 were used. Fibroblast purity was tested by flow cytometry for PDPN as a pan-marker of fibroblasts. All cell lines were tested negative for mycoplasma.

Tumor cell suspension derived after tumor harvest (detailed below) was plated on collagen-coated tissue culture flasks under standard antibiotics for the generation of 2D cell culture. Cell suspension derived after tumor harvest (detailed below) was plated on Matrigel (Cultrex® Organoid Qualified BME, Type 2) dome under standard antibiotics for the generation of 3D organoid cell culture. Protocol for the generation of 3D organoid cell

culture was adapted from Dr. Tuveson's laboratory (Cold Spring Harbor Laboratory)[293]. GFP^+ tumor cells were sorted on FACSAria-II (BD Biosciences), and re-plated in complete medium until stable cell lines were established. All 2D cell lines were cultured in complete medium (DMEM-F12 with 10% FBS and 1% PenStrep) at 37° C and 5% CO_2. All 3D cell lines were cultured in complete medium (Advanced DMEM-F12 with 1% HEPES, 1% L-glutamine, and 1% PenStrep) at 37°C and 5% CO_2. All cell lines were passaged <6 times and were tested positive for cytokeratin-19, and negative for smooth muscle actin and vimentin to verify their carcinoma identity and purity. All cell lines were tested negative for mycoplasma using 2 independent commercial kits (Sigma and Lonza).

Tissue harvest

Mice were euthanized by trans-cardiac perfusion using 15 mL of PBS-heparin under isoflurane anesthesia. When taken for histology, tumor tissues were fixed in 10% neutral-buffered formalin overnight at 4°C. When taken for cellular assays, tumor tissues or respective lymph nodes were manually minced and digested in 20 mL of sterile 1X HBSS (Thermo Fisher) containing 2 mg/mL of collagenase A (Roche) and 1X DNase-I (Sigma) for 30 min at 37°C with constant stirring. Digestion was quenched in 5 mL of sterile fetal bovine serum (FBS, Atlanta Biologicals) filtered through 40 μm Nylon mesh, pelleted through centrifugation (2000 RPM for 5 min at 4°C), and resuspended in required media/buffer as single cell suspensions.

Orthotopic and syngeneic implantations

Age-matched 6–8-week-old female C57BL/6 and FVB/NJ mice were used for orthotopic/transplantable mouse models. Syngeneic orthotopic PDAC tumors were established by surgical implantation, as previously described[214]. To establish orthotopic models, 100,000 cells in 50 µL of Cultrex (Trevigen) were injected into the pancreas of sex-matched C57BL/6 or FVB/NJ mice as previously described[294]. Cohorts of mice were randomized into different treatment groups by gross tumor diameter using thrice-weekly palpation, external caliper measurement, and ultrasound measurement. To establish subcutaneous models, 250,000 cells in 50 µL of Cultrex (Trevigen) were injected into the mammary fat pad of sex-matched C57BL/6 mice as previously described. Cohorts of mice were randomized into different treatment groups by gross tumor diameter using thrice-weekly external caliper measurement.

Pharmacologic inhibitors

FAKi (VS-4718), provided by Verastem, Inc., is a selective bispecific inhibitor with activity against FAK1/PTK2 and Pyk2/PTK2b kinases. Cell-based assays have determined it has biochemical half-maximal inhibitory concentrations (IC_{50}) of 6.0 nM and 20 nM for FAK and Pyk2. For animal experiments, 75mg/kg VS-4718 was formulated in vehicle (0.5% carboxymethyl cellulose and 0.1% Tween-80 (Sigma-Aldrich) in sterile water) and administered by oral gavage twice a day. For *in-vitro* studies 0.25, 0.5, or 1.0 µM of VS-4718 in DMSO was used.

Radiation therapy

Mice received Radiation Therapy (RT) as five daily hypofractionated doses (6Gy x 5) using the Small Animal Radiation Research Platform (SARRP200, XStrahl Life Sciences). Mice were injected i.p. with an iodine contrast agent (2100mg/kg) before being placed on the irradiation platform one at a time under isoflurane anesthesia. Conebeam computed tomography (CT) imaging was performed for each individual mouse to pinpoint the pancreas, images were imported into Muriplan and used to select an isocenter. The tumor was then irradiated using anterior-posterior-opposed beams using either the 5mm x 5mm or 10mm x 10mm collimator at a dose rate of 3.9 Gy/min. Mice were monitored over 2 weeks for signs of radiation sickness or weight-loss. DietGel recovery gel was provided for 14-day window immediately following radiation therapy in survival studies.

For *in-vitro* radiation experiments, RS2000 160kV X-ray Irradiator using a 0.3 mm copper filter (Rad Source Technologies) was used.

Immunotherapeutic antibodies

For immunotherapy regimen, 250 µg of agonist antibodies (α-CTLA4 clone UC10-4F10-11; α-PD1 clone RMP1-14; BioXCell) were given by intraperitoneal (i.p.) injection; α-PD1 was given every 4 days for a total of 30 days and α-CTLA4 was given every 5 days for a total of 4 doses from beginning of treatment. Treatments were discontinued after 30 days to prevent α-rat IgG reaction.

Organoid cultures

3D organoid cell lines derived from KPC-OG mice, called KPOG, were passaged in Cultrex® Organoid Qualified BME, Type 2. Pancreatic fibroblasts were derived from

C57Bl/6J mice. Organoid cells (~50 structures in a dome of 50μL of Cultrex® Organoid Qualified BME, Type 2) were cultured with or without 10^5 pancreatic fibroblasts per dome. Collagen-I concentrations (1.0 mg/mL) were modulated in the ECM matrix. One day post organoid culture preparation, organoid cultures were treated with FAKi at varying dose concentrations. Two hours post FAKi treatment, culture was treated with radiation.

All organoid experiments were done in 24-well tissue culture treated plates. At least n=3/group was used for statistical power analysis. KPOG organoid growth was monitored using the GFP marker. Fluorescence images were taken using Nikon AZ100 microscope daily and images were analyzed using Metamorph and HALO imaging software for analyses.

Immunohistochemical staining

Tissues were fixed in 10% neutral formalin for 18-24 hours, embedded in paraffin after graded-ethanol dehydration, and sectioned into 5-μm sections using a microtome. Where applicable, formalin-fixed, paraffin embedded (FFPE) tissue sections were stained for Hematoxylin & Eosin (Thermo Fisher), Picro-Sirius Red (Sigma-Aldrich) and Masson's Trichrome (Diagnostic Biosystems) according to manufacturer's instructions. Automated staining of tissues was carried out on the Bond RX^m (Leica Biosystems) following dewaxing and appropriate antigen retrieval. Immunostaining was chromogenically visualized using the Bond Polymer Refine Detection alone or in conjunction with Bond Intense R Detection Systems (DS9263, Leica Biosystems). Slides were dehydrated through graded ethanol, followed by xylene, then mounted using Xylene-based Cytoseal (Thermo Fisher) or Vectamount (Vector Labs) as appropriate.

Staining was performed with the following antibodies: αSMA (Abcam ab5694), Podoplanin (Biolegend 127402), Ki67 (Abcam ab15580), BrdU (Abcam ab2284), CC3 (Cell Signaling 9661S), Cytokeratin 19 (DSHB TROMA-III), Cytokeratin 17/19 (Cell Signaling 12434S), CD8α (Cell Signaling 98941), pSTAT1 (Cell Signaling 8826s), CD4 (Abcam ab183685), Foxp3 (eBioscience 14-5773-82), γH2Ax (Cell Signaling 9718S).

Flow cytometry

Following tissue digestion, single cell suspensions were resuspended in flow cytometry buffer (PBS containing 1% BSA and 5 mM EDTA), FcR blocked with rat α-mouse CD16/CD32 antibodies (EBioscience) for 10 min and pelleted by centrifugation. Where applicable, $CD8^+$ T cells specific for antigen OVA were labeled by incubating cell suspension with H2Kb::SIINFEKL-specific MHCI dextramer (1:5; Immudex protocol) for 10 min at room temperature prior to extracellular staining. Cells were consequently labeled with 100 µL of fluorophore-conjugated α-mouse extracellular antibodies at recommended dilutions for 25 min on ice. Intracellular staining for intracellular markers was conducted subsequently using the EBioscience Transcription Factor Staining buffer set, according to manufacturer's instructions. All antibodies are listed in Key Resources Table. FCS Data were acquired on BD Fortessa X-20 (BD Biosciences) within 3-4 days and analyzed using FlowJo software (v10).

Staining was performed with the following antibodies: CD45 (eBioscience 25-0451), CD45 (BD Biosciences 564225), CD3ε (eBioscience 17-0031-82), CD11b (eBioscience 56-0112-82), MHC-II (eBioscience 48-5321-82), Ly6G (Biolegend 127608), Ly6C (eBioscience 45-5932), F4/80 (eBioscience 15-4801-82), CD11c (eBioscience 47-0114-

82), CD24 (eBioscience 11-0241-82), CD24 (eBioscience 11-0242-82), CD103 (Biolegend 121423), CD8α (BD Biosciences 563786), CD8α (BD Biosciences 562283), CD4 (eBioscience 11-0043-82), CD62L (Biolegend 104437), CD44 (eBioscience 48-0441-82), PD1 (eBioscience 12-9985-82), Tim3 (Biolegend (119715), Ki67 (eBioscience 50-5698-82), Foxp3 (eBioscience 35-5773-82), MHC-I (eBioscience 11-5998-82), B220 (Biolegend 103212), SIINFEKL Dextramer (Immudex JD2163).

Mass cytometry

Tumor samples were digested in HBSS supplemented with 2mg/ml collagenase A (Roche), 2.5U/ml hyaluronidase and DNase I at 37C for 30 min with agitation to generate single-cell suspensions. Cell suspensions were counted and stained in 5 μM cisplatin per million cells for exactly 3 min on ice and washed with Cy-FACS buffer (PBS, 0.1% BSA, 0.02% NaN_3, 2 mM EDTA) twice. Cells were incubated with FcR blocking reagent plus surface-antibody cocktail for 40 min on ice. After incubation, surface-marker stained cells were washed twice with Cy-FACS buffer. Cells were then fixed with 4% PFA for 10 min on ice and permeabilized with permeabilization buffer (Invitrogen) for 40 min containing the intracellular stain cocktail. All antibodies are listed in Key Resources Table. Cells were then washed twice with PBS and stained with 200 μl of DNA intercalator per million cells. Cells were acquired on a CyTOF2 mass cytometer (Fluidigm) and data were uploaded to Cytobank for further analysis. Events were gated on singlets, live, and $CD45^+$. A maximum of 100,000 events were then visualized using standard t-SNE algorithm. Populations of interest were manually gated and verified based on lineage marker-expression.

Staining was performed with the following antibodies: CD45 (Fluidigm 3089005B), CD90 (Biolegend 105202), CD11c (Fluidigm 3142003B), CD68 (Biolegend 137001), MHC-I (Fluidigm 3144016B), CD206 (Biolegend 141702), F4/80 (Fluidigm 3146008B), MHC-II (Biolegend 107602), CD11b (Fluidigm 3148003B), CD172α/SIRPα (Biolegend 144002), Ly6C (Fluidigm 3150010B), Ly6G (Fluidigm 3151010B), CD64 (Biolegend 139301), XCR1 (Biolegend 148202), CD103 (Biolegend 121402), NK1.1 (BioXcell BE0036), Bst2 (Novous/imgenx DDX0390P-100), IRF4 (Biolegend 646402), CD83 (Thermofisher Scientific 14-0831-82), CD40 (Fluidigm 124601), Ox40L (Biolegend 108802), CCR2 (RnD systems MAB55381-100), Cx3CR1 (Fluidigm 3164023B), CCR7 (Biolegend 120101), PDL2 (BioXCell BE0112), VISTA (Biolegend 150202), Tim3 (BioXcell BE0115), PDL1 (BioXCell BE0101), CD80 (Biolegend 104702), CD135/FLT3 (Thermofisher Scientific 14-1351-82), CD86 (Fluidigm 3172016B), Tim4 (Biolegend 130002), B220 (Fluidigm 3144011B), CD44 (Leinco C382), GITR (BioXcell BE0063), CD25 (Leinco C1194), CD38 (eBioscience 14-0381-82), CD90 (Biolegend 105202), Lag3 (Leinco L306), CD27 (eBioscience 50-124-94), KLRG1 (Bioxcell BE0201), CD103 (Biolegend 121402), CD4 (BioXcell BE0003-1), CD45 (Fluidigm 3089005B), CD62L (Leinco C2118), ICOS (eBioscience 14-9949-82), OX-40 (BioXcell BE0031), PD-1 (eBioscience 14-9981-82), TIGIT (BioXcell BE0274), CD69 (eBioscience 14-0691-82), TCRβ (BioXcell BE0102), CD127 (BioXcell BE0065), CD39 (Biolegend 143802), NK1.1 (BioXcell BE0036), CD8α (Leinco C375), TCRγδ (eBioscience 14-5711-82), Tim3 (BioXcell BE0115), H2-Kb OVA (WUSTL CHiiPs core), Ki67 (Novus NBP2-22112), Foxp3 (eBioscience 14-5773-82), GATA3 (eBioscience 14-9966-82), Granzyme B (eBioscience

MA1-80734), CTLA-4 (eBioscience 50-129-16), TCF1 (R&D MAB8224), ROR-γt (eBioscience 14-6988-82), Eomes (eBioscience 50-245-556), T-bet (Biolegend 644802).

Western immunoblot

Cell lysates were harvested using radioimmunoprecipitation assay (RIPA) lysis buffer [25 mM Tris-HCl pH 7.5, 150 mM NaCl, 1% NP-40, 0.5% DOC, 0.1% SDS] supplemented with protease and phosphatase inhibitors (Roche). Cell lysates were resolved in Tris-glycine sodium dodecyl sulfate/polyacrylamide gel electrophoresis (SDS/PAGE) gels and transferred to polyvinylidene difluoride (PVDF) membranes (Invitrogen). After blocking in 1X TBST buffer with 5% w/v BSA, membranes were probed with primary antibodies overnight at 4°C. Membranes were washed thrice in 1X TBST and probed with HRP-conjugated secondary antibody for 1 hour at RT. Membranes were developed with Pierce ECL Western Blotting Substrates and detected using a ChemiDoc XRS+ system (Bio-Rad).

Staining was performed with the following antibodies: β-actin (Cell Signaling 4970), p-IRF3 (Cell Signaling 29047S), IRF3 (Cell Signaling 4302S), STING (Cell Signaling 13647S), γH2Ax (Cell Signaling 9718S).

RNA and cDNA isolation

Total RNA was extracted from live cultured cells using an E.Z.N.A.® Total RNA kit (OMEGA) according to manufacturer's instructions and banked in -80° C until use. cDNA for downstream applications were synthesized using qScript cDNA SuperMix kit (QuantaBio) according to manufacturer's instructions.

RNA sequencing and analysis

RNA samples from treated KPOG organoid cultures were prepared according to kit manufacturer's protocol, ribo-depleted using RiboZero protocol and subsequently indexed, pooled, and sequenced on HiSeq 3000 (Illumina) at the Genome Technology Access Center (GTAC), Washington University. Differential expression analysis of normalized counts (after standard base calling and demultiplexing) was performed to analyze for differences between conditions and the results were filtered for only those genes with Benjamini-Hochberg FDR adjusted p values ≤ 0.05. For each contrast extracted with *Limma*, global perturbations in known Gene Ontology (GO) terms and KEGG pathways were detected using the R/Bioconductor package *GAGE* to test for changes in expression of the reported log2 fold-changes reported for each term versus the background log2 fold-changes of all genes found outside the respective term.

Mouse tissue single cell RNA (scRNA) sequencing data analysis

PDAC tissues were taken from Vehicle-treated, RT-treated, FAKi-treated, or RT+FAKi-treated KPC pancreatic tumor 14 days post treatment start. Cells were sorted into two samples: Immune cells ($CD45^+$) and CAFs ($CD45^-$ $CD31^-$ $Epcam^-$ $PDPN^+$) using Aria-II cell sorter (BD Biosciences). Each sample was generated from a pooled of 2-3 mice/treatment group. For a total of 4 treatment groups and 2 different cell types, we made 8 total libraries to be sequenced.

Sorted cells from each sample were encapsulated into droplets and libraries were prepared using Chromium Single Cell 3'v3 Reagent kits according to the manufacturer's

protocol (10x Genomics, Pleasanton, CA, USA). The generated libraries were sequenced by a NovaSeq 6000 sequencing system (Illumina, San Diego, CA, USA) to an average of 50,000 mean reads per cell. Cellranger mkfastq pipeline (10X Genomics) was used to demultiplex illumine base call files to FASTQ files. Files from the KPC tumors were demultiplexed with > 97% valid barcodes, and > 94% q30 reads. Afterwards, fastq files from each sample were processed with Cellranger counts and aligned to the mm10 reference (v.3.1.0, 10X Genomics, mouse reference mm10-2020-A from https://cf.10xgenomics.com/supp/cell-exp/refdata-gex-mm10-2020-A.tar.gz) to generate feature barcode matrix.

The filtered feature barcode matrices from were loaded into Seurat as Seurat objects (Seurat v4). For each Seurat object, genes that were expressed in less than 3 cells and cells that expressed less than 1000 or more than 6000 genes, were excluded. Cells with greater than 10% mitochondrial RNA content were also excluded. SCTransform with default parameters was used on each individual sample to normalize and scale the expression matrix against the sequence depths and percentages of mitochondrial genes (Hafemeister and Satija, 2019). Cell cycle scores and the corresponding cell cycle phase for each cell were calculated and assigned after SCTransform based on the expression signatures for S and G2/M genes (CellCycleScoring). The differences between the S phase score and G2/M score were regressed-out by SCTransform on individual samples. Variable features were calculated for each sample independently and ranked, based on the number of samples they were independently identified (SelectIntegrationFeatures). The top 3,000 shared variable features were used for multi-set canonical correlation analysis to reduce dimensions and identify projection vectors that defined shared

biological states among samples and maximized overall correlations across datasets. Multiple datasets were then integrated based using Harmony Integration (RunHarmony). Principle component analysis (PCA) was performed on the 3000 variable genes calculated earlier (function RunPCA). A UMAP dimensional reduction was performed on the scaled matrix using the first 30 PCA components to obtain a two-dimensional representation of cell states. Then, these defined 30 dimensionalities were used to refine the edge weights between any two cells based on Jaccard similarity (FindNeighbors), and were used to cluster cells through FindClusters functions, which implemented shared nearest neighbor modularity optimization. To characterize clusters, the FindAllMarkers function with logfold threshold = 0.25 and minimum 0.25-fold difference and MAST test was used to identify signatures alone with each cluster. Then, the TAMs, cDCs, and adaptive immune (B cells, T cells, NK cells, $\gamma\delta$T cells) were selected and top 3000 variable features were recalculated to re-cluster. Differently expressed genes (DEGs) between the two groups were calculated for each dataset with min.pct of 0.1 and logfc.threshold of 0.01 and MAST test (FindMarkers). Then the DEG lists from each dataset were filtered with p.value <0.05 and ranked based on foldchange. These ranked gene sets were fed into Gene Set Enrichment Analysis (GSEA) to test for GO terms, KEGG pathways, Reactome and Molecular Signatures Database (MSigDB) gene sets with FDR < 0.05 in ClusterProfiler (Wu et al., 2021).

Human sample single cell RNA (scRNA) sequencing data analysis

PDAC tissues were taken from patients using ultrasound-guided biopsies and details of the trial design are available on clincaltrials.gov (NCT04331041) and briefly here.

Patients received SBRT with a total of 50Gy given in 5 fractions. FAKi (VS-6063) was given at a dose of 400mg BID starting the end of day 2 post-SBRT and continued up to one year. Tissues were obtained pre-treatment and after 12-14 weeks post-SBRT. Biopsy tissues were processed and digested as described above. Following tissue digestion, processed cells from each sample were encapsulated into droplets and libraries using BD Rhapsody Single-Cell Capture and cDNA Synthesis Analysis System (BD Biosciences) according to the manufacturer's protocol. For a total of 6 pre- and post-treatment groups, we made 10 total libraries to be sequenced.

The generated libraries were sequenced by a NovaSeq 6000 sequencing system (Illumina, San Diego, CA, USA) to an average of 50,000 mean reads per cell. FASTQ files from each sample were processed and aligned with BD Rhapsody WTA Analysis Pipeline (SevenBridges) using reference genome (GRCh38-PhiX-gencodev29.tar.gz) to generate feature barcode matrix.

The filtered feature barcode matrices were loaded into Seurat as Seurat objects (Seurat v4). For each Seurat object, genes that were expressed in less than 3 cells and cells that expressed less than 1000 or more than 6000 genes, were excluded. Cells with greater than 25% mitochondrial RNA content were also excluded. Seurat NormalizeData and ScaleData with default parameters was used on each individual sample to normalize and scale the expression matrix against sequence depth and percentage of mitochondrial genes. Variable features were calculated for each sample independently and ranked based on the number of samples they were independently identified (FindVariableFeatures). The top 3000 shared variable features were used for multi-set canonical correlation analysis to reduce dimension and identify projection vectors that

define shared biological states among samples and maximize overall correlation across datasets. Multiple datasets were then integrated based using Harmony Integration (RunHarmony). Principle component analysis (PCA) was performed on the 3000 variable genes calculated earlier (function RunPCA). A UMAP dimensional reduction was performed on the scaled matrix using the first 30 PCA components to obtain a two-dimensional representation of cell states. Then, these defined 30 dimensionalities were used to refine the edge weights between any two cells based on Jaccard similarity (FindNeighbors), and were used to cluster cells through FindClusters functions, which implemented shared nearest neighbor modularity optimization. To characterize clusters, the FindAllMarkers function with logfold threshold = 0.25 and minimum 0.25-fold difference and MAST test was used to identify signatures alone with each cluster. Differently expressed genes (DEGs) between the two groups were calculated for each dataset with min.pct of 0.1 and logfc.threshold of 0.01 and MAST test (FindMarkers). Then the DEG lists from each dataset were filtered with p.value <0.05 and ranked based on foldchange. These ranked gene sets were fed into Gene Set Enrichment Analysis (GSEA) to test for GO terms, KEGG pathways, Reactome and Molecular Signatures Database (MSigDB) gene sets with FDR < 0.05 in ClusterProfiler (Wu et al., 2021).

Reverse Phase Protein Array (RPPA)

Cell extracts were lysed using (RIPA) lysis buffer [25 mM Tris-HCl pH 7.5, 150 mM NaCl, 1% NP-40, 0.5% DOC, 0.1% SDS] supplemented with protease and phosphatase inhibitors (Roche). Samples were then submitted to the MD Anderson Cancer Center for

the RPPA assay. The Functional Proteomics RPPA Core is supported by MD Anderson Cancer Center Support Grant # 5 P30 CA016672-40.

Image analysis

Whole-tissue scans at 10X or 20X magnification were obtained on a Zeiss Axio Scan Z1 brightfield/fluorescence Slide Scanner. Whole-tissue scans were analyzed with HALO software (Indica Labs) using Area quantification, Cytonuclear, or HighPlex modules. Where noted, grading was conducted by a trained pathologist in a blinded fashion and verified by principal investigator post-hoc.

Multiplex IHC (mIHC)

Serial staining was performed with multiple markers as indicated, adapted from a previously published study (Tsujikawa et al., 2017). FFPE tissue sections were loaded onto the BOND RX^m autostainer (Leica Biosystems) for iterative staining cycles for markers including CK19, CD8, CD4, Foxp3, PDPN, and pSTAT1. Slides were baked for 60 minutes and deparaffinized prior to the first cycle. Based on antibody host species, default manufacturer protocols and reagents were used up to labeling with HRP. Antigen labeling was chromogenically visualized with a ready-to-use AEC substrate (Abcam). Post-staining, the slides were manually counterstained for hematoxylin, coverslipped using VectaMount AQ Aqueous mounting media (Vector), then scanned using an Axio Scan Z1 (Zeiss). The slides were then decoverslipped and destained using an ethanol gradient, including a 1% hydrochloric acid wash and blocked, as needed, with avidin/biotin blocking kit (Vector Laboratories) and anti-rabbit or anti-rat Fab fragments to

eliminate carryover signal from previous cycles, prior to starting another staining cycle. Citrate based antigen retrieval was performed before each staining cycle.

Images of the same specimen but different stains were cropped into multiple segments using ZEN software (Zeiss). Using HALO image analysis software (Indica Labs), each marker was then converted into pseudocolors using the Deconvolution algorithm and compiled into composite multi-marker images. Markers of interest were pseudo-colored and quantified through the HighPlex FL algorithm in HALO software.

Statistical analysis

All statistical analyses were performed using GraphPad Prism software v9, with input from a Biostatistics core expert at Washington University. All data are representative of at least two independent experiments, unless specifically noted. Sample size was pre-calculated to satisfy power-requirements (with >85% confidence) in most experiments. To accomplish randomization for orthotopic or syngeneic tumor experiments, animals were sorted by a blinded investigator with tumor sizes in ascending order and then groups were assigned in descending order. Each group was checked *post-hoc* to verify no statistical difference in average starting tumor size. Data are shown as mean ± SEM, unless otherwise noted. Statistical tests such as unpaired parametric Student's t-test, ANOVA analysis (Bonferroni multiple comparison), or unpaired non-parametric Mann–Whitney U test were used appropriately based on normality of data. For survival analyses, Log-Rank (Mantel-Cox) test was used. $p < 0.05$ was considered statistically significant for all studies; ns denotes not significant.

Data availability

Bulk-RNA and scRNA sequencing data from KPC pancreatic lesions can be found at the Gene Expression Omnibus Repository (GEO) accession number #####. All software packages used are publicly available through commercial vendors.

Chapter 3: Conclusions and Future Directions

3.1. Conclusions

Many factors contribute to the recalcitrant nature of PDAC to therapy[8-11,259]. Here, we show that the PDAC stroma can lead to RT resistance. These data are in agreement with other studies, which showed that direct ECM-mediated signaling through β1-integrin[101,121,295] and Caveolin[296] can play a role in regulating RT sensitivity in multiple cancer models. ECM can impact RT response *in-vivo* by several mechanisms, which include directly signaling to tumor cells through integrins and other receptors[117-121], acting as a reservoir for secreted mitogens[122-124] and as a major oxygen bioavailability[132,225]. All these studies showed that the stromal ECM can promote survival of cancer cells following RT; however, how the PDAC stroma might affect RT-induced immune priming is less clear. Interestingly, our data here suggest that collagen-rich ECMs not only promote cancer cell survival but also repress RT-induced IFN signaling, which may be critical to RT-induced tumor immunity.

In these studies, using KPC GEMMs, we found that even though RT could have temporary short-term tumor control, it fails to prime T cells responses, which translates to failure of long-term tumor control and no survival benefit. This is noteworthy because in many other cancer models, RT is perfectly capable of priming T cells and controlling tumor growth[141,297] and we ourselves observed this in KP-driven sarcomas (**Fig. 2.1K**). Even though our PDAC and sarcoma GEMMs have the same mutations in Kras and p53 driving tumorigenesis, we noted one of the major differences was in the amount of stromal desmoplasia. The PDAC stroma is abundant compared to genetically equivalent sarcomas[52,298]. In our current study, we found collagen and pancreatic fibroblasts synergistically mitigate RT efficacy and ability to induce tumor cell death *in-vitro*, which is

in part mediated through fibroblasts' support of PDAC cell proliferation and collagen's ability to blunt of RT-induced IFN signaling. Similar data have been reported, in which pancreatic stellate cells (PSCs) can secrete factors, such as IL-1α and TGFβ, which dose-dependently enhanced PDAC cell proliferation, migration, invasion, and colony formation and caused resistance to gemcitabine and RT through the activation of MAPK AKT pathways[94]. Furthermore, PSCs can directly interact with PDAC cells to promote radioprotection and stimulate the proliferation of tumor cells through β1 integrin signaling, which is independent of phosphoinositide 3-kinase but depends on FAK[101,102]. The presence of extensive desmoplasia and its role to promote tumor proliferation in PDAC further explains that unlike in the sarcoma model, in PDAC, RT counterintuitively increases proliferation instead of decreasing proliferation. This suggests that RT may perform differently in a tumor which is stroma-rich versus stroma-light, which is in part mediated through FAK.

Prior studies have observed that inhibition of FAK signaling changes the phenotype of both the PDAC tumor cells themselves as well as non-malignant stromal cells in PDAC tumors, such as the endothelial cells and CAFs[214,257,284,299]. This prompted us to see if we can overcome this stromal-induced protection to RT-induced tumor death by adding FAKi. To our surprise, we found that FAKi completely reversed RT resistance in PDAC through multiple different cellular pathways, including, but not limited to, regulation of DNA damage repair/responses, ROS responses, cell cycle checkpoint regulation, inflammatory pathways, MAPK pathways, mTOR/autophagy, and pro-survival signaling. This is supported by the fact that FAKi can resensitize lung cancer cells through modulating DNA damage responses[252] and melanoma and lung carcinoma cells through

NFκB activity[257]. These FAKi-specific pathways may play a role in controlling RT efficacy in PDAC that may or may not be mutually exclusive to its effects on stromal cells, and hence, further work needs to be done to delve deeper into the mechanisms of each of these broad signaling mechanisms in each cellular compartment.

In addition to tumor cell-directed effects of the combination treatment, by blocking FAK signaling, RT now successfully induces immune priming and modulates the immune and stromal TME in PDAC to participate better in anti-tumor functions. This is demonstrated by the presence of increased cDC1s and tumor-antigen specific T cells and shifts in TAMs, cDCs, and T cells toward anti-tumor phenotypes. We postulate that these changes in tumor immunity facilitate RT's ability to prime better anti-tumor T cell responses, both in targeted tumor tissue and systemically. One possible explanation for the ability of FAK inhibition to rescue RT-induced immune priming effect is through altering collagen interactions in the stroma and how they contribute to IFN signaling, as seen by the increase in both types I and II IFN responses/pathways in the dual RT+FAKi treatment, which are not present in either RT or FAKi monotherapy alone.

Another contributor to stromal modulation of treatment response may be the heterogeneity of CAF populations[21,22,276,277]. Studies on the PDAC's TME have been linked to PDAC resistance to both chemo- and immuno-therapies[48-51]. Our understanding about the PDAC CAFs is still limited and rapidly changing. Besides knowing that they play diverse roles and can dictate divergent treatment outcomes[14,15,19], we still do not know enough whether and how much they are interchangeable from one another, how plastic they are, and how treatments affect them. Surprisingly, we found the RT+FAKi treatment causes tremendous changes in the composition of CAFs and skews their phenotype

toward one that participates more in anti-tumor immunity. Studies have shown that CAFs can play a role in tumor immunity through IL-1 and TGFβ signaling[21,22,277] and our study identifies a novel role for CAFs in anti-tumor immunity through IFN signaling. It will be interesting to further elucidate how the inhibition of FAK signaling changes this aspect of CAFs, considering CAFs express FAK at a high level.

Adding another layer of complication to understanding the role of CAFs in our study, it is known that CAFs are resistant to RT[92], and therefore we have yet to understand the nuances of how RT may affect CAF subpopulations and subsequently affect their interactions with immune cells and anti-tumor immunity. Moreover, while some studies show stiffer matrix reduces efficacy of DNA damaging agents[279,280], it is still unknown whether the presence of stroma and CAFs contribute to the capability of RT to induce immunogenic cell death and whether the addition of FAKi changes this. The role of PDAC stroma, including CAFs and its ECM, to immunogenic cell death, amongst many other mechanisms of cell death, needs to be further clarified.

Overall, this study presents compelling data to suggest that stromal modulation through FAKi sensitizes PDAC to RT-induced anti-tumor immunity, and furthermore, unlocks sustained checkpoint immunotherapy efficacy. Currently, FAK inhibition is already being tested in combination with SBRT in patients with locally advanced PDAC (NCT04331041), but these data support expanding this approach to include immune checkpoint blockade.

3.2. Open Questions and Future Directions

What is the mechanism by which the combination of RT and FAKi regresses PDAC tumors? What is the mechanism of tumor cell death by the combination of RT and FAKi? Are the cancer cells dying in an immunogenic way?

We saw that the combination of RT and FAKi regressed PDAC tumors, which was associated with decreased proliferation of tumor cells and increased apoptosis (**Fig. 2.7B-F**). However, these phenotypes we observed have not entirely elucidated how the dual treatment mechanistically kills the PDAC tumor cells.

It is well established that there are many ways a cell can die including, but not limited to: 1) Apoptosis (intrinsic and extrinsic), 2) Immunogenic cell death (ICD); 3) Autophagy-dependent cell death; 4) Lysosome-dependent cell death; 5) Necrosis; 6) Pyroptosis; 7) Ferroptosis; 8) Necroptosis; 9) Cellular senescence; 10) Mitotic catastrophe; 11) Entotic cell death; and 12) Mitochondrial permeability transition (MPT)-driven necrosis[300]. Galluzzi et al. wrote a comprehensive review on the molecular mechanisms of cell death in 2018[300]. Because of the importance in answering mechanistically how the PDAC cells died due to RT+FAKi treatment, I will highlight and list out a couple definitions directly from this review article below:

1. Extrinsic apoptosis: "specific variant of regulated cell death initiated by perturbations of the extracellular microenvironment detected by plasma membrane receptors, propagated by CASP8 and precipitated by executioner caspases, mainly CASP3"

2. Intrinsic apoptosis: “type of regulated cell death initiated by perturbations of the extracellular or intracellular microenvironment, demarcated by mitochondrial outer membrane permeabilization, and precipitated by executioner caspases, mainly CASP3”
    a. Anoikis: “specific variant of intrinsic apoptosis initiated by the loss of integrin-dependent anchorage”
3. Immunogenic cell death (ICD): “a form of regulated cell death that is sufficient to activate an adaptive immune response in immunocompetent hosts”
4. Autophagy-dependent cell death: “a form of regulated cell death that mechanistically depends on the autophagic machinery (or components thereof)”
5. Lysosome-dependent cell death: “a type of regulated cell death demarcated by primary lysosomal membrane permeabilization and precipitated by cathepsins, with optional involvement of mitochondrial outer membrane permeability and caspases”
6. Pyroptosis: “a type of regulated cell death that critically depends on the formation of plasma membrane pores by members of the gasdermin protein family, often (but not always) as a consequence of inflammatory caspase activation”
7. Ferroptosis: “a form of regulated cell death initiated by oxidative perturbations of the intracellular microenvironment that is under constitutive control by GPX4 and can be inhibited by iron chelators and lipophilic antioxidants”
8. Necroptosis: “a modality of regulated cell death triggered by perturbations of extracellular or intracellular homeostasis that critically depends on MLKL, RIPK3, and (at least in some settings) on the kinase activity of RIPK1”

9. Cellular senescence: “irreversible loss of proliferative potential associated with specific morphological and biochemical features, including the senescence-associated secretory phenotype”
10. Mitotic catastrophe: “oncosuppressive mechanism for the control of mitosis-incompetent cells by regulated cell death or cellular senescence”
11. Entotic cell death: “a type of regulated cell death that originates from actomyosin-dependent cell-in-cell internalization (entosis) and is executed by lysosomes”
12. Mitochondrial permeability transition (MPT)-driven necrosis: “specific form of regulated cell death triggered by perturbations of the intracellular microenvironment and relying on cyclophilin D”

For my thesis project, I mainly focused on looking at apoptosis, measured by cleaved caspase 3 (CC3), as a form of cell death due to treatment. However, all the other mechanisms of cell death just mentioned above are possible means of how the PDAC cells died from the RT + FAKi treatment combination. For instance, we saw that our treatments not only caused increased apoptosis, but the combination also caused necrosis in parts of the tumor which may very possibly have induced an immunogenic cell death. More recent data suggest that there is a complex interconnectivity of these cell death mechanisms and they further recommend that therapies should aim to target more than a single cell death routine to achieve more success[300]. Hence, it is important to elucidate these cell death mechanisms by which our dual treatment works to fully understand how we can prevent treatment resistance and achieve better success.

By inhibiting FAK signaling, we were able to increase apoptosis in RT-treated PDAC GEMMs that we did not see with RT monotherapy alone (**Fig. 2.7F**). Apoptosis happens

when there are perturbations in the cellular microenvironment, such as growth factor withdrawal, DNA damage, endoplasmic reticulum (ER) stress, ROS overload, replication stress, microtubular alterations, or mitotic defects[300]. Our data suggest that there is DNA damage, ER stress, and ROS overload, so it makes sense that we see an increase in apoptosis in the RT+FAKi-treated group. Apoptotic cells usually retain their plasma membrane integrity and metabolic integrity which allows the rapid clearance of debris by phagocytes which then completes the whole process. This process was originally thought to not be highly inflammatory because it is tightly regulated and thus immunologically silent[300,301]. Apoptosis is very different from necrosis where the cells die while invoking a highly inflammatory environment. However, what is interesting is that now we have evidence that intrinsic and extrinsic apoptosis and their consequent disposal by phagocytes are not always immunologically silent as originally thought before[300,302,303]. This is important because we know that even though we showed that apoptosis is higher in the dual treatment compared to vehicle or either monotherapy alone, the dual treatment still generates a robust anti-tumor immune response.

Another important question to note is whether the way the PDAC cells are dying is immunogenic, i.e., are the cancer cells dying through immunogenic cell death? We know one characteristic of ICD that causes an activation of the immune system is through the secretion, release, or surface exposure of damage-associated molecular patterns (DAMPs)[304]. DAMPs are released by apoptotic, necrotic, and autophagic cells, which alert the host to cause cell death and trigger a pro-inflammatory immune response. Some key DAMPs include surface-exposed Calreticulin (CRT), actively secreted adenosine triphosphate (ATP), and passively released high-mobility group box 1 protein

(HMGB1)[305,306]. These DAMPs are beneficial in anti-cancer therapy and their balance can determine the outcome of the induced immunologic response[307]. We know to some extent that the way the RT+FAKi-treated PDAC cells die is highly inflammatory and this likely contributes to the recruitment of immune cells into the TME through the secretion of IFN-related proteins and CXCL9, CXCL10, and CXCL11. However, we have not successfully measured these three DAMPs before. Hence, it is important to study whether our RT+FAKi-treated mice express these DAMPs and whether the balance of these DAMPs is skewed toward a more immunostimulatory versus inhibitory environment.

What is the mechanism by which the combination of RT and FAKi induces increases in cDC1 and CD8$^+$ tumor specific T cell numbers in PDAC? Is the increase of CD8$^+$ tumor specific T cell number dependent on cDC1 increase?

We observed that the dual RT and FAKi treatment induced a dramatic increase in the total number of cDC1 and CD8$^+$ tumor specific T cells (**Fig. 2.7I,K**). However, we still do not have a clear understanding of the mechanisms at play. There are a couple possibilities that could explain our observation: 1) shifted differentiation and mobilization of myeloid precursors in the bone marrow to bias towards more dendritic cells; 2) increased priming and proliferation of dendritic cells and T cells in the lymph nodes; 3) targeted recruitment and retention of dendritic cells and T cells from the periphery into the tumor microenvironment through cytokines and/or chemokines; 4) increased survival of these immune cells in the TME through a change in cell transcription and/or translation, epigenetic, or metabolism; and 5) modulations in the PDAC TME that support the direct and indirect recruitment of these cells into the TME.

PDAC tumors engage several immunosuppressive mechanisms to evade the immune system, which include the expansion of immunosuppressive granulocytic and myeloid progenitors in the bone marrow and its consequential enrichment of tumor associated macrophages (TAMs) and granulocytes at the expense of immunostimulatory tumor-infiltrating conventional dendritic cells[308]. Meyer et al. showed that PDAC and breast cancers secrete GCSF which causes the downregulation of transcription factor interferon regulatory factor 8 (IRF8) in bone marrow progenitors. Because both TAMs and cDCs arise from the same bone marrow progenitors, the granulocyte-macrophage progenitor (GMP) and macrophage-dendritic cell progenitor (MDP), the balance of TAMs and cDCs depend on signals received in the bone marrow. Furthermore, Hegde et al. showed that compared to lung cancers, PDAC has a dearth of cDCs[24], which could be explained by the tumor-induced myelopoiesis skewing into more tumor-promoting TAMs instead of cDCs. Furthermore, many other groups have shown that as tumor develops, the TME alters the balance of these myeloid cells and converts them into immunosuppressive cells[309-311]. It is not surprising that myeloid cells in many cancers are immunosuppressive and contribute to poor treatment response and overall survival[25,26,165,202,312-315]. We found that the RT+FAKi-treated mice have a >20-fold increase in the ratio of cDC1 to TAMs, while the monotherapy was unable to achieve this impressive ratio (**Fig. 2.7K**). This data adds the question as to whether the bone marrow progenitors in these mice are skewed to produce more cDCs versus TAMs and granulocytes. This could be studied by looking at the progenitor cells in the bone marrow and blood by flow cytometry and measuring serum proteins for possible growth factors that can explain this finding. This information

could open up new therapeutic approaches to skew bone marrow progenitor cells into the more tumor-suppressive population.

The next big question is whether the increase in the number of $CD8^+$ tumor specific T cells depend on cDC1 directly and whether priming in the lymph node is responsible for this phenomenon. cDCs from tumors can take up antigens and migrate into the draining lymph nodes to expand naïve $CD8^+$ T cells[316-319]. Through eloquent two-photon microscopy studies, it was revealed that T cell priming by cDCs occurs in three successive stages: 1) transient serial encounters, followed by 2) upregulation of activation markers and stable contacts of T cell and cDC culminating in cytokine production of IL-2 and IFNγ, and ends with 3) rapid proliferation and high motility of T cells[318]. This data showed the dependence of cDCs for T cell expansion through priming in the lymph node. However, we have not directly tested this hypothesis yet. This could be done through using a cDC-specific depleting mice (Zbtb46-DTR[320]) to test the dependence of cDCs for T cell expansion and by using an agonist of the sphingosine 1-phosphate receptor ($S1P_1R$), FTY720, to block the egress of T cells from the lymph node. I hypothesize that cDCs play a role in the increase of $CD8^+$ T cells number; however, whether $CD8^+$ T cells expansion in our RT+FAKi-treated mice is fully or partially dependent on cDCs is still debatable.

Based on our data which point to the inflammatory environment where the tumor cells are dying (**Fig. 2.3F-I**), it is logical to think that these inflammatory signals recruit the cDC1 and $CD8^+$ T cells in the PDAC tumors of RT+FAKi-treated mice. We found that the dual-treated mice and/or cells have increases in inflammatory cytokines and chemokines, such as CXCL9, CXCL10, CXCL11, CCL5, CXCL5, and CX3CL1, and increases in IFN-related proteins, such as IRF1, IRF7, IFNγR2, and IFNAR1. These cytokines have been shown

to be able to recruit tumor-suppressive immune cells[321]. It will be interesting to see if the influx of these cDCs and $CD8^+$ T cells we saw was dependent on any of these cytokines/chemokines. Currently, there are multiple blocking antibodies targeting these proteins, such as αCXCL9, αCXCR3, αIFNAR1, αIFNγ, etc. – it would be insightful to know which of these proteins, if not all, are responsible for the increase of anti-tumor immune cells in our treated mice.

The next possibility for the high number of tumor-infiltrating cDC1 and $CD8^+$ T cells in RT+FAKi-treated mice is the change in the survival capability of these immune cells in the harsh PDAC TME. There are multiple ways this can happen: a cell can change its transcription and/or translation, epigenetic signatures, or metabolism. First, the anti-apoptotic proteins BCL-2, MCL-1, and A1 can influence and control survival of T cells, cDCs, and B cells[322,323]. When looking at our scRNA seq data on the immune compartment, we did see apoptosis gene signature being downregulated and many metabolism pathways being changed when compared to vehicle (data not shown). This makes us wonder whether there are transcriptional and/or translational changes in these anti-apoptotic and metabolism genes that give the immune cells better survival signals. We have not directly tested changes in these genes by RT-PCR or proteins by Western Blot, but it is possible to test this hypothesis to see if the immune cells have better survival signals in the TME due to the combination treatment. Newer tools such as ATAC-seq will help us investigate epigenetic changes in a genome-wide scale. We could look at the chromatin accessibility for these anti- and pro-apoptotic genes using this technique to test this hypothesis of epigenetic modulation. Lastly, it is becoming clearer that metabolic pathways and metabolites play a role in providing energy and substrates for cell growth

and survival, but also instruct effector function, differentiation, and gene expression[324,325]. This immunometabolism can be studied to better understand changes brought upon by RT and/or FAKi by using tools such as Seahorse metabolism analyzer. Understanding how the immune cells survive better in the harsh PDAC TME will help us develop better strategies of improving immune cell longevity to fight tumors in the future.

Lastly, but not the least, we know that the PDAC TME harbors a very harsh environment for immune cell function. However, we disclosed from multiple approaches that there are many changes brought upon the PDAC TME once we block FAK signaling in combination with RT. Among these changes, we observed the destruction of tumor cells, induction of IFN and inflammatory signaling, changes in tumor cellular metabolism, reduction of immunosuppressive immune cells and CAFs, improvement of anti-tumor immune cell phenotypes, and alteration of CAFs to participate in anti-tumor immunity. I have hypothesized above how some of these observations could help explain the increase of cDC1 and $CD8^+$ T cell number in the PDAC TME. In this paragraph, I would like to rationalize how changes in the immune cells and CAFs themselves could play a role in the influx of cDC1 and $CD8^+$ T cells in PDAC, either directly or indirectly. There are two possibilities that these immune cells are more likely to be honed and to survive in the harsh TME: 1) there is a “better” environment in which these cells can be recruited to live and survive or 2) there is a newly “open and permissive” milieu for which the cells can thrive. First, it has been shown previously that immune cells and CAFs can recruit other immune cells into the TME through the secretion of cytokines/chemokines among many other mechanisms[326-329]. **Figures 2.11-2.14** presented the phenotypic changes in both the immune cell and the CAF compartments in RT+FAKi-treated mice. These changes

include the skewing of these cells to have substantially more type-I and type-II IFNs signatures, which are well known to be good anti-tumor phenotypes[330,331]. Changes in these immune cells and CAFs can directly or indirectly recruit cDC1s and $CD8^+$ T cells from the circulation or induce their proliferation *in situ*. For instance, these cells can now create a new "better" environment where the anti-tumor immune cells are more likely to be recruited to from the bone marrow or circulation. Additionally, as mentioned earlier, TAMs, granulocytes, eosinophils, and myCAFs are reduced after the RT+FAKi treatment (**Fig. 2.7K, 2.11D**). The loss of these immunosuppressive cells might possibly have created an "open and permissive" space for new immune cells to be recruited into the PDAC TME. To test the impact these immune cells and CAFs have for the recruitment of anti-tumor immune cells found in our RT+FAKi-treated mice, we could do cellular depletion strategies. We have tested the dependence of the treatment on $CD4^+$ and $CD8^+$ T cells and found that they are not important for initial tumor regression but important for long-term tumor control (**Fig. 2.7L-M**). Next, we could give αCSF-1 and clodronate to deplete TAMs, we could utilize Zbtb46-DTR mice to deplete cDCs themselves, and we could use αSMA-tk mice to deplete αSMA^+ CAFs[332]. By doing these depletion studies, we could test whether these immune cells and CAFs are necessary and/or sufficient for the recruitment of cDC1s and $CD8^+$ T cells to come infiltrate the PDAC TME after the combination of RT and FAKi treatment. Understanding this aspect of cellular-cellular interaction will help us develop novel therapeutic strategies focusing on specific aspects of these interactions.

How does a dense ECM abrogate RT response mechanistically? How does collagen abrogate RT-induced IFN signaling? Does a dense ECM impair the ability of tumor cells to fix DNA double strand breaks?

The recalcitrant nature of PDAC has been linked in part to its unique TME, which is characterized by a fibrotic and desmoplastic stroma composed of dense collagen-rich ECM and abundant CAFs[8-11]. It is not surprising that the dense ECM of PDAC has been correlated with poor response to chemotherapies and immune-directed therapies as it can hinder the penetrance of chemotherapeutic agents and anti-tumor immune cells[48-51]. However, it was not clear, until now, how PDAC associated fibrosis might impact the efficacy of RT. We found out that this dense ECM in PDAC (composed mainly of Collagen-I) abrogates RT-induced IFN responses (**Fig. 2.3F**). This is interesting because, unlike chemo- and immune-directed therapies, which are distributed through the blood or lymphatic vessels which is affected by the characteristic of ECM, RT does not need to go through these various tissues or cells to reach its target. However, we still do not have a clear understanding of how RT-induced IFN responses are dampened. There are multiple possible hypotheses: 1) in a dense ECM, the cellular architecture (microtubules, stress fibers, focal adhesions, and intermediate filaments) is altered/impaired causing the cells to be less responsive to changes caused by RT; 2) in a dense ECM, cells are less able to or less efficient at releasing the specific inflammatory-inducing molecules needed to induce IFN responses, for example DNA which can activate STING signaling; 3) in a dense ECM, cells are more capable at fixing double strand DNA breaks from RT; 4) in a dense ECM, there are unusual receptor-ligand interactions which change the cell's inherent ability to respond to RT; and lastly 5) in a dense ECM, other components of the

TME, such as the dendritic cells or other tumor-suppressing immune cells, are hindered from performing their anti-tumor IFN secretory function.

One of the most important anti-tumor responses of RT is the induction of IFN signaling along with its succeeding immune responses. Thus, it is important to understand how IFN responses are triggered due to RT. DNA is considered a key PAMP that can trigger an immune response; thus, a strict compartmentalization of cellular DNA in the nucleus and mitochondria is necessary to avoid aberrant immune response[333]. Radiation damages DNA either by directly depositing energy or indirectly by the ionization of water molecules to produce hydroxyl radicals that attack the DNA[334]. Damage caused by radiation can cause DNA double strand breaks (DSBs), which are the most cytotoxic type of DNA lesion[334]. The cytosolic DNA sensor cyclic GMP-AMP (cGAMP) synthase (cGAS) is an important cytosolic nucleic acid sensor[335] that localizes to micronuclei formed after DNA damage. The breakdown of micronuclear envelope leads to the rapid accumulation of cGAS, which then allows self-DNA to become exposed to the cytosol[139]. The accumulation of dsDNA present in the cell cytosol activates the cGAS, which then generate cGAMP, which in turn activates the transcription factor IRF3 and induces a type-I IFN response via the adaptor protein STING (stimulator of interferon genes)[336]. In response to DNA damage, the transcription factor NFκB is also activated, which directs the induction of IFN signaling as a stress response pathway[337,338]. Numerous studies have shown that RT-induced DNA DSBs are important to activate IFN signaling, which is an important tumor-suppressing function[179,194,201,339-342]. Both type-I and type-II IFNs have been shown to be necessary for RT-immediate tumor control, as the abrogation of IFN abolishes the anti-tumor effects of RT[194,340]. In summary, this DNA sensing process can

in turn activate both innate and adaptive immune responses to produce anti-tumor IFNs[343].

Our findings point to the importance of this dense ECM in abolishing RT-induced IFN responses (**Fig. 2.3F**). It makes one wonder whether this is related with the DNA sensing cGAS-STING pathway mentioned above. Post DNA damage, DNA must be secreted into the cytosol from the nucleus or mitochondria for cGAS to be activated[333]. This process of DNA transfer requires a functional microtubule network[344]. Studies have suggested that alterations in ECM force will change a cell's phenotype and its microtubule network system[345]. Thus, it is logical to think that a dense ECM will have a different cellular architecture which may hinder the process of DNA transfer into the cytosol for cGAS-STING to be activated. First, we could test out if cellular architecture and microtubule network are different in a low vs. dense ECM condition by using either two-photon microscopy or electron microscopy. Next, it will be interesting to test this hypothesis using a STING KO cells to see if cGAS-STING pathway is impaired in a dense ECM environment.

Another hypothesis is that in a dense ECM, cells are more capable at fixing DNA breaks caused by RT. Some studies have shown that microtubules regulate the repair response to DNA DSBs in a process called DMSR (DSB-induced microtubule dynamics stress response), which is important for canonical nonhomologous end joining (c-NHEJ)[346]. Because of the possible modification of cellular architecture in a dense ECM, this DNA DSBs repair process may be altered, causing changes in how soon and how long cells are stimulated by the DNA DAMPs. Furthermore, another group also showed that ECM mechanical signals regulate DSB repair efficiency and genotoxic stress in a

process that is dependent on MAP4K4/6/7 kinases[279]. They demonstrated that cells in lower ECM impairs DSB repair and renders cells sensitive to genotoxic stress when compared to cells in dense ECM. These studies point to the importance of ECM in DNA repair process, which could potentially explain why PDAC cells grown in dense ECM are less responsive to RT and induce less IFN response. We could test out the time needed for the cells to repair their DNA DSBs post-RT when they are grown in a low vs. dense ECM. If it is true that cells in a higher ECM is more able to repair DNA breaks, this could point to the possibility that dense ECM induces a more radioresistant environment for cancer cells.

Next, ECM is an important component that dictates cellular interactions in the TME, including cell-to-cell signaling and ECM-to-cell signaling[347]. ECM proteins and structures dictate cellular behavior, migration, differentiation, proliferation, and survival and accordingly determine different consequences in tumorigenesis, metastasis, and treatment outcomes[348]. Inside the cell, integrins, in association with other cofactors such as growth factors, cytokine, and intracellular adapter molecules such as FAK and Src family kinases, play an integral role in transmitting ECM-induced signaling pathways. The external physical and biochemical properties of the ECM also have a role in the signaling processes important in cancers[347]. The biochemical and biophysical properties of different ECM can consequently determine different receptor-ligand interactions that may be important in how cells respond to RT, especially the different integrins. Integrin signaling have been implicated in radioresistance in multiple cancer models[101,121,349]. More importantly, integrin crosstalk has been implicated in radioresistance by rapidly normalizing DNA damage and preferentially surviving post-RT[350]. Thus, it is reasonable

to hypothesize that a dense ECM will have different receptor-ligand interactions that may confer different sensitivities to RT. It has been shown before that cells grown in a dense ECM have a higher pFAK level[214]. To look at other receptor-ligand interactions that may be different in a low vs. dense ECM, we could perform RNA seq or scRNA seq and use analysis tools such as CellChat Explorer[351] which will allow us to observe receptor-ligand interaction and cell-cell communication atlas.

Lastly, different ECM phenotypes dictate how cancers behave and are associated with distinct cellular composition as a whole[352-356]. For example, tumor-associated collagen signatures (TACS) describe different collagen architecture in cancers, which have distinctive metastasis and response to therapies patterns[356]. Likewise, in pancreatic cancer, it has been recognized that there are different histological and molecular subtypes associated with different molecular and cellular composition and survival statistics[354,355]. I have discussed earlier in the Introduction that different stromal and immune cells can have different roles in regulating RT efficacy. Thus, it is possible that not only do different cells exist in different ECM architecture, but they also behave differently in different ECM. Immune cells migrate differently based on the ECM they reside in[357,358]. Therefore, it will be interesting to elucidate the phenotypes, functions, and responses of immune cells grown in low vs. dense ECM post-RT. To do this, we can utilize a 3D *in-vitro* culture system where we can manipulate the tumor, stromal, ECM, and immune components to test in different treatment conditions.

Overall, there are many ways in which the ECM can dictate cellular responses to treatment. Understanding how the different ECM architecture directs RT efficacy is

important to help us design a more personalized treatment options for different patients in the future.

What can we learn from the FAKi- and RT+FAKi-induced CAF subsets? How different are they phenotypically and functionally from the well-studied myCAFs, iCAFs, and apCAFs in PDAC? What is the cellular origin of these CAFs?

Many studies have elegantly illustrated how the PDAC's TME contributes to PDAC's recalcitrant nature and resistance to both chemo- and immuno-therapies[48-51]. It is obvious now that the abundant and heterogeneous PDAC CAF populations play a role in treatment response[21,22,276,277]. However, unlike our knowledge of the heterogenous immune cells, our understanding about the PDAC CAFs is still very limited and rapidly changing. We know that different PDAC CAFs play diverse roles and can dictate divergent treatment outcomes[14,15,19]; however, we still do not know enough whether and how much they are interchangeable from one another, how plastic they are, how they communicate with other cells in the TME, where they come from, how their proportions change with tumor progression, and how treatments affect them.

Our studies found FAKi and RT+FAKi treatments caused tremendous changes in the composition of CAFs and skewed their phenotype toward one that participates more in anti-tumor immunity (**Fig. 2.11-2.12**). Multiple groups have shown that CAFs are not uniform in composition and are constantly altered during tumor progression and that they can play a role in tumor immunity through IL-1, TGFβ, and IL-6 signaling[17,21,22,277,359]. Adding to this, my own current study identified a novel role for CAFs in anti-tumor immunity through IFN signaling. Furthermore, many groups have also displayed that

CAFs present functional diversity which has therapeutic implications in PDAC's treatment outcomes[14,17,19,213]. Moreover, they have also shown the importance of spatial orientation of the CAFs in respect to tumor cells and that there is a lineage-dependent relationship between preexisting fibroblasts to CAFs as baseline PSC heterogeneity regulates subsequent CAF development during tumorigenesis[17,21,22,277,359-361]. This section below highlights some new data on PDAC CAFs to show just how important, unique, and complex they are.

Previously, studies on PDAC CAFs were difficult due to the lack of specific markers. Although there are no specific markers identified for different CAFs, there have been multiple studies which employed scRNA seq to cluster CAFs into transcriptionally defined clusters in PDAC[17,21,22,277,359,361,362]. Some of these studies include: 1) the αSMA$^+$ myCAFs and LRRC15$^+$ CAFs which are located closer to tumor ducts and depend on TGFβ signaling; 2) the Ly6C$^+$ iCAFs which reside further away from tumor ducts within the stroma and display IL-1 and JAK/STAT signaling pattern; 3) the CD74$^+$ MHC-II$^+$ apCAFs which have immunomodulatory functions and are characterized by the activation of STAT1, MTORC1, MYC, and antigen presentation pathways; 4) NetrinG1$^+$ CAFs which are immunosuppressive, inhibit NK cell-mediated anti-tumor activity, and support PDAC survival through glutamate/glutamine metabolism; and 5) the tumor restraining αSMA$^+$ CAFs vs. tumor-promoting FAP$^+$ CAFs which have two polarizing immunomodulating roles.

Many of these studies have revealed the complexity of CAF biology in PDAC. The findings on myCAFs, iCAFs, and apCAFs by the Tuveson lab highlight the heterogeneity of CAFs based on the signaling gradients and spatial proximity from tumor cells in the

TME. We do not yet know what signaling processes define FAKi- and RT+FAKi-induced CAFs we found in our data set. Furthermore, we also do not yet know the spatial proximity of these treatment-induced CAFs from tumor cells and other immune cells. Using newer technologies such as Imaging Mass Cytometry[363,364] will enable us to do high dimensional *in situ* single cell analysis of unique CAFs in their native spatial TME within the preserved architecture of the tumor itself. This technique will allow us to know more about the heterogeneous PDAC CAFs, which will make it more likely we will be able to better understand cancer progression and its resistance mechanisms and how to overcome them.

Signaling gradients and spatial proximity in the TME are not the only contributors to the heterogeneity of PDAC CAFs. Recently, multiple studies on the origin of PDAC CAFs[360,362] have brought up another important question with regards to our FAKi- and RT+FAKi-treated CAFs – where do these treatment-induced CAFs come from? It was originally thought that PDAC CAFs arise from a common cell of origin, the pancreatic stellate cells (PSCs), which diversify based on cytokines and growth factors and other conditions in the TME. However, unforeseen to this original idea, newer studies showed that the diverse PDAC CAFs actually arise not just from PSCs but from a heterogenous mesenchymal lineage, mesothelial cells, pancreas-resident fibroblast populations, and potentially from the bone marrow[360,362]. Currently, there is no mouse models we can use to fully elucidate every single possible cellular origin of PDAC CAFs. However, there are a couple mouse models and experimental studies which we can use to study the cellular origin of these FAKi- and RT+FAKi-induced PDAC CAFs: 1) the Fabp4-Cre;Rosa26^{mTmG} uses GFP to mark PSCs and their progeny during tumorigenesis[360]; 2) bone marrow

transplant using a different congenic mice (for example CD90.1 vs. CD90.2) to track for bone marrow precursors; and 3) we can potentially generate new mouse models using Lrrn4-Cre as a specific marker for mesothelial cells or Tie1-Cre as a specific marker for endothelial cells. These studies will help shine a light into the unique functions of CAFs from a defined cellular origin.

Lastly, many of these elegant studies on the PDAC CAFs have shown the nonredundant functions of specific CAF population in shaping PDAC TME and treatment response among many other things[17,21,22,277,359,361,362]. Helms et al. showed that Tie1$^+$ PSC-derived CAFs are involved highly in cell adhesion, ECM-receptor interaction, and axon guidance, while non-PSC derived CAFs are more enriched for immunomodulatory and metabolic processes[360]. These PSC-derived CAFs uniquely expressed ECM components at a higher level including those associated with tissue stiffness and PDAC aggressive nature, such as tenascins and perlecan. They further showed that the PSC-associated ECM signature was associated with a worse prognosis in PDAC patients. Moreover, McAndrews et al. showed tumor-protective αSMA$^+$ CAF depletion was associated with epithelial migration, cell proliferation, cytokine production, and inflammatory responses, while tumor-promoting FAP$^+$ CAF depletion was associated with protein processing, proteolysis, and pancreatic secretion[17]. Interestingly, not only are the myCAFs in our dataset showed a lot of pathways associated with ECM components like the PSC-derived CAFs signature in the Helms et al. data set, but the FAKi- and RT+FAKi-induced CAFs showed upregulation of pathways associated with proteolysis and pancreatic secretion similar to the gene signatures that are upregulated when the tumor-promoting FAP$^+$ CAFs are deleted. Since FAKi- and RT+FAKi-treated mice have a

change in CAF phenotype at the expense of this stereotypical myCAFs, it will be interesting to see if these treatment-induced CAFs have distinct signatures associated with better prognosis in PDAC patients. As there are more and more publicly available data sets correlating different CAF signatures with patient prognosis available online[360,365], it will be interesting to compare our FAKi- and RT+FAKi-induced CAFs signatures to these datasets.

Altogether, these studies suggest that CAF heterogeneity in PDAC arise from at least multiple sources including different cytokine and growth factor signaling gradients within the TME and mesenchymal lineage heterogeneity. There are so much more that we do not yet understand about CAFs and its complex and unique biology. Understanding CAF biology will help shine some light on how we can target and manipulate them better to fight cancer more effectively.

How does the combination of RT and FAKi treatment affect the anti-tumor functions of the tumor-infiltrating immune cells? Is there an abscopal effect? Is there long-term immune memory? How is the T cell repertoire (TCR clonality and diversity)? Are cDCs better at antigen uptake and migration to lymph node to initiate priming?

Together with the many changes in CAFs to be more anti-tumor, RT+FAKi-treated mice also have a shift in the phenotype of their immune cells to be more tumor-suppressing (**Fig. 2.7I-K ,2.9-2.10**). We have utilized flow cytometry, mass cytometry, and scRNA seq to evaluate changes in the immune cell compartment to show that $CD8^+$ T cells have better effector functions and both TAMs and cDCs are more pro-inflammatory, anti-tumor, and have better antigen processing and presentation signatures. However,

these positive changes in the immune cells brought up more in-depth and detailed questions regarding their phenotypes and functions. More specifically, we do not yet know whether there is an abscopal effect from RT+FAKi treatment, whether there is long-term immune memory, whether there is an increase in the TCR diversity and/or clonality, and the functions of the cDCs. Understanding these immune changes in our treatment will help us better design future therapeutic options which will aim to utilize the immune system.

One important question regarding the anti-tumor immune changes in our treatment is whether there is an abscopal effect from the treatment. Abscopal effect is a term used to describe systemic anti-cancer responses from RT[366,367]. This tumor regression at non-irradiated distant sites has been connected to mechanisms involving the anti-tumor immune system. Abscopal effect is one of the incentives for the combination of radiotherapy and immunotherapies – to extend the efficacy of RT to provide benefits at both local and metastatic distant sites[134,151,181,367-369]. Our current study did not answer whether combining FAKi with RT can cause abscopal effect like the combination of RT with ICB. To investigate abscopal effect in our treatment model, I propose the use of primary and secondary tumor implantation model. Once mice are treated, we need to observe the growth of irradiated and non-irradiated flanks and check whether RT combined with FAKi can control tumor growth at both primary and remote sites, which is the very definition of abscopal effect.

The next question is whether our treated mice retain long-term $CD8^+$ T cells memory. This question stemmed from the fact that 8 out of the 9 RT+FAKi+ICB-treated mice completely regressed their tumors after treatment (**Fig. 2.13I**). Even after 250 days post

tumor implant when mice are no longer receiving treatment for the past 100 days, there is no evidence of tumor in these mice. We have new data which suggests that these mice retained long-term memory cells (data not shown). Mice were rechallenged by tumor implantation at the opposite flank and 75% of the mice completely rejected the tumors while 100% of the tumor-naïve mice succumbed to tumor burden. It will be interesting to see whether this is completely dependent on $CD8^+$ T cells and what can we learn from these cells which retained long-term memory.

Still relating to $CD8^+$ T cells changes brought upon the treatment, the next question is in regard to the T cell repertoire – how our treatment changed TCR clonality and diversity. It is now well established that T cell infiltration is paramount for effective anti-tumor immune responses and that TCR repertoire can change with treatment[370,371]. Recent studies have also showed that TCR diversity at baseline can be a prognostic indicator in various cancers and TCR clonality can be predictive for the efficacy of PD1-blockade immunotherapy[372,373]. One study showed that RT can remodel the intratumoral T cell responses by increasing TCR clonality[374]. All these studies showed that both immunotherapies and RT can change TCR repertoire and that TCR repertoire is an important element, which could be a good biomarker for treatment efficacy and prognosis. We saw an increase in the number of antigen-specific $CD8^+$ T cells post-treatment (**Fig. 2.7I**), which suggests an increase in TCR clonality. However, we have not excluded the possibility of a change in TCR diversity. Thus, it will be interesting to see how our treatment changes the intratumoral TCR repertoire by performing TCR sequencing.

Lastly, even though we have both CyTOF and scRNA seq data on the function of the cDCs from the treated mice, we still have not done *ex vivo* functional assays or assess

their functions *in vivo*. Like the $CD8^+$ T cells, it is now well-established that cDCs are also necessary for anti-tumor immune functions, including in the context of radiation. RT generates inflammatory signals in the TME, including the generation of tumor-specific antigens from dying tumor cells thus promoting the cGAS-STING pathway and initiating IFN signaling cascade, which then promotes the maturation and migration of cDCs to facilitate antigen processing and presentation and stimulation of $CD8^+$ T cells[366]. Our CyTOF data showed that RT indeed increased MHC-I, MHC-II, and CD80 and CD86 activation markers on cDCs (data not shown) as part of the maturation signals from RT, which are retained in the RT+FAKi-treated mice when compared to vehicle. However, we have not done *ex vivo* functional assays on these cDCs. To do this, I propose to do dendritic cell APC assay, which involves the analysis of T cell activation. Through IFNγ ELISPOT measurement, how well antigen-loaded FACS-sorted cDCs activate T cells can be measured. Next, we also do not know how efficient these cDCs migrate from the tumor into the draining lymph node to activate naïve T cells. To study this, we need to utilize *in vivo* imaging technique of fluorescent-labeled cDCs to assess for their migration and interaction with T cells. These functional assays will enable us to look at how well the RT+FAKi-treated cDCs cross present and prime T cells to be fully functional.

It is critical to have a functional immune system to fight cancers. We observed countless alterations in the innate and adaptive immune systems in our RT+FAKi-treated mice, which point to more tumor-suppressing phenotypes and functions. Understanding these changes deeper will be important to help strategize better combinatorial immunotherapy treatment options for PDAC in the future.

Mechanistically, how does FAKi re-sensitize PDAC to RT?

Our study highlights the importance of blocking FAK signaling to sensitize PDAC to RT *in vitro* and *in vivo* (**Fig. 2.5-2.8**). However, we have not elucidated yet the ways FAK inhibition can achieve this sensitization of PDAC to RT. Our RPPA and RNA-seq data gave us a couple clues as to how: 1) changes in cell cycle checkpoint pathways; 2) changes in DNA damage response/repair pathways; and 3) changes in mTOR and autophagy pathways. Alterations in one or more of these pathways could explain why PDAC is more sensitive to RT after FAK inhibition.

Cell cycle regulation is one of the most important determinants of RT sensitivity[375]. After DNA damage by RT, cell cycle checkpoints are activated to either permit cells for genetic repair or induce irreversible growth arrest leading to cell death. These DNA checkpoint regulators include the DNA damage sensor (RAD, BRCA, NBS1), transducer (ATM, CHK), and effector (p53, p21, CDK) genes[375]. Cells are most radiosensitive in the G2-M phase of the cell cycle, less radiosensitive in G1 phase, and most radioresistant during the latter part of S cell cycle phase[375]. This knowledge has led to the development of fractionated RT strategy to partially synchronize the tumor cells to be at the most radiosensitive phase. FAK inhibition has been associated as a mediator of cell cycle regulation[376]. One study showed that dominant negative FAK mutant cells inhibited cell cycle progression at G1 phase, blocked cyclin D1 upregulation, and induced p21 expression[376]. The FAK inhibitor we used, VS-4718, has been shown to decrease S phase and increase G0/G1 and G2 levels in ovarian carcinoma HEY and OVCAR8 cells[377]. Another studied also showed suppression of FAK led to growth arrest of NSCLC cells in the G2 phase of the cell cycle[252]. We have not tested the cell cycle progression in

our PDAC cells when given FAKi ± RT. Performing flow cytometry cell survival and cell cycle progression analysis with 7-AAD, Annexin V, and Propidium Iodide will be an interesting way to assess whether FAKi changes the PDAC's cell cycle to become more proportionally radiosensitive.

Next, it is plausible that FAKi changes the ability of cells to repair DNA in response to DNA damage. We have data that showed the combination of FAKi and RT led to persistent γH2Ax protein after 24 hours (**Fig. 2.6D**) and γH2Ax^{+} cells after 3 days (**Fig. 3.1**). One group indicated that FAK suppression in NSCLC led to the activation and maintenance of DNA damage response as demonstrated by the increase in γH2Ax protein and increase in both γH2Ax and TP53BP1 to DNA damage foci[252]. They mentioned the possibility of these effects caused by inhibition of DSB repair proteins, such as ATM, ATR, or DNA-PKcs which affect DSB repair and cell cycle checkpoint control. Thus, it will be interesting if we saw such changes in these DSB repair proteins in our FAKi-treated cells that may explain why there is persistent DNA damage in our combination RT+FAKi treatment.

Lastly, mTOR inhibitors have been exposed to have radiosensitizing ability[378,379]. Multiple groups showed that inhibiting mTOR pathway can inhibit ATM and DNA-PKcs and block both nonhomologous end joining and homologous recombination of DNA repair pathways which result from DNA DSBs. Cells treated with the mTOR inhibitors are much more sensitive to RT and a majority of them end up dying from being incapable to repair DNA breaks. It is interesting to see that the changes we saw with our FAKi complexly implicate mTOR signaling pathways (**Fig. 2.5E, 2.6C**). Because changes in the mTOR signaling were revealed to be involved in DNA DSBs and repair pathways, it will be

interesting to see the changes from blocking FAK signaling in the context of mTOR pathway.

Which immunotherapies will work the best when combined with RT and FAKi (innate immune cell directed vs. adaptive immune cell directed)?

Our study highlights the benefit of adding immune checkpoint blockade (αPD1/αCTLA4, ICB, **Fig. 2.13G-I**) to the combination of RT+FAKi to improve long-term survival. We also tested another immunotherapy combination αPD1 and OX40 with RT+FAKi and found similar efficacy in the KP2 syngeneic tumor model when compared with the RT+FAKi+αPD1/αCTLA4 treatment combination (data not shown). In this model, RT-treated mice had a median survival of 40 days, RT+αPD1/αCTLA4 and RT+αPD1/OX40 groups had a median survival of 37 and 40 days respectively, RT+FAKi dual combination had a median survival of 65 days, while RT+FAKi+αPD1/αCTLA4 and RT+FAKi+αPD1/OX40 groups had a median survival of 77 and 81 days respectively. Because there is no statistically significant difference in the RT+FAKi+αPD1/αCTLA4 and RT+FAKi+αPD1/OX40 groups, and because the combination of αPD1/αCTLA4 has already been well characterized in PDAC cases, we went ahead and continue our subsequent study with αPD1/αCTLA4 combination as our immunotherapeutic agents.

Although αPD1 and αCTLA4 immunotherapies are T cell-directed checkpoint antibodies, recent studies showed that the efficacy of these checkpoint immunotherapies is also attributable to the innate immune system as the therapies impact innate immune cells both directly and indirectly[45,380,381]. This highlights the importance of both the innate and adaptive immune system working together to shape clinical efficacy. However, PDAC

is known to be lacking in the numbers of cDCs[24] and one of most dramatic improvements in number of immune cells post RT+FAKi treatment is of cDC1 (**Fig. 2.7K**). This begs the question as to whether the innate-directed immunotherapies such as CD40 agonist and Flt3L would work better in the combination of RT+FAKi. There is no doubt that RT and FAKi treatments play a role in changing both the innate and adaptive immune compartments. Thus, finding the "better" immunotherapies will help us strategize better combinatorial treatment strategy in the future to further improve the efficacy of RT+FAKi. If our first in-human clinical trial (NCT04331041) which combines SBRT with FAKi shows promising results, we can propose to combine it with immunotherapy to show an even better treatment response and long term protection as we saw in our preclinical data.

How will different RT regimens affect the combination treatment with FAKi? How will the future of RT, such as FLASH RT, change this effect?

Even though the concept of radiotherapy is not new, RT is still a rapidly evolving field. The goal of RT is to deliver the highest possible dose of radiation to the tumor while also sparing normal healthy tissues around it. For that purpose, researchers these days are aiming to adjust RT dose or schedule to reach the total radiation more quickly while limiting damage to normal tissues. However, it has been previously described that different RT regimens can have diverse impact on the immune system and efficacy when combined with immunotherapies, all of which were nicely reviewed by Demaria and Formenti[382,383]. Vanpouille-Box et al. showed that the efficacy of controlling primary tumor was not different when comparing 8Gyx3 vs. 30Gyx1 RT regimen. However, abscopal effects was not induced by 30Gyx1 high dose radiation due to the induction of DNA

exonuclease, Trex1, by RT doses above 12-18Gy, which ultimately attenuates the immunogenicity by degrading the accumulated cytosolic DNA upon irradiation[384]. Furthermore, Dewan et al. showed that while primary tumors treated with 20Gyx1, 8Gyx3, vs. 6Gyx5 did not show any differences in tumor burden, there was a dramatic improvement of the secondary tumor growth control when mice were treated with either of the two fractionated RT regimens (8Gyx3 and 6Gyx5) with 8Gyx3 RT regimen being superior to 6Gyx5 at the induction of abscopal effect and tumor-specific T cells[385]. Overall, all these studies showed that there are differences to the immune system with different RT regimens and that there exists a therapeutic window for the optimal use of fractionated RT in combination with immunotherapies.

Our study outlined here was done using the concept of hypofractionated RT, which gives larger doses of radiation less often to reduce the number of treatments, instead of the old-fashioned conventional RT regimen. These newer hypofractionated radiation delivery techniques have been recently tested and shown to have similar efficacy and adverse effects in multiple cancer types, including PDAC[386-389]. However, using our PDAC GEMMs, we have not tested the difference of the hypofractionated RT dose we chose (6Gyx5) vs. the more “immunogenic” RT dose (8Gyx3) Dewan et al. elegantly showed being better at inducing abscopal effect and T cell immunity when combined with αCTLA4[385]. I think it will be important going forward to test these two different RT regimens, especially when we want to combine the RT+FAKi therapy with immunotherapies. We may even be able to use Trex1 to guide the selection of RT dose and fractionation in patients who will be treated with immunotherapy. Moreover, we do not have studies yet showing the differential impact of various RT regimens on the PDAC

CAFs. As we showed in our study, CAFs can play a role in anti-tumor immunity and thus understanding their changes due to treatment may be as important as studying the immune system.

Lastly, ultra-high dose rate of RT (FLASH-RT) is a new technology that enables the ultra-fast delivery of doses (≥40Gy/s) while sparing normal tissues[231,232]. The idea was that very short pulses of radiation elicit less genomic instability than continuous radiation at the same dose. However, many studies now have shown that this FLASH-RT regimen was as efficient as conventional RT in repression of primary tumor growth without causing damage to normal cells[390-394], which have generated positive enthusiasm on the field. Although there have been some explanations of the benefits of FLASH-RT, including reduced TGFβ, TNFα, and ROS when compared to conventional RT, the mechanisms of how FLASH-RT changes the immune system and the TME have not yet been elucidated. It will be important to see how FLASH-RT influences the immune system and CAFs, the tumor-stroma communications, and stromal-mediated radioresistance. It will also be interesting to see if we have the same effect of tumor regression and T cell priming in our PDAC model when combining FAK inhibition with FLASH-RT vs. fractionated RT dose.

Despite many recent discoveries, there are still many remaining questions in the field to be addressed with regards to different RT dosing and regimen. Future discoveries about these mechanisms can be used for the design of novel RT and drug combinations to target stromal-mediated RT resistance we observed in PDAC.

3.3. Figures

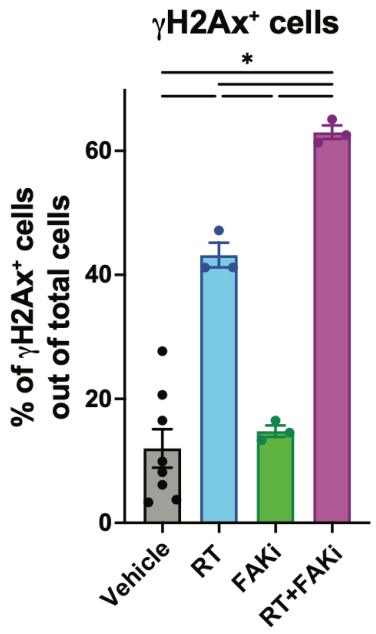

Figure 3.1: The combination of FAK inhibition and RT retained DNA damage

Analysis of γH2Ax by IHC on KPOG organoid cultures taken 3 days post RT. n = at least 3/group.

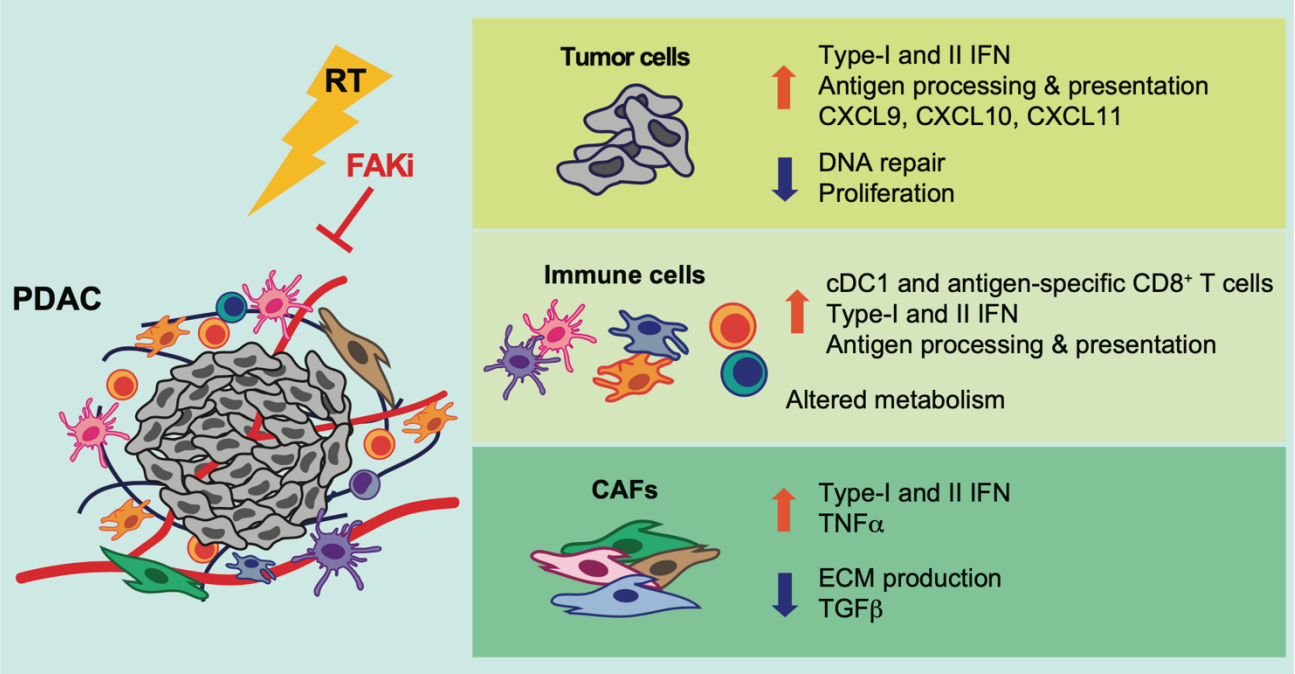

Figure 3.2: Summary of thesis dissertation

We found that fibroblasts and collagen work synergistically to mitigate RT efficacy, which is mediated in part through Focal Adhesion Kinase (FAK). In mice, FAK inhibitor (FAKi) rescued RT resistance leading to significant tumor regression and enhanced survival. Associated with this regression, we found generalized increases in type-I and II interferon signaling in the tumor cells, immune cells, and the CAFs. Specifically in the tumor cells, we found increased antigen processing and presentation and increased inflammatory signaling including chemokines CXCL9, CXCL10, and CXCL10. Furthermore, we found increased dendritic cells and tumor specific $CD8^+$ T cells numbers. Single cell RNA seq and CyTOF revealed that the dual RT+FAKi treatment primed immune cells and cancer associated fibroblasts to participate in better anti-tumor immunity in the form of enhanced antigen processing and presentation and T cell activation. Moreover, there are metabolic changes in the immune compartment and altered phenotype in the CAFs to be high in

TNFα and low in TGFβ signaling. Altogether, these data showed that the combination of RT and FAKi remodels the PDAC TME to promote immunogenicity.

References

1 Siegel, R. L., Miller, K. D. & Jemal, A. Cancer Statistics, 2017. *CA Cancer J Clin* **67**, 7-30, doi:10.3322/caac.21387 (2017).

2 Orth, M. *et al.* Pancreatic ductal adenocarcinoma: biological hallmarks, current status, and future perspectives of combined modality treatment approaches. *Radiation Oncology* **14**, 141, doi:10.1186/s13014-019-1345-6 (2019).

3 Ryan, D. P., Hong, T. S. & Bardeesy, N. Pancreatic Adenocarcinoma. *New England Journal of Medicine* **371**, 1039-1049, doi:10.1056/NEJMra1404198 (2014).

4 Fan, J.-q. *et al.* Current advances and outlooks in immunotherapy for pancreatic ductal adenocarcinoma. *Mol Cancer* **19**, 32, doi:10.1186/s12943-020-01151-3 (2020).

5 Hester, R., Mazur, P. K. & McAllister, F. Immunotherapy in Pancreatic Adenocarcinoma: Beyond “Copy/Paste”. *Clinical Cancer Research* **27**, 6287-6297, doi:10.1158/1078-0432.CCR-18-0900 (2021).

6 Hezel, A. F., Kimmelman, A. C., Stanger, B. Z., Bardeesy, N. & Depinho, R. A. Genetics and biology of pancreatic ductal adenocarcinoma. *Genes Dev* **20**, 1218-1249, doi:10.1101/gad.1415606 (2006).

7 Yarchoan, M., Hopkins, A. & Jaffee, E. M. Tumor Mutational Burden and Response Rate to PD-1 Inhibition. *New England Journal of Medicine* **377**, 2500-2501, doi:10.1056/NEJMc1713444 (2017).

8 Feig, C. *et al.* The pancreas cancer microenvironment. *Clinical cancer research : an official journal of the American Association for Cancer Research* **18**, 4266-4276, doi:10.1158/1078-0432.CCR-11-3114 (2012).

9 Ohlund, D. *et al.* Type IV collagen is a tumour stroma-derived biomarker for pancreas cancer. *British journal of cancer* **101**, 91-97, doi:10.1038/sj.bjc.6605107 (2009).

10 Whatcott, C. J. *et al.* Desmoplasia in Primary Tumors and Metastatic Lesions of Pancreatic Cancer. *Clin Cancer Res* **21**, 3561-3568, doi:10.1158/1078-0432.Ccr-14-1051 (2015).

11 Leca, J. *et al.* Cancer-associated fibroblast-derived annexin A6+ extracellular vesicles support pancreatic cancer aggressiveness. *The Journal of Clinical Investigation* **126**, 4140-4156, doi:10.1172/JCI87734 (2016).

12 Norton, J., Foster, D., Chinta, M., Titan, A. & Longaker, M. Pancreatic Cancer Associated Fibroblasts (CAF): Under-Explored Target for Pancreatic Cancer Treatment. *Cancers* **12**, 1347, doi:10.3390/cancers12051347 (2020).

13 Öhlund, D. *et al.* Distinct populations of inflammatory fibroblasts and myofibroblasts in pancreatic cancer. *J Exp Med* **214**, 579-596, doi:10.1084/jem.20162024 (2017).

14 Özdemir, B. C. *et al.* Depletion of carcinoma-associated fibroblasts and fibrosis induces immunosuppression and accelerates pancreas cancer with reduced survival. *Cancer Cell* **25**, 719-734, doi:10.1016/j.ccr.2014.04.005 (2014).

15 Lo, A. *et al.* Fibroblast activation protein augments progression and metastasis of pancreatic ductal adenocarcinoma. *JCI Insight* **2**, e92232, doi:10.1172/jci.insight.92232 (2017).
16 Lo, A. *et al.* Tumor-Promoting Desmoplasia Is Disrupted by Depleting FAP-Expressing Stromal Cells. *Cancer Research* **75**, 2800-2810, doi:10.1158/0008-5472.CAN-14-3041 (2015).
17 McAndrews, K. M. *et al.* Identification of Functional Heterogeneity of Carcinoma-Associated Fibroblasts with Distinct IL-6 Mediated Therapy Resistance in Pancreatic Cancer. *Cancer Discovery*, candisc.1484.2020, doi:10.1158/2159-8290.CD-20-1484 (2022).
18 Chen, Y., McAndrews, K. M. & Kalluri, R. Clinical and therapeutic relevance of cancer-associated fibroblasts. *Nature Reviews Clinical Oncology* **18**, 792-804, doi:10.1038/s41571-021-00546-5 (2021).
19 Chen, Y. *et al.* Type I collagen deletion in αSMA+ myofibroblasts augments immune suppression and accelerates progression of pancreatic cancer. *Cancer Cell* **39**, 548-565.e546, doi:https://doi.org/10.1016/j.ccell.2021.02.007 (2021).
20 von Ahrens, D., Bhagat, T. D., Nagrath, D., Maitra, A. & Verma, A. The role of stromal cancer-associated fibroblasts in pancreatic cancer. *Journal of Hematology & Oncology* **10**, 76, doi:10.1186/s13045-017-0448-5 (2017).
21 Biffi, G. *et al.* IL1-Induced JAK/STAT Signaling Is Antagonized by TGFβ to Shape CAF Heterogeneity in Pancreatic Ductal Adenocarcinoma. *Cancer Discovery* **9**, 282, doi:10.1158/2159-8290.CD-18-0710 (2019).
22 Elyada, E. *et al.* Cross-species single-cell analysis of pancreatic ductal adenocarcinoma reveals antigen-presenting cancer-associated fibroblasts. *Cancer Discov*, CD-19-0094, doi:10.1158/2159-8290.CD-19-0094 (2019).
23 Karamitopoulou, E. Tumour microenvironment of pancreatic cancer: immune landscape is dictated by molecular and histopathological features. *British Journal of Cancer* **121**, 5-14, doi:10.1038/s41416-019-0479-5 (2019).
24 Hegde, S. *et al.* Dendritic Cell Paucity Leads to Dysfunctional Immune Surveillance in Pancreatic Cancer. *Cancer Cell* **37**, 289-307.e289, doi:10.1016/j.ccell.2020.02.008 (2020).
25 Panni, R. Z. *et al.* Agonism of CD11b reprograms innate immunity to sensitize pancreatic cancer to immunotherapies. *Sci Transl Med* **11**, doi:10.1126/scitranslmed.aau9240 (2019).
26 DeNardo, D. G. & Ruffell, B. Macrophages as regulators of tumour immunity and immunotherapy. *Nat Rev Immunol* **19**, 369-382, doi:10.1038/s41577-019-0127-6 (2019).
27 Steele, N. G. *et al.* Multimodal mapping of the tumor and peripheral blood immune landscape in human pancreatic cancer. *Nature Cancer* **1**, 1097-1112, doi:10.1038/s43018-020-00121-4 (2020).
28 Lohneis, P. *et al.* Cytotoxic tumour-infiltrating T lymphocytes influence outcome in resected pancreatic ductal adenocarcinoma. *European Journal of Cancer* **83**, 290-301, doi:https://doi.org/10.1016/j.ejca.2017.06.016 (2017).
29 Nagl, S. *et al.* Cell-to-cell distances between tumor-infiltrating inflammatory cells have the potential to distinguish functionally active from suppressed inflammatory

cells. *Oncoimmunology* **5**, e1127494, doi:10.1080/2162402x.2015.1127494 (2016).
30 Boissonnas, A. *et al.* CD8+ tumor-infiltrating T cells are trapped in the tumor-dendritic cell network. *Neoplasia* **15**, 85-94, doi:10.1593/neo.121572 (2013).
31 Peranzoni, E. *et al.* Ex Vivo Imaging of Resident CD8 T Lymphocytes in Human Lung Tumor Slices Using Confocal Microscopy. *J Vis Exp*, 55709, doi:10.3791/55709 (2017).
32 Wculek, S. K. *et al.* Dendritic cells in cancer immunology and immunotherapy. *Nature Reviews Immunology* **20**, 7-24, doi:10.1038/s41577-019-0210-z (2020).
33 Mellman, I. & Steinman, R. M. Dendritic cells: specialized and regulated antigen processing machines. *Cell* **106**, 255-258, doi:10.1016/s0092-8674(01)00449-4 (2001).
34 Murphy, T. L. *et al.* Transcriptional Control of Dendritic Cell Development. *Annual Review of Immunology* **34**, 93-119, doi:10.1146/annurev-immunol-032713-120204 (2016).
35 Murphy, T. L. & Murphy, K. M. Dendritic cells in cancer immunology. *Cell Mol Immunol* **19**, 3-13, doi:10.1038/s41423-021-00741-5 (2022).
36 Joffre, O. P., Segura, E., Savina, A. & Amigorena, S. Cross-presentation by dendritic cells. *Nature Reviews Immunology* **12**, 557-569, doi:10.1038/nri3254 (2012).
37 Jung, S. *et al.* In vivo depletion of CD11c+ dendritic cells abrogates priming of CD8+ T cells by exogenous cell-associated antigens. *Immunity* **17**, 211-220, doi:10.1016/s1074-7613(02)00365-5 (2002).
38 Bourgeois, C., Rocha, B. & Tanchot, C. A role for CD40 expression on CD8+ T cells in the generation of CD8+ T cell memory. *Science* **297**, 2060-2063, doi:10.1126/science.1072615 (2002).
39 Smith, C. M. *et al.* Cognate CD4+ T cell licensing of dendritic cells in CD8+ T cell immunity. *Nature Immunology* **5**, 1143-1148, doi:10.1038/ni1129 (2004).
40 Janssen, E. M. *et al.* CD4+ T cells are required for secondary expansion and memory in CD8+ T lymphocytes. *Nature* **421**, 852-856, doi:10.1038/nature01441 (2003).
41 Ferris, S. T. *et al.* cDC1 prime and are licensed by CD4(+) T cells to induce anti-tumour immunity. *Nature* **584**, 624-629, doi:10.1038/s41586-020-2611-3 (2020).
42 Spranger, S., Dai, D., Horton, B. & Gajewski, T. F. Tumor-Residing Batf3 Dendritic Cells Are Required for Effector T Cell Trafficking and Adoptive T Cell Therapy. *Cancer cell* **31**, 711-723.e714, doi:10.1016/j.ccell.2017.04.003 (2017).
43 Fuertes, M. B., Woo, S.-R., Burnett, B., Fu, Y.-X. & Gajewski, T. F. Type I interferon response and innate immune sensing of cancer. *Trends in Immunology* **34**, 67-73, doi:https://doi.org/10.1016/j.it.2012.10.004 (2013).
44 Padovan, E., Spagnoli, G. C., Ferrantini, M. & Heberer, M. IFN-alpha2a induces IP-10/CXCL10 and MIG/CXCL9 production in monocyte-derived dendritic cells and enhances their capacity to attract and stimulate CD8+ effector T cells. *J Leukoc Biol* **71**, 669-676 (2002).
45 Gubin, M. M. *et al.* Checkpoint blockade cancer immunotherapy targets tumour-specific mutant antigens. *Nature* **515**, 577-581, doi:10.1038/nature13988 (2014).

46 Edelson, B. T. *et al.* Peripheral CD103+ dendritic cells form a unified subset developmentally related to CD8alpha+ conventional dendritic cells. *J Exp Med* **207**, 823-836, doi:10.1084/jem.20091627 (2010).
47 Broz, Miranda L. *et al.* Dissecting the Tumor Myeloid Compartment Reveals Rare Activating Antigen-Presenting Cells Critical for T Cell Immunity. *Cancer Cell* **26**, 638-652, doi:10.1016/j.ccell.2014.09.007 (2014).
48 DuFort, C. C. *et al.* Interstitial Pressure in Pancreatic Ductal Adenocarcinoma Is Dominated by a Gel-Fluid Phase. *Biophys J* **110**, 2106-2119, doi:10.1016/j.bpj.2016.03.040 (2016).
49 Nieskoski, M. D. *et al.* Collagen Complexity Spatially Defines Microregions of Total Tissue Pressure in Pancreatic Cancer. *Scientific Reports* **7**, 10093, doi:10.1038/s41598-017-10671-w (2017).
50 Trédan, O., Galmarini, C. M., Patel, K. & Tannock, I. F. Drug resistance and the solid tumor microenvironment. *J Natl Cancer Inst* **99**, 1441-1454, doi:10.1093/jnci/djm135 (2007).
51 Netti, P. A., Berk, D. A., Swartz, M. A., Grodzinsky, A. J. & Jain, R. K. Role of extracellular matrix assembly in interstitial transport in solid tumors. *Cancer Res* **60**, 2497-2503 (2000).
52 Krisnawan, V. E., Stanley, J. A., Schwarz, J. K. & DeNardo, D. G. Tumor Microenvironment as a Regulator of Radiation Therapy: New Insights into Stromal-Mediated Radioresistance. *Cancers (Basel)* **12**, doi:10.3390/cancers12102916 (2020).
53 Valkenburg, K. C., De Groot, A. E. & Pienta, K. J. Targeting the tumour stroma to improve cancer therapy. *Nat Rev Clin Oncol* **15**, 366-381, doi:10.1038/s41571-018-0007-1 (2018).
54 Mueller, M. M. & Fusenig, N. E. Friends or foes - Bipolar effects of the tumour stroma in cancer. *Nat Rev Cancer* **4**, 839-849, doi:10.1038/nrc1477 (2004).
55 Kalluri, R. The biology and function of fibroblasts in cancer. *Nat Rev Cancer* **16**, 582-598, doi:10.1038/nrc.2016.73 (2016).
56 Kalluri, R. & Zeisberg, M. Fibroblasts in cancer. *Nat Rev Cancer* **6**, 392-401, doi:10.1038/nrc1877 (2006).
57 D'Arcangelo, E., Wu, N. C., Cadavid, J. L. & McGuigan, A. P. The life cycle of cancer-associated fibroblasts within the tumour stroma and its importance in disease outcome. *Br J Cancer*, doi:10.1038/s41416-019-0705-1 (2020).
58 Junttila, M. R. & De Sauvage, F. J. Influence of tumour micro-environment heterogeneity on therapeutic response. *Nature* **501**, 346-354, doi:10.1038/nature12626 (2013).
59 Turley, S. J., Cremasco, V. & Astarita, J. L. Immunological hallmarks of stromal cells in the tumour microenvironment. *Nat Rev Immunol* **15**, 669-682, doi:10.1038/nri3902 (2015).
60 Gilkes, D. M., Semenza, G. L. & Wirtz, D. Hypoxia and the extracellular matrix: Drivers of tumour metastasis. *Nat Rev Cancer* **14**, 430-439, doi:10.1038/nrc3726 (2014).
61 Iyer, S. P., Hunt, C. R. & Pandita, T. K. Cross Talk between Radiation and Immunotherapy: The Twain Shall Meet. *Radiat Res* **189**, 219-224, doi:10.1667/rr14941.1 (2018).

62 Barcellos-Hoff, M. H., Park, C. & Wright, E. G. Radiation and the microenvironment - Tumorigenesis and therapy. *Nat Rev Cancer* **5**, 867-875, doi:10.1038/nrc1735 (2005).
63 McLaughlin, M. *et al.* Inflammatory microenvironment remodelling by tumour cells after radiotherapy. *Nat Rev Cancer*, doi:10.1038/s41568-020-0246-1 (2020).
64 Barker, H. E., Paget, J. T. E., Khan, A. A. & Harrington, K. J. The tumour microenvironment after radiotherapy: Mechanisms of resistance and recurrence. *Nat Rev Cancer* **15**, 409-425, doi:10.1038/nrc3958 (2015).
65 Weichselbaum, R. R., Liang, H., Deng, L. & Fu, Y. X. Radiotherapy and immunotherapy: A beneficial liaison? *Nat Rev Clin Oncol* **14**, 365-379, doi:10.1038/nrclinonc.2016.211 (2017).
66 Hwang, W. L., Pike, L. R. G., Royce, T. J., Mahal, B. A. & Loeffler, J. S. Safety of combining radiotherapy with immune-checkpoint inhibition. *Nat Rev Clin Oncol* **15**, 477-494, doi:10.1038/s41571-018-0046-7 (2018).
67 Schaue, D. & McBride, W. H. Opportunities and challenges of radiotherapy for treating cancer. *Nat Rev Clin Oncol* **12**, 527-540, doi:10.1038/nrclinonc.2015.120 (2015).
68 Grassberger, C., Ellsworth, S. G., Wilks, M. Q., Keane, F. K. & Loeffler, J. S. Assessing the interactions between radiotherapy and antitumour immunity. *Nat Rev Clin Oncol* **16**, 729-745, doi:10.1038/s41571-019-0238-9 (2019).
69 van Leeuwen, C. M. *et al.* The alfa and beta of tumours: a review of parameters of the linear-quadratic model, derived from clinical radiotherapy studies. *Radiat Oncol* **13**, 96, doi:10.1186/s13014-018-1040-z (2018).
70 Hall, E. & Giaccia, A. in *Radiobiology for the radiologist* 35-53 (Lippincott Williams & Wilkins, 2012).
71 Papiez, L. & Timmerman, R. Hypofractionation in radiation therapy and its impact. *Med Phys* **35**, 112-118, doi:10.1118/1.2816228 (2008).
72 Mahajan, A. *et al.* Post-operative stereotactic radiosurgery versus observation for completely resected brain metastases: a single-centre, randomised, controlled, phase 3 trial. *Lancet Oncol* **18**, 1040-1048, doi:10.1016/S1470-2045(17)30414-X (2017).
73 Qiu, H., Moravan, M. J., Milano, M. T., Usuki, K. Y. & Katz, A. W. SBRT for Hepatocellular Carcinoma: 8-Year Experience from a Regional Transplant Center. *J Gastrointest Cancer* **49**, 463-469, doi:10.1007/s12029-017-9990-1 (2018).
74 Kishan, A. U. & King, C. R. Stereotactic Body Radiotherapy for Low- and Intermediate-Risk Prostate Cancer. *Semin Radiat Oncol* **27**, 268-278, doi:10.1016/j.semradonc.2017.02.006 (2017).
75 Aridgides, P. & Bogart, J. Stereotactic Body Radiation Therapy for Stage I Non-Small Cell Lung Cancer. *Thorac Surg Clin* **26**, 261-269, doi:10.1016/j.thorsurg.2016.04.008 (2016).
76 Mole, R. H. Whole body irradiation; radiobiology or medicine? *Br J Radiol* **26**, 234-241, doi:10.1259/0007-1285-26-305-234 (1953).
77 Dewan, M. Z. *et al.* Fractionated but not single-dose radiotherapy induces an immune-mediated abscopal effect when combined with anti-CTLA-4 antibody. *Clin Cancer Res* **15**, 5379-5388, doi:10.1158/1078-0432.CCR-09-0265 (2009).

78 Lee, Y. *et al.* Therapeutic effects of ablative radiation on local tumor require CD8+ T cells: changing strategies for cancer treatment. *Blood* **114**, 589-595, doi:10.1182/blood-2009-02-206870 (2009).
79 Reits, E. A. *et al.* Radiation modulates the peptide repertoire, enhances MHC class I expression, and induces successful antitumor immunotherapy. *J Exp Med* **203**, 1259-1271, doi:10.1084/jem.20052494 (2006).
80 Reynders, K., Illidge, T., Siva, S., Chang, J. Y. & De Ruysscher, D. The abscopal effect of local radiotherapy: using immunotherapy to make a rare event clinically relevant. *Cancer Treat Rev* **41**, 503-510, doi:10.1016/j.ctrv.2015.03.011 (2015).
81 Riaz, N. *et al.* The role of neoantigens in response to immune checkpoint blockade. *Int Immunol* **28**, 411-419, doi:10.1093/intimm/dxw019 (2016).
82 Leroi, N., Lallemand, F., Coucke, P., Noel, A. & Martinive, P. Impacts of ionizing radiation on the different compartments of the tumor microenvironment. *Front Pharmacol* **7**, 1-9, doi:10.3389/fphar.2016.00078 (2016).
83 Straub, J. M. *et al.* Radiation-induced fibrosis: mechanisms and implications for therapy. *J Cancer Res Clin Oncol* **141**, 1985-1994, doi:10.1007/s00432-015-1974-6 (2015).
84 Arnold, K. M. *et al.* The Impact of Radiation on the Tumor Microenvironment: Effect of Dose and Fractionation Schedules. *Cancer Growth Metastasis* **11**, 117906441876163-117906441876163, doi:10.1177/1179064418761639 (2018).
85 Penney, D. P. & Wayne A. Rosenkrans, J. Cell-Cell Matrix Interactions in Induced Lung Injury: I. The Effects of X-Irradiation on Basal Laminar Proteoglycans. *Radiat Res* **99**, 410-419, doi:10.2307/3576383 (1984).
86 Barcellos-Hoff, M. H. Radiation-induced Transforming Growth Factor β and Subsequent Extracellular Matrix Reorganization in Murine Mammary Gland. *Cancer Res* **53**, 3880-3886 (1993).
87 Remy, J., Wegrowski, J., Crechet, F., Martin, M. & Daburon, F. Long-Term Overproduction of Collagen in Radiation-Induced Fibrosis. *Radiat Res* **125**, 14-19, doi:10.2307/3577976 (1991).
88 Chargari, C., Clemenson, C., Martins, I., Perfettini, J.-L. & Deutsch, E. Understanding the functions of tumor stroma in resistance to ionizing radiation: emerging targets for pharmacological modulation. *Drug Resist Updat* **16**, 10-21, doi:10.1016/j.drup.2013.01.001 (2013).
89 Kamochi, N. *et al.* Irradiated fibroblast-induced bystander effects on invasive growth of squamous cell carcinoma under cancer-stromal cell interaction. *Cancer Sci* **99**, 2417-2427, doi:10.1111/j.1349-7006.2008.00978.x (2008).
90 Ohuchida, K. *et al.* Radiation to Stromal Fibroblasts Increases Invasiveness of Pancreatic Cancer Cells through Tumor-Stromal Interactions. *Cancer Res* **64**, 3215-3222, doi:10.1158/0008-5472.CAN-03-2464 (2004).
91 Tommelein, J. *et al.* Cancer-Associated Fibroblasts Connect Metastasis-Promoting Communication in Colorectal Cancer. *Front Oncol* **5**, 1-11, doi:10.3389/fonc.2015.00063 (2015).
92 Wang, Z., Tang, Y., Tan, Y., Wei, Q. & Yu, W. Cancer-associated fibroblasts in radiotherapy: Challenges and new opportunities. *Cell Commun Signal* **17**, 1-12, doi:10.1186/s12964-019-0362-2 (2019).

93 Boelens, M. C. *et al.* Exosome transfer from stromal to breast cancer cells regulates therapy resistance pathways. *Cell* **159**, 499-513, doi:10.1016/j.cell.2014.09.051 (2014).
94 Hwang, R. F. *et al.* Cancer-associated stromal fibroblasts promote pancreatic tumor progression. *Cancer Res* **68**, 918-926, doi:10.1158/0008-5472.CAN-07-5714 (2008).
95 Hardee, M. E. *et al.* Resistance of glioblastoma-initiating cells to radiation mediated by the tumor microenvironment can be abolished by inhibiting transforming growth factor-β. *Cancer Res* **72**, 4119-4129, doi:10.1158/0008-5472.CAN-12-0546 (2012).
96 Wang, Y. *et al.* Cancer-associated Fibroblasts Promote Irradiated Cancer Cell Recovery Through Autophagy. *EBioMedicine* **17**, 45-56, doi:10.1016/j.ebiom.2017.02.019 (2017).
97 Acharyya, S. *et al.* A CXCL1 paracrine network links cancer chemoresistance and metastasis. *Cell* **150**, 165-178, doi:10.1016/j.cell.2012.04.042 (2012).
98 Zhang, H. *et al.* CAF-secreted CXCL1 conferred radioresistance by regulating DNA damage response in a ROS-dependent manner in esophageal squamous cell carcinoma. *Cell Death Dis* **8**, e2790-e2790, doi:10.1038/cddis.2017.180 (2017).
99 Downward, J. Targeting RAS signalling pathways in cancer therapy. *Nat Rev Cancer* **3**, 11-22, doi:10.1038/nrc969 (2003).
100 Dhillon, A. S., Hagan, S., Rath, O. & Kolch, W. MAP kinase signalling pathways in cancer. *Oncogene* **26**, 3279-3290, doi:10.1038/sj.onc.1210421 (2007).
101 Cordes, N. Integrin-mediated cell-matrix interactions for prosurvival and antiapoptotic signaling after genotoxic injury. *Cancer Lett* **242**, 11-19, doi:10.1016/j.canlet.2005.12.004 (2006).
102 Mantoni, T. S., Lunardi, S., Al-Assar, O., Masamune, A. & Brunner, T. B. Pancreatic stellate cells radioprotect pancreatic cancer cells through β1-integrin signaling. *Cancer Res* **71**, 3453-3458, doi:10.1158/0008-5472.CAN-10-1633 (2011).
103 Al-Assar, O. *et al.* Contextual regulation of pancreatic cancer stem cell phenotype and radioresistance by pancreatic stellate cells. *Radiotherapy and Oncology* **111**, 243-251, doi:10.1016/j.radonc.2014.03.014 (2014).
104 Chen, W. J. *et al.* Cancer-associated fibroblasts regulate the plasticity of lung cancer stemness via paracrine signalling. *Nat Commun* **5**, doi:10.1038/ncomms4472 (2014).
105 Osuka, S. *et al.* IGF1 receptor signaling regulates adaptive radioprotection in glioma stem cells. *Stem Cells* **31**, 627-640, doi:10.1002/stem.1328 (2013).
106 Hawsawi, N. M. *et al.* Breast carcinoma-associated fibroblasts and their counterparts display neoplastic-specific changes. *Cancer Res* **68**, 2717-2725, doi:10.1158/0008-5472.CAN-08-0192 (2008).
107 Tang, F. R. & Loke, W. K. Molecular mechanisms of low dose ionizing radiation-induced hormesis, adaptive responses, radioresistance, bystander effects, and genomic instability. *Int J Radiat Biol* **91**, 13-27, doi:10.3109/09553002.2014.937510 (2015).

108 Sun, Y. *et al.* Treatment-induced damage to the tumor microenvironment promotes prostate cancer therapy resistance through WNT16B. *Nat Med* **18**, 1359-1368, doi:10.1038/nm.2890 (2012).
109 Tsai, K. K. C., Stuart, J., Chuang, Y.-Y. E., Little, J. B. & Yuan, Z.-M. Low-Dose Radiation-Induced Senescent Stromal Fibroblasts Render Nearby Breast Cancer Cells Radioresistant. *Radiat Res* **172**, 306-313, doi:10.1667/rr1764.1 (2009).
110 Pazolli, E. *et al.* Chromatin remodeling underlies the senescence- associated secretory phenotype of tumor stromal fibroblasts that supports cancer progression. *Cancer Res* **72**, 2251-2261, doi:10.1158/0008-5472.CAN-11-3386 (2012).
111 Li, D. *et al.* Radiation promotes epithelial-to-mesenchymal transition and invasion of pancreatic cancer cell by activating carcinoma-associated fibroblasts. *Am J Cancer Res* **6**, 2192-2206 (2016).
112 Hellevik, T. *et al.* Cancer-associated fibroblasts from human NSCLC survive ablative doses of radiation but their invasive capacity is reduced. *Radiat Oncol* **7**, doi:10.1186/1748-717X-7-59 (2012).
113 Rhim, A. D. *et al.* Stromal elements act to restrain, rather than support, pancreatic ductal adenocarcinoma. *Cancer Cell* **25**, 735-747, doi:10.1016/j.ccr.2014.04.021 (2014).
114 Jiang, H., Hegde, S. & DeNardo, D. G. Tumor-associated fibrosis as a regulator of tumor immunity and response to immunotherapy. *Cancer Immunology, Immunotherapy* **66**, 1037-1048, doi:10.1007/s00262-017-2003-1 (2017).
115 Lu, P., Weaver, V. M. & Werb, Z. The extracellular matrix: a dynamic niche in cancer progression. *J Cell Biol* **196**, 395-406, doi:10.1083/jcb.201102147 (2012).
116 Poltavets, V., Kochetkova, M., Pitson, S. M. & Samuel, M. S. The Role of the Extracellular Matrix and Its Molecular and Cellular Regulators in Cancer Cell Plasticity. *Front Oncol* **8**, 431-431, doi:10.3389/fonc.2018.00431 (2018).
117 Weichselbaum, R. R. *et al.* An interferon-related gene signature for DNA damage resistance is a predictive marker for chemotherapy and radiation for breast cancer. *Proceedings of the National Academy of Sciences of the United States of America* **105**, 18490-18495, doi:10.1073/pnas.0809242105 (2008).
118 Puthawala, K. *et al.* Inhibition of integrin αvβ6, an activator of latent transforming growth factor-β, prevents radiation-induced lung fibrosis. *American Journal of Respiratory and Critical Care Medicine* **177**, 82-90, doi:10.1164/rccm.200706-806OC (2008).
119 Park, C. C. *et al.* B1 Integrin Inhibitory Antibody Induces Apoptosis of Breast Cancer Cells, Inhibits Growth, and Distinguishes Malignant From Normal Phenotype in Three Dimensional Cultures and in Vivo. *Cancer Research* **66**, 1526-1535, doi:10.1158/0008-5472.CAN-05-3071 (2006).
120 Park, C. C., Zhang, H. J., Yao, E. S., Park, C. J. & Bissell, M. J. B1 Integrin Inhibition Dramatically Enhances Radiotherapy Efficacy in Human Breast Cancer Xenografts. *Cancer Res* **68**, 4398-4405, doi:10.1158/0008-5472.CAN-07-6390 (2008).
121 Cordes, N., Seidler, J., Durzok, R., Geinitz, H. & Brakebusch, C. B1-Integrin-Mediated Signaling Essentially Contributes To Cell Survival After Radiation-Induced Genotoxic Injury. *Oncogene* **25**, 1378-1390, doi:10.1038/sj.onc.1209164 (2006).

122 Biswas, S. *et al.* Inhibition of TGF Beta with neutralizing antibodies prevents radiation-induced acceleration of metastatic cancer progression Find the latest version : Inhibition of TGF- β with neutralizing antibodies prevents radiation-induced acceleration of metastatic. *Journal of Clinical Investigation* **117**, 1305-1313, doi:10.1172/JCI30740.Some (2007).
123 Hellevik, T. & Martinez-Zubiaurre, I. Radiotherapy and the tumor stroma: The importance of dose and fractionation. *Front Oncol* **4 JAN**, 1-12, doi:10.3389/fonc.2014.00001 (2014).
124 Chetty, C., Bhoopathi, P., Rao, J. S. & Lakka, S. S. Inhibition of matrix metalloproteinase-2 enhances radiosensitivity by abrogating radiation-induced FoxM1-mediated G2/M arrest in A549 lung cancer cells. *Int J Cancer* **124**, 2468-2477, doi:10.1002/ijc.24209 (2009).
125 Bertout, J. A., Patel, S. A. & Simon, M. C. The impact of O2 availability on human cancer. *Nat Rev Cancer* **8**, 967-975, doi:10.1038/nrc2540 (2008).
126 Gray, L. H., Conger, A. D., Ebert, M., Hornsey, S. & Scott, O. C. A. The Concentration of Oxygen Dissolved in Tissues at the Time of Irradiation as a Factor in Radiotherapy. *Br J Radiol* **26**, 638-648, doi:10.1259/0007-1285-26-312-638 (1953).
127 Brown, J. M. The hypoxic cell: A target for selective cancer therapy - Eighteenth Bruce F. Cain Memorial Award Lecture. *Cancer Res* **59**, 5863-5870 (1999).
128 Brown, J. M. Vasculogenesis: A crucial player in the resistance of solid tumours to radiotherapy. *Br J Radiol* **87**, doi:10.1259/bjr.20130686 (2014).
129 Frérart, F. *et al.* The acidic tumor microenvironment promotes the reconversion of nitrite into nitric oxide: Towards a new and safe radiosensitizing strategy. *Clin Cancer Res* **14**, 2768-2774, doi:10.1158/1078-0432.CCR-07-4001 (2008).
130 Mitchell, J. B. *et al.* Hypoxic mammalian cell radiosensitization by nitric oxide. *Cancer Res* **53**, 5845-5848 (1993).
131 Winkler, F. *et al.* Kinetics of vascular normalization by VEGFR2 blockade governs brain tumor response to radiation. *Cancer Cell* **6**, 553-563, doi:10.1016/j.ccr.2004.10.011 (2004).
132 Ansiaux, R. *et al.* Thalidomide radiosensitizes tumors through early changes in the tumor microenvironment. *Clin Cancer Res* **11**, 743-750 (2005).
133 Crokart, N. *et al.* Tumor radiosensitization by antiinflammatory drugs: Evidence for a new mechanism involving the oxygen effect. *Cancer Res* **65**, 7911-7916, doi:10.1158/0008-5472.CAN-05-1288 (2005).
134 Demaria, S. & Formenti, S. C. Radiation as an immunological adjuvant: current evidence on dose and fractionation. *Frontiers in Oncology* **2**, 1-7, doi:10.3389/fonc.2012.00153 (2012).
135 Formenti, S. C. *et al.* Radiotherapy induces responses of lung cancer to CTLA-4 blockade. *Nat Med* **24**, 1845-1851, doi:10.1038/s41591-018-0232-2 (2018).
136 Golden, E. B. *et al.* Radiation fosters dose-dependent and chemotherapy-induced immunogenic cell death. *Oncoimmunology* **3**, e28518, doi:10.4161/onci.28518 (2014).
137 Harding, S. M. *et al.* Mitotic progression following DNA damage enables pattern recognition within micronuclei. *Nature* **548**, 466-470, doi:10.1038/nature23470 (2017).

138 Dillon, M. T. *et al.* ATR Inhibition Potentiates the Radiation-induced Inflammatory Tumor Microenvironment. *Clin Cancer Res* **25**, 3392-3403, doi:10.1158/1078-0432.Ccr-18-1821 (2019).
139 Mackenzie, K. J. *et al.* cGAS surveillance of micronuclei links genome instability to innate immunity. *Nature* **548**, 461-465, doi:10.1038/nature23449 (2017).
140 Blair, T. C. *et al.* Dendritic Cell Maturation Defines Immunological Responsiveness of Tumors to Radiation Therapy. *J Immunol* **204**, doi:10.4049/jimmunol.2000194 (2020).
141 Gupta, A. *et al.* Radiotherapy Promotes Tumor-Specific Effector CD8 + T Cells via Dendritic Cell Activation. *J Immunol* **189**, 558-566, doi:10.4049/jimmunol.1200563 (2012).
142 Gerber, S. A. *et al.* IFN-γ mediates the antitumor effects of radiation therapy in a murine colon tumor. *Am J Pathol* **182**, 2345-2354, doi:10.1016/j.ajpath.2013.02.041 (2013).
143 Filatenkov, A. *et al.* Ablative tumor radiation can change the tumor immune cell microenvironment to induce durable complete remissions. *Clin Cancer Res* **21**, 3727-3739, doi:10.1158/1078-0432.CCR-14-2824 (2015).
144 Sharabi, A. B. *et al.* Stereotactic radiation therapy augments antigen-specific PD-1-mediated antitumor immune responses via cross-presentation of tumor antigen. *Cancer Immunol Res* **3**, 345-355, doi:10.1158/2326-6066.CIR-14-0196 (2015).
145 Yoshimoto, Y. *et al.* Radiotherapy-induced anti-tumor immunity contributes to the therapeutic efficacy of irradiation and can be augmented by CTLA-4 blockade in a mouse model. *PLoS ONE* **9**, 1-8, doi:10.1371/journal.pone.0092572 (2014).
146 Gerber, S. A. *et al.* Radio-responsive tumors exhibit greater intratumoral immune activity than nonresponsive tumors. *Int J Cancer* **134**, 2383-2392, doi:10.1002/ijc.28558 (2014).
147 Vanpouille-Box, C. *et al.* TGFβ Is a Master Regulator of Radiation Therapy-Induced Antitumor Immunity. *Cancer Res* **75**, 2232-2242, doi:10.1158/0008-5472.Can-14-3511 (2015).
148 Deng, L. *et al.* Irradiation and anti-PD-L1 treatment synergistically promote antitumor immunity in mice. *J Clin Invest* **124**, 687-695, doi:10.1172/jci67313 (2014).
149 Dovedi, S. J. *et al.* Acquired resistance to fractionated radiotherapy can be overcome by concurrent PD-L1 blockade. *Cancer Res* **74**, 5458-5468, doi:10.1158/0008-5472.Can-14-1258 (2014).
150 Park, S. S. *et al.* PD-1 Restrains Radiotherapy-Induced Abscopal Effect. *Cancer Immunol Res* **3**, 610-619, doi:10.1158/2326-6066.Cir-14-0138 (2015).
151 Formenti, S. C. & Demaria, S. Systemic effects of local radiotherapy. *Lancet Oncol* **10**, 718-726, doi:10.1016/s1470-2045(09)70082-8 (2009).
152 Shaverdian, N. *et al.* Previous radiotherapy and the clinical activity and toxicity of pembrolizumab in the treatment of non-small-cell lung cancer: a secondary analysis of the KEYNOTE-001 phase 1 trial. *Lancet Oncol* **18**, 895-903, doi:10.1016/s1470-2045(17)30380-7 (2017).
153 Kang, J., Demaria, S. & Formenti, S. Current clinical trials testing the combination of immunotherapy with radiotherapy. *J Immunother Cancer* **4**, 51, doi:10.1186/s40425-016-0156-7 (2016).

154 Milas, L. Tumor Bed Effect in Murine Tumors: Relationship to Tumor Take and Tumor Macrophage Content. *Radiat Res* **123**, 232-232, doi:10.2307/3577551 (1990).
155 Vatner, R. E. & Formenti, S. C. Myeloid-derived cells in tumors: effects of radiation. *Semin Radiat Oncol* **25**, 18-27, doi:10.1016/j.semradonc.2014.07.008 (2015).
156 Xu, J. *et al.* CSF1R signaling blockade stanches tumor-infiltrating myeloid cells and improves the efficacy of radiotherapy in prostate cancer. *Cancer Res* **73**, 2782-2794, doi:10.1158/0008-5472.CAN-12-3981 (2013).
157 Ceradini, D. J. *et al.* Progenitor cell trafficking is regulated by hypoxic gradients through HIF-1 induction of SDF-1. *Nat Med* **10**, 858-864, doi:10.1038/nm1075 (2004).
158 Meng, Y. *et al.* Blockade of tumor necrosis factor α signaling in tumor-associated macrophages as a radiosensitizing strategy. *Cancer Res* **70**, 1534-1543, doi:10.1158/0008-5472.CAN-09-2995 (2010).
159 Prakash, H. *et al.* Low doses of gamma irradiation potentially modifies immunosuppressive tumor microenvironment by retuning tumor-associated macrophages: lesson from insulinoma. *Carcinogenesis* **37**, 301-313, doi:10.1093/carcin/bgw007 (2016).
160 Klug, F. *et al.* Low-dose irradiation programs macrophage differentiation to an iNOS^{+}/M1 phenotype that orchestrates effective T cell immunotherapy. *Cancer Cell* **24**, 589-602, doi:10.1016/j.ccr.2013.09.014 (2013).
161 Chiang, C. S. *et al.* Irradiation promotes an m2 macrophage phenotype in tumor hypoxia. *Front Oncol* **2**, 89, doi:10.3389/fonc.2012.00089 (2012).
162 Okubo, M. *et al.* M2-polarized macrophages contribute to neovasculogenesis, leading to relapse of oral cancer following radiation. *Sci Rep* **6**, 27548, doi:10.1038/srep27548 (2016).
163 Seifert, L. *et al.* Radiation Therapy Induces Macrophages to Suppress T-Cell Responses Against Pancreatic Tumors in Mice. *Gastroenterology* **150**, 1659-1672.e1655, doi:10.1053/j.gastro.2016.02.070 (2016).
164 Crittenden, M. R. *et al.* Expression of NF-κb p50 in tumor stroma limits the control of tumors by radiation therapy. *PLoS ONE* **7**, doi:10.1371/journal.pone.0039295 (2012).
165 Shiao, S. L. *et al.* TH2-polarized CD4+ T Cells and macrophages limit efficacy of radiotherapy. *Cancer Immunol Res* **3**, 518-525, doi:10.1158/2326-6066.CIR-14-0232 (2015).
166 Chen, H. M. *et al.* Myeloid-derived suppressor cells as an immune parameter in patients with concurrent sunitinib and stereotactic body radiotherapy. *Clin Cancer Res* **21**, 4073-4085, doi:10.1158/1078-0432.CCR-14-2742 (2015).
167 Ko, J. S. *et al.* Sunitinib mediates reversal of myeloid-derived suppressor cell accumulation in renal cell carcinoma patients. *Clin Cancer Res* **15**, 2148-2157, doi:10.1158/1078-0432.CCR-08-1332 (2009).
168 Persa, E., Balogh, A., Sáfrány, G. & Lumniczky, K. The effect of ionizing radiation on regulatory T cells in health and disease. *Cancer Lett* **368**, 252-261, doi:10.1016/j.canlet.2015.03.003 (2015).

169 Facciabene, A., Motz, G. T. & Coukos, G. T-Regulatory cells: Key players in tumor immune escape and angiogenesis. *Cancer Res* **72**, 2162-2171, doi:10.1158/0008-5472.CAN-11-3687 (2012).
170 Kachikwu, E. L. *et al.* Radiation enhances regulatory T cell representation. *Int J Radiat Oncol Biol Phys* **81**, 1128-1135, doi:10.1016/j.ijrobp.2010.09.034 (2011).
171 Qinfeng, S. *et al.* In situ observation of the effects of local irradiation on cytotoxic and regulatory T lymphocytes in cervical cancer tissue. *Radiat Res* **179**, 584-589, doi:10.1667/rr3155.1 (2013).
172 Komatsu, N. & Hori, S. Full restoration of peripheral Foxp3+ regulatory T cell pool by radioresistant host cells in scurfy bone marrow chimeras. *Proc Natl Acad Sci U S A* **104**, 8959-8964, doi:10.1073/pnas.0702004104 (2007).
173 Schaue, D., Xie, M. W., Ratikan, J. A. & McBride, W. H. Regulatory T cells in radiotherapeutic responses. *Front Oncol* **2**, 90, doi:10.3389/fonc.2012.00090 (2012).
174 Bos, P. D., Plitas, G., Rudra, D., Lee, S. Y. & Rudensky, A. Y. Transient regulatory T cell ablation deters oncogene-driven breast cancer and enhances radiotherapy. *J Exp Med* **210**, 2435-2466, doi:10.1084/jem.20130762 (2013).
175 Oweida, A. J. *et al.* STAT3 Modulation of Regulatory T Cells in Response to Radiation Therapy in Head and Neck Cancer. *J Natl Cancer Inst* **111**, 1339-1349, doi:10.1093/jnci/djz036 (2019).
176 Oweida, A. *et al.* Resistance to Radiotherapy and PD-L1 Blockade Is Mediated by TIM-3 Upregulation and Regulatory T-Cell Infiltration. *Clin Cancer Res* **24**, 5368-5380, doi:10.1158/1078-0432.Ccr-18-1038 (2018).
177 Bhatia, S. *et al.* Inhibition of EphB4-Ephrin-B2 Signaling Reprograms the Tumor Immune Microenvironment in Head and Neck Cancers. *Cancer Res* **79**, 2722-2735, doi:10.1158/0008-5472.Can-18-3257 (2019).
178 Schaue, D., Ratikan, J. A., Iwamoto, K. S. & McBride, W. H. Maximizing tumor immunity with fractionated radiation. *Int J Radiat Oncol Biol Phys* **83**, 1306-1310, doi:10.1016/j.ijrobp.2011.09.049 (2012).
179 Lugade, A. A. *et al.* Local radiation therapy of B16 melanoma tumors increases the generation of tumor antigen-specific effector cells that traffic to the tumor. *J Immunol* **174**, 7516-7523, doi:10.4049/jimmunol.174.12.7516 (2005).
180 Apetoh, L. *et al.* Toll-like receptor 4-dependent contribution of the immune system to anticancer chemotherapy and radiotherapy. *Nat Med* **13**, 1050-1059, doi:10.1038/nm1622 (2007).
181 Demaria, S., Golden, E. B. & Formenti, S. C. Role of Local Radiation Therapy in Cancer Immunotherapy. *JAMA Oncol* **1**, 1325-1332, doi:10.1001/jamaoncol.2015.2756 (2015).
182 Obeid, M. *et al.* Calreticulin exposure dictates the immunogenicity of cancer cell death. *Nat Med* **13**, 54-61, doi:10.1038/nm1523 (2007).
183 Ghiringhelli, F. *et al.* Activation of the NLRP3 inflammasome in dendritic cells induces IL-1beta-dependent adaptive immunity against tumors. *Nat Med* **15**, 1170-1178, doi:10.1038/nm.2028 (2009).
184 Gulley, J. L. *et al.* Combining a recombinant cancer vaccine with standard definitive radiotherapy in patients with localized prostate cancer. *Clin Cancer Res* **11**, 3353-3362, doi:10.1158/1078-0432.Ccr-04-2062 (2005).

185 Schaue, D. *et al.* T-cell responses to survivin in cancer patients undergoing radiation therapy. *Clin Cancer Res* **14**, 4883-4890, doi:10.1158/1078-0432.Ccr-07-4462 (2008).
186 Rutkowski, J., Ślebioda, T., Kmieć, Z. & Zaucha, R. Changes in systemic immune response after stereotactic ablative radiotherapy. Preliminary results of a prospective study in patients with early lung cancer. *Pol Arch Intern Med* **127**, 245-253, doi:10.20452/pamw.3997 (2017).
187 Wasserman, J., Blomgren, H., Rotstein, S., Petrini, B. & Hammarström, S. Immunosuppression in irradiated breast cancer patients: in vitro effect of cyclooxygenase inhibitors. *Bull N Y Acad Med* **65**, 36-44 (1989).
188 Rödel, F. *et al.* Immunomodulatory properties and molecular effects in inflammatory diseases of low-dose x-irradiation. *Front Oncol* **2**, 120, doi:10.3389/fonc.2012.00120 (2012).
189 Trowell, O. A. The sensitivity of lymphocytes to ionising radiation. *J Pathol Bacteriol* **64**, 687-704, doi:10.1002/path.1700640403 (1952).
190 Frey, B. *et al.* Hypofractionated Irradiation Has Immune Stimulatory Potential and Induces a Timely Restricted Infiltration of Immune Cells in Colon Cancer Tumors. *Front Immunol* **8**, 231-231, doi:10.3389/fimmu.2017.00231 (2017).
191 Wisdom, A. J. *et al.* Neutrophils promote tumor resistance to radiation therapy. *Proc Natl Acad Sci U S A* **116**, 18584-18589, doi:10.1073/pnas.1901562116 (2019).
192 Matsumura, S. & Demaria, S. Up-regulation of the pro-inflammatory chemokine CXCL16 is a common response of tumor cells to ionizing radiation. *Radiat Res* **173**, 418-425, doi:10.1667/rr1860.1 (2010).
193 Matsumura, S. *et al.* Radiation-induced CXCL16 release by breast cancer cells attracts effector T cells. *J Immunol* **181**, 3099-3107, doi:10.4049/jimmunol.181.5.3099 (2008).
194 Lugade, A. A. *et al.* Radiation-induced IFN-gamma production within the tumor microenvironment influences antitumor immunity. *J Immunol* **180**, 3132-3139, doi:10.4049/jimmunol.180.5.3132 (2008).
195 Hallahan, D. E., Spriggs, D. R., Beckett, M. A., Kufe, D. W. & Weichselbaum, R. R. Increased tumor necrosis factor alpha mRNA after cellular exposure to ionizing radiation. *Proc Natl Acad Sci U S A* **86**, 10104-10107, doi:10.1073/pnas.86.24.10104 (1989).
196 Barcellos-Hoff, M. H., Derynck, R., Tsang, M. L. & Weatherbee, J. A. Transforming growth factor-beta activation in irradiated murine mammary gland. *J Clin Invest* **93**, 892-899, doi:10.1172/jci117045 (1994).
197 Marincola, F. M., Jaffee, E. M., Hicklin, D. J. & Ferrone, S. Escape of human solid tumors from T-cell recognition: molecular mechanisms and functional significance. *Adv Immunol* **74**, 181-273, doi:10.1016/s0065-2776(08)60911-6 (2000).
198 Klein, B. *et al.* The effect of irradiation on expression of HLA class I antigens in human brain tumors in culture. *J Neurosurg* **80**, 1074-1077, doi:10.3171/jns.1994.80.6.1074 (1994).
199 Santin, A. D. *et al.* Effects of irradiation on the expression of major histocompatibility complex class I antigen and adhesion costimulation molecules

ICAM-1 in human cervical cancer. *Int J Radiat Oncol Biol Phys* **39**, 737-742, doi:10.1016/s0360-3016(97)00372-6 (1997).
200 Santin, A. D. *et al.* Effects of irradiation on the expression of surface antigens in human ovarian cancer. *Gynecol Oncol* **60**, 468-474, doi:10.1006/gyno.1996.0075 (1996).
201 Wan, S. *et al.* Chemotherapeutics and radiation stimulate MHC class I expression through elevated interferon-beta signaling in breast cancer cells. *PLoS One* **7**, e32542, doi:10.1371/journal.pone.0032542 (2012).
202 Zhu, Y. *et al.* Tissue-Resident Macrophages in Pancreatic Ductal Adenocarcinoma Originate from Embryonic Hematopoiesis and Promote Tumor Progression. *Immunity* **47**, 323-338.e326, doi:10.1016/j.immuni.2017.07.014 (2017).
203 Wynn, T. A., Chawla, A. & Pollard, J. W. Macrophage biology in development, homeostasis and disease. *Nature* **496**, 445-455, doi:10.1038/nature12034 (2013).
204 Kraman, M. *et al.* Suppression of Antitumor. *Science* **330**, 827-830 (2010).
205 Lourdes Mora-García, M. *et al.* Mesenchymal stromal cells derived from cervical cancer produce high amounts of adenosine to suppress cytotoxic T lymphocyte functions. *J Transl Med* **14**, 1-14, doi:10.1186/s12967-016-1057-8 (2016).
206 Erez, N., Truitt, M., Olson, P. & Hanahan, D. Cancer-Associated Fibroblasts Are Activated in Incipient Neoplasia to Orchestrate Tumor-Promoting Inflammation in an NF-κB-Dependent Manner. *Cancer Cell* **17**, 135-147, doi:10.1016/j.ccr.2009.12.041 (2010).
207 Liu, T. *et al.* Cancer-associated fibroblasts: an emerging target of anti-cancer immunotherapy. *J Hematol Oncol* **12**, 86, doi:10.1186/s13045-019-0770-1 (2019).
208 Wynn, T. A. & Ramalingam, T. R. Mechanisms of fibrosis: therapeutic translation for fibrotic disease. *Nat Med* **18**, 1028-1040, doi:10.1038/nm.2807 (2012).
209 Cheng, J. t. *et al.* Hepatic carcinoma-associated fibroblasts induce IDO-producing regulatory dendritic cells through IL-6-mediated STAT3 activation. *Oncogenesis* **5**, e198-e198, doi:10.1038/oncsis.2016.7 (2016).
210 Khosravi-Maharlooei, M. *et al.* Tolerogenic effect of mouse fibroblasts on dendritic cells. *Immunology* **148**, 22-33, doi:10.1111/imm.12584 (2016).
211 Mace, T. A. *et al.* Pancreatic Cancer-Associated Stellate Cells Promote Differentiation of Myeloid-Derived Suppressor Cells in a STAT3-Dependent Manner. *Cancer Res* **73**, 3007, doi:10.1158/0008-5472.CAN-12-4601 (2013).
212 Kim, J. H. *et al.* The role of myofibroblasts in upregulation of S100A8 and S100A9 and the differentiation of myeloid cells in the colorectal cancer microenvironment. *Biochem Biophys Res Commun* **423**, 60-66, doi:https://doi.org/10.1016/j.bbrc.2012.05.081 (2012).
213 Feig, C. *et al.* Targeting CXCL12 from FAP-expressing carcinoma-associated fibroblasts synergizes with anti–PD-L1 immunotherapy in pancreatic cancer. *Proceedings of the National Academy of Sciences* **110**, 20212, doi:10.1073/pnas.1320318110 (2013).
214 Jiang, H. *et al.* Targeting focal adhesion kinase renders pancreatic cancers responsive to checkpoint immunotherapy. *Nat Med* **22**, 851-860, doi:10.1038/nm.4123 (2016).

215 Serrels, A. *et al.* Nuclear FAK Controls Chemokine Transcription, Tregs, and Evasion of Anti-tumor Immunity. *Cell* **163**, 160-173, doi:https://doi.org/10.1016/j.cell.2015.09.001 (2015).
216 Ager, E. I. *et al.* Blockade of MMP14 activity in murine breast carcinomas: Implications for macrophages, vessels, and radiotherapy. *J Natl Cancer Inst* **107**, 1-12, doi:10.1093/jnci/djv017 (2015).
217 Shibuya, M. Vascular endothelial growth factor and its receptor system: Physiological functions in angiogenesis and pathological roles in various diseases. *J Biochem* **153**, 13-19, doi:10.1093/jb/mvs136 (2013).
218 Kibria, G., Hatakeyama, H. & Harashima, H. Cancer multidrug resistance: Mechanisms involved and strategies for circumvention using a drug delivery system. *Arch Pharm Res* **37**, 4-15, doi:10.1007/s12272-013-0276-2 (2014).
219 Lanitis, E., Irving, M. & Coukos, G. Targeting the tumor vasculature to enhance T cell activity. *Curr Opin Immunol* **33**, 55-63, doi:10.1016/j.coi.2015.01.011 (2015).
220 Tsai, C. S. *et al.* Macrophages from irradiated tumors express higher levels of iNOS, arginase-I and COX-2, and promote tumor growth. *Int J Radiat Oncol Biol Phys* **68**, 499-507, doi:10.1016/j.ijrobp.2007.01.041 (2007).
221 Park, H. J., Griffin, R. J., Hui, S., Levitt, S. H. & Song, C. W. Radiation-induced vascular damage in tumors: implications of vascular damage in ablative hypofractionated radiotherapy (SBRT and SRS). *Radiat Res* **177**, 311-327, doi:10.1667/rr2773.1 (2012).
222 Hasmim, M. *et al.* Cutting edge: Hypoxia-induced Nanog favors the intratumoral infiltration of regulatory T cells and macrophages via direct regulation of TGF-β1. *J Immunol* **191**, 5802-5806, doi:10.4049/jimmunol.1302140 (2013).
223 Kocher, M. *et al.* Computer simulation of cytotoxic and vascular effects of radiosurgery in solid and necrotic brain metastases. *Radiother Oncol* **54**, 149-156, doi:10.1016/s0167-8140(99)00168-1 (2000).
224 Sonveaux, P. *et al.* Modulation of the tumor vasculature functionality by ionizing radiation accounts for tumor radiosensitization and promotes gene delivery. *FASEB J* **16**, 1979-1981, doi:10.1096/fj.02-0487fje (2002).
225 Crokart, N. *et al.* Early reoxygenation in tumors after irradiation: determining factors and consequences for radiotherapy regimens using daily multiple fractions. *Int J Radiat Oncol Biol Phys* **63**, 901-910, doi:10.1016/j.ijrobp.2005.02.038 (2005).
226 Rao, S. S. *et al.* Axitinib sensitization of high Single Dose Radiotherapy. *Radiotherapy and Oncology* **111**, 88-93, doi:10.1016/j.radonc.2014.02.010 (2014).
227 Choi, J., Cha, Y. J. & Koo, J. S. Adipocyte biology in breast cancer: From silent bystander to active facilitator. *Prog Lipid Res* **69**, 11-20, doi:10.1016/j.plipres.2017.11.002 (2018).
228 Bochet, L. *et al.* Cancer-associated adipocytes promotes breast tumor radioresistance. *Biochem Biophys Res Commun* **411**, 102-106, doi:10.1016/j.bbrc.2011.06.101 (2011).
229 Meng, G. *et al.* Implications for breast cancer treatment from increased autotaxin production in adipose tissue after radiotherapy. *FASEB Journal* **31**, 4064-4077, doi:10.1096/fj.201700159R (2017).
230 Begg, A. C., Stewart, F. A. & Vens, C. Strategies to improve radiotherapy with targeted drugs. *Nat Rev Cancer* **11**, 239-253, doi:10.1038/nrc3007 (2011).

231 Vozenin, M. C., Hendry, J. H. & Limoli, C. L. Biological Benefits of Ultra-high Dose Rate FLASH Radiotherapy: Sleeping Beauty Awoken. *Clin Oncol* **31**, 407-415, doi:https://doi.org/10.1016/j.clon.2019.04.001 (2019).
232 Harrington, K. J. Ultrahigh dose-rate radiotherapy: Next steps for FLASH-RT. *Clin Cancer Res*, clincanres.1796.2018, doi:10.1158/1078-0432.CCR-18-1796 (2018).
233 Mitra, S. K., Hanson, D. A. & Schlaepfer, D. D. Focal adhesion kinase: in command and control of cell motility. *Nat Rev Mol Cell Biol* **6**, 56-68, doi:10.1038/nrm1549 (2005).
234 Cance, W. G. *et al.* Immunohistochemical analyses of focal adhesion kinase expression in benign and malignant human breast and colon tissues: correlation with preinvasive and invasive phenotypes. *Clin Cancer Res* **6**, 2417-2423 (2000).
235 Sulzmaier, F. J., Jean, C. & Schlaepfer, D. D. FAK in cancer: mechanistic findings and clinical applications. *Nat Rev Cancer* **14**, 598-610, doi:10.1038/nrc3792 (2014).
236 Levental, K. R. *et al.* Matrix Crosslinking Forces Tumor Progression by Enhancing Integrin Signaling. *Cell* **139**, 891-906, doi:https://doi.org/10.1016/j.cell.2009.10.027 (2009).
237 Hauck, C. R., Hsia, D. A., Ilic, D. & Schlaepfer, D. D. v-Src SH3-enhanced Interaction with Focal Adhesion Kinase at β1 Integrin-containing Invadopodia Promotes Cell Invasion∗. *Journal of Biological Chemistry* **277**, 12487-12490, doi:https://doi.org/10.1074/jbc.C100760200 (2002).
238 Jean, C. *et al.* Inhibition of endothelial FAK activity prevents tumor metastasis by enhancing barrier function. *J Cell Biol* **204**, 247-263, doi:10.1083/jcb.201307067 (2014).
239 Tavora, B. *et al.* Endothelial FAK is required for tumour angiogenesis. *EMBO Mol Med* **2**, 516-528, doi:10.1002/emmm.201000106 (2010).
240 Owen, K. A. *et al.* Regulation of lamellipodial persistence, adhesion turnover, and motility in macrophages by focal adhesion kinase. *J Cell Biol* **179**, 1275-1287, doi:10.1083/jcb.200708093 (2007).
241 Stokes, J. B. *et al.* Inhibition of focal adhesion kinase by PF-562,271 inhibits the growth and metastasis of pancreatic cancer concomitant with altering the tumor microenvironment. *Mol Cancer Ther* **10**, 2135-2145, doi:10.1158/1535-7163.Mct-11-0261 (2011).
242 Lagares, D. *et al.* Inhibition of focal adhesion kinase prevents experimental lung fibrosis and myofibroblast formation. *Arthritis Rheum* **64**, 1653-1664, doi:10.1002/art.33482 (2012).
243 Barker, H. E., Bird, D., Lang, G. & Erler, J. T. Tumor-secreted LOXL2 activates fibroblasts through FAK signaling. *Mol Cancer Res* **11**, 1425-1436, doi:10.1158/1541-7786.Mcr-13-0033-t (2013).
244 Greenberg, R. S. *et al.* FAK-dependent regulation of myofibroblast differentiation. *Faseb j* **20**, 1006-1008, doi:10.1096/fj.05-4838fje (2006).
245 Despeaux, M. *et al.* Critical features of FAK-expressing AML bone marrow microenvironment through leukemia stem cell hijacking of mesenchymal stromal cells. *Leukemia* **25**, 1789-1793, doi:10.1038/leu.2011.145 (2011).

246 Lim, Y. *et al.* PyK2 and FAK connections to p190Rho guanine nucleotide exchange factor regulate RhoA activity, focal adhesion formation, and cell motility. *J Cell Biol* **180**, 187-203, doi:10.1083/jcb.200708194 (2008).
247 Cabrita, M. A. *et al.* Focal adhesion kinase inhibitors are potent anti-angiogenic agents. *Mol Oncol* **5**, 517-526, doi:10.1016/j.molonc.2011.10.004 (2011).
248 Infante, J. R. *et al.* Safety, pharmacokinetic, and pharmacodynamic phase I dose-escalation trial of PF-00562271, an inhibitor of focal adhesion kinase, in advanced solid tumors. *J Clin Oncol* **30**, 1527-1533, doi:10.1200/jco.2011.38.9346 (2012).
249 Kang, Y. *et al.* Role of focal adhesion kinase in regulating YB-1-mediated paclitaxel resistance in ovarian cancer. *J Natl Cancer Inst* **105**, 1485-1495, doi:10.1093/jnci/djt210 (2013).
250 Diaz Osterman, C. J. *et al.* FAK activity sustains intrinsic and acquired ovarian cancer resistance to platinum chemotherapy. *Elife* **8**, doi:10.7554/eLife.47327 (2019).
251 Skinner, H. D. *et al.* Proteomic Profiling Identifies PTK2/FAK as a Driver of Radioresistance in HPV-negative Head and Neck Cancer. *Clin Cancer Res* **22**, 4643-4650, doi:10.1158/1078-0432.Ccr-15-2785 (2016).
252 Tang, K.-J. *et al.* Focal Adhesion Kinase Regulates the DNA Damage Response and Its Inhibition Radiosensitizes Mutant KRAS Lung Cancer. *Clinical cancer research : an official journal of the American Association for Cancer Research* **22**, 5851-5863, doi:10.1158/1078-0432.CCR-15-2603 (2016).
253 Williams, K. E., Bundred, N. J., Landberg, G., Clarke, R. B. & Farnie, G. Focal adhesion kinase and Wnt signaling regulate human ductal carcinoma in situ stem cell activity and response to radiotherapy. *Stem Cells* **33**, 327-341, doi:10.1002/stem.1843 (2015).
254 Canel, M. *et al.* T-cell co-stimulation in combination with targeting FAK drives enhanced anti-tumor immunity. *Elife* **9**, doi:10.7554/eLife.48092 (2020).
255 Halder, J. *et al.* Therapeutic efficacy of a novel focal adhesion kinase inhibitor TAE226 in ovarian carcinoma. *Cancer Res* **67**, 10976-10983, doi:10.1158/0008-5472.Can-07-2667 (2007).
256 Bagi, C. M. *et al.* Sunitinib and PF-562,271 (FAK/Pyk2 inhibitor) effectively block growth and recovery of human hepatocellular carcinoma in a rat xenograft model. *Cancer Biol Ther* **8**, 856-865, doi:10.4161/cbt.8.9.8246 (2009).
257 Tavora, B. *et al.* Endothelial-cell FAK targeting sensitizes tumours to DNA-damaging therapy. *Nature* **514**, 112-116, doi:10.1038/nature13541 (2014).
258 Cid-Arregui, A. & Juarez, V. Perspectives in the treatment of pancreatic adenocarcinoma. *World J Gastroenterol* **21**, 9297-9316, doi:10.3748/wjg.v21.i31.9297 (2015).
259 Sarantis, P., Koustas, E., Papadimitropoulou, A., Papavassiliou, A. G. & Karamouzis, M. V. Pancreatic ductal adenocarcinoma: Treatment hurdles, tumor microenvironment and immunotherapy. *World J Gastrointest Oncol* **12**, 173-181, doi:10.4251/wjgo.v12.i2.173 (2020).
260 McGuigan, A. *et al.* Pancreatic cancer: A review of clinical diagnosis, epidemiology, treatment and outcomes. *World J Gastroenterol* **24**, 4846-4861, doi:10.3748/wjg.v24.i43.4846 (2018).

261 Hull, A. *et al.* Radioimmunotherapy of Pancreatic Ductal Adenocarcinoma: A Review of the Current Status of Literature. *Cancers* **12**, doi:10.3390/cancers12020481 (2020).
262 Hazard, L. The role of radiation therapy in pancreas cancer. *Gastrointest Cancer Res* **3**, 20-28 (2009).
263 Goodman, K. A. & Hajj, C. Role of radiation therapy in the management of pancreatic cancer. *J Surg Oncol* **107**, 86-96, doi:10.1002/jso.23137 (2013).
264 Yao, W., Maitra, A. & Ying, H. Recent insights into the biology of pancreatic cancer. *EBioMedicine* **53**, 102655, doi:10.1016/j.ebiom.2020.102655 (2020).
265 Zhang, Y. *et al.* Myeloid cells are required for PD-1/PD-L1 checkpoint activation and the establishment of an immunosuppressive environment in pancreatic cancer. *Gut* **66**, 124-136, doi:10.1136/gutjnl-2016-312078 (2017).
266 Stromnes, I. M. *et al.* Targeted depletion of an MDSC subset unmasks pancreatic ductal adenocarcinoma to adaptive immunity. *Gut* **63**, 1769-1781, doi:10.1136/gutjnl-2013-306271 (2014).
267 Buscail, L., Bournet, B. & Cordelier, P. Role of oncogenic KRAS in the diagnosis, prognosis and treatment of pancreatic cancer. *Nature Reviews Gastroenterology & Hepatology* **17**, 153-168, doi:10.1038/s41575-019-0245-4 (2020).
268 Gandhi, L. *et al.* Pembrolizumab plus Chemotherapy in Metastatic Non–Small-Cell Lung Cancer. *New England Journal of Medicine* **378**, 2078-2092, doi:10.1056/NEJMoa1801005 (2018).
269 Larkin, J. *et al.* Combined Nivolumab and Ipilimumab or Monotherapy in Untreated Melanoma. *New England Journal of Medicine* **373**, 23-34, doi:10.1056/NEJMoa1504030 (2015).
270 Robert, C. *et al.* Pembrolizumab versus Ipilimumab in Advanced Melanoma. *New England Journal of Medicine* **372**, 2521-2532, doi:10.1056/NEJMoa1503093 (2015).
271 Kunk, P. R., Bauer, T. W., Slingluff, C. L. & Rahma, O. E. From bench to bedside a comprehensive review of pancreatic cancer immunotherapy. *Journal for immunotherapy of cancer* **4**, 14-14, doi:10.1186/s40425-016-0119-z (2016).
272 O'Reilly, E. M. *et al.* Durvalumab With or Without Tremelimumab for Patients With Metastatic Pancreatic Ductal Adenocarcinoma: A Phase 2 Randomized Clinical Trial. *JAMA Oncology* **5**, 1431-1438, doi:10.1001/jamaoncol.2019.1588 (2019).
273 Neoptolemos, J. P. *et al.* A Randomized Trial of Chemoradiotherapy and Chemotherapy after Resection of Pancreatic Cancer. *New England Journal of Medicine* **350**, 1200-1210, doi:10.1056/NEJMoa032295 (2004).
274 Wainberg, Z. A. *et al.* Open-label, Phase I Study of Nivolumab Combined with nab-Paclitaxel Plus Gemcitabine in Advanced Pancreatic Cancer. *Clinical Cancer Research* **26**, 4814, doi:10.1158/1078-0432.CCR-20-0099 (2020).
275 Gajiwala, S., Torgeson, A., Garrido-Laguna, I., Kinsey, C. & Lloyd, S. Combination immunotherapy and radiation therapy strategies for pancreatic cancer—targeting multiple steps in the cancer immunity cycle. *Journal of Gastrointestinal Oncology* **9**, 1014-1026 (2018).
276 Biffi, G. & Tuveson, D. A. Diversity and Biology of Cancer-Associated Fibroblasts. *Physiol Rev* **101**, 147-176, doi:10.1152/physrev.00048.2019 (2021).

277 Ohlund, D. *et al.* Distinct populations of inflammatory fibroblasts and myofibroblasts in pancreatic cancer. *J Exp Med* **214**, 579-596, doi:10.1084/jem.20162024 (2017).
278 Baskar, R., Dai, J., Wenlong, N., Yeo, R. & Yeoh, K.-W. Biological response of cancer cells to radiation treatment. *Frontiers in molecular biosciences* **1**, 24-24, doi:10.3389/fmolb.2014.00024 (2014).
279 Deng, M. *et al.* Extracellular matrix stiffness determines DNA repair efficiency and cellular sensitivity to genotoxic agents. *Science Advances* **6**, eabb2630, doi:10.1126/sciadv.abb2630.
280 Deville, S. S. & Cordes, N. The Extracellular, Cellular, and Nuclear Stiffness, a Trinity in the Cancer Resistome—A Review. *Frontiers in Oncology* **9**, 1376 (2019).
281 Kaur, P. & Asea, A. Radiation-induced effects and the immune system in cancer. *Front Oncol* **2**, 191, doi:10.3389/fonc.2012.00191 (2012).
282 Zhao, X.-K. *et al.* Focal Adhesion Kinase Regulates Fibroblast Migration via Integrin beta-1 and Plays a Central Role in Fibrosis. *Scientific Reports* **6**, 19276, doi:10.1038/srep19276 (2016).
283 Schlaepfer, D. D. & Hunter, T. Signal transduction from the extracellular matrix--a role for the focal adhesion protein-tyrosine kinase FAK. *Cell Struct Funct* **21**, 445-450, doi:10.1247/csf.21.445 (1996).
284 Laklai, H. *et al.* Genotype tunes pancreatic ductal adenocarcinoma tissue tension to induce matricellular fibrosis and tumor progression. *Nature medicine* **22**, 497-505, doi:10.1038/nm.4082 (2016).
285 Venkatesulu, B. P., Hsieh, C.-E., Sanders, K. L. & Krishnan, S. Recent advances in radiation therapy of pancreatic cancer. *F1000Res* **7**, F1000 Faculty Rev-1931, doi:10.12688/f1000research.16272.1 (2018).
286 Li, D., Xie, K., Wolff, R. & Abbruzzese, J. L. Pancreatic cancer. *The Lancet* **363**, 1049-1057, doi:https://doi.org/10.1016/S0140-6736(04)15841-8 (2004).
287 Hingorani, S. R. *et al.* Trp53R172H and KrasG12D cooperate to promote chromosomal instability and widely metastatic pancreatic ductal adenocarcinoma in mice. *Cancer Cell* **7**, 469-483, doi:10.1016/j.ccr.2005.04.023 (2005).
288 Wong, J. *et al.* High-resolution, small animal radiation research platform with x-ray tomographic guidance capabilities. *International journal of radiation oncology, biology, physics* **71**, 1591-1599, doi:10.1016/j.ijrobp.2008.04.025 (2008).
289 Mills, B. N. *et al.* Stereotactic Body Radiation and Interleukin-12 Combination Therapy Eradicates Pancreatic Tumors by Repolarizing the Immune Microenvironment. *Cell Rep* **29**, 406-421.e405, doi:10.1016/j.celrep.2019.08.095 (2019).
290 Kirsch, D. G. *et al.* A spatially and temporally restricted mouse model of soft tissue sarcoma. *Nat Med* **13**, 992-997, doi:10.1038/nm1602 (2007).
291 Thomas, D. & Radhakrishnan, P. Tumor-stromal crosstalk in pancreatic cancer and tissue fibrosis. *Mol Cancer* **18**, 14-14, doi:10.1186/s12943-018-0927-5 (2019).
292 Apte, M. V. *et al.* Desmoplastic reaction in pancreatic cancer: role of pancreatic stellate cells. *Pancreas* **29**, 179-187, doi:10.1097/00006676-200410000-00002 (2004).
293 Boj, S. F. *et al.* Organoid models of human and mouse ductal pancreatic cancer. *Cell* **160**, 324-338, doi:10.1016/j.cell.2014.12.021 (2015).

294 Kim, M. P. *et al.* Generation of orthotopic and heterotopic human pancreatic cancer xenografts in immunodeficient mice. *Nat Protoc* **4**, 1670-1680, doi:10.1038/nprot.2009.171 (2009).
295 Goel, H. L. *et al.* β1 integrins mediate resistance to ionizing radiation in vivo by inhibiting c-Jun amino terminal kinase 1. *J Cell Physiol* **228**, 1601-1609, doi:10.1002/jcp.24323 (2013).
296 Klein, D. *et al.* Endothelial Caveolin-1 regulates the radiation response of epithelial prostate tumors. *Oncogenesis* **4**, e148-e148, doi:10.1038/oncsis.2015.9 (2015).
297 Lee, Y. *et al.* Therapeutic effects of ablative radiation on local tumor require CD8+ T cells: changing strategies for cancer treatment. *Blood* **114**, 589-595, doi:10.1182/blood-2009-02-206870 (2009).
298 Hosein, A. N., Brekken, R. A. & Maitra, A. Pancreatic cancer stroma: an update on therapeutic targeting strategies. *Nature Reviews Gastroenterology & Hepatology* **17**, 487-505, doi:10.1038/s41575-020-0300-1 (2020).
299 Dawson, J. C., Serrels, A., Stupack, D. G., Schlaepfer, D. D. & Frame, M. C. Targeting FAK in anticancer combination therapies. *Nature Reviews Cancer* **21**, 313-324, doi:10.1038/s41568-021-00340-6 (2021).
300 Galluzzi, L. *et al.* Molecular mechanisms of cell death: recommendations of the Nomenclature Committee on Cell Death 2018. *Cell Death & Differentiation* **25**, 486-541, doi:10.1038/s41418-017-0012-4 (2018).
301 Szondy, Z., Sarang, Z., Kiss, B., Garabuczi, É. & Köröskényi, K. Anti-inflammatory Mechanisms Triggered by Apoptotic Cells during Their Clearance. *Frontiers in immunology* **8**, 909-909, doi:10.3389/fimmu.2017.00909 (2017).
302 Yatim, N., Cullen, S. & Albert, M. L. Dying cells actively regulate adaptive immune responses. *Nat Rev Immunol* **17**, 262-275, doi:10.1038/nri.2017.9 (2017).
303 Green, D. R., Ferguson, T., Zitvogel, L. & Kroemer, G. Immunogenic and tolerogenic cell death. *Nat Rev Immunol* **9**, 353-363, doi:10.1038/nri2545 (2009).
304 Hou, W. *et al.* Strange attractors: DAMPs and autophagy link tumor cell death and immunity. *Cell Death & Disease* **4**, e966-e966, doi:10.1038/cddis.2013.493 (2013).
305 Vénéreau, E., Ceriotti, C. & Bianchi, M. E. DAMPs from Cell Death to New Life. *Front Immunol* **6**, 422, doi:10.3389/fimmu.2015.00422 (2015).
306 Krysko, O., Løve Aaes, T., Bachert, C., Vandenabeele, P. & Krysko, D. V. Many faces of DAMPs in cancer therapy. *Cell death & disease* **4**, e631-e631, doi:10.1038/cddis.2013.156 (2013).
307 Hayashi, K. *et al.* Tipping the immunostimulatory and inhibitory DAMP balance to harness immunogenic cell death. *Nature Communications* **11**, 6299, doi:10.1038/s41467-020-19970-9 (2020).
308 Meyer, M. A. *et al.* Breast and pancreatic cancer interrupt IRF8-dependent dendritic cell development to overcome immune surveillance. *Nature Communications* **9**, 1250, doi:10.1038/s41467-018-03600-6 (2018).
309 Gabrilovich, D. I., Ostrand-Rosenberg, S. & Bronte, V. Coordinated regulation of myeloid cells by tumours. *Nat Rev Immunol* **12**, 253-268, doi:10.1038/nri3175 (2012).
310 Qian, B.-Z. *et al.* CCL2 recruits inflammatory monocytes to facilitate breast-tumour metastasis. *Nature* **475**, 222-225, doi:10.1038/nature10138 (2011).

311 Geissmann, F. *et al.* Development of monocytes, macrophages, and dendritic cells. *Science* **327**, 656-661, doi:10.1126/science.1178331 (2010).
312 Kitamura, T., Qian, B. Z. & Pollard, J. W. Immune cell promotion of metastasis. *Nat Rev Immunol* **15**, 73-86, doi:10.1038/nri3789 (2015).
313 Noy, R. & Pollard, J. W. Tumor-associated macrophages: from mechanisms to therapy. *Immunity* **41**, 49-61, doi:10.1016/j.immuni.2014.06.010 (2014).
314 DeNardo, D. G. *et al.* Leukocyte complexity predicts breast cancer survival and functionally regulates response to chemotherapy. *Cancer discovery* **1**, 54-67, doi:10.1158/2159-8274.CD-10-0028 (2011).
315 DeNardo, D. G. *et al.* CD4(+) T cells regulate pulmonary metastasis of mammary carcinomas by enhancing protumor properties of macrophages. *Cancer Cell* **16**, 91-102, doi:10.1016/j.ccr.2009.06.018 (2009).
316 Bousso, P. & Robey, E. Dynamics of CD8+ T cell priming by dendritic cells in intact lymph nodes. *Nat Immunol* **4**, 579-585, doi:10.1038/ni928 (2003).
317 Stoll, S., Delon, J., Brotz, T. M. & Germain, R. N. Dynamic imaging of T cell-dendritic cell interactions in lymph nodes. *Science* **296**, 1873-1876, doi:10.1126/science.1071065 (2002).
318 Mempel, T. R., Henrickson, S. E. & Von Andrian, U. H. T-cell priming by dendritic cells in lymph nodes occurs in three distinct phases. *Nature* **427**, 154-159, doi:10.1038/nature02238 (2004).
319 von Andrian, U. H. & Mempel, T. R. Homing and cellular traffic in lymph nodes. *Nat Rev Immunol* **3**, 867-878, doi:10.1038/nri1222 (2003).
320 Meredith, M. M. *et al.* Expression of the zinc finger transcription factor zDC (Zbtb46, Btbd4) defines the classical dendritic cell lineage. *J Exp Med* **209**, 1153-1165, doi:10.1084/jem.20112675 (2012).
321 Tokunaga, R. *et al.* CXCL9, CXCL10, CXCL11/CXCR3 axis for immune activation - A target for novel cancer therapy. *Cancer treatment reviews* **63**, 40-47, doi:10.1016/j.ctrv.2017.11.007 (2018).
322 Carrington, E. M. *et al.* Anti-apoptotic proteins BCL-2, MCL-1 and A1 summate collectively to maintain survival of immune cell populations both in vitro and in vivo. *Cell Death & Differentiation* **24**, 878-888, doi:10.1038/cdd.2017.30 (2017).
323 Droin, N. M. & Green, D. R. Role of Bcl-2 family members in immunity and disease. *Biochimica et Biophysica Acta (BBA) - Molecular Cell Research* **1644**, 179-188, doi:https://doi.org/10.1016/j.bbamcr.2003.10.011 (2004).
324 Jung, J., Zeng, H. & Horng, T. Metabolism as a guiding force for immunity. *Nature Cell Biology* **21**, 85-93, doi:10.1038/s41556-018-0217-x (2019).
325 Buck, M. D., Sowell, R. T., Kaech, S. M. & Pearce, E. L. Metabolic Instruction of Immunity. *Cell* **169**, 570-586, doi:10.1016/j.cell.2017.04.004 (2017).
326 Rot, A. & von Andrian, U. H. Chemokines in innate and adaptive host defense: basic chemokinese grammar for immune cells. *Annu Rev Immunol* **22**, 891-928, doi:10.1146/annurev.immunol.22.012703.104543 (2004).
327 Luster, A. D. Chemokines--chemotactic cytokines that mediate inflammation. *N Engl J Med* **338**, 436-445, doi:10.1056/nejm199802123380706 (1998).
328 Luster, A. D., Alon, R. & von Andrian, U. H. Immune cell migration in inflammation: present and future therapeutic targets. *Nature Immunology* **6**, 1182-1190, doi:10.1038/ni1275 (2005).

329 Monteran, L. & Erez, N. The Dark Side of Fibroblasts: Cancer-Associated Fibroblasts as Mediators of Immunosuppression in the Tumor Microenvironment. *Frontiers in Immunology* **10**, doi:10.3389/fimmu.2019.01835 (2019).
330 Huber, J. P. & Farrar, J. D. Regulation of effector and memory T-cell functions by type I interferon. *Immunology* **132**, 466-474, doi:10.1111/j.1365-2567.2011.03412.x (2011).
331 Jorgovanovic, D., Song, M., Wang, L. & Zhang, Y. Roles of IFN-γ in tumor progression and regression: a review. *Biomarker Research* **8**, 49, doi:10.1186/s40364-020-00228-x (2020).
332 LeBleu, V. S. *et al.* Origin and function of myofibroblasts in kidney fibrosis. *Nat Med* **19**, 1047-1053, doi:10.1038/nm.3218 (2013).
333 Roers, A., Hiller, B. & Hornung, V. Recognition of Endogenous Nucleic Acids by the Innate Immune System. *Immunity* **44**, 739-754, doi:10.1016/j.immuni.2016.04.002 (2016).
334 Mahaney, B. L., Meek, K. & Lees-Miller, S. P. Repair of ionizing radiation-induced DNA double-strand breaks by non-homologous end-joining. *Biochem J* **417**, 639-650, doi:10.1042/BJ20080413 (2009).
335 Sun, L., Wu, J., Du, F., Chen, X. & Chen Zhijian, J. Cyclic GMP-AMP Synthase Is a Cytosolic DNA Sensor That Activates the Type I Interferon Pathway. *Science* **339**, 786-791, doi:10.1126/science.1232458 (2013).
336 Ablasser, A. *et al.* cGAS produces a 2′-5′-linked cyclic dinucleotide second messenger that activates STING. *Nature* **498**, 380-384, doi:10.1038/nature12306 (2013).
337 Brzostek-Racine, S., Gordon, C., Van Scoy, S. & Reich, N. C. The DNA damage response induces IFN. *Journal of immunology (Baltimore, Md. : 1950)* **187**, 5336-5345, doi:10.4049/jimmunol.1100040 (2011).
338 Li, N. *et al.* ATM is required for IkappaB kinase (IKKk) activation in response to DNA double strand breaks. *J Biol Chem* **276**, 8898-8903, doi:10.1074/jbc.M009809200 (2001).
339 Lim, J. Y. H., Gerber, S. A., Murphy, S. P. & Lord, E. M. Type I interferons induced by radiation therapy mediate recruitment and effector function of CD8(+) T cells. *Cancer Immunol Immunother* **63**, 259-271, doi:10.1007/s00262-013-1506-7 (2014).
340 Burnette, B. C. *et al.* The Efficacy of Radiotherapy Relies upon Induction of Type I Interferon–Dependent Innate and Adaptive Immunity. *Cancer Research* **71**, 2488-2496, doi:10.1158/0008-5472.CAN-10-2820 (2011).
341 Weichselbaum Ralph, R. *et al.* An interferon-related gene signature for DNA damage resistance is a predictive marker for chemotherapy and radiation for breast cancer. *Proceedings of the National Academy of Sciences* **105**, 18490-18495, doi:10.1073/pnas.0809242105 (2008).
342 Minn, A. J. Interferons and the Immunogenic Effects of Cancer Therapy. *Trends Immunol* **36**, 725-737, doi:10.1016/j.it.2015.09.007 (2015).
343 Deng, L. *et al.* STING-Dependent Cytosolic DNA Sensing Promotes Radiation-Induced Type I Interferon-Dependent Antitumor Immunity in Immunogenic Tumors. *Immunity* **41**, 843-852, doi:10.1016/j.immuni.2014.10.019 (2014).

344 Bai, H., Lester, G. M. S., Petishnok, L. C. & Dean, D. A. Cytoplasmic transport and nuclear import of plasmid DNA. *Biosci Rep* **37**, BSR20160616, doi:10.1042/BSR20160616 (2017).
345 Putnam, A. J., Schultz, K. & Mooney, D. J. Control of microtubule assembly by extracellular matrix and externally applied strain. *American Journal of Physiology-Cell Physiology* **280**, C556-C564, doi:10.1152/ajpcell.2001.280.3.C556 (2001).
346 Ma, S. *et al.* DNA damage promotes microtubule dynamics through a DNA-PK-AKT axis for enhanced repair. *Journal of Cell Biology* **220**, e201911025, doi:10.1083/jcb.201911025 (2021).
347 Kim, S. H., Turnbull, J. & Guimond, S. Extracellular matrix and cell signalling: the dynamic cooperation of integrin, proteoglycan and growth factor receptor. *J Endocrinol* **209**, 139-151, doi:10.1530/joe-10-0377 (2011).
348 Winkler, J., Abisoye-Ogunniyan, A., Metcalf, K. J. & Werb, Z. Concepts of extracellular matrix remodelling in tumour progression and metastasis. *Nature Communications* **11**, 5120, doi:10.1038/s41467-020-18794-x (2020).
349 Beinke, C., Van Beuningen, D. & Cordes, N. Ionizing radiation modules of the expression and tyrosine phosphorylation of the focal adhesion-associated proteins focal adhesion kinase (FAK) and its substrates p130cas and paxillin in A549 human lung carcinoma cells in vitro. *International Journal of Radiation Biology* **79**, 721-731, doi:10.1080/09553000310001610231 (2003).
350 Haeger, A. *et al.* Collective cancer invasion forms an integrin-dependent radioresistant niche. *J Exp Med* **217**, doi:10.1084/jem.20181184 (2020).
351 Jin, S. *et al.* Inference and analysis of cell-cell communication using CellChat. *Nature Communications* **12**, 1088, doi:10.1038/s41467-021-21246-9 (2021).
352 Nallanthighal, S., Heiserman, J. P. & Cheon, D.-J. The Role of the Extracellular Matrix in Cancer Stemness. *Frontiers in Cell and Developmental Biology* **7**, doi:10.3389/fcell.2019.00086 (2019).
353 Walker, C., Mojares, E. & Del Río Hernández, A. Role of Extracellular Matrix in Development and Cancer Progression. *Int J Mol Sci* **19**, 3028, doi:10.3390/ijms19103028 (2018).
354 Moffitt, R. A. *et al.* Virtual microdissection identifies distinct tumor- and stroma-specific subtypes of pancreatic ductal adenocarcinoma. *Nat Genet* **47**, 1168-1178, doi:10.1038/ng.3398 (2015).
355 Martens, S. *et al.* Different shades of pancreatic ductal adenocarcinoma, different paths towards precision therapeutic applications. *Annals of Oncology* **30**, 1428-1436, doi:10.1093/annonc/mdz181 (2019).
356 Brett, E. A., Sauter, M. A., Machens, H.-G. & Duscher, D. Tumor-associated collagen signatures: pushing tumor boundaries. *Cancer & Metabolism* **8**, 14, doi:10.1186/s40170-020-00221-w (2020).
357 McMahon, M., Ye, S., Pedrina, J., Dlugolenski, D. & Stambas, J. Extracellular Matrix Enzymes and Immune Cell Biology. *Frontiers in Molecular Biosciences* **8**, doi:10.3389/fmolb.2021.703868 (2021).
358 Bhattacharjee, O., Ayyangar, U., Kurbet, A. S., Ashok, D. & Raghavan, S. Unraveling the ECM-Immune Cell Crosstalk in Skin Diseases. *Frontiers in Cell and Developmental Biology* **7**, doi:10.3389/fcell.2019.00068 (2019).

359 Buechler, M. B. *et al.* Cross-tissue organization of the fibroblast lineage. *Nature* **593**, 575-579, doi:10.1038/s41586-021-03549-5 (2021).
360 Helms, E. J. *et al.* Mesenchymal Lineage Heterogeneity Underlies Nonredundant Functions of Pancreatic Cancer–Associated Fibroblasts. *Cancer Discovery* **12**, 484-501, doi:10.1158/2159-8290.CD-21-0601 (2022).
361 Francescone, R. *et al.* Netrin G1 Promotes Pancreatic Tumorigenesis through Cancer-Associated Fibroblast-Driven Nutritional Support and Immunosuppression. *Cancer Discov* **11**, 446-479, doi:10.1158/2159-8290.Cd-20-0775 (2021).
362 Dominguez, C. X. *et al.* Single-Cell RNA Sequencing Reveals Stromal Evolution into LRRC15(+) Myofibroblasts as a Determinant of Patient Response to Cancer Immunotherapy. *Cancer Discov* **10**, 232-253, doi:10.1158/2159-8290.Cd-19-0644 (2020).
363 Gohil, S. H., Iorgulescu, J. B., Braun, D. A., Keskin, D. B. & Livak, K. J. Applying high-dimensional single-cell technologies to the analysis of cancer immunotherapy. *Nat Rev Clin Oncol* **18**, 244-256, doi:10.1038/s41571-020-00449-x (2021).
364 Giesen, C. *et al.* Highly multiplexed imaging of tumor tissues with subcellular resolution by mass cytometry. *Nat Methods* **11**, 417-422, doi:10.1038/nmeth.2869 (2014).
365 Obradovic, A. *et al.* Immunostimulatory cancer-associated fibroblast subpopulations can predict immunotherapy response in head and neck cancer. *Clin Cancer Res*, doi:10.1158/1078-0432.Ccr-21-3570 (2022).
366 Craig, D. J. *et al.* The abscopal effect of radiation therapy. *Future Oncology* **17**, 1683-1694, doi:10.2217/fon-2020-0994 (2021).
367 Ngwa, W. *et al.* Using immunotherapy to boost the abscopal effect. *Nature Reviews Cancer* **18**, 313-322, doi:10.1038/nrc.2018.6 (2018).
368 Formenti, S. C. & Demaria, S. Combining Radiotherapy and Cancer Immunotherapy: A Paradigm Shift. *JNCI: Journal of the National Cancer Institute* **105**, 256-265, doi:10.1093/jnci/djs629 (2013).
369 Demaria, S. *et al.* Ionizing radiation inhibition of distant untreated tumors (abscopal effect) is immune mediated. *International Journal of Radiation Oncology*Biology*Physics* **58**, 862-870, doi:https://doi.org/10.1016/j.ijrobp.2003.09.012 (2004).
370 Reuben, A. *et al.* TCR Repertoire Intratumor Heterogeneity in Localized Lung Adenocarcinomas: An Association with Predicted Neoantigen Heterogeneity and Postsurgical Recurrence. *Cancer Discovery* **7**, 1088-1097, doi:10.1158/2159-8290.CD-17-0256 (2017).
371 Rudqvist, N.-P. *et al.* Radiotherapy and CTLA-4 Blockade Shape the TCR Repertoire of Tumor-Infiltrating T Cells. *Cancer immunology research* **6**, 139-150, doi:10.1158/2326-6066.CIR-17-0134 (2018).
372 Valpione, S. *et al.* The T cell receptor repertoire of tumor infiltrating T cells is predictive and prognostic for cancer survival. *Nature Communications* **12**, 4098, doi:10.1038/s41467-021-24343-x (2021).

373 Postow, M. A. *et al.* Peripheral T cell receptor diversity is associated with clinical outcomes following ipilimumab treatment in metastatic melanoma. *Journal for ImmunoTherapy of Cancer* **3**, 23, doi:10.1186/s40425-015-0070-4 (2015).
374 Chow, J. *et al.* Radiation induces dynamic changes to the T cell repertoire in renal cell carcinoma patients. *Proceedings of the National Academy of Sciences* **117**, 23721-23729, doi:10.1073/pnas.2001933117 (2020).
375 Pawlik, T. M. & Keyomarsi, K. Role of cell cycle in mediating sensitivity to radiotherapy. *Int J Radiat Oncol Biol Phys* **59**, 928-942, doi:10.1016/j.ijrobp.2004.03.005 (2004).
376 Zhao, J. H., Reiske, H. & Guan, J. L. Regulation of the cell cycle by focal adhesion kinase. *J Cell Biol* **143**, 1997-2008, doi:10.1083/jcb.143.7.1997 (1998).
377 Tancioni, I. *et al.* FAK Inhibition Disrupts a β5 Integrin Signaling Axis Controlling Anchorage-Independent Ovarian Carcinoma Growth. *Molecular Cancer Therapeutics* **13**, 2050-2061, doi:10.1158/1535-7163.MCT-13-1063 (2014).
378 Mukherjee, B. *et al.* The dual PI3K/mTOR inhibitor NVP-BEZ235 is a potent inhibitor of ATM- and DNA-PKCs-mediated DNA damage responses. *Neoplasia* **14**, 34-43, doi:10.1593/neo.111512 (2012).
379 Konstantinidou, G. *et al.* Dual phosphoinositide 3-kinase/mammalian target of rapamycin blockade is an effective radiosensitizing strategy for the treatment of non-small cell lung cancer harboring K-RAS mutations. *Cancer research* **69**, 7644-7652, doi:10.1158/0008-5472.CAN-09-0823 (2009).
380 Gubin, M. M. *et al.* High-Dimensional Analysis Delineates Myeloid and Lymphoid Compartment Remodeling during Successful Immune-Checkpoint Cancer Therapy. *Cell* **175**, 1014-1030.e1019, doi:10.1016/j.cell.2018.09.030 (2018).
381 Liu, X., Hogg, G. D. & DeNardo, D. G. Rethinking immune checkpoint blockade: 'Beyond the T cell'. *Journal for immunotherapy of cancer* **9**, e001460, doi:10.1136/jitc-2020-001460 (2021).
382 Demaria, S. & Formenti, S. Radiation as an immunological adjuvant: current evidence on dose and fractionation. *Frontiers in Oncology* **2**, doi:10.3389/fonc.2012.00153 (2012).
383 Formenti, S. C. & Demaria, S. Combining radiotherapy and cancer immunotherapy: a paradigm shift. *J Natl Cancer Inst* **105**, 256-265, doi:10.1093/jnci/djs629 (2013).
384 Vanpouille-Box, C. *et al.* DNA exonuclease Trex1 regulates radiotherapy-induced tumour immunogenicity. *Nature Communications* **8**, 15618, doi:10.1038/ncomms15618 (2017).
385 Dewan, M. Z. *et al.* Fractionated but Not Single-Dose Radiotherapy Induces an Immune-Mediated Abscopal Effect when Combined with Anti–CTLA-4 Antibody. *Clinical Cancer Research* **15**, 5379-5388, doi:10.1158/1078-0432.CCR-09-0265 (2009).
386 Hassanzadeh, C. *et al.* Ablative Five-Fraction Stereotactic Body Radiation Therapy for Inoperable Pancreatic Cancer Using Online MR-Guided Adaptation. *Advances in Radiation Oncology* **6**, 100506, doi:https://doi.org/10.1016/j.adro.2020.06.010 (2021).

387 Huguet, F. *et al.* Chemotherapy and intensity-modulated radiation therapy for locally advanced pancreatic cancer achieves a high rate of R0 resection*. *Acta Oncologica* **56**, 384-390, doi:10.1080/0284186X.2016.1245862 (2017).
388 Widmark, A. *et al.* Ultra-hypofractionated versus conventionally fractionated radiotherapy for prostate cancer: 5-year outcomes of the HYPO-RT-PC randomised, non-inferiority, phase 3 trial. *The Lancet* **394**, 385-395, doi:10.1016/S0140-6736(19)31131-6 (2019).
389 Gu, L. *et al.* Comparing Hypofractionated With Conventional Fractionated Radiotherapy After Breast-Conserving Surgery for Early Breast Cancer: A Meta-Analysis of Randomized Controlled Trials. *Frontiers in Oncology* **11**, doi:10.3389/fonc.2021.753209 (2021).
390 Favaudon, V. *et al.* Ultrahigh dose-rate FLASH irradiation increases the differential response between normal and tumor tissue in mice. *Sci Transl Med* **6**, 245ra293, doi:10.1126/scitranslmed.3008973 (2014).
391 Girdhani, S. *et al.* Abstract LB-280: FLASH: A novel paradigm changing tumor irradiation platform that enhances therapeutic ratio by reducing normal tissue toxicity and activating immune pathways. *Cancer Research* **79**, LB-280-LB-280, doi:10.1158/1538-7445.AM2019-LB-280 (2019).
392 Loo, B. W. *et al.* (P003) Delivery of Ultra-Rapid Flash Radiation Therapy and Demonstration of Normal Tissue Sparing After Abdominal Irradiation of Mice. *International Journal of Radiation Oncology, Biology, Physics* **98**, E16, doi:10.1016/j.ijrobp.2017.02.101 (2017).
393 Montay-Gruel, P. *et al.* Long-term neurocognitive benefits of FLASH radiotherapy driven by reduced reactive oxygen species. *Proceedings of the National Academy of Sciences* **116**, 10943-10951, doi:10.1073/pnas.1901777116 (2019).
394 Montay-Gruel, P. *et al.* Irradiation in a flash: Unique sparing of memory in mice after whole brain irradiation with dose rates above 100Gy/s. *Radiotherapy and Oncology* **124**, 365-369, doi:https://doi.org/10.1016/j.radonc.2017.05.003 (2017).